

SYNTHESIS AND APPLICATION OF CHIRAL PALLADIUM-PHOSPHANE
PRECATALYST IN ENANTIOSELECTIVE C-N CROSS-COUPLING

by Nande Abena Wright
Bachelor of Science Chemistry,
Ryerson University Toronto, ON, Canada, 2013

A thesis presented to Ryerson University
in partial fulfillment of the requirements for the degree of
Master of Science in the Program of
Molecular Science

Toronto, Ontario, Canada, 2016
© Nande Abena Wright 2016

Author's Declaration

I hereby declare that I am the sole author of this thesis. This is a true copy of the thesis, including any required final revisions, as accepted by my examiners.

I authorize Ryerson University to lend this thesis to other institutions or individuals for the purpose of scholarly research.

I further authorize Ryerson University to reproduce this thesis by photocopying or by other means, in total or in part, at the request of other institutions or individuals for the purpose of scholarly research.

I understand that my thesis may be made electronically available to the public.

SYNTHESIS AND APPLICATION OF CHIRAL PALLADIUM-PHOSPHANE PRECATALYST IN ENANTIOSELECTIVE C-N CROSS-COUPLING

Nande Abena Wright

Master of Science in the Program of Molecular Science
Ryerson University, 2016

Abstract

The various strategies and reaction conditions towards the synthesis of benzene-, naphthalene-, and phenanthrene-based dicyclohexylbiaryl phosphanes are presented. A chiral third generation Buchwald-type precatalyst has been synthesized, employing the non-commercially available ligand, (*R*)-dicyclohexyl(2'-methoxy-[1,1'-binaphth-2-yl])phosphane, (*R*)-Cy₂MOP, and a dimeric methanesulfonate-bridged palladacycle based on a 2-aminobiphenyl scaffold. Application of the palladacyclic precatalyst in an enantioselective variant of the Buchwald-Hartwig reaction is demonstrated in the desymmetrization of prochiral α -(2-bromobenzyl)malonamides *via* intramolecular *N*-arylation. The scope of the catalysis in the presence of the precatalyst has been investigated with efforts towards optimizing yields, catalyst loading, and enantioselectivities. Attempts towards the isolation of a potential reaction intermediate in the form of a stable amido-bound palladium complex are discussed. Finally, strategies towards gaining mechanistic insight on the origin of the enantiomeric excess are discussed.

Acknowledgements

I would like to say thank you to my supervisor Dr. Russell Viirre for granting me the opportunity to carry out my graduate thesis under his supervision. His patience and knowledge in the area of synthetic organic chemistry have allowed me to grow and progress as a synthetic chemist. I want express my gratitude to my supervisory committee members Dr. Gossage and Dr. Koivisto for their support over these past years. The sharing of ideas has been invaluable and our discussions have helped me to improve the way that I troubleshoot in the laboratory. Another influential figure who has inspired and supported me throughout my graduate degree is Dr. Foucher, who is on my examination committee. I would also like to thank Dr. Alan Lough for carrying out the X-ray crystallographic analysis.

As a graduate student, much of my time has been spent working alongside my peers and I must say that it has been a pleasure. Lab members both past and present have truly shaped my experience and I have enjoyed many fun times with them, learning and working together, and sharing music and laughs. I am grateful to Rob Denning, Khrystyna Herasymchuk, Grace Luk, and Maja Chojnacka for their support when I first started my research. To Vassili Kanellis, I am glad that I met you and got to spend time expanding on ideas and sharing jokes with you in the lab. Many others have contributed to my memorable time here including my favourite lab technologist, Shawn McFadden, and my friends and colleagues, Phillip, Christopher, Kevin, Mohammad, Kathy May, Krimo, Jennifer, Maryam, Jeffrey, Sara, Burhan, Nora, Jee In, Aju-sue, Victoria, Donna, Amir, and more friends in the science research labs.

Finally, I want to thank my family and friends for being there for me throughout these years, especially during challenging times. To my parents, Ras Iville and Ikeila, and siblings, Nzinga, Nkosi, Nefertiti, and Nigisti Wright, I thank you all for keeping me going. Nkosi, your

ambition and motivation inspire me every day and I appreciate your encouragement. Nigisti, your trust and friendship mean the world to me. To my Auntie Yolisa, thank you for being so positive and enthusiastic about my studies over the years. I want to thank the Azubuikes, Janice Ruck, and Lorrie Simunovic for their support and kindness during a very challenging time in my life. I must say a special thank you to my mom for her unyielding love, and infinite support and encouragement. Thank you for always believing in me and for being a voice of reason in my life. I am truly grateful for all of you and as my brilliant family always says, “we did it!”

To my grandmother,
Mabel Eugene Anderson-Meikle

Table of Contents

Author's Declaration.....	ii
Abstract	iii
Acknowledgements.....	iv
Dedication	vi
List of Figures	ix
List of Schemes.....	x
List of Tables	xii
List of Abbreviations	xiii
1 Introduction.....	1
1.1 Pd-catalyzed cross-coupling reactions.....	1
1.2 Catalytic cycle	4
1.3 Nature of the ligand	7
1.4 Preformed palladium catalysts.....	14
1.5 Palladium-catalyzed enantioselective C-N cross-coupling	25
1.6 Research objectives	37
2 Results and Discussion	39
2.1 Towards the synthesis of bulky dialkylbiaryl phosphanes	39
2.2 Synthesis of Buchwald-type precatalyst.....	56
2.3 Synthesis of quinolinones <i>via</i> palladacycle-catalyzed Buchwald-Hartwig reaction ..	64
2.4 Investigating the origin of selectivity in the desymmetrization of malonamides	69
3 Experimental	74
3.1 General information.....	74
3.2 Towards benzene-based <i>ortho</i> -bromobiaryl	75
3.3 Synthesis of binaphthyl-based chiral phosphanes	79
3.4 Synthesis of 2-aminobiphenyl-based palladium methanesulfonate dimer	83
3.5 General procedure for the synthesis of third generation palladium precatalysts.....	84
3.6 General procedure for the synthesis of α -(2-bromobenzyl)malonamides	86
3.7 General procedure for the <i>N</i> -arylation of α -(2-bromobenzyl)malonamides.....	93
4 Conclusion	95
5 Appendix.....	96
5.1 NMR spectroscopy data.....	96

5.2	HPLC chromatograms	146
5.3	X-ray crystallography data for Cy ₂ MOP-Pd precatalyst	152
References		180

List of Figures

Figure 1 – General catalytic cycle for Pd-catalyzed cross-coupling reactions	1
Figure 2 – Catalytic cycle for the Buchwald-Hartwig amination	4
Figure 3 – β -Hydride elimination of intermediate Pd-amido species	5
Figure 4 – Mechanism for the generation of active Pd(0) catalyst using an amine	6
Figure 5 – Reduction of Pd(II) source to Pd(0) by triphenylphosphane	6
Figure 6 – Diphosphanes with bite angles larger than 100° in van Leeuwen's study	9
Figure 7 – Dialkylbiphenyl phosphane ligands	11
Figure 8 – Conformations of monophosphane-Pd complexes in <i>N</i> -arylation reaction	12
Figure 9 – 1,6-Diene Pd(0) monophosphane complexes	15
Figure 10 – Mode of Buchwald-type precatalyst activation	21
Figure 11 – Target chiral dialkylbiarylphosphanes	39
Figure 12 – ^{31}P NMR spectrum of complex reaction mixture from attempted benzyne pathway towards diphenyl biarylphosphane in CDCl_3	51
Figure 13 – ^{19}F NMR spectrum confirming the presence of $\text{BINOL}(\text{OTf})_2$ in CDCl_3	55
Figure 14 – ^{31}P NMR spectrum of the methanesulfonate dimer bridge-splitting reaction with Cy_2MOP after 20 minutes in CDCl_3	58
Figure 15 – ^{31}P NMR spectrum of Cy_2MOP coordination reaction after 15 hours	59
Figure 16 – ^1H NMR spectrum of product mixture from the C-P coupling reaction towards (<i>R</i>)-MOP ligand in CDCl_3	63
Figure 17 – Investigating the origin of selectivity in the amidation reaction	69
Figure 18 – ^{31}P NMR spectrum of reaction of 1:1:0.25 eq 22/31 / KO^tBu in C_6D_6	71
Figure 19 – ^{31}P NMR spectrum of reaction of 1:1:0.25 eq 22/31 / KO^tBu in THF in C_6D_6	72
Figure 20 – ^{31}P NMR spectrum of reaction of 1:1:1 eq 22/31 / KO^tBu in THF in C_6D_6	72
Figure 21 – ^1H NMR expansion of characteristic diastereotopic proton signals of dibenzyl quinolinone 35 in CDCl_3	73

List of Schemes

Scheme 1 – General Buchwald-Hartwig cross-coupling reaction	2
Scheme 2 – First reported Pd-catalyzed aromatic amination.....	2
Scheme 3 – Transamination and subsequent Pd-catalyzed aromatic amination.....	3
Scheme 4 – Aryl bromide amination under tin-free conditions reported by Buchwald	3
Scheme 5 – Aryl bromide amination under tin-free conditions reported by Hartwig	3
Scheme 6 – PdCl ₂ (dppf)-catalyzed Kumada and Negishi coupling	8
Scheme 7 – Original synthetic route towards dialkylbiaryl phosphanes	10
Scheme 8 – One-pot procedure towards dialkylbiaryl phosphanes <i>via</i> benzyne route.....	11
Scheme 9 – Preparation of air and moisture stable PEPPSI precatalyst complexes.....	16
Scheme 10 – Coupling of electron-poor anilines with aryl chlorides using a weak base.....	17
Scheme 11 – First reported Pd-catalyzed amination of aryl chlorides	18
Scheme 12 – Amination of aryl chlorides catalyzed by highly active precatalyst	19
Scheme 13 – Synthesis of palladacyclic phenethylamine-based precatalyst.....	20
Scheme 14 – Comparison of traditional Pd sources and precatalyst in <i>N</i> -arylation	20
Scheme 15 – Coupling of electron-poor anilines with aryl chlorides using a weak base.....	21
Scheme 16 – Synthesis of palladacyclic 2-aminobiphenyl-based precatalyst	23
Scheme 17 – Suzuki-Miyaura coupling of unstable boronic acids using precatalyst.....	23
Scheme 18 – Synthesis of 2-aminobiphenyl methanesulfonate precatalyst	24
Scheme 19 – Arylation of primary amides using precatalyst	25
Scheme 20 – Kinetic resolution of <i>rac</i> -4,12-dibromo[2.2]paracyclophane	26
Scheme 21 – Kinetic resolution for the phenylation of <i>rac</i> -NOBIN	27
Scheme 22 – Kinetic resolution for the phenylation of <i>rac</i> -BINAM	27
Scheme 23 – Kinetic resolution of racemic primary amines	28
Scheme 24 – Kinetic resolution of optically active primary amines	29
Scheme 25 – Synthesis of atropisomeric anilides <i>via</i> intermolecular <i>N</i> -arylation	30
Scheme 26 – Synthesis of atropisomeric lactams <i>via</i> intramolecular <i>N</i> -arylation.....	30
Scheme 27 – Synthesis of atropisomeric 2-aryl-4-quinolinones <i>via</i> tandem amination.....	31
Scheme 28 – Intramolecular double cyclization <i>via</i> <i>N</i> -arylation of malonamides	32
Scheme 29 – Desymmetrization of malonamides <i>via</i> enantioselective <i>N</i> -arylation.....	33
Scheme 30 – Enantioselective synthesis of azamacrocycle <i>via</i> Buchwald-Hartwig amination using dichloroanthraquinone and dioxadamine	34

Scheme 31 – Enantioselective synthesis of azamacrocyclic <i>via</i> Buchwald-Hartwig amination using dichloroanthraquinone and trioxadiazine.....	35
Scheme 32 – Enantioselective synthesis of azamacrocyclic <i>via</i> Buchwald-Hartwig amination using dichloroanthracene and dioxadiazine.....	35
Scheme 33 – Enantioselective synthesis of azamacrocyclic <i>via</i> Buchwald-Hartwig amination using dichloroanthracene and trioxadiazine	36
Scheme 34 – Enantioselective synthesis nitrogen-bridged azacalix[4]arene	36
Scheme 35 – Synthesis of chiral methanesulfonate precatalyst based on (<i>R</i>)-Cy ₂ MOP	37
Scheme 36 – Enantio- and diastereoselective Buchwald-Hartwig reactions.....	38
Scheme 37 – Methylation of 1-bromo-2-naphthol using iodomethane	40
Scheme 38 – Synthesis of 1-bromo-2-methoxynaphthalene from 2-naphthol	41
Scheme 39 – Strategy towards benzene-based dialkylbiaryl phosphane.....	41
Scheme 40 – Aryl lithium strategy towards benzene-based dialkylbiaryl phosphane.....	42
Scheme 41 – Synthesis of 2-methoxynaphthylboronic acid for Suzuki-Miyaura coupling	43
Scheme 42 – Strategy towards phenanthrene-based dialkylbiaryl phosphane	46
Scheme 43 – Synthesis of monobrominated phenanthrene towards target dibromide	49
Scheme 44 – Generation and reaction of benzene-based biaryl Grignard reagent towards benzene-based dialkylbiaryl phosphane	50
Scheme 45 – Li/Br exchange of <i>ortho</i> -bromobiaryl towards dialkylbiaryl phosphane.....	51
Scheme 46 – Phosphination of benzene-based <i>ortho</i> -bromobiaryl	52
Scheme 47 – Methylation of BINOL using iodomethane	54
Scheme 48 – Triflation of Me-BINOL using triflic anhydride.....	54
Scheme 49 – Synthesis of Cy ₂ MOP following improved protocol	55
Scheme 50 – Modified procedure towards cyclopalladated 2-aminobiphenyl and ¹ H NMR spectrum of isolated crude product	56
Scheme 51 – Synthesis of 2-aminobiphenyl-based palladium methanesulfonate dimer.....	57
Scheme 52 – Synthesis of chiral methanesulfonate precatalyst based on Cy ₂ MOP.....	58
Scheme 53 – Synthesis of chiral methanesulfonate precatalyst based on (<i>R</i>)-MOP	62
Scheme 54 – Synthesis of malonic acid from diethyl methylmalonate	64
Scheme 55 – Synthesis of <i>N</i> -substituted malonamides.....	65
Scheme 56 – Towards the synthesis of a palladium-amido species of the catalytic cycle	71

List of Tables

Table 1. Cross-coupling of 2-butybmagnesium chloride with bromobenzene	9
Table 2. Optimization of Suzuki-Miyaura cross coupling reaction conditions	45
Table 3. Bromination reaction conditions towards 9,10-dibromophenanthrene.....	48
Table 4. X-ray structure of Cy ₂ MOP-Pd precatalyst and relevant bond angles	60
Table 5. X-ray structure of Cy ₂ MOP-Pd precatalyst and related structures	61
Table 6. Dihedral angles of phosphane moiety of Cy ₂ MOP-Pd precatalyst.....	62
Table 7. Optimization of malonamide cyclization reaction conditions	66

List of Abbreviations

Ac	Acetyl
Ar	Aryl
BINAM	1,1'-Binaphthyl-2,2'-diamine
BINAP	2,2'-Bis(diphenylphosphanyl)-1,1'-binaphthalene
BINOL	1,1'-Bi-2-naphthol
Bn	Benzyl
Bu	Butyl
cat.	Catalyst
CTAB	Cetyltrimethylammonium bromide
Cy	Cyclohexyl
Cy ₂ MOP	Dicyclohexyl(2'-methoxy-[1,1'-binaphthalen]-2-yl)phosphane
dba	Dibenzylideneacetone
DCM	Dichloromethane
<i>de</i>	Diastereomeric excess
DFT	Density functional theory
DIPEA	<i>N,N</i> -Diisopropylethylamine
DiPPF	1,1'-Bis(diisopropylphosphino)ferrocene
DME	Dimethoxyethane
DMPU	<i>N,N'</i> -Dimethylpropylene urea
DMSO	Dimethyl sulfoxide
DPEphos	Bis[(2-diphenylphosphino)phenyl] ether
DPPB	1,4-Bis(diphenylphosphino)butane
DPPE	1,2-Bis(diphenylphosphino)ethane
DPPF	1,1'-Bis(diphenylphosphino)ferrocene
DPPP	1,3-Bis(diphenylphosphino)propane
DTBM	Di- <i>tert</i> -butylmethoxy
DTBNpP	Di(<i>tert</i> -butyl)neopentylphosphane

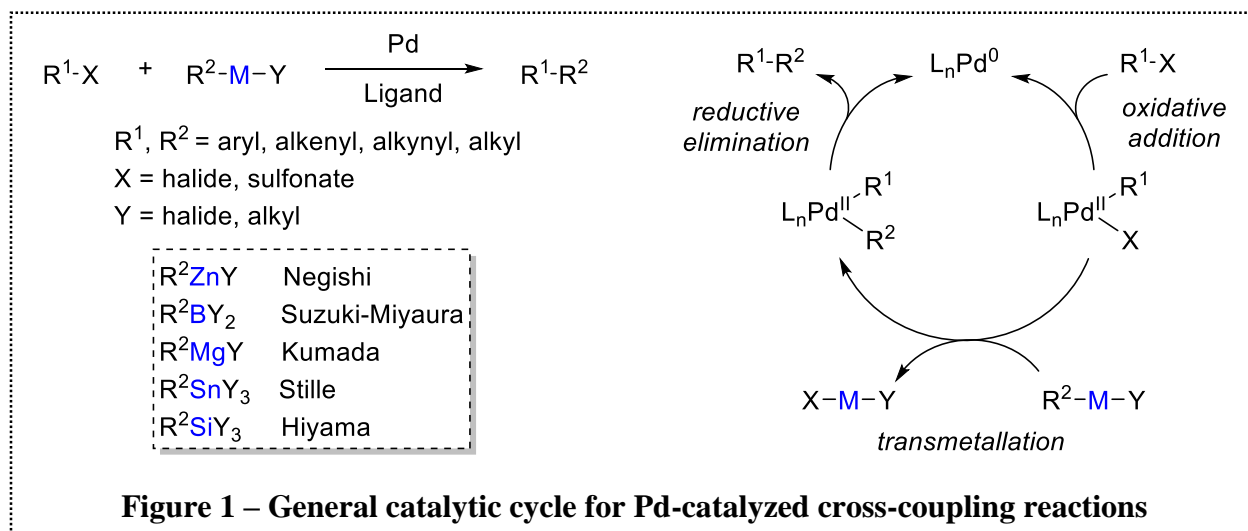
<i>ee</i>	Enantiomeric excess
eq	Equivalent
Et	Ethyl
HPLC	High-performance liquid chromatography
LiHMDS	Lithium bis(trimethylsilyl)amide
MAP	2-Diphenylphosphino-2'-(<i>N,N'</i> -dimethylamino)-1,1'-binaphthalene
Me	Methyl
Ms	Methanesulfonyl (mesyl)
MOP	2-Diphenylphosphino-2'-methoxy-1,1'-binaphthyl
MTBE	Methyl <i>tert</i> -butyl ether
n.d.	Not determined
NET	Norepinephrine transporter
NHC	<i>N</i> -heterocyclic carbene
NMR	Nuclear magnetic resonance
NOBIN	2-Amino-2'-hydroxy-1,1'-binaphthalene
PEPPSI	Pyridine-enhanced precatalyst preparation stabilization and initiation
Ph	Phenyl
PHANEPHOS	4,12-Bis(diphenylphosphino)-[2.2]-paracyclophane
PPFA	(<i>R</i>)- <i>N,N</i> -Dimethyl-1-[(<i>S</i>)-2-(diphenylphosphino)ferrocenyl]ethylamine
Pr	Propyl
QUINAP	1-(2-Diphenylphosphino-1-naphthyl)isoquinoline
R _f	Retention factor
rt	Room temperature
SEGPPOS	5,5'-Bis(diphenylphosphino)-4,4'-bi-benzo[1,3]dioxole
Tf	Trifluoromethanesulfonyl
THF	Tetrahydrofuran
TLC	Thin layer chromatography
TMEDA	Tetramethylethylenediamine

TMS	Tetramethylsilane
TOF	Turn over frequency
Tol	Tolyl
Ts	Toluenesulfonyl (tosyl)

1 Introduction

1.1 Pd-catalyzed cross-coupling reactions

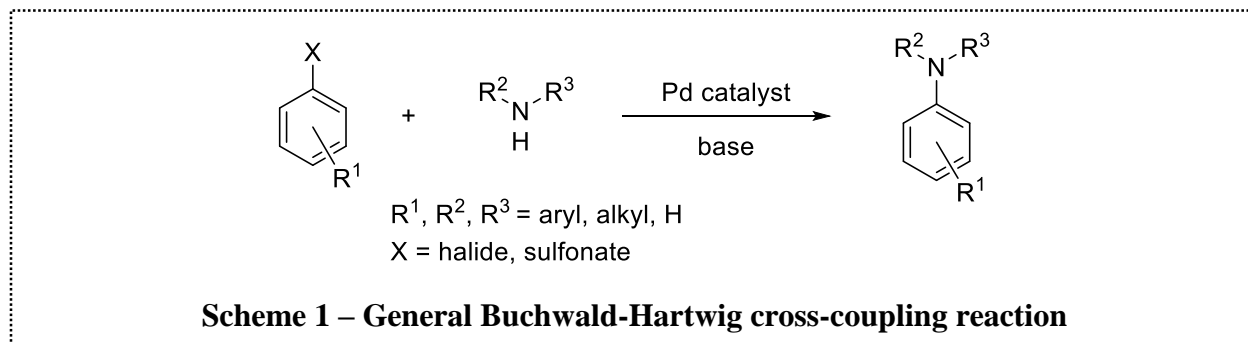
Cross-coupling reactions are transition-metal catalyzed substitutions of an aryl, alkenyl, alkynyl, or alkyl halide (or pseudohalide) by an organometallic nucleophile which follows the general accepted pathway depicted in Figure 1 proceeding by oxidative addition, transmetallation,



and reductive elimination.¹ Specifically, palladium-catalyzed cross-coupling reactions have emerged as a powerful synthetic tool for carbon-carbon and carbon-heteroatom bond formation. The significance and impact of these transformations on synthetic chemistry over the past few decades was recognized with the Nobel Prize in chemistry in 2010, awarded to R. F. Heck, E. Negishi, and A. Suzuki “for palladium-catalyzed cross couplings in organic synthesis”. These reactions are categorized based on the type of organometallic nucleophile involved and the scientists who discovered and developed them.^{1,2}

1.1.1 Buchwald-Hartwig reaction

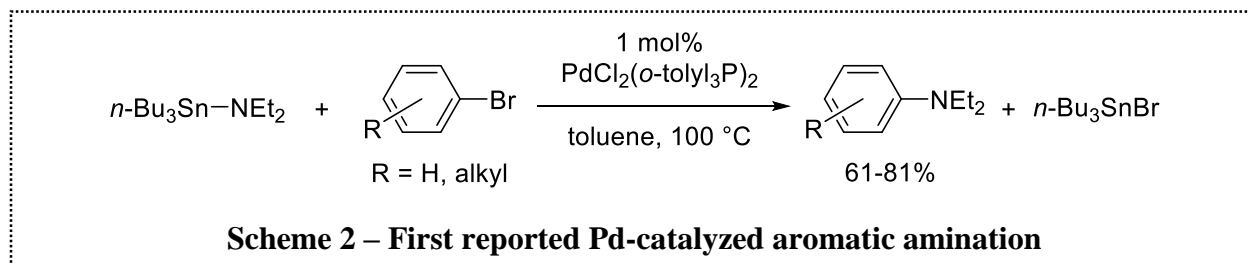
The general Buchwald-Hartwig reaction involves the cross-coupling of an aryl halide with an amine in the presence of a palladium catalyst and a base (Scheme 1). This cross-coupling



methodology has been extended to include the formation of the C-O, C-P, and C-S bonds in ether, phosphane, and thioether products.³

1.1.2 History of C-N cross-coupling reaction

The first palladium-catalyzed C-N cross-coupling reaction was reported by Migita and co-workers in 1983 (Scheme 2).⁴ This amination involved the reaction of *N,N*-diethylamino-



tributyltin with aryl bromides, affording *N,N*-diethylaminobenzene derivatives. The major drawback of this seminal discovery was the lack of generality for other types of amines; also, aminostannanes are thermally and moisture sensitive which inhibited the practicality of their isolation and further derivatization. In 1994, overcoming this limitation, Buchwald and Guram demonstrated that a broad range of aminostannanes could be generated *in situ via* transamination and subsequently employed in the amination of various aryl bromides, as shown in Scheme 3.⁵



In 1995, Buchwald and Hartwig independently developed tin-free cross-coupling conditions, nearly simultaneously, where a variety of amines and aryl bromides were coupled in the presence of a palladium catalyst and a base (Scheme 4 and Scheme 5).^{7,8} This breakthrough

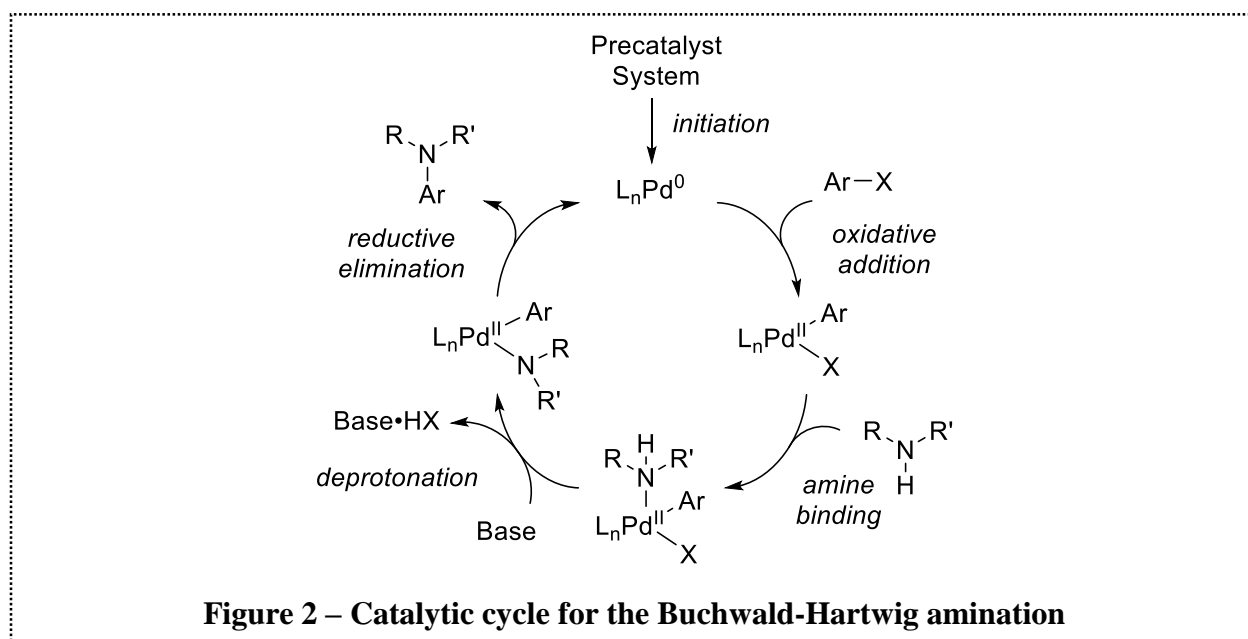


3

side reactions and improve functional group compatibility. The amination of aryl halides has since become a powerful tool in organic synthesis, pharmaceuticals, and materials chemistry.⁹

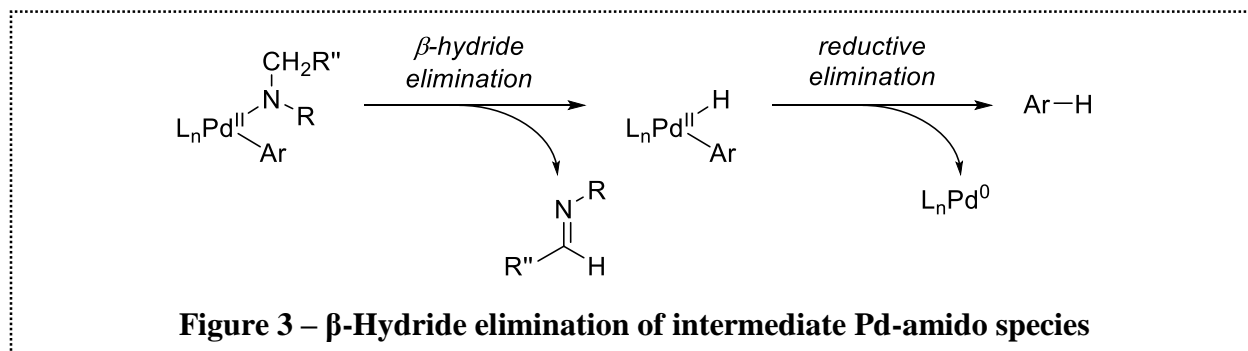
1.2 Catalytic cycle

The generally accepted mechanism for the catalytic cycle of the C-N cross-coupling reaction is presented in Figure 2.^{7,10-13} Initiation of the palladium source to form the catalytically active palladium(0) species is followed by oxidative addition of the aryl halide to give the arylpalladium(II) species, coordination of the amine, then deprotonation of the palladium-bound amine and finally, reductive elimination of the coupled *N*-aryl product, regenerating the active



catalyst. In certain cases, especially when electron-rich (deactivated) aryl halides are employed, the amide-bound palladium species can react by an undesired alternate pathway during the cycle.

β -Hydride elimination of the palladium-amido species can occur in the cases where the amine substrate possesses a β -hydrogen, generating an imine and a palladium(II) aryl hydride which subsequently undergoes reductive elimination, forming an arene byproduct and regenerating the active palladium(0) catalyst (Figure 3).⁷ Electron-deficient palladium-amido complexes on the



other hand undergo reductive elimination more readily, thereby avoiding the competitive hydrodehalogenation of the aryl halide. This particular problem in addition to the extension of this cross-coupling methodology to more challenging substrates, such as aryl chlorides, which are readily available and inexpensive compared to their bromide and iodide counterparts, have been major focuses with regards to the development of this reaction.

1.2.1 Precatalyst system activation

The active catalyst of the Buchwald-Hartwig reaction is a low coordinate palladium(0) complex. Typically, these catalyst systems are designed to include an electron-rich palladium centre, which has a greater propensity for electron-donation in the oxidative addition step. In the case where a palladium(II) source such as $\text{Pd}(\text{OAc})_2$ is used, it must be reduced to palladium(0) to enter the catalytic cycle. Typically, the reducing agent constitutes the amine nucleophile or an

exogenous reducing agent such as *n*-tributylamine,¹⁴ as highlighted in Figure 4.¹⁵ In order to serve as a reducing agent the amine must possess a β -hydrogen for β -hydride elimination of the generated

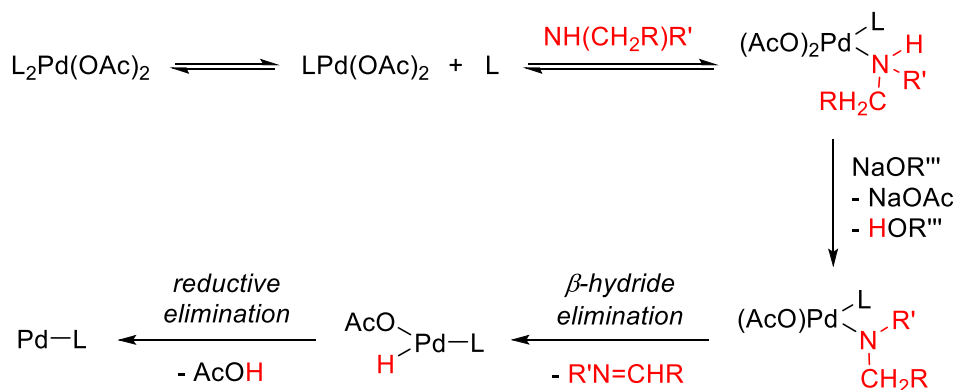


Figure 4 – Mechanism for the generation of active Pd(0) catalyst using an amine

palladium(II) amine complex to be possible. The phosphane ligand can also facilitate the formation of the active catalyst;^{16,17} however, the mode of this transformation is likely hindered in the presence of bulky substituents on the phosphorus. Phosphanes such as triphenylphosphane or

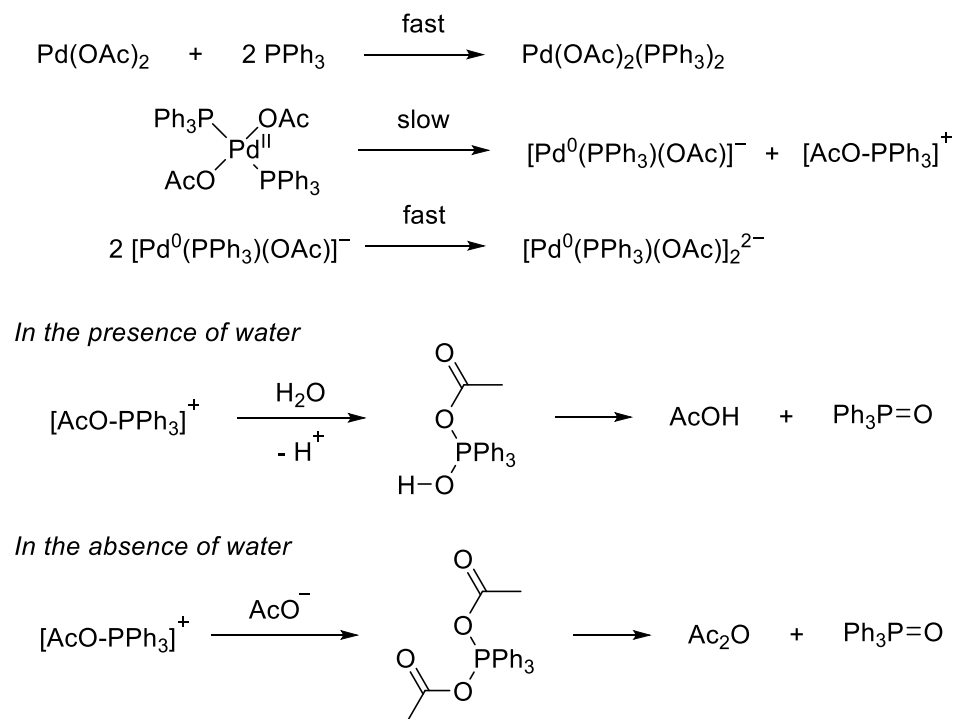


Figure 5 – Reduction of Pd(II) source to Pd(0) by triphenylphosphane

BINAP generate the phosphane oxide species and acetic anhydride upon activation of the palladium catalyst, as highlighted in Figure 5.¹⁶ Reduction of the palladium(II) species by triphenylphosphane occurs upon exposure to an oxygenated ligand such as hydroxide or acetate. In the presence of water, oxide formation can be represented as the coordination of water to the intermediate species $[\text{AcO-PPh}_3]^+$ followed by the elimination of acetic acid. Formation of the phosphane oxide in the absence of water involves the coordination of the acetate ligand to $[\text{AcO-PPh}_3]^+$ followed by elimination of acetic anhydride. This *in situ* activation of the catalyst step is often inadequate under certain reaction conditions.

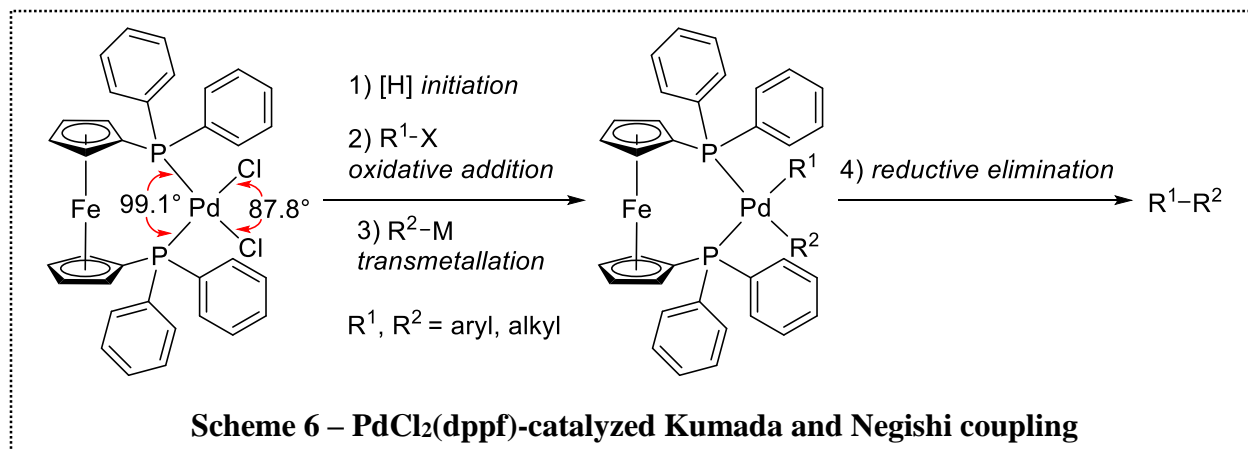
To obviate the need for an activation step, stable, palladium(0) sources have been employed in several reports along with the selected ligand source. The commercially available palladium(0) source, $\text{Pd}_2(\text{dba})_3$, has traditionally been used, however it can vary in content and purity, often containing palladium nanoparticles, which can interfere with the reaction and most importantly with the quality of the results.¹⁸ It has also been observed that dba can hinder the formation and activity of the active catalyst species.¹⁹ Still commonly used, especially in larger scale processes, are the palladium(0) complex, $\text{Pd}(\text{PPh}_3)_4$, and palladium(II) catalyst, $\text{PdCl}_2(\text{PPh}_3)_4$, which avoid the formation of deleterious palladium species. These complexes are restricted by triphenylphosphane however, since it is less active than many of the more recently developed ligands which limits the substrate scope to aryl iodides and activated aryl bromides.¹⁸

1.3 Nature of the ligand

The efficiency of catalyst complexes is influenced by the properties of the transition metal and the associated ligand. The structural features of the ancillary ligand used in a palladium-catalyzed cross-coupling reaction has been demonstrated to dictate catalytic activity and selectivity,^{20,21} therefore highlighting the significance of ligand choice for the success of a reaction.

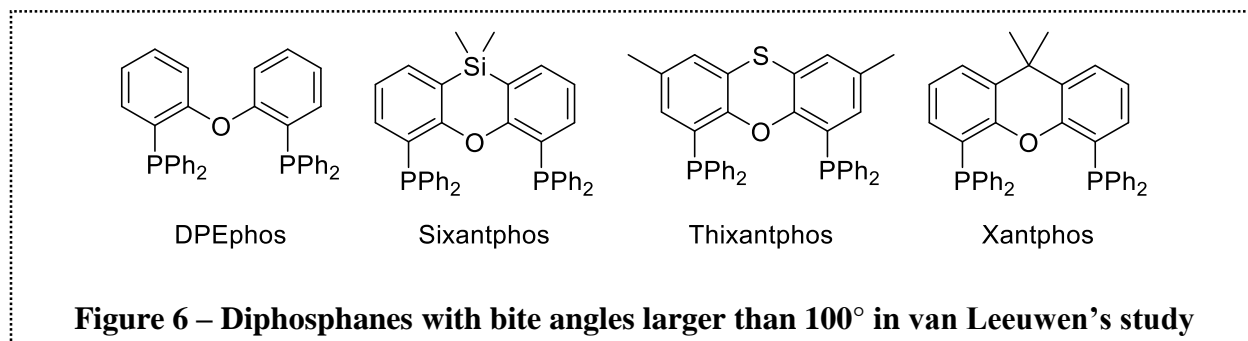
A wide variety of ligands have been developed for the catalysis of different transformations and this steady progress has contributed greatly to the expansion of the reaction scope of the Buchwald-Hartwig amination and has enabled its success under milder conditions. The steric and electronic properties of the phosphane can have extreme implications on the activity and selectivity of a catalyst system and therefore structural modifications can facilitate the tuning of a catalyst for a given reaction.

An early observation made by Hayashi highlighted the significance of the structural features of the ligand used in cross-coupling reactions.²² Employing $\text{PdCl}_2(\text{dppf})$ as a ligand, it was found that its relatively large P-Pd-P bite angle and smaller Cl-Pd-Cl bite angle highlighted in Scheme 6,²² led to an enhanced rate of reductive elimination compared to the rates achieved using



other diphosphane ligands including dppe, dppp, and dppb, which have smaller bite angles between the two phosphane groups within the ligand. This feature enabled the coupling of previously challenging alkyl Grignard and alkylzinc reagents with organohalides in Kumada and Negishi cross-coupling reactions, respectively. Furthermore, increased selectivity for the desired cross-coupling product was also observed with increasing bite angle. Building upon these results van Leeuwen *et al.* investigated the activity and selectivity achieved using diphosphanes shown in Figure 6, with bite angles larger than 100° (determined *via* computational methods),²³ a range

which was not covered in Hayashi's report. This study revealed that an optimum P-Pd-P bite angle was about 102°, as demonstrated by the results obtained using DPEphos, which led to greater



catalyst efficiency and comparable yield of the coupled product. The results from these studies are summarized for the cross-coupling of 2-butylmagnesium chloride with bromobenzene in Table 1 below.²³

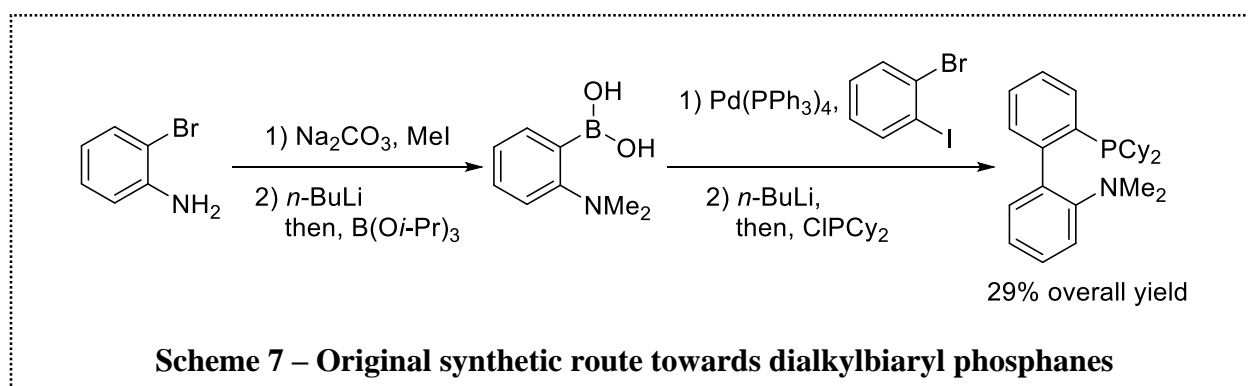
Table 1. Cross-coupling of 2-butylmagnesium chloride with bromobenzene

Diphosphane Ligand	Bite Angle (°)	TOF (mol (mol Pd) ⁻¹ h ⁻¹)	Time (h)	Conversion (%)	Yield (%)			
					A	B	C	
dppe	78.1	n.d.	48	4	0	0	n.d.	
dppp	86.2	n.d.	24	67	69	31	n.d.	
dppb	98.7	n.d.	8	98	51	25	n.d.	
dppf ^a	99.07	79	2	100	95	2	3	
DPEphos	102.9	181	2	100	98	1	1	
Sixantphos	106.5	36	16	58.8	67	17	16	
Thixantphos	107.2	24	16	36.5	51	17	32	
Xantphos	110.0	24	16	23.6	41	19	40	

^a The natural bite angle for dppf was unable to be accurately calculated due to the challenges associated with modelling the ferrocene-units, so the P-Pd-P angle from the PdCl₂(dppf) X-ray crystal structure was used.

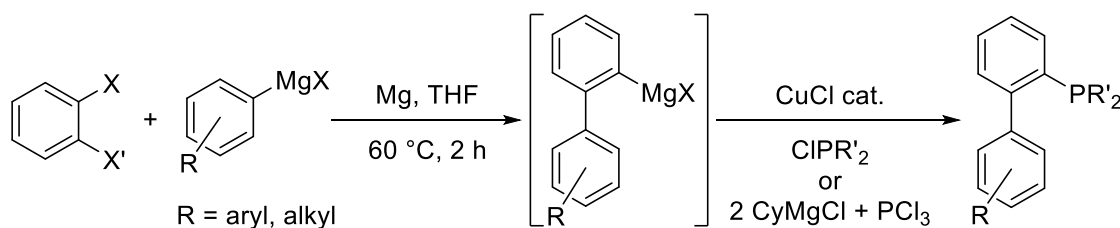
1.3.1 Dialkylbiaryl phosphane ligands

In 1998, Buchwald introduced a new class of relatively air-stable dialkylbiaryl phosphane ligands that showed high activity for palladium-catalyzed amination and Suzuki-Miyaura cross-coupling reactions of aryl chlorides, in various catalyst systems.²⁴ Despite the high activity observed using the palladium catalyst based on this ligand, the utility was compromised since accessing the featured dialkylaminophosphane ligand required four steps, as presented in Scheme 7. Further studies revealed that ligands with a bulkier phosphane (*e.g.* *tert*-butyl substituted in



place of cyclohexyl group) showed superior results for certain substrates. In addition, the importance of the amino group was studied by analyzing the readily available desamino analogs, which were found to be equally effective but for only certain substrates. Sparked by the outstanding results obtained, researchers focused on developing an efficient synthetic route to render this class of ligands more readily available.

In 2000, Buchwald showed that dialkylbiaryl phosphanes ligands can be accessed *via* a less expensive, scalable one-pot procedure displayed in Scheme 8 involving the reaction of a benzyne generated *in situ* from a dihalobenzene, with an arylmagnesium halide followed by the reaction of the generated *ortho*-metallated biphenyl with a chlorodialkylphosphane.²⁵ Subsequent findings improved upon the synthesis by employing a copper chloride catalyst in the reaction of chlorodialkylphosphanes with Grignard reagents.²⁶ Dialkylbiaryl phosphanes continue to play a



Scheme 8 – One-pot procedure towards dialkylbiaryl phosphanes *via* benzyne route

significant role in palladium-catalyzed cross-coupling reaction as supporting ligands, allowing the use of mild reaction conditions, lower catalyst loading, and they can be employed in a variety of cross-coupling reactions including C-N, C-O, Suzuki-Miyaura, and Negishi with wide substrate scopes (Figure 7).^{21,27}

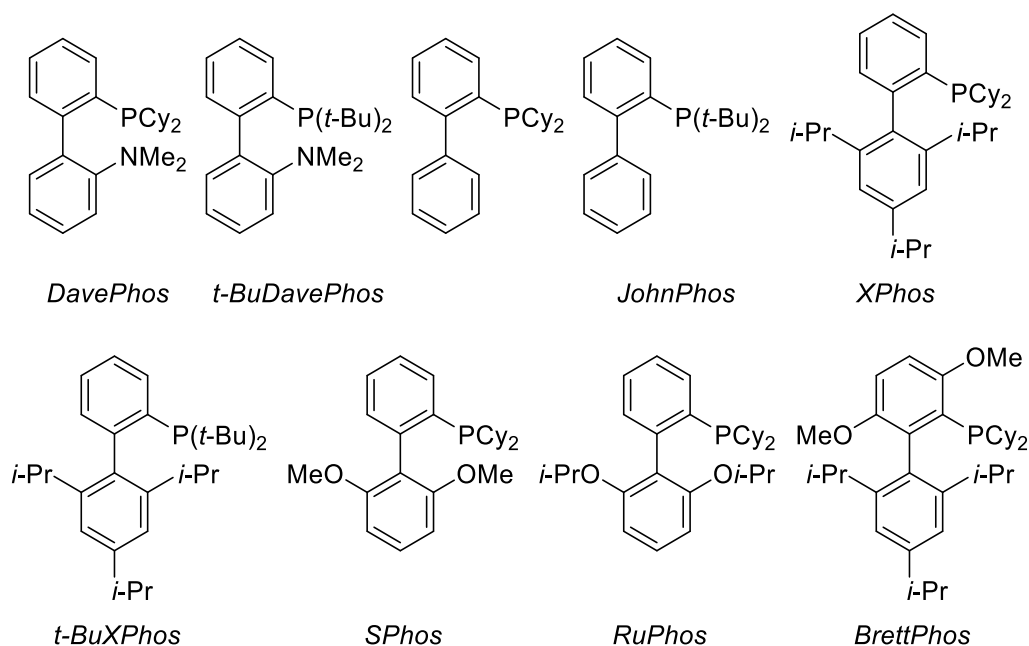
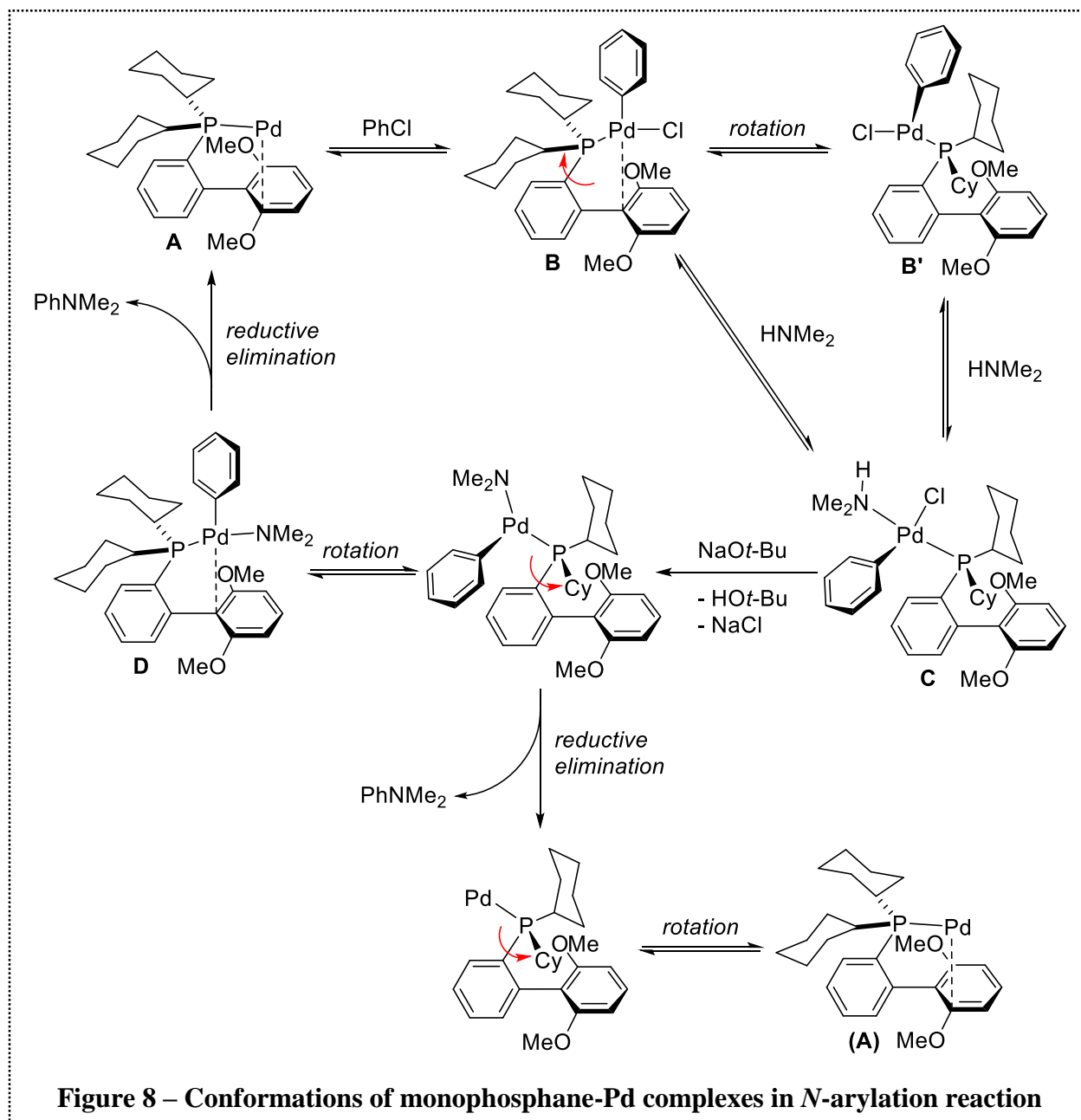


Figure 7 – Dialkylbiphenyl phosphane ligands

It can be challenging to obtain structural information about the reaction intermediates within the catalytic cycle and to isolate such species. Towards unveiling the origins of the success obtained using these highly efficient supporting ligands, Barder and Buchwald investigated the amination mechanism in the presence of biaryl phosphanes by conducting an all-atom density

functional theory (DFT) study.²⁷ The various conformations of the monophosphane-palladium complexes accessed throughout the catalytic cycle in the amination of chlorobenzene with dimethylamine, are exhibited in Figure 8 below.²⁷



The active catalyst monophosphane species **A** is stabilized by Pd-arene interactions (or Pd-O interactions where applicable). The most favourable geometry of the subsequent complex **B**

following oxidative addition also relies on these metal-arene stabilizing interactions. Binding of the amine nucleophile however, is more facile when the arene ring is in the distal position relative to the palladium centre, as in the structure of **B'**. Therefore, rotation about the phosphorus centre in the oxidative addition complex formed is required. Deprotonation of the palladium-bound amine is readily achieved since even a relatively bulky base such as NaOtBu can access the proton due to the absence of steric crowding from the non-phosphane bearing arene of the ligand in **C**. Rotation about the phosphorus centre is necessary to re-establish the former interactions between the π -system of the non-phosphane bearing arene of **D** and the palladium centre, and enforce a *cis* geometry between the aryl and amide ligands which is necessary for reductive elimination to occur. As a result of the metal-arene stabilizing interactions for intermediates throughout the catalytic cycle described above, these types of phosphane ligands, especially those containing ortho-substituents relative to the phosphorus, promote longer catalyst lifetime and this in turn may contribute to lower catalyst loadings.³

1.3.1.1 Influence of phosphane on oxidative addition

The oxidative addition step involves the reaction of the aryl halide with the low valent coordinatively unsaturated palladium complex, forming two new bonds with the metal centre following the Ar-X bond cleavage.² The oxidation state of palladium increases by two since its former non-bonding electrons are involved in the new coordinative bonds. In general, greater electron density of the metal facilitates oxidative addition² and electron-rich sigma donors such as phosphanes, coordinated to the palladium centre, serve this role. It has been supported through ¹H and ³¹P NMR spectroscopic studies of palladium-catalyzed amination reactions that oxidative addition of the aryl halide is the rate determining step.^{24,28} This is especially apparent in the case of unactivated substrates such as aryl chlorides and tosylates.

In order to enhance the rate of oxidative addition a considerable amount of research towards more active catalyst systems has been conducted by various groups focusing on ligand design. The employment of electron-rich phosphane ligands for the purpose of increasing the electron density at the palladium centre was suggested to achieve faster reaction rates *via* enhancement of oxidative addition. However, generation of the palladium(0) complex can involve complete dissociation of a chelating phosphane, therefore, an electron-rich ligand that could also facilitate ligand dissociation was the target.²⁸ This was another driving force for the investigation of sterically hindered alkylphosphanes in the coupling of unactivated substrates.

1.3.1.2 Influence of phosphane on reductive elimination

Reductive elimination in the Buchwald-Hartwig reaction typically occurs in a square planar palladium(II) system from a four-coordinate complex directly or dissociation of one ligand to generate a three-coordinate intermediate may be required.^{2,28} In contrast to oxidative addition, formally the opposite transformation, reductive elimination is more favourable in electron-poor complexes since a more electron-poor palladium has a greater propensity to accept electrons. Sterically hindered complexes encourage dissociation of the product since bulky ligands occupy more space around the metal centre. The pseudobidentate interaction of the phosphane-ligated palladium centre with the π -electrons of the non-phosphane bearing arene enforces the coupling partners into a *cis* geometry, necessary for reductive elimination of the product to occur, which consequently enhances the rate of reductive elimination (refer to 1.3.1, Figure 8).²⁷

1.4 Preformed palladium catalysts

For over a decade, there has been an emphasis on the development of robust preformed palladium catalysts towards simplified catalyst activation, improved activity and selectivity, reduced metal loading, in addition to reduced ligand-to-metal ratios in cross-coupling reactions.²⁹

From an empirical standpoint, precatalysts circumvent the employment of air-sensitive ligands such as the often pyrophoric phosphanes (*e.g.* DTBNpP)³⁰ which have the potential to form catalyst complexes with high activity in palladium-catalyzed cross-coupling reactions. Also, the formation of the active catalyst has traditionally been associated with challenges such as inefficient *in situ* formation of the active complex, requiring elevated temperatures and excess ligand, or accessibility of multiple unique catalytic species in a single reaction giving rise to reproducibility issues. These commonly encountered complications associated with the formation of the active palladium(0) catalyst has inspired the research of many scientists including Buchwald, in the development of precatalysts comprised of the palladium and the ligand, to allow efficient catalyst activation under mild conditions.

1.4.1 Monoligated Pd-L catalysts

It is notable that progress in the area of coupling the more economically attractive substrates aryl chlorides has been made possible by the use of monoligated Pd-L catalyst based on electron-rich ligands including dialkylaryl phosphanes²¹ and *N*-heterocyclic carbenes (NHCs).³¹ Foundational research was conducted by Fu^{20,32} and Koie³³ in the employment of highly active, sterically hindered, electron-rich trialkylphosphanes for the activation of more challenging substrates in cross-coupling reactions such as aryl chlorides. The shortcomings of these trialkylphosphanes ligands are that they are air-sensitive and often pyrophoric which precludes their use for scaled up procedures and industrial processes. These problems associated

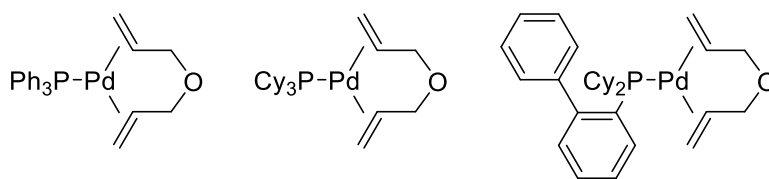
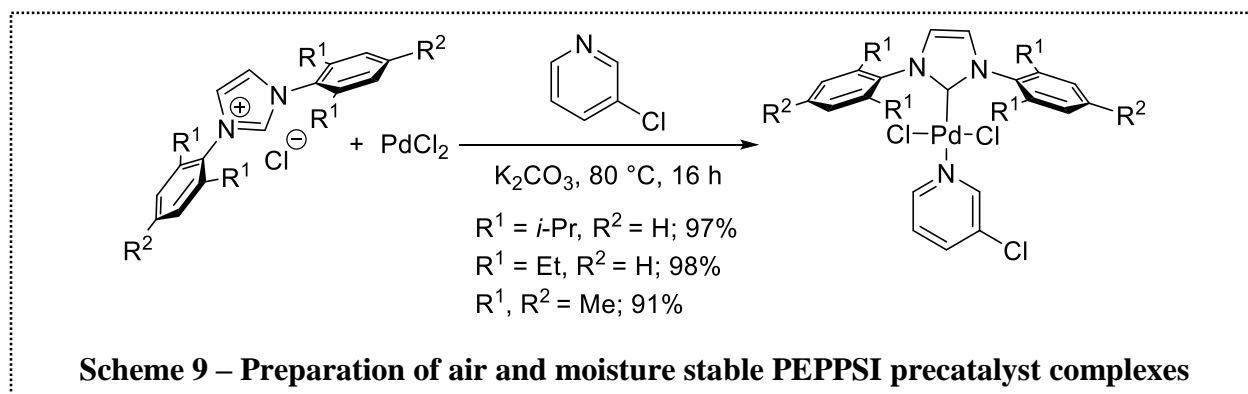


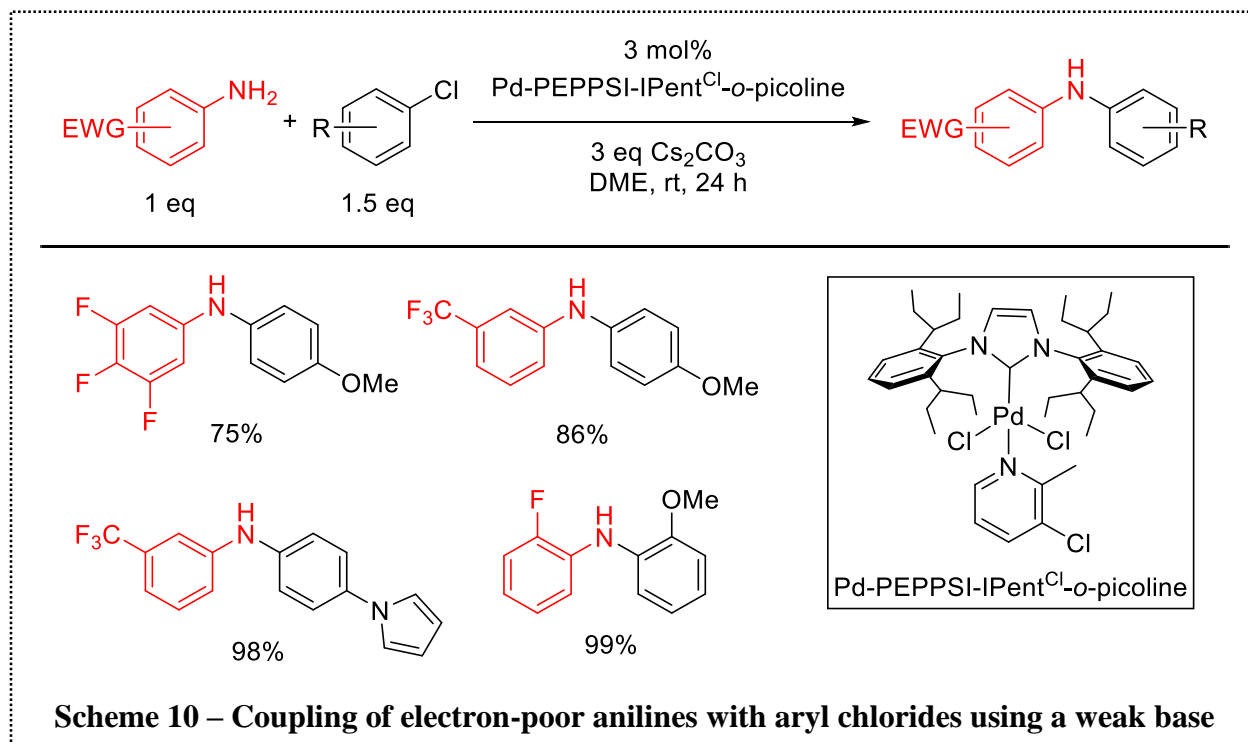
Figure 9 – 1,6-Diene Pd(0) monophosphane complexes

trialkylphosphanes served as a major driving force for the development of a precatalyst with the Pd-PR₃ bond already installed. The first monophosphane palladium(0) complexes, presented in Figure 9, were presented by Beller in 2000, incorporating the electron-rich, air-sensitive ligands triphenylphosphane, tricyclohexylphosphane and *ortho*-biphenyldicyclohexylphosphane, previously developed by Buchwald.³⁴ Authors demonstrated their superiority in the Suzuki-Miyaura coupling of aryl chlorides compared to *in situ*-formed catalysts Pd₂(dba)₃/PCy₃ or Pd(OAc)₂/PCy₃, and the tunability of these precatalysts.

While NHCs can be isolated and stored, they are still sensitive and require handling under inert conditions. Due to their electron-donating capacity and ability to incorporate bulky substituents, they have been used as ligands in (NHC)Pd(II) dimeric precatalysts toward (NHC)Pd(0).³⁵ In addition, the Pd-carbene bond can tolerate harsher heating conditions and this attribute might overcome Pd-L bond lability which is usually compensated for by using an excess of the ligand. Several monoligated Pd-NHC precatalysts have also been demonstrated to have high activity in palladium-catalyzed cross-coupling reactions. An enormous breakthrough in this area was made by Organ and co-workers with the preparation of a PEPPSI-pyridine-stabilized NHC precatalyst which unlike former examples was accessed using air-stable starting materials which were inexpensive.³⁶ The NHC-PdCl₂-3-chloropyridine complexes were readily prepared from solutions of the imidazolium salts, PdCl₂ and potassium carbonate in neat 3-chloropyridine, as



outlined in Scheme 9. Since this report, the versatility of PEPPSI-type precatalysts in cross-coupling reactions has been demonstrated in several examples.^{36–38} Further development in this area led to the observation that structural modifications to the backbone of the NHC core



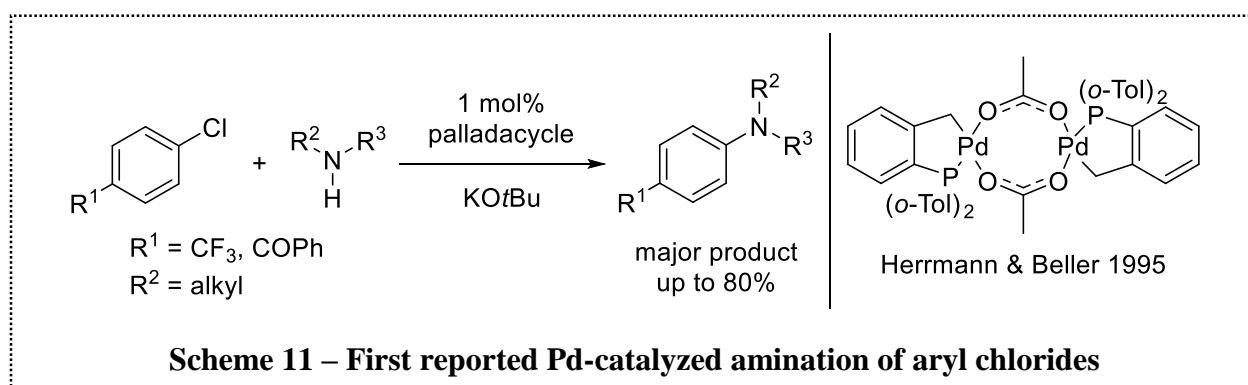
significantly affects reactivity and selectivity. Later, Organ reported design of a Pd-PEPPSI-IPent^{Cl}-*o*-picoline complex which efficiently catalyzed the coupling of challenging coupling partners, specifically, weakly nucleophilic (*i.e.* electron-poor) anilines and deactivated (*i.e.* electron-rich or sterically hindered) aryl chlorides using carbonate bases at room temperature (Scheme 10).³⁷

1.4.2 Palladacycle precatalysts

Precatalysts comprised of tertiary phosphane ligands and the palladium moiety can either give way to the L₂Pd(0) or LPd(0) active catalyst species. Although moderately air-sensitive, the L₂Pd(0) catalyst can be synthesized and isolated, or generated *in situ* from L₂Pd(II)X₂ precursors. L₂Pd(0) complexes typically have the shortcoming of air and moisture sensitivity while L₂Pd(II)X₂

precatalysts are relatively air, moisture, and thermally stable. Conversely, LPd(0) catalysts have not been isolated thus far and instead are generated from various palladium precursors including palladacycles. Palladacycles were the first class of precursors to be used towards LPd(0) in cross-couplings. They offer several advantages to catalysts formed *in situ* from a palladium precursor and free ligand including stability in open air and lower palladium to ligand ratios are required, which reduces cost, and allows shorter reaction times to be achieved while maintaining yields.³⁹

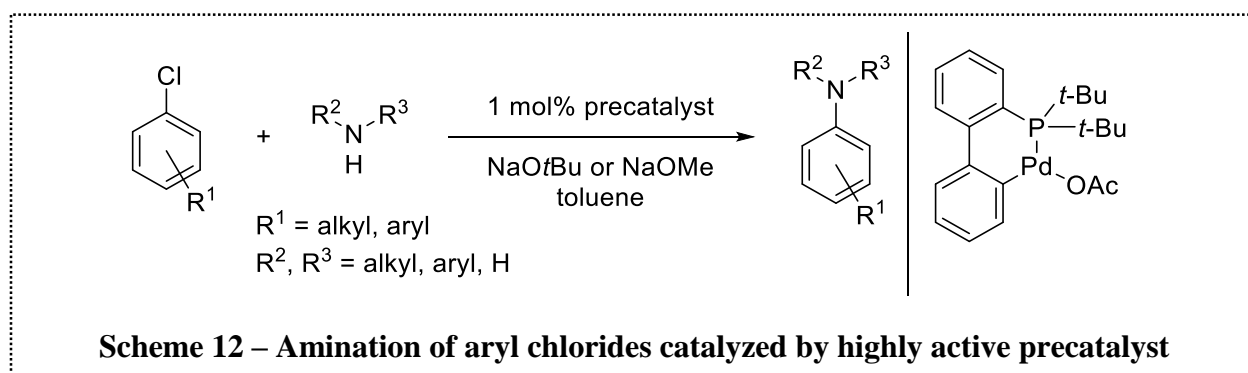
In 1995, Herrmann and Beller reported the synthesis of a thermally stable palladacyclic dimer catalyst from the reaction of P(*o*-tolyl)₃ with Pd(OAc)₂,⁴⁰ and demonstrated its utility in the Heck reaction and later the Suzuki coupling reaction.⁴¹ Following the demonstrated utility of the precatalyst in different coupling reactions, Hartwig and Louie employed it in the amination of aryl bromides, marking the first application of a palladacycle precatalyst in the Buchwald-Hartwig reaction.⁴² Authors provided mechanistic insight to support that the palladacycle precatalyst provides a precursor to the active catalyst, P(*o*-tolyl)₃-Pd(0).⁴² The first palladium-catalyzed amination of aryl chlorides with amines, displayed in Scheme 11, was reported in 1997 by Beller and co-workers using the previously developed cyclopalladated tri-*ortho*-tolylphosphane,



demonstrating its utility and wide applicability.⁴³ Following these reports, expectations were high for this class of precatalysts with its demonstrated ability to activate more economically attractive substrates, such as aryl chlorides rather than the traditionally used aryl iodides or triflates.

1.4.3 Buchwald precatalysts

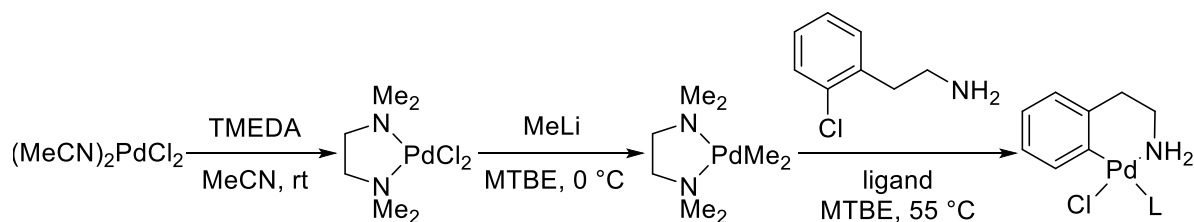
There have been many examples reported by Buchwald's group where these precatalyst systems have been shown to promote otherwise difficult cross-coupling reactions or transformations involving reactive functional groups requiring lower reaction temperatures. In 2003, Buchwald reported the preparation of an air, moisture, and thermally stable palladacyclic precatalyst based on their previously developed biaryl phosphanes, and demonstrated its utility and versatility for the amination of aryl chlorides (Scheme 12).⁴⁴ This precatalyst offered a



convenient single-component system which precludes the use of a glovebox for the coupling reaction. The isolation of this palladacycle set the foundation for the development of the next generations of stable monoligated precatalysts.

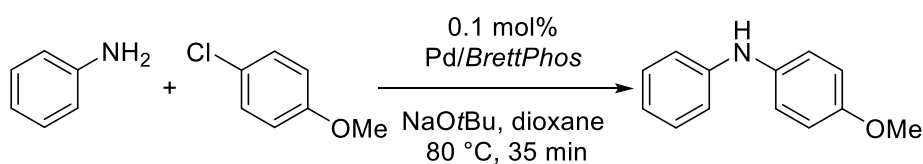
1.4.4 First generation Buchwald precatalyst

In 2008, Buchwald introduced a new class of palladacyclic precatalysts (now referred to as Buchwald's first generation precatalyst) based on an intramolecularly coordinated phenethylamine complex.⁴⁵ Preparation of the precatalyst complex, outlined in Scheme 13, proceeds by ligand exchange of (MeCN)₂PdCl₂ with TMEDA followed by the reaction of the generated (tmeda)PdCl₂ complex with MeLi at 0 °C to afford the thermally sensitive, (tmeda)PdMe₂. Treatment of



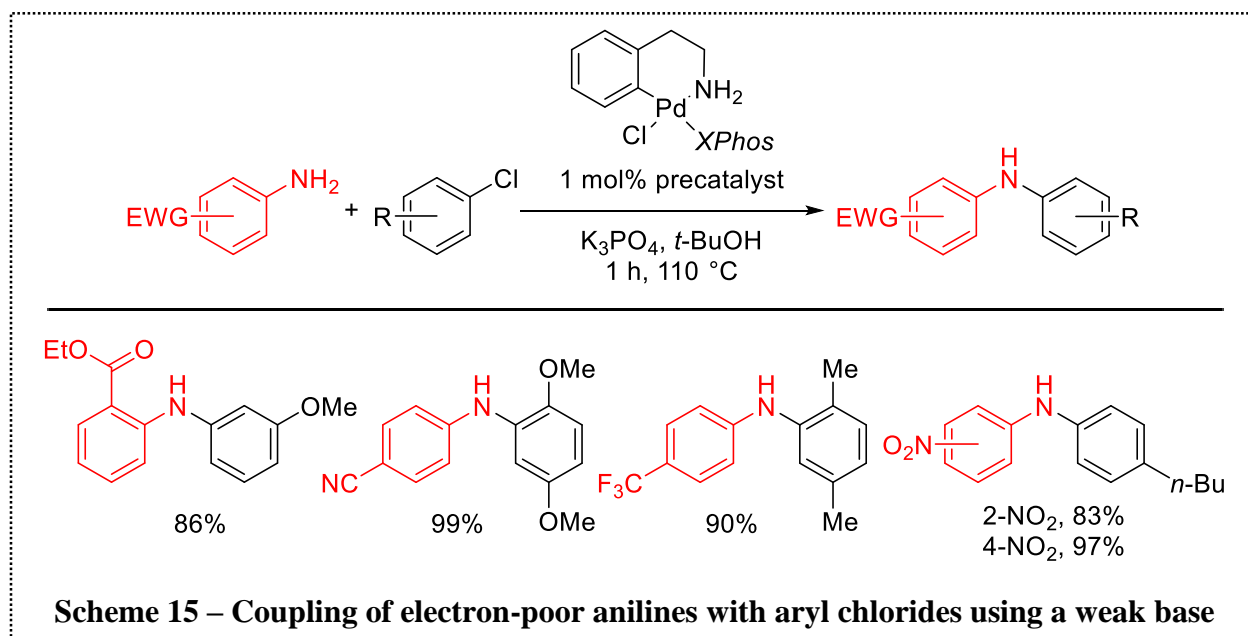
Scheme 13 – Synthesis of palladacyclic phenethylamine-based precatalyst

(*tmeda*)PdMe₂ with 2-chlorophenethylamine in the presence of the desired phosphane generates the corresponding precatalyst complex. This palladacycle is compatible with a variety of phosphane ligands including *XPhos*, *SPhos*, *RuPhos*, and *BrettPhos* (refer to 1.3.1, Figure 7). The performance of the palladacycle in the cross-coupling of 4-chloroanisole and aniline in the presence of 0.1 mol% Pd, employing *BrettPhos* as the supporting ligand, was compared to that of traditionally used palladium sources. The precatalyst provided a highly active system, reaching complete conversion after 35 min. Following the appropriate activation mode for the other catalysts, complexes formed using Pd(OAc)₂/PhB(OH)₂, [Pd(allyl)Cl]₂, and Pd₂dba₃, each combined with *BrettPhos*, led to a maximum conversion of *ca.* 25%, as highlighted in Scheme 14. The authors also demonstrated the utility of the phenethylamine-based palladacycle in the arylation



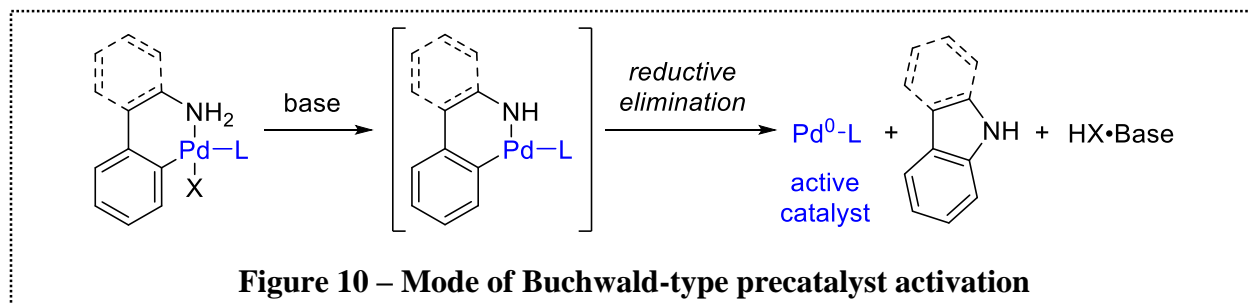
Pd source	Conversion
Palladacycle	>99%
Pd ₂ (dba) ₃	25%
Pd(OAc) ₂	<10%
[(allyl)PdCl] ₂	<10%

Scheme 14 – Comparison of traditional Pd sources and precatalyst in *N*-arylation



of aryl chlorides with electron-poor anilines, which are typically challenging coupling partners (Scheme 15).

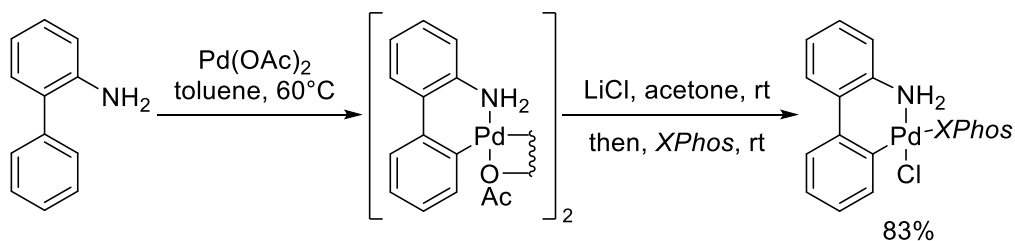
The great success of the precatalyst is in part due to the efficient catalyst activation achieved *via* intramolecular reductive elimination under mild basic reaction conditions. As shown in Figure 10, precatalyst activation requires deprotonation of the ligated amine followed by reductive elimination of the palladium-amido intermediate species to generate the active monoligated palladium-catalyst. In the case of the first generation precatalyst, indoline is generated as a byproduct and can be easily removed during the workup procedure. This precatalyst activation obviates the need for any exogenous reducing agent. Following the formation of the active catalyst species, Pd-L, can undergo oxidative addition of aryl chlorides at temperatures as low as $-40\text{ }^{\circ}\text{C}$.⁴⁵



Despite the efficient activation that can be achieved with this precatalyst, there are various shortcomings, such as the difficulties associated with its synthesis. There are three reaction steps which involve the handling of unstable organometallic reaction intermediates, as demonstrated in Scheme 13 above. In addition, activation in the presence of weak bases such as carbonates, is slow and requires elevated temperatures to proceed. In 2011, Vicente and Saura-Llamas presented an alternative procedure for the cyclopalladation of primary amines and secondary amines towards first generation Buchwald-type precatalysts that offered several advantages over the procedure previously reported.⁴⁶ This protocol proceeds by a C-H activation sequence involving phenethylammonium triflate and Pd(OAc)₂. The use of the superacid, triflic acid, was required to access the triflate salt and an additional ligand exchange step was required. Efforts to overcome these and previous limitations associated with the first generation precatalyst led to the investigation of a new class wherein the aromatic amine, 2-aminobiphenyl, is used in place of phenethylamine.

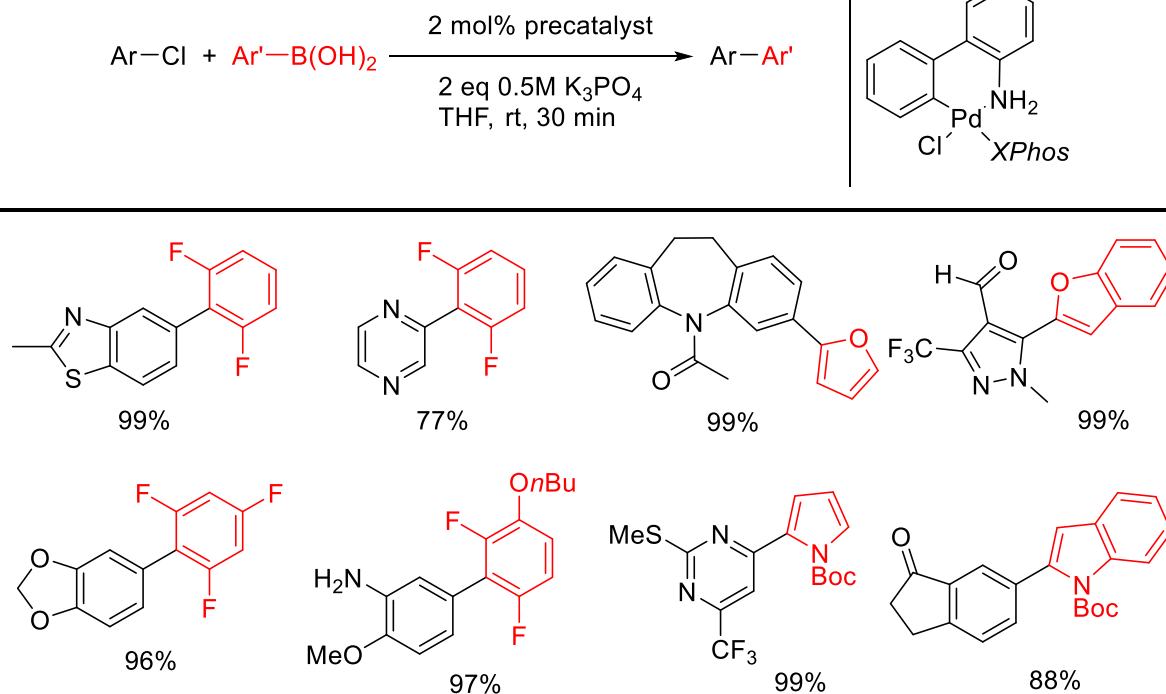
1.4.5 Second generation Buchwald precatalyst

Traditionally, the cyclopalladation of primary amines is difficult to achieve in high yields but Albert *et al.* discovered an efficient one-pot protocol to achieve this transformation towards triphenylphosphane- and pyridine-ligated palladacycles of 2-aminobiphenyl.⁴⁷ Adapting this methodology, the second generation Buchwald precatalyst was accessed *via* C-H activation of 2-aminobiphenyl using Pd(OAc)₂ followed by an ion exchange and the reaction of the generated binuclear cyclopalladated complex with a phosphane ligand, as depicted in Scheme 16.⁴⁸ The chlorido bridging units are installed by a metathesis reaction of the initial acetato-bridged complex with LiCl. The acidity of the palladium-amido species of this aromatic analog is enhanced compared to the previous aliphatic amine-based complex and consequently the activation can be



Scheme 16 – Synthesis of palladacyclic 2-aminobiphenyl-based precatalyst

achieved using weak bases at room temperature. In the case of the 2-aminobiphenyl-based precatalysts, carbazole is generated as a byproduct and can be easily removed during the purification process. The utility of these precatalysts in Suzuki-Miyaura reaction of polyfluorophenyl and 2-heteroaryl boronic acids, which are prone to rapid protodeboronation under basic conditions, was demonstrated.⁴⁸ Selected examples of the coupling of these challenging boronic acid coupling partners are presented in Scheme 17.

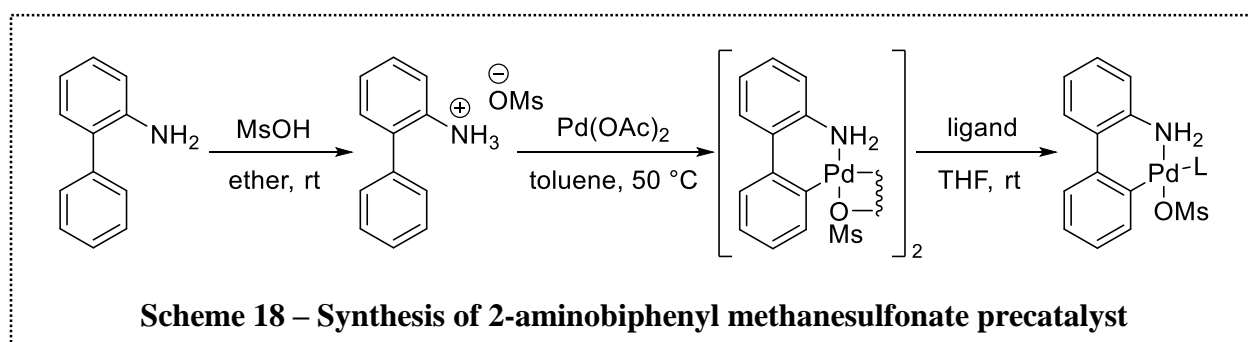


Scheme 17 – Suzuki-Miyaura coupling of unstable boronic acids using precatalyst

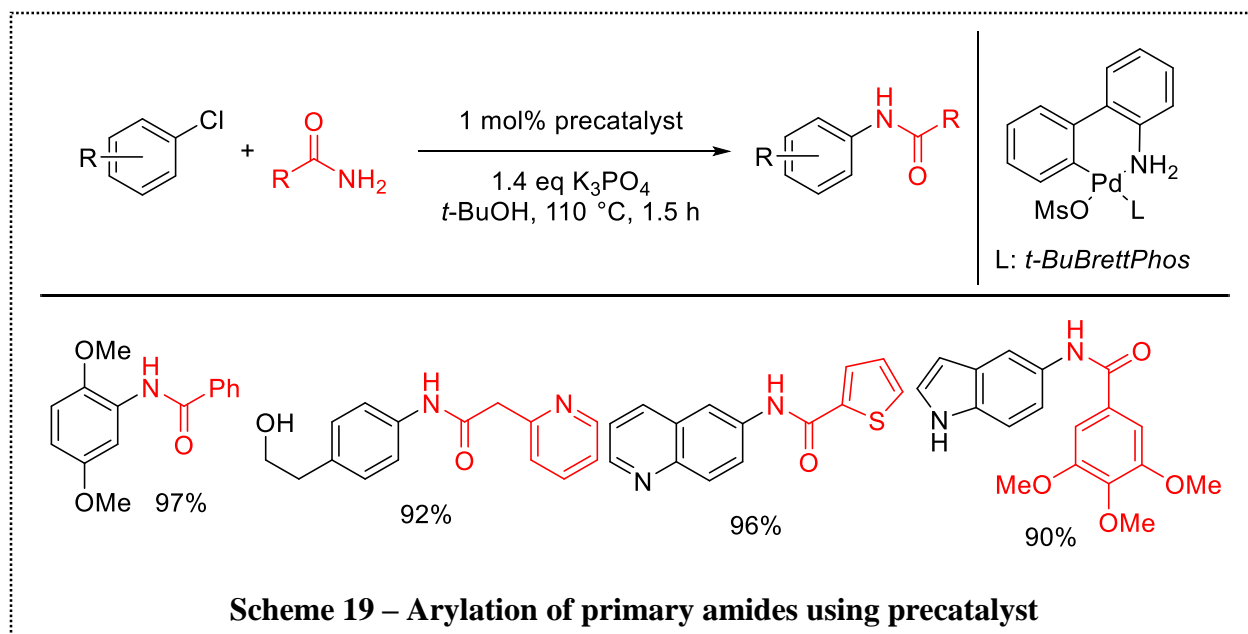
1.4.6 Third generation Buchwald precatalyst

Improving upon the second generation precatalyst the aim was focused on modifying the palladium complex in a way that would allow accommodation of bulkier phosphane ligands which could not previously be used in these systems. The third generation precatalyst, presented in Scheme 18 below, was developed in 2013 by Buchwald and Tudge.⁴⁹ The new design is based on the use of methanesulfonate, a weaker donor ligand, since the inability of chloride to dissociate from the precatalyst complex contributes to the difficulties encountered when attempting to include bulkier phosphane ligands. The negative charge on methanesulfonate is strongly delocalized through resonance, contributing to the non-coordinating nature of the anion which provides bulky phosphane ligands access to the palladium centre. As a result, the mesylate anion can also provide a counterion to a palladium complex with enhanced electrophilicity, contrary to the chloride anion which has a localized negative charge and is therefore a stronger ligand.

The synthesis of the third generation precatalyst involves the formation of the 2-biphenylammonium mesylate salt from 2-aminobiphenyl and MsOH, followed by cyclopalladation using Pd(OAc)₂, then coordination of the phosphane, as presented in Scheme 18.



Preliminary computational studies using DFT revealed that the replacing the chloride as in the second generation precatalyst with a mesylate anion rendered the palladium(II) centre more electropositive although other structural features are quite similar.⁴⁹ High reactivity of these



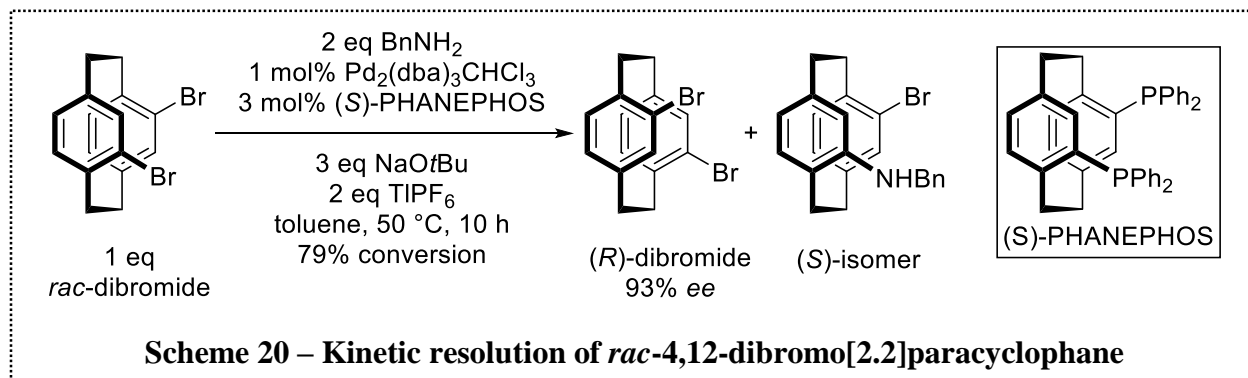
precatalysts in various C-C, C-N and C-O bond forming reactions has been demonstrated.^{49,50} As demonstrated in Scheme 19, high yields and good functional group tolerance were achieved in the coupling of functionalized aryl chlorides and primary amides.

1.5 Palladium-catalyzed enantioselective C-N cross-coupling

Over the past 15 years, a number of enantioselective *N*-arylation examples have been reported comprising of various methods including kinetic resolution, desymmetrizations and other symmetry breaking strategies that result in the formation of a chiral centre, axis or plane.^{51–62} The substrate scope of the asymmetric Buchwald-Hartwig procedure has expanded to include other C(sp²)-heteroatom bond forming reactions including C-O examples^{63,64} and C-P examples.^{65–70} Research towards developing a practical methodology for enantioselective carbon-heteroatom coupling is still underway as most reports feature systems that provide modest enantioselectivities.

1.5.1 Kinetic resolution

The first enantioselective Buchwald-Hartwig reaction describing the kinetic resolution of 4,12-dibromo[2.2]paracyclophane was reported by Rossen and Pye in 1997 (Scheme 20).⁵¹ The

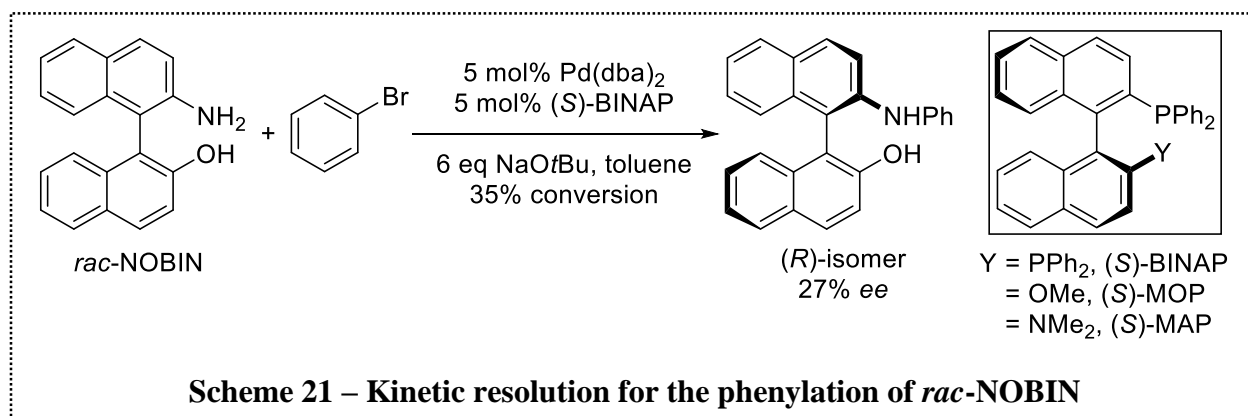


performance of (*S*)-PHANEPHOS/ $\text{Pd}_2(\text{dba})_3$ was superior to that of (*R*)-BINAP/ $\text{Pd}_2(\text{dba})_3$ in terms of activity and enantiodiscrimination observed as demonstrated through the calculated enantiomeric discrimination factor*. Practical kinetic resolution of the (*S*)-dibromide was achieved with a 3 to 4 times faster reaction rate than the (*R*)-enantiomer at 50 °C. Employing a halide anion scavenger, TIPF_6 , led to a significant decrease in the reaction rate; however the kinetic resolution was greatly improved with the (*S*)-dibromide at 50 °C, with an enantiomeric discriminating factor of 10 to 13. When the reaction was driven to a fairly high conversion of 79%, the unreacted (*R*)-dibromide had 93% *ee* (42% resolution yield). On the other hand, the (*R*)-BINAP/ $\text{Pd}_2(\text{dba})_3$ catalyst system performed poorly in respect to selectivity and led to only a two-fold difference between the enantiomers.

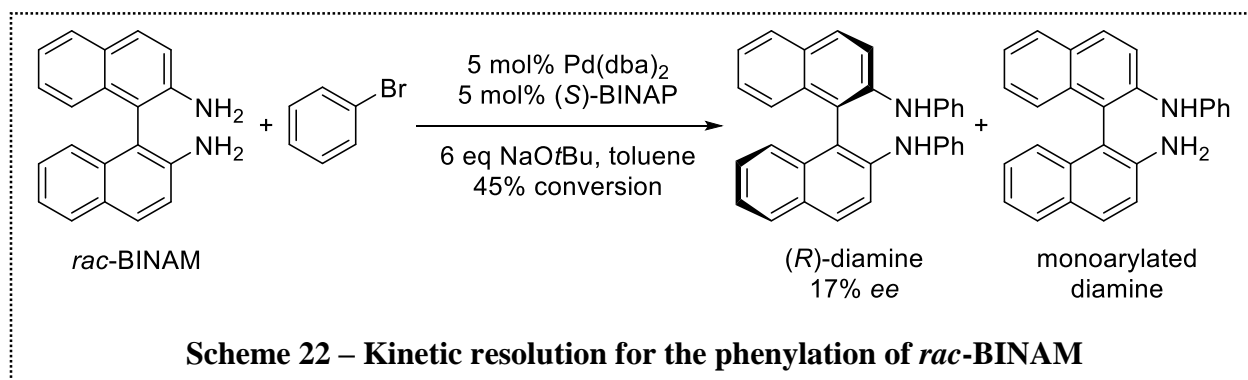
The following year, Vyskočil and Kočovský reported the partial kinetic resolution of axial chiral amines through *N*-arylation in the presence of (*S*)-BINAP.⁵² This was observed while investigating the efficacy of the bidentate MAP ligand in the model reaction of NOBIN and the

* The enantiomeric discrimination or selectivity factor (*s*) is a measure of the relative rate of the faster reacting enantiomer to the slower one in a kinetic resolution, and is calculated from the conversion (*C*) and the *ee* of remaining starting material as determined by $s = \ln[(1-C)(1-ee)]/\ln[(1-C)(1+ee)]$.^{101,102} For a nonselective reaction *s* = 1.

corresponding diamine, 1,1'-binaphthyl-2,2'-diamine or BINAM, with bromobenzene compared to that of bidentate ligands BINAP and MOP which have been successfully employed in various Pd-catalyzed transformations. In the cross-coupling reaction with the amino alcohol shown in Scheme

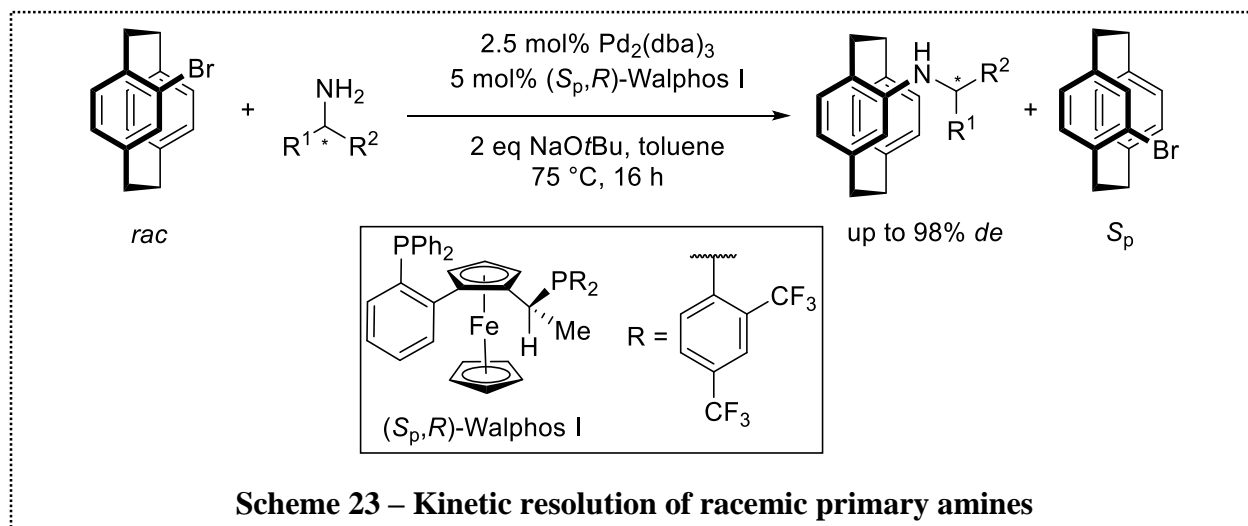


21, a preference for the (*R*)-enantiomer was observed in the coupled product with up to 27% *ee* using (*S*)-BINAP at 35% conversion. Coupling of the analogous diamine showed a preference for the (*R*)-bisarylated product with up to 17% *ee* achieved at 45% conversion using (*S*)-BINAP (Scheme 22). No enantioselectivity was reported for the monoarylated diamine product. A marked increase in the reaction rate was observed when using (*R*)-MAP compared to the results obtained



for (*S*)-BINAP or (*R*)-MOP; however, kinetic resolution was not observed in the reactions where (*R*)-MOP was employed and negligible in the case of (*R*)-MAP. While the observed enantiomeric excess was low in either case, this example served as a proof of principle of the possibility of kinetic resolution of chiral amines *via* Buchwald-Hartwig reaction.

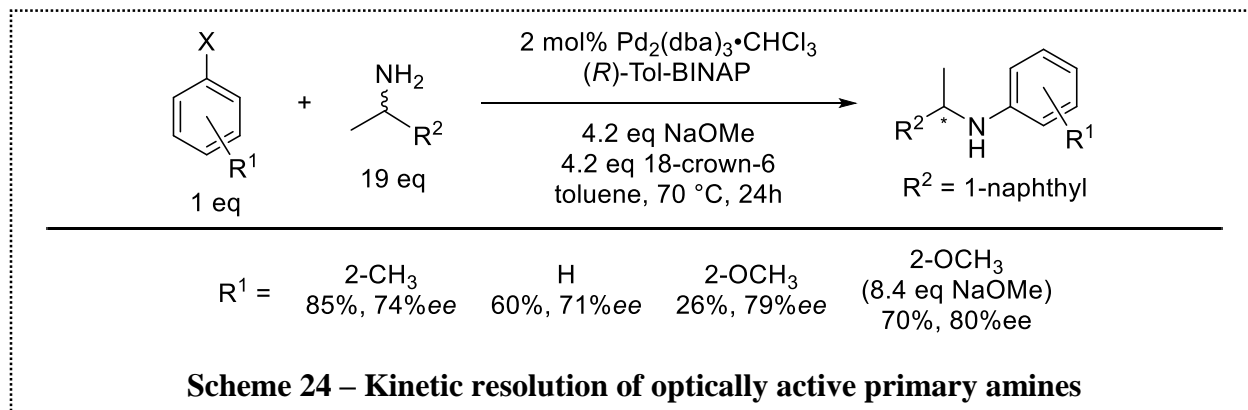
In 2005, Bräse and co-workers reported the first diastereoselective Buchwald-Hartwig reaction where chiral amines were arylated with racemic 4-bromo-[2.2]paracyclophane under kinetic resolution, as presented in Scheme 23 below.⁵³ This procedure provided rapid easy access



to enantiopure 4-bromo-[2.2]paracyclophane in a single reaction step, an improvement from the former four-step procedure.⁷¹ The highest diastereoselectivity was achieved in the reaction of the bulky chiral (1*S*,2*S*)-2-(benzyloxy)cyclohexylamine with the bromide using BINAP/ $\text{Pd}_2(\text{dba})_3$ giving 70% yield and 98% *de*. In the reaction of 4-bromo-[2.2]paracyclophane with 0.5 equivalents of (*S*)-1-phenylethylamine, the best catalyst system was (*S_p*,*R*)-Walphos 1/ $\text{Pd}_2(\text{dba})_3$ providing the coupled product in 92% yield and 86% *de*. The authors also successfully coupled (4-[2.2]paracyclophane)triflate with (*S*)-1-phenylethylamine and achieved 91% *de*. Several amines with varying electronic and steric properties were tolerated in the reaction. Also noteworthy, this protocol facilitated the coupling of an electron-rich aryl halide which can be challenging in the Buchwald-Hartwig reaction. In general, high enantioselectivities were accessed when the stereochemical configuration of the ligand compared to the amine were appropriately paired. For each of the screened chiral amines, the excess diastereomer was independent of the BINAP

enantiomer employed, indicating that substrate control of stereoselectivity was superior to catalyst control.

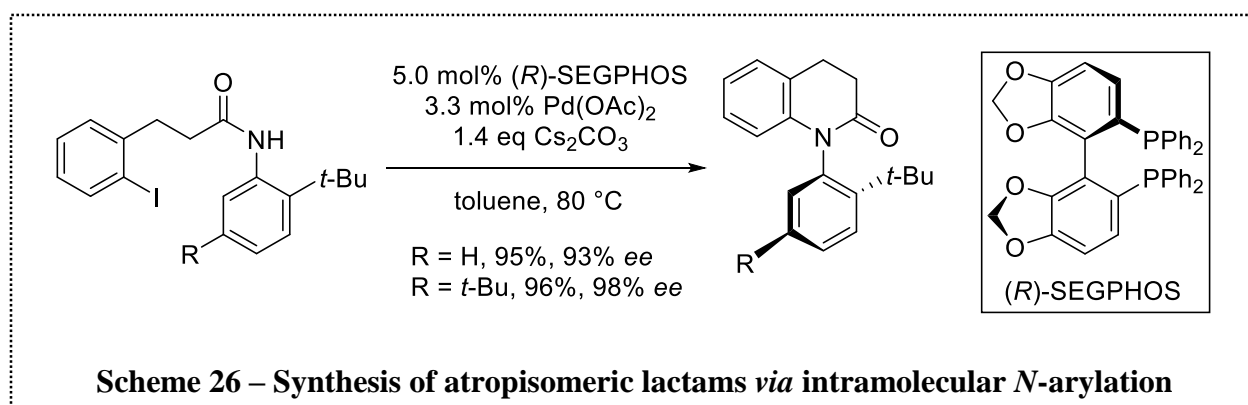
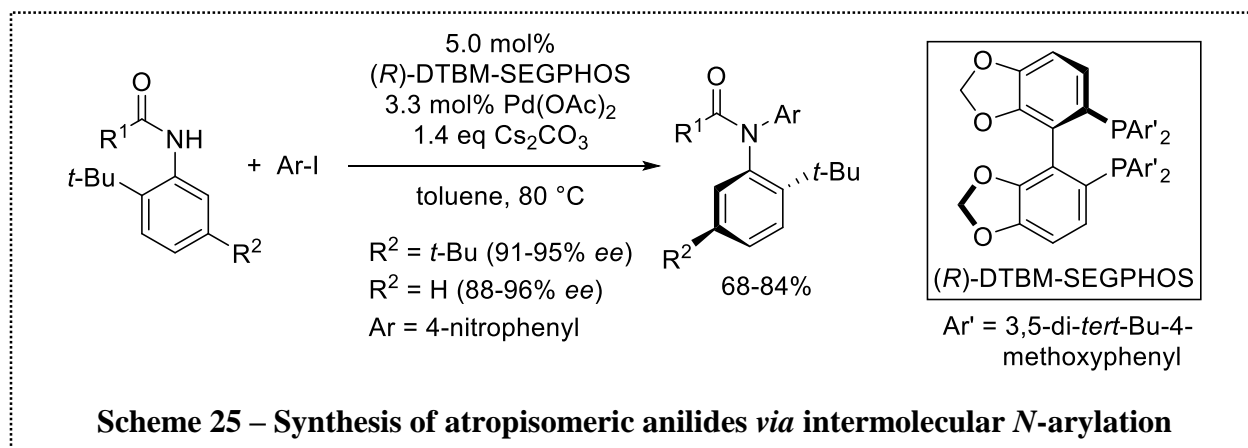
In a related study also reported in 2005, the kinetic resolution of racemic primary amines *via* selective *N*-arylation using a palladium-complex with a chiral ligand, as shown in Scheme 24, was described.⁵⁴ Enantioenriched aniline derivatives were afforded in good yields and low to



moderate enantiopurity. The reaction of 2-iodoanisole with 19 equivalents of racemic 1-(1-naphthyl)ethylamine in the presence of sodium methoxide and 18-crown-6 by (*R*)-Tol-BINAP/ $\text{Pd}_2(\text{dba})_3 \cdot \text{CHCl}_3$ gave the best result with 70% yield with 80% *ee* achieved.

1.5.2 Formation of N-C chiral axis

Traditionally, optically active atropisomeric compounds have been prepared predominantly *via* optical resolution of the racemate by chiral column chromatography or using chiral resolving agents.⁷² In the past 10 years, Kitagawa and co-workers have done extensive work towards the development of protocols for the preparation of N-C axially chiral compounds *via* variations of the enantioselective Buchwald-Hartwig reaction. The first practical methodology towards atropisomeric anilides was described in 2005 where the generation of an N-C chiral axis

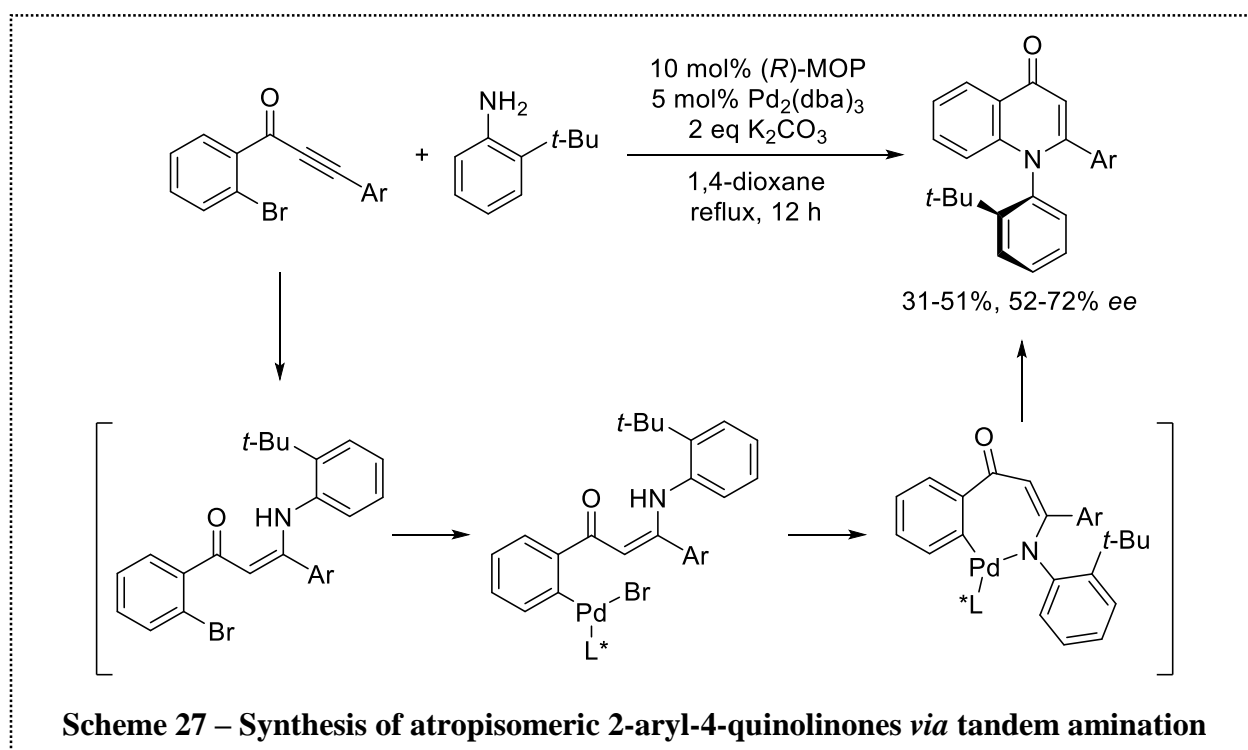


was achieved through inter- and intramolecular *N*-arylation of *ortho-tert*-butylanilides in the presence of Pd(OAc)₂ and a chiral ligand (Scheme 25 and Scheme 26).^{55–58}

This report marked the first enantioselective catalytic *N*-arylation using achiral substrates. In the intermolecular examples (*R*)-DTBM-SEGPHOS gave the best results in the reactions of 4-iodonitrobenzene with a variety of *ortho-tert*-butylanilide derivatives. Counterintuitively, the intermolecular reactions proceeded at a faster rate than the intramolecular lactamizations where (*R*)-SEGPHOS was demonstrated to be the most efficient ligand for cyclization. Di-*tert*-butylanilides gave increased enantioselectivity in both the inter- and intramolecular reactions compared to the analogous mono-*tert*-butylanilides. High selectivities were attributed to the preference towards the *E*-rotamer for *ortho-tert*-butylanilide derivatives regardless of the electronic properties (rotamers of *ortho-tert*-butylanilide with varied electronic properties due to

varied substituents at the *para*-position of the phenyl ring showed this preference also).⁵⁶ In a follow up report, Kitagawa demonstrated the application of these atropisomeric anilide derivatives to asymmetric enolate chemistry.⁵⁶ These developments led to the synthesis of key intermediates towards norepinephrine transporter (NET) inhibitors using the atropisomeric lactams.⁵⁸

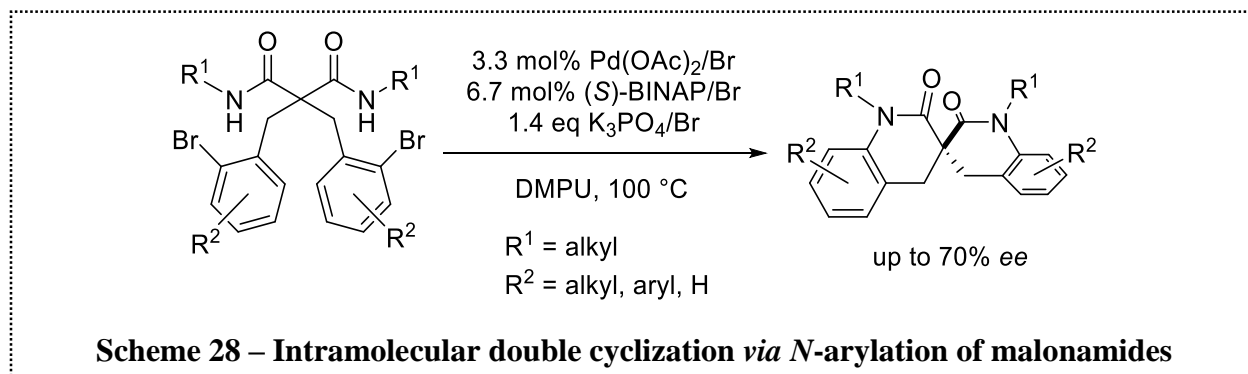
Expanding upon the reaction scope, the synthesis of new N-C axial chiral compounds 2-aryl-4-quinolinones was presented by Kitagawa in 2012.⁵⁹ In this example, the reaction proceeds by 1,4-addition of *ortho-tert*-butylaniline to a 2-bromophenyl arylethynyl ketone, isomerization of the generated enamine intermediate and finally, intramolecular aryl amination in the presence of (*R*)-MOP/ $\text{Pd}_2(\text{dba})_3$, affording the 2-aryl-4-quinolinones, as shown in Scheme 27. Low yields of



up to 51%, and low to moderate enantioselectivities, up to 72% *ee*, were achieved using the (*R*)-MOP/ $\text{Pd}_2(\text{dba})_3$ catalyst system.

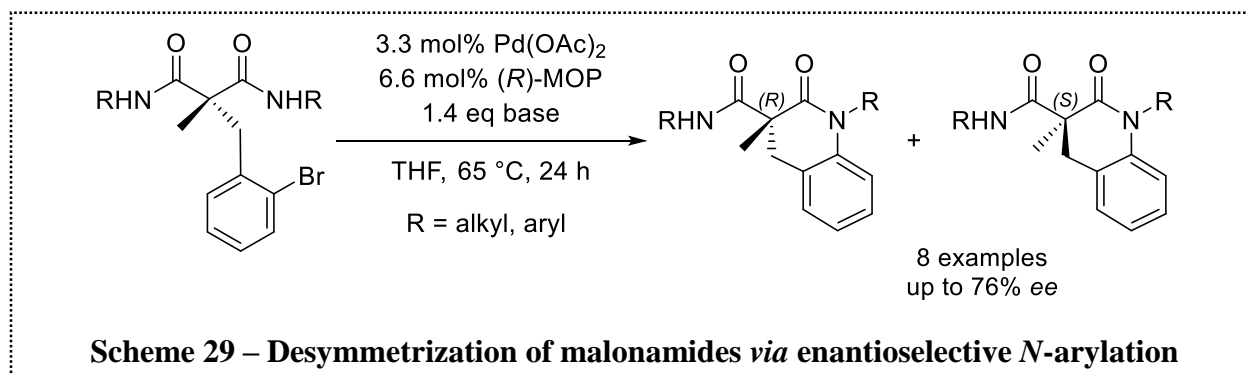
1.5.3 Desymmetrization *via* *N*-arylation

The desymmetrization methodology has been used in a variety of synthetic venues including natural product total synthesis *via* formation of a chiral axis⁷³ and in the development of molecular rotors.⁷⁴ In a report by Sasai in 2009, an enantioselective double *N*-arylation was employed to access *C*₂-symmetric spiranes from malonamides (Scheme 28).⁶⁰ Two sequential



Buchwald-Hartwig amidations take place where the first cyclization determines the enantioselectivity and the second cyclization was found not to involve a kinetic resolution process. Various nitrogen substituents were tolerated on the malonamide, giving high yields and moderate selectivities (up to 70% *ee*). The trend observed was that as the bulkiness of the *N*-substituent increases, the enantioselectivity achieved decreases. This is likely due to the absence of adequate steric bias present as the bulkiness of the *N*-substituent approaches that of the benzyl halide moiety of the malonamide. Such was the case with the benzyl *N*-substituent which led to the poor enantioselectivity with only 49% *ee* obtained.

In 2009, our group developed an enantioselective Buchwald-Hartwig reaction presented in Scheme 29, where various α -(2-bromobenzyl)malonamides were cyclized, thereby forming a stereogenic carbon centre and generating chiral quinolinone derivatives with in good yields and moderate enantioselectivities.⁶¹ The best results were obtained when a $\text{Pd}(\text{OAc})_2/(\text{R})\text{-MOP}$



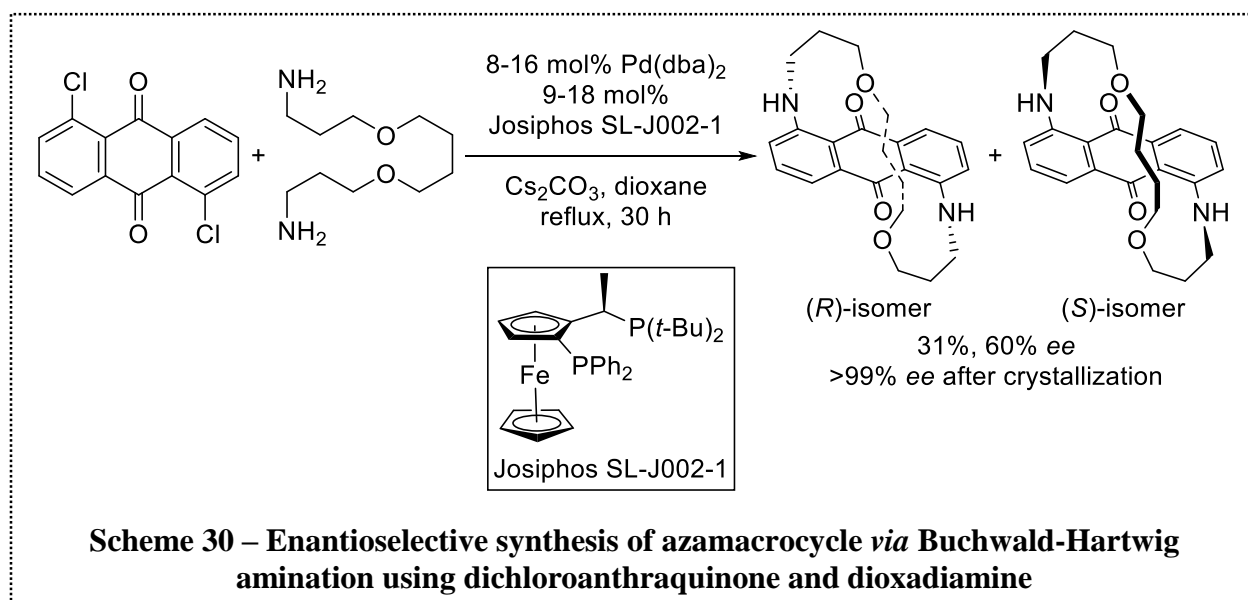
catalyst system was employed with either potassium or cesium carbonate as a base in THF with good yields and up to 76% *ee*. In our example, asymmetric induction arises from the interaction of the chiral catalyst with the substituents at the alpha carbon position, methyl versus bromobenzyl group. Presumably, the steric bias present within the malonamides influences enantioselectivity by causing the *N*-alkyl group to point away from the sterically encumbered space of amide-bound palladium complex leaving the comparatively small methyl group pointing in that direction leading to a preference for the arylation of one of the amide nitrogen atoms.

1.5.4 Formation of planar chiral macrocycles

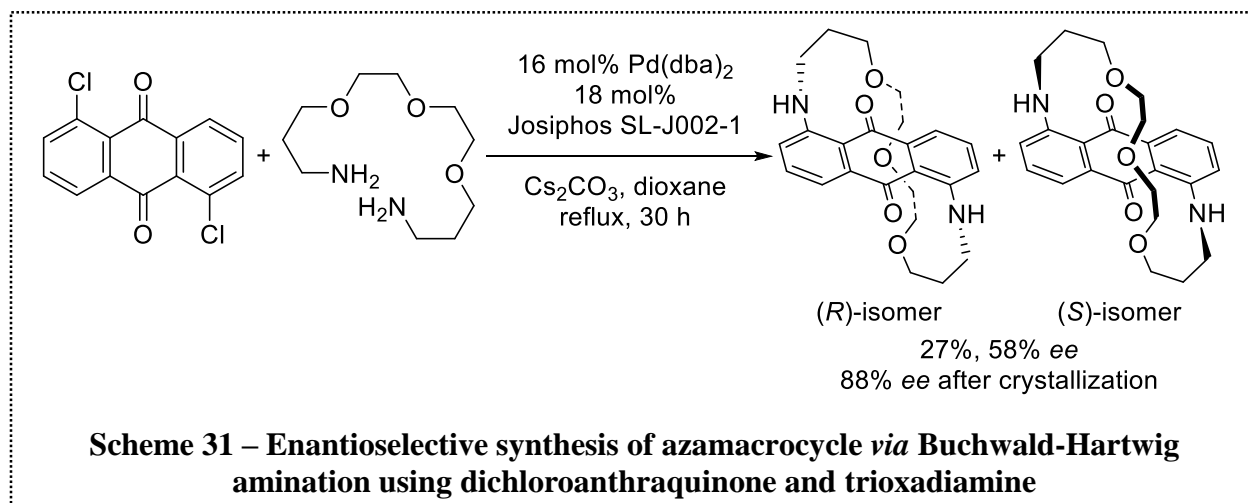
Enantioselectivity in the Buchwald-Hartwig amination *via* generation of a chiral plane has also been accomplished. In 2010, Averin and co-workers reported the amination of dihaloarenes, 1,5-dichloroanthraquinone and 1,5-dichloroanthracene, with di- and trioxadiazines in the presence of chiral bidentate ligands with $\text{Pd}(\text{dba})_2$. This was the first example of the synthesis of macrocycles with planar chirality *via* enantioselective palladium-catalyzed amination. The first amination generates a linear molecule; however, there is facial selectivity in the second amination

resulting in planar chiral products. Comparable yields were obtained using the di- and trioxadiazines with either dichloroarene.

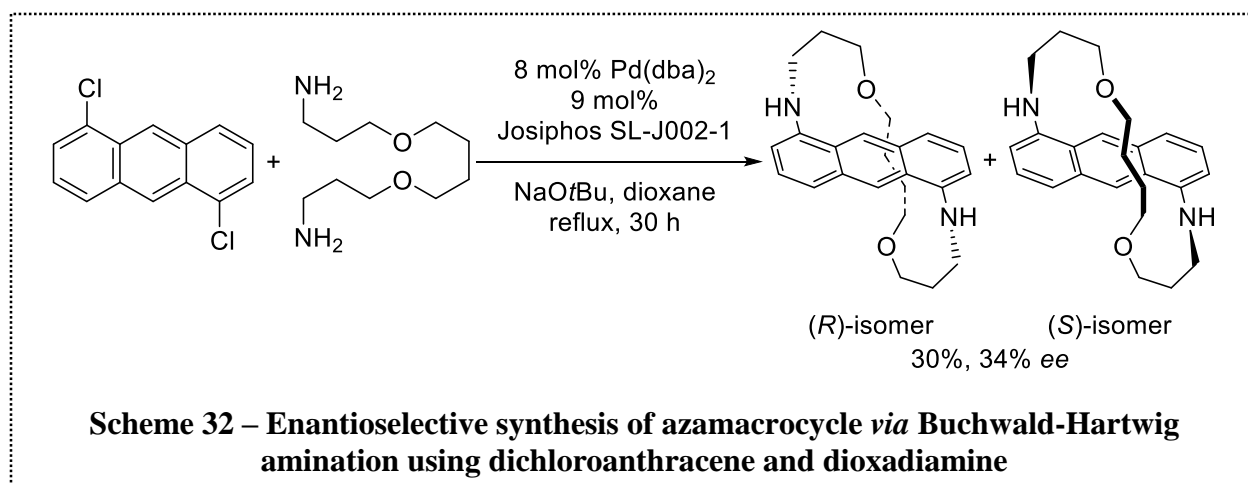
Initially $\text{Pd}(\text{dba})_2$ paired with BINAP and selected derivatives were tested in the reaction of 1,5-dichloroanthraquinone and the dioxadiazine, however, employing a phosphane ferrocene ligand, PPFA, led to improved selectivity (30% *ee* from this catalyst system compared to 2% *ee* using (*R*)-BINAP), which sparked the screening of other Josiphos-type ligands. Josiphos SL-J002-1 gave the best results, affording the azamacrocyclic in 60% *ee* and 31% yield, shown in Scheme 30. Upon recrystallization of the enantioenriched azamacrocyclic, spontaneous resolution occurred,



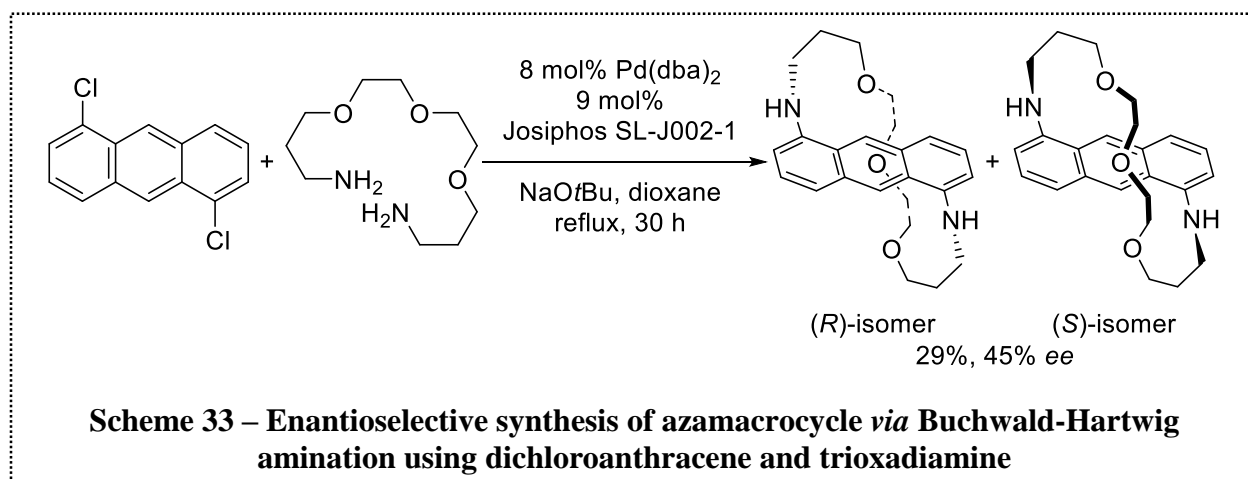
yielding 19% of the homochiral crystals with 99% *ee*. In the case of the azamacrocyclic comprised of anthraquinone and trioxadiazine moieties, (*R*)-BINAP gave 35% which was the highest yield however it was virtually inactive in asymmetric induction, as was the case in the synthesis of the analogous dioxadiazine-based azamacrocyclic. The most efficient ligand in this system was found to be Josiphos SL-J002-1 which gave the highest, albeit modest yield of 27% and selectivity of 58% *ee*, as highlighted in Scheme 31. The enantiomeric mixture was recrystallized affording the product in 88% *ee* and 11% yield.



Further investigation of the reaction scope was conducted through the reactions of 1,5-dichloroanthracene with the di- and trioxadiazines. The chiral phosphane ligands, (*R*)-BINAP, (*R,S*)-PPFA and Josiphos SL-J002-1 were tested. In the reaction with the dioxadiazine, presented in Scheme 32, Josiphos SL-J002-1 gave the best yield and *ee* value (30% and 34% *ee*). Crystals of



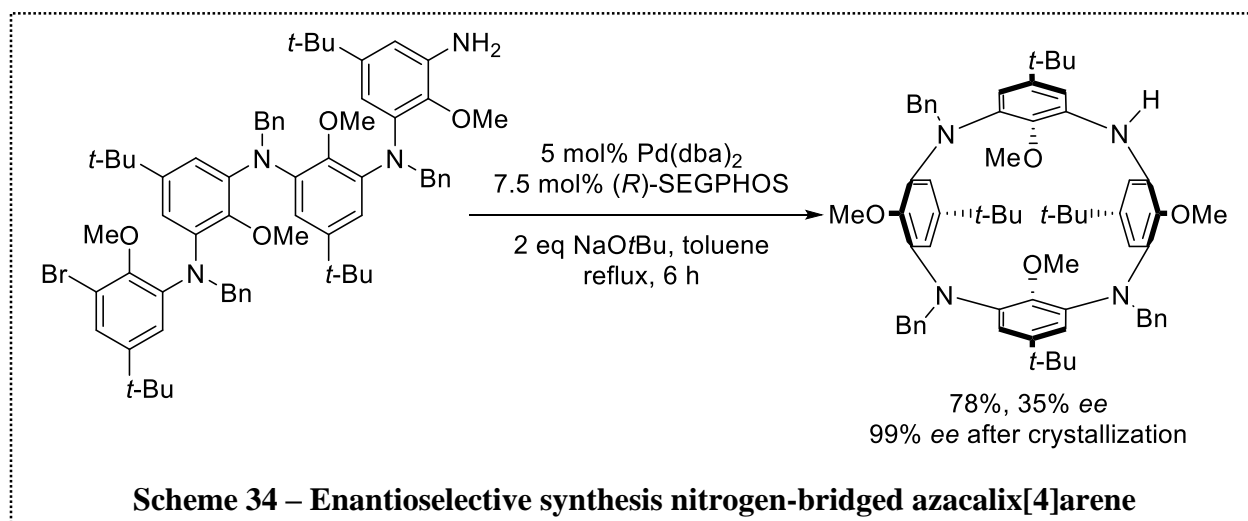
the azamacrocycle could not be obtained through recrystallization towards improving the enantiopurity. Conversely to the performance of (*R*)-BINAP in the reactions of dichloroanthraquinone, asymmetric induction was achieved in the dichloroanthracene and dioxadiazine system leading to 12% *ee* in the product. In the reaction of 1,5-dichloroanthracene with the trioxadiazine shown in Scheme 33, Josiphos SL-J002-1 was the best performing ligand



of the three tested, providing the azamacrocycles in 29% yield and 45% *ee*. Also noteworthy, (*R*)-BINAP showed improved asymmetric induction compared to the reactions of 1,5-dichloroanthraquinone generating the azamacrocycles in 27% *ee*. Efforts to increase the enantioenrichment of this anthracene-based azamacrocycles *via* recrystallization were also unsuccessful.

1.5.5 Formation inherently chiral calixarenes

The first inherently chiral nitrogen-bridged azacalix[4]arene was prepared in an intramolecular cyclization *via* Buchwald-Hartwig amination by Ishibashi and co-workers in 2009, as shown in Scheme 34.⁷⁵ Several chiral phosphane ligands were screened towards the cyclization

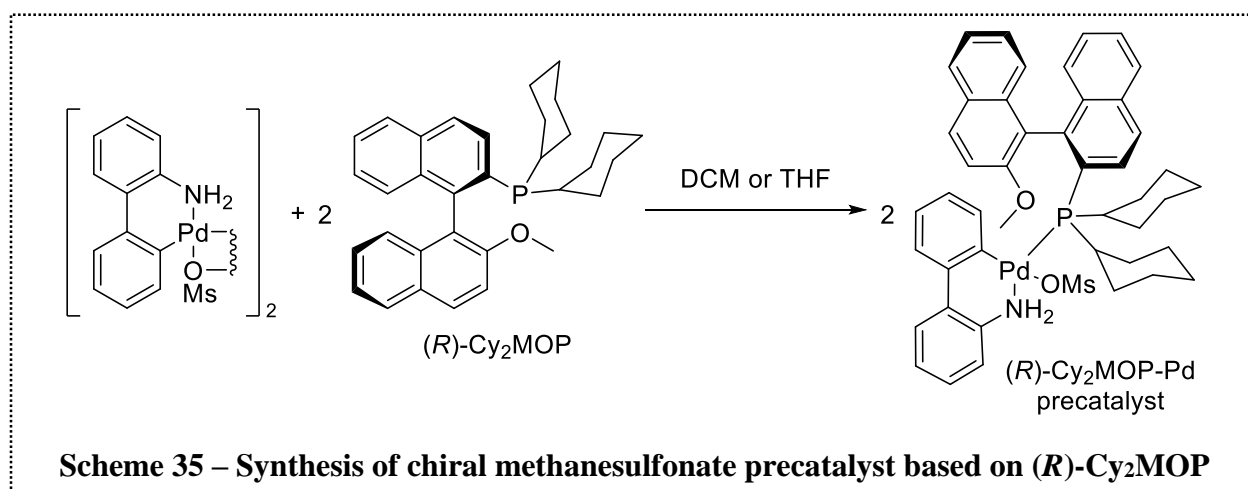


of the acyclic tetramer. (*R*)-BINAP/Pd₂(dba)₃ led to 81% of the desired product, however only 21% *ee* was obtained. (*R*)-SEGPHOS/Pd₂(dba)₃ was found to be most efficient catalyst generating the azacalix[4]arene in its 1,3-alternate conformation in 78% yield and 35% *ee*. Resolution of the enantiomeric mixture by crystallization afforded the (–)-calix[4]arene in 99% *ee*.

1.6 Research objectives

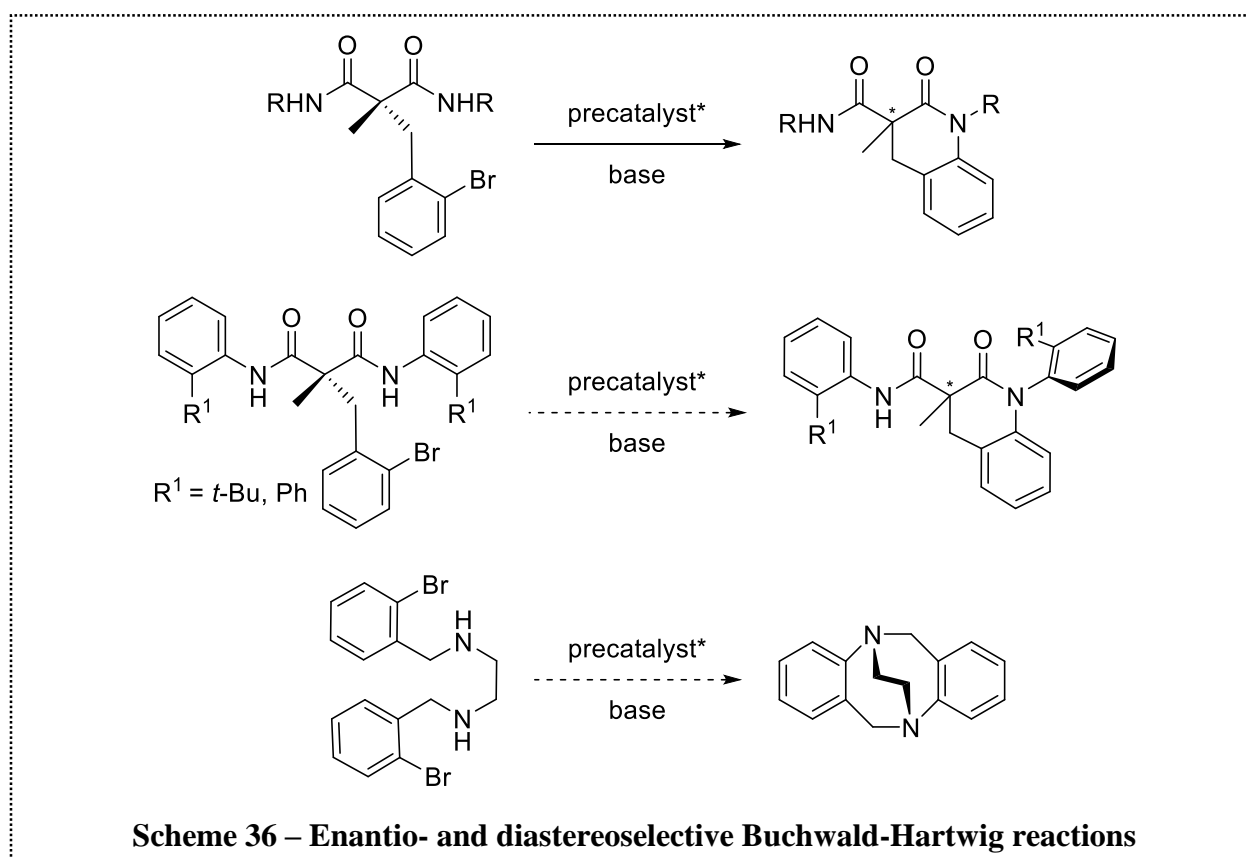
There are many examples where superior results are obtained from precatalyst systems in cross-coupling reactions compared to analogous catalysts formed *in situ* from a palladium precursor and the free ligand. This research has focused on the development of a palladium precatalyst that incorporates a chiral phosphane ligand to facilitate selectivity in asymmetric synthesis. The objectives include the synthesis of a third generation Buchwald-type palladium precatalyst using a chiral dialkylbiaryl phosphane and its application in the catalysis of an enantioselective Buchwald-Hartwig reaction.

Though not commercially available, we found that the employment of (*R*)-dicyclohexyl(2'-methoxy-[1,1'-binaphthalen]-2-yl)phosphane (hereafter referred to as (*R*)-Cy₂MOP) was more efficient compared to the previously employed ligand, (*R*)-MOP, in the cyclization of the *tert*-butylphenyl and biphenyl malonamides,⁷⁶ thus it was selected as the ligand in the first target



precatalyst. The aim is to synthesize and characterize a chiral palladium-phosphane precatalyst based on the previously investigated (*R*)-Cy₂MOP ligand following the reaction outlined in Scheme 35.

Following the isolation of a third generation Buchwald-type precatalyst with the added feature of chirality the objective is to improve the activity and selectivity achieved in the desymmetrization reaction of α -bromobenzyl malonamides through optimization of the reaction conditions. Ultimately, extension of this methodology to a wider scope of structurally related substrates such as those highlighted in Scheme 36, towards enantio- and diastereoselective *N*-arylation, is desired. This work focuses primarily on the synthesis and characterization of a

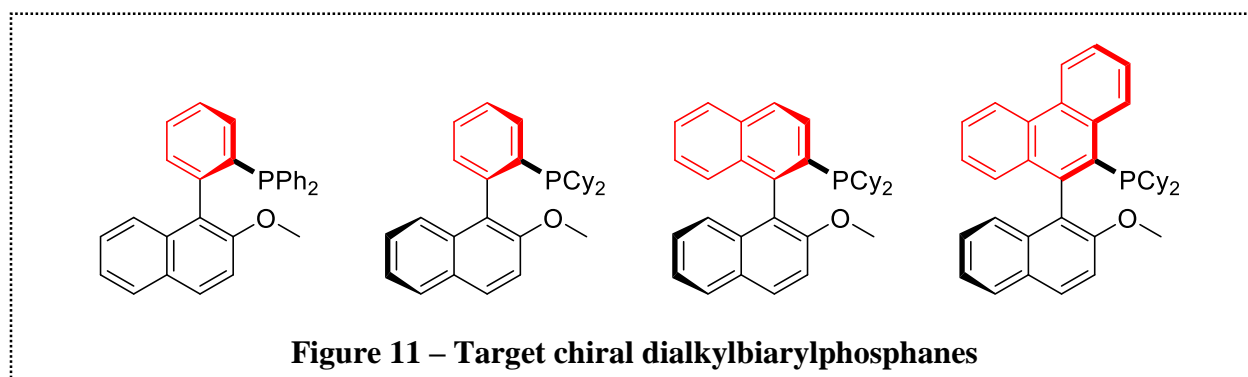


Cy₂MOP-Pd precatalyst and its application in an enantioselective intramolecular *N*-arylation of prochiral malonamides.

2 Results and Discussion

2.1 Towards the synthesis of bulky dialkylbiaryl phosphanes

The enormous success of bulky, electron-rich dialkylbiaryl phosphanes in cross-coupling reactions⁷⁷ inspired our ligand targets. Towards investigating the role of the size of the phosphane-bound aryl moiety highlighted in red in Figure 11, the aim was to synthesize the benzene-, naphthalene-, and phenanthrene-based biarylphosphanes shown below. The size of the two aryl



moieties of the biaryl scaffold influences the dihedral angles of the system which can affect enantioselectivities.^{78,79} Also, increased steric bulk of the phosphorus substituents can lead to a higher barrier to rotation about the chiral axis which may increase the stereochemical integrity of the ligand. The objective was to evaluate the effect of greater steric bulk on the phosphane-bearing arene of the ligand. We predicted that increased benzofusion might force the palladium-amido moiety of the intermediate complex closer to the chiral phosphane during C-N bond formation thereby facilitating a more efficient transfer of chiral information from the catalyst to the substrate.

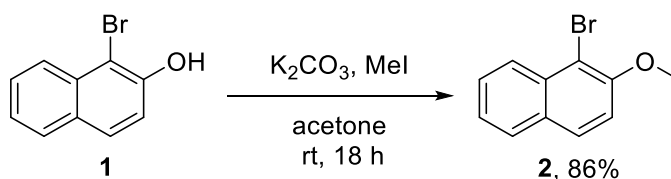
Each of the target chiral dialkylbiaryl phosphanes has the potential for favourable stabilizing interactions with the palladium(II) centre, presumably at the *ipso*-carbon of the methoxy-bearing arene or potentially at the methoxy oxygen, thereby protecting the coordination sphere of palladium from potentially detrimental premature amide binding, binding of several molecules of the amide nucleophile, or bidentate *N,O*-binding of the amide nucleophile. The

generation of κ^2 -amidate complexes inhibits the reactivity of a catalyst for palladium-catalyzed amidation,⁸⁰ therefore the target ligands would circumvent these challenges for various substrates.

2.1.1 Benzyne route towards dialkylbiaryl phosphane

The strategy investigated towards the synthesis of a benzene-based biarylphosphane was the benzyne route described by Buchwald wherein a one-pot procedure is used.²⁵ This protocol takes place over two stages: 1) *in situ* formation and reaction of a benzyne and an aryl Grignard reagent and 2) copper-catalyzed reaction with a chlorodialkylphosphane to form the C-P bond. The procedure outlined by Buchwald relies on the *in situ* formation of a benzyne intermediate from a dihaloarene alongside the generation of an arylmagnesium halide from the corresponding aryl halide. The benzyne and the aryl Grignard reagent subsequently react generating a biaryl Grignard reagent. In the second stage, a chlorodialkylphosphane is added to the biaryl Grignard reagent in the presence of a copper catalyst, forming a dialkylbiaryl phosphane.

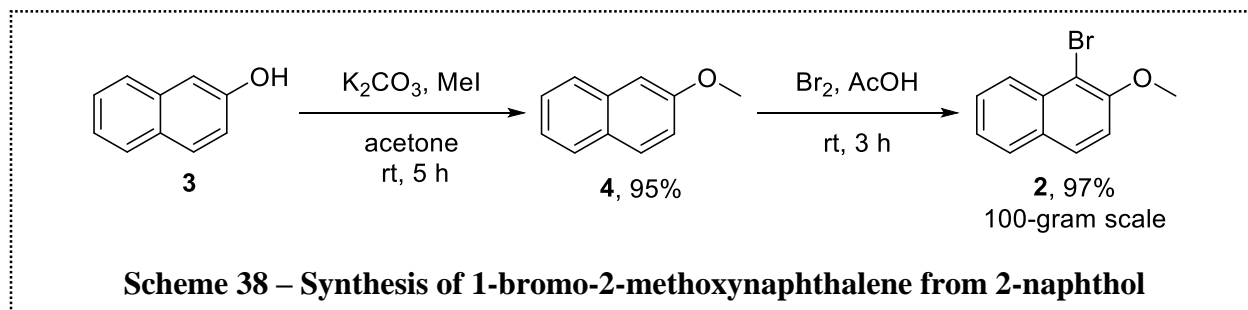
The target aryl bromide, 1-bromo-2-methoxynaphthalene **2**, was accessed from 1-bromo-2-naphthol **1** following the Williamson ether synthesis protocol using potassium carbonate to deprotonate the alcohol and iodomethane as the methylating agent (Scheme 37). Following the



Scheme 37 – Methylation of 1-bromo-2-naphthol using iodomethane

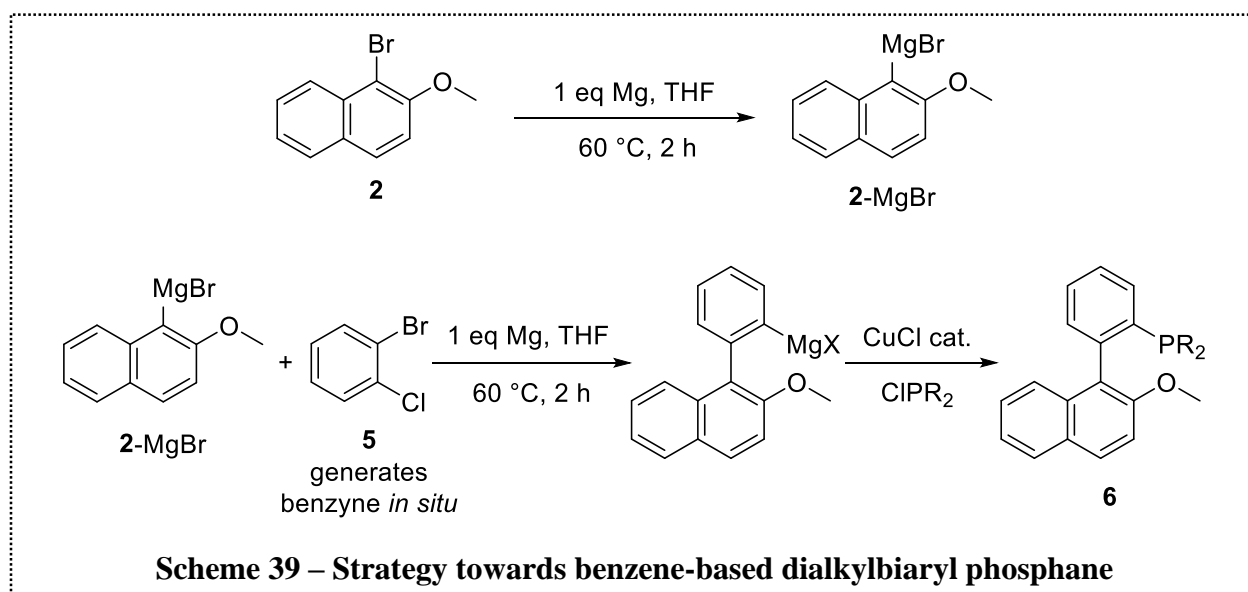
workup, the product was purified by recrystallization in hexanes, which provided the product as colourless crystals in 86% yield. Due to the large quantities of 2-naphthol in stock, moving forward, the methylation of 2-naphthol was conducted to generate 2-methoxynaphthalene to be used towards **2** in a scaled up procedure. The product was derived from the bromination of 2-

methoxynaphthalene **4** in acetic acid using bromine, as shown in Scheme 38. The product crystallized from the reaction mixture and was then filtered and washed with distilled water to give



2 as a white solid in 92% yield over 2 steps.

The aryl Grignard of 1-bromo-2-methoxynaphthalene **2** was prepared under an inert atmosphere using magnesium turnings along with a small crystal of iodine in THF (Scheme 39).

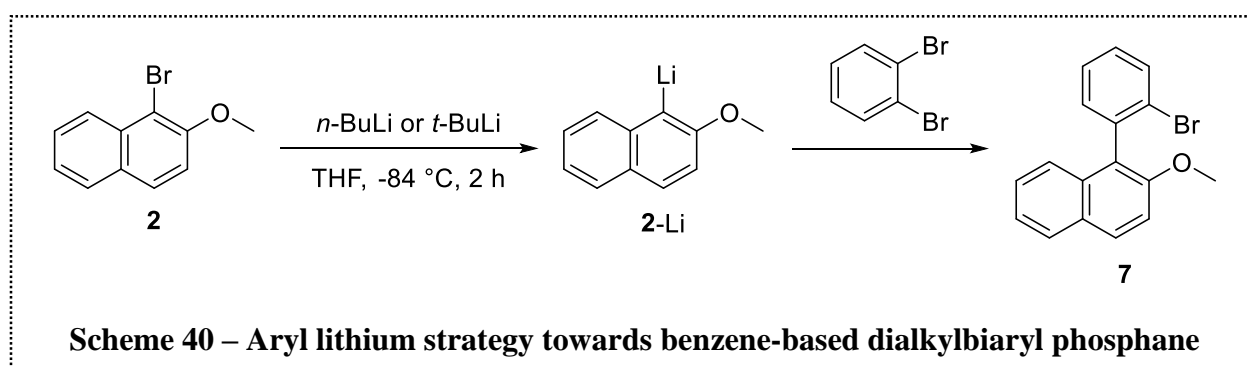


The reaction mixture took on a yellow-brown colour due to the presence of iodine, which was employed to increase the reactivity of the metal surface.^{81,82} A colour change from yellow-brown to colourless indicates consumption of the iodine and provides evidence of magnesium “activation”. Following this activation, 1-bromo-2-methoxynaphthalene was dissolved in THF and added dropwise to the magnesium. Monitoring the reaction progress by TLC analysis, upon

complete disappearance of the aryl bromide, bromochlorobenzene was added dropwise to facilitate the generation of the biaryl Grignard reagent as depicted in Scheme 39. Chlorodiphenylphosphane was used rather than the desired chlorodicyclohexylphosphane as a cost saving strategy while the reaction conditions were being optimized. Confirming the successful formation of the Grignard reagent was challenging since multiple products were formed as indicated *via* TLC analysis. The troubleshooting conducted did not improve the outcome of the reaction and a complex product mixture was consistently formed. With only small variations in the retention factors of the compounds present in the mixture using various solvent systems, separating the components by column chromatography or preparative TLC could not be achieved.

2.1.2 Aryl lithium coupling route towards dialkylbiaryl phosphane

Following the challenges encountered attempting the synthesis of the biarylphosphane *via* the benzyne route, an aryl lithium coupling strategy was investigated towards the benzene-based *ortho*-bromobiaryl which would then be subjected to C-P cross-coupling conditions. There is literature precedent for the generation of a biaryl bromide through the reaction of an aryl lithium with a dihaloarene.^{83,84} The synthetic pathway is outlined in Scheme 40.

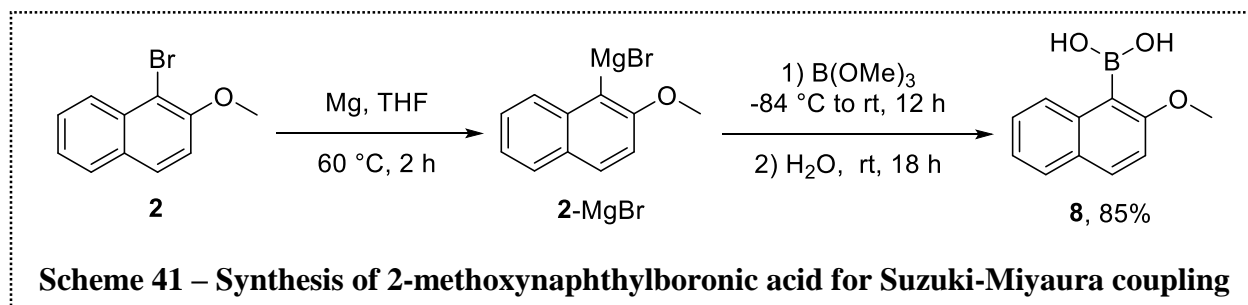


Monitoring the reaction by TLC analysis, once there was evidence of complete consumption of 1-bromo-2-methoxynaphthalene **2**, the reaction was allowed to warm to room temperature before adding 1,2-dibromobenzene. Several trials were conducted, however the

addition of *n*-BuLi consistently led to the generation of multiple products. The reaction was later attempted using *t*-BuLi in place of *n*-BuLi but this did not improve the reaction outcome. The crude mixture contained starting material, the reduced arene, and several unidentified byproducts. A minor signal at δ 4.04 ppm in the ^1H NMR spectrum indicated the presence of the starting reagent, 1-bromo-2-methoxynaphthalene, and the major signal at *ca.* δ 3.94 ppm is characteristic of 2-methoxynaphthalene whose presence was also supported by the signals in the aromatic region. The identity of the compounds giving rise to other major signals were not determined. The results obtained using *t*-BuLi were similar with variations in the ratios of byproducts.

2.1.3 Synthesis of *ortho*-bromobiaryl via Suzuki-Miyaura coupling reaction

Following the lack of success with the benzyne and organolithium strategies towards the biarylphosphane, an alternative indirect route was envisioned wherein a benzene-based *ortho*-bromobiaryl would be synthesized *via* a Suzuki-Miyaura coupling and used towards generating the desired phosphane in subsequent reactions. The synthesis of 2-methoxy-1-naphthylboronic



acid, outlined in Scheme 41, was the first step towards the intended Suzuki-Miyaura coupling with 1,2-dibromobenzene. Employing Schlenk techniques, 1-bromo-2-methoxynaphthalene was transformed into the corresponding magnesium halide reagent using magnesium turnings in the presence of a crystal of iodine in THF. The reaction progress was monitored periodically by TLC analysis (10% ethyl acetate in hexanes) by quenching a drop of the reaction mixture with methanol and observing the conversion of the aryl bromide **2** (R_f = 0.42) to the reduced arene, 2-

methoxynaphthalene **4** ($R_f = 0.44$). Formation of the boronate ester towards the synthesis of the corresponding boronic acid was accomplished by reacting the Grignard reagent, formed *in situ*, with trimethylborate. The Grignard reagent was separated from the remaining magnesium turnings by transferring the mixture to a clean Schlenk flask *via* cannula needle. An important observation made at this stage was that upon slight cooling of the formed Grignard reagent, the reaction mixture thickened which impeded the intended cannula transfer. Therefore, it was necessary to transfer the reaction mixture promptly following the confirmation of complete conversion of **2** by TLC analysis to avoid the challenge of removing magnesium turnings from the final product. Using a liquid nitrogen/ethyl acetate bath, the reaction was cooled to $-84\text{ }^{\circ}\text{C}$ and trimethylborate was added before warming the mixture to room temperature and stirring for 18 hours. The boronic acid **8** was obtained following a standard aqueous workup to hydrolyze the labile boronate ester substituents of the generated dimethyl(2-methoxy-1-naphthyl)boronate ester. Allowing ample time for the generation of a homogeneous solution following the addition of water proved key for a simplified workup. The volatiles were removed under reduced pressure and the remaining solid was stirred in DCM and then collected by filtration. A final suspension of the product in DCM followed by filtration and a wash using cold DCM was conducted to afford 2-methoxy-1-naphthylboronic acid **8** as a white solid. The boronic acid had poor solubility in most of the common laboratory solvents and the sample for NMR spectroscopic analysis was dissolved in deuterated DMSO.

Under inert atmosphere, the Suzuki-Miyaura coupling of 2-methoxy-1-naphthylboronic acid and 1,2-dibromobenzene was conducted in degassed THF and 2M K_2CO_3 using 2.5 mol% $\text{Pd}(\text{PPh}_3)_4$. The reaction was carried out at $60\text{ }^{\circ}\text{C}$, monitoring periodically by TLC analysis. The reactant to product ratio was not improved beyond the 72-hour reaction period, and thus towards achieving shorter reaction time and higher conversion, dioxane was employed in place of THF in

order to access higher reaction temperatures. This led to a slightly greater yield, 53% compared to the highest achieved yield of 45% under various conditions using THF. The degassing procedure was conducted under vacuum and backfilling the system with nitrogen rather than by bubbling nitrogen gas through the dioxane, as done for THF. The aqueous basic mixture was degassed separately from the organic mixture and was subsequently added to the reaction flask. Results and observations from selected trials of conditions screening for the Suzuki-Miyaura coupling are included in Table 2. The best results were achieved when 2.5 mol% Pd(PPh₃)₄ in dioxane and water were used (Table 2, entry 3).

Table 2. Optimization of Suzuki-Miyaura cross coupling reaction conditions^a

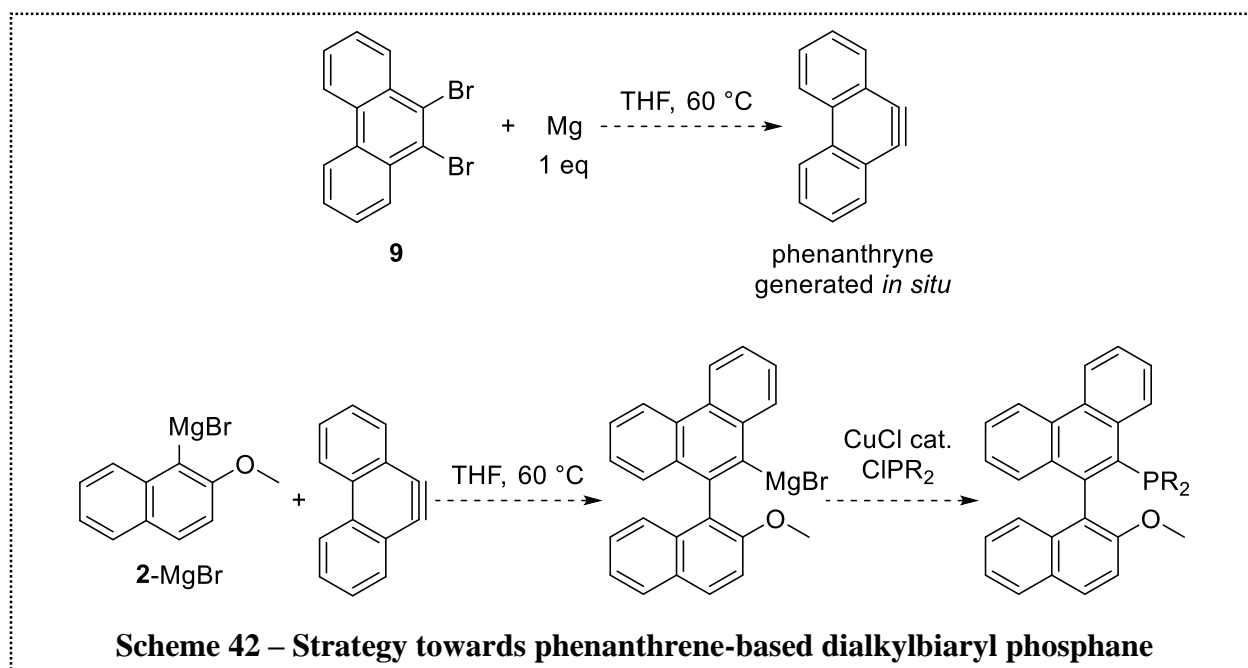
Entry	Pd(PPh ₃) ₄ (mol%)	Solvent	T (°C)	Time	Yield (%)
1	2.5	THF:water	60	72 h	45
2	2.5	THF:water	160 ^b	5 min	n.d. ^c
3	2.5	dioxane:water	100	72 h	53
4	1.25	dioxane:water	100	72 h	38
5	2.5	dioxane:water	180 ^b	6 min	n.d. ^c
^a Reaction conditions: 1.0 eq boronic acid 8 , 2 eq 1,2-dibromobenzene in THF or dioxane and 1.5 eq aqueous K ₂ CO ₃ . ^b Reactions were conducted using a microwave synthesizer. ^c Major product was the protodeboronated byproduct.					

Experiments were conducted using the microwave reactor in attempts to lower the reaction time for the Suzuki-Miyaura coupling (Table 2, entries 2 and 5). Boronic acid **8** and THF were added to a 20-mL microwave vial equipped with a magnetic stir bar and the solution was degassed by bubbling nitrogen gas through the solution. Dibromobenzene was added to the vial followed by a degassed aqueous solution of K₂CO₃, then Pd(PPh₃)₄ over a flow of nitrogen gas. The vial was

sealed promptly after all of the reagents were combined and then heated at 160 °C for 5 min with stirring. The major product formed was the protodeboronated arene, 2-methoxynaphthalene **4**. Next, the reaction was attempted using dioxane since the reaction had proceeded with greater yield using this organic solvent with conventional heating. Dioxane and aqueous base solution were degassed and then quickly transferred to a microwave reaction vial containing the boronic acid **8** and Pd(PPh₃)₄. Dibromobenzene was added to the mixture over a gentle flow of nitrogen and the vial was sealed. The reaction was set to 180 °C for 6 minutes. The crude product mixture contained the desired coupled product along with the byproduct, **4**, accessed *via* protodeboronation of the boronic acid, and several other minor impurities that do not coincide with starting material as indicated in the ¹H NMR spectrum. Efforts to minimize the reaction time from 72 hours to 6 minutes by employing the microwave reactor were unsuccessful.

2.1.4 Towards the synthesis of phenanthrene-based biarylphosphane

The strategy towards the phenanthrene-based biarylphosphane, presented in Scheme 42, followed the same protocol towards the benzene-based system. Instead of forming a benzyne



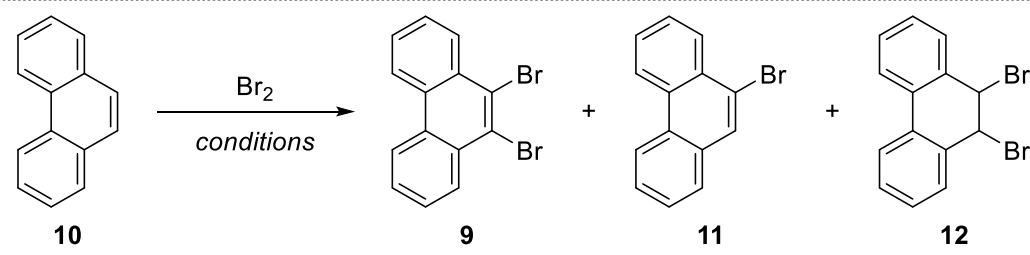
intermediate from a dihalobenzene, we proposed transforming dibromophenanthrene into the analogous phenanthryne species *in situ* to react with the generated aryl Grignard reagent. The biaryl system afforded would be comprised of the 2-methoxynaphthyl base and the upper bulky phenanthryl moiety. Successful formation of the 2-methoxyl-1-naphthyl Grignard reagent had already been achieved consistently, therefore steps towards this biaryl system began with efforts to generate the 9,10-dibrominated phenanthrene precursor.

2.1.4.1 Strategies towards 9,10-dibromophenanthrene

Following a literature procedure for the synthesis of 9,10-dibromophenanthrene,⁸⁵ the tungstophosphoric acid cesium salt, $\text{Cs}_x\text{H}_{3-x}\text{PW}_{12}\text{O}_{40}$,[†] and cetyltrimethylammonium bromide (CTAB) were dissolved in DCM, followed by the addition of phenanthrene. A diluted solution of bromine was added dropwise with vigorous stirring at room temperature over 10 minutes. The reaction was left to stir for an additional 5 minutes and the resulting mixture was filtered and the collected solid was washed with water. Analysis of the ^1H NMR spectrum of the crude product revealed that three different compounds were present (Table 3, entry 1). This was evidenced by three unique singlets: the major signal at δ 5.71 ppm arising from the proton at the 9- and 10-position in the dibrominated addition product **12**; the signal at δ 7.75 ppm which is characteristic of the starting reagent, phenanthrene **10**; and the monobrominated phenanthrene product **11** which gives a signal at δ 8.12 ppm for the proton at the 10-position. The reaction was repeated to ensure that the slightly longer reaction time than described in the literature procedure did not negatively impact the results. The undesired products described above were consistently formed when shorter reaction times were employed.

[†]The tungstophosphoric acid cesium salt was prepared by former thesis student Maja Chojnacka¹⁰³ following the literature procedure.¹⁰⁴

Table 3. Bromination reaction conditions towards 9,10-dibromophenanthrene

						
Entry	Catalyst	Additive	Solvent	T (°C)	t (min)	Results
1	Cs salt/CTAB	---	DCM	rt	5	11 and 12 formed
2	FeBr ₃	---	AcOH	160 ^a	5	11 and bromoacetic acid formed
3	FeBr ₃	---	<i>t</i> -BuOH	120 ^a	10	11 and volatile substance formed
4	FeBr ₃	KO <i>t</i> -Bu	<i>t</i> -BuOH	120 ^a	10	Incomplete conversion to 11

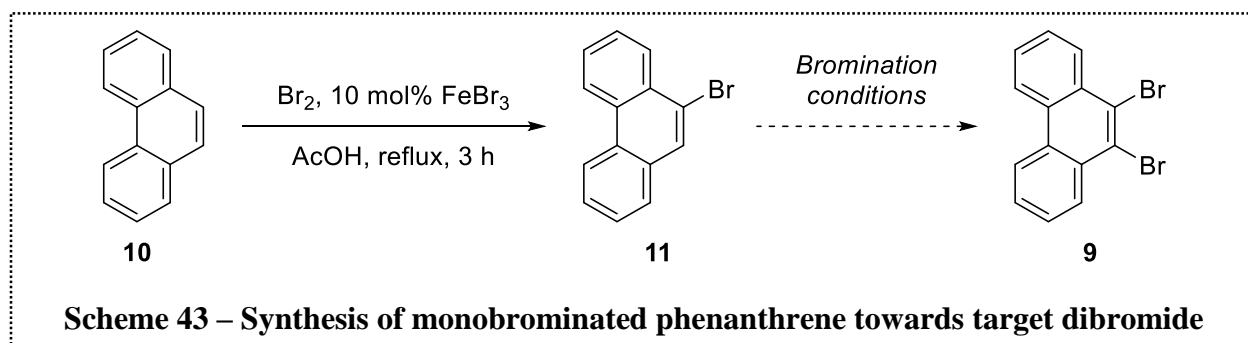
^a Reactions were conducted using a microwave synthesizer.

Next, the dibromination was attempted using 2 equivalents of bromine and 10 mol% of FeBr₃ in acetic acid at 160 °C for 5 minutes in the microwave reactor (Table 3, entry 2). The pressure in the reaction vial did not stabilize and instead increased over the course of the reaction. Once the reaction was complete, sodium thiosulfate solution, a mild reducing agent, was used in the workup as a quenching agent for the excess bromine. The ¹H NMR spectrum of the crude product had a signal at δ 3.90 ppm which indicated that a different compound was formed compared to the byproducts formed in the previous trials. This new singlet signal is characteristic of bromoacetic acid.⁸⁶ The singlet at δ 8.12 ppm for the monobrominated product **11** was observed and the characteristic signal for the addition product **12** at δ 5.71 ppm was absent.

The microwave reaction was repeated using *tert*-butanol except at 120 °C for 10 minutes to manage the pressure levels of the vial (Table 3, entry 3). The reaction solvent, *tert*-butanol was selected based on its reasonably high boiling point and the fact that the molecule cannot be readily oxidized and therefore would not pose an issue in the reaction where bromine is used. The pressure

rose steadily over the course of the reaction due to the generation of a gas. The pressure in the vial was slowly relieved by intermittently venting the evolved gas through a needle following the 10-minute reaction period to avoid violent bubbling of the mixture. The probable identity of the generated gas is 2-methylpropene from the elimination reaction of *tert*-butanol. In attempts to resolve this issue, the reaction was repeated with the addition of 2 equivalents of KO*t*Bu, in order to prevent the protonation of the *tert*-butanol. The major components of the crude mixture determined *via* ^1H NMR spectroscopy were starting material along with monobrominated phenanthrene.

The limited success with affording 9-bromophenanthrene inspired the idea to intentionally isolate the monobromophenanthrene **11** and subject it to varied brominating conditions to achieve the target dibromophenanthrene product as shown in Scheme 43. The separation of **11** from the

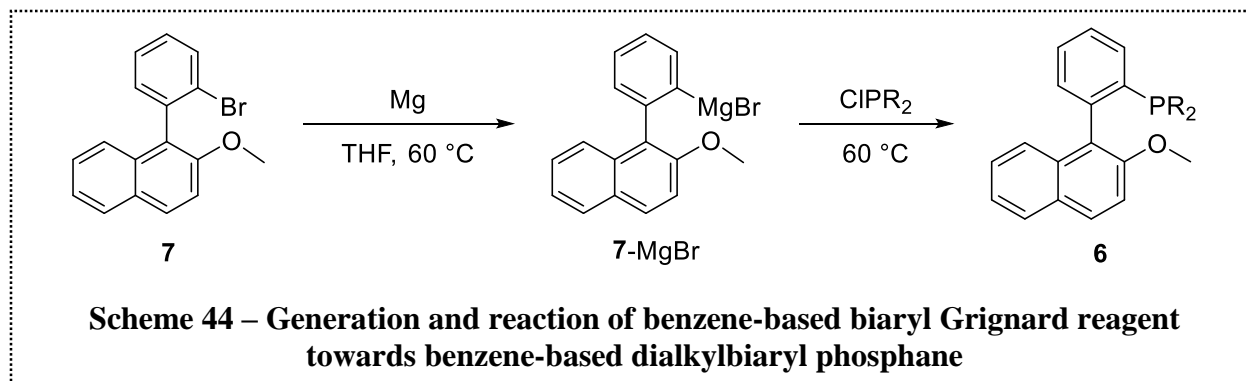


product mixture proved difficult *via* flash chromatography and further investigation is required to determine the feasibility of this strategy.

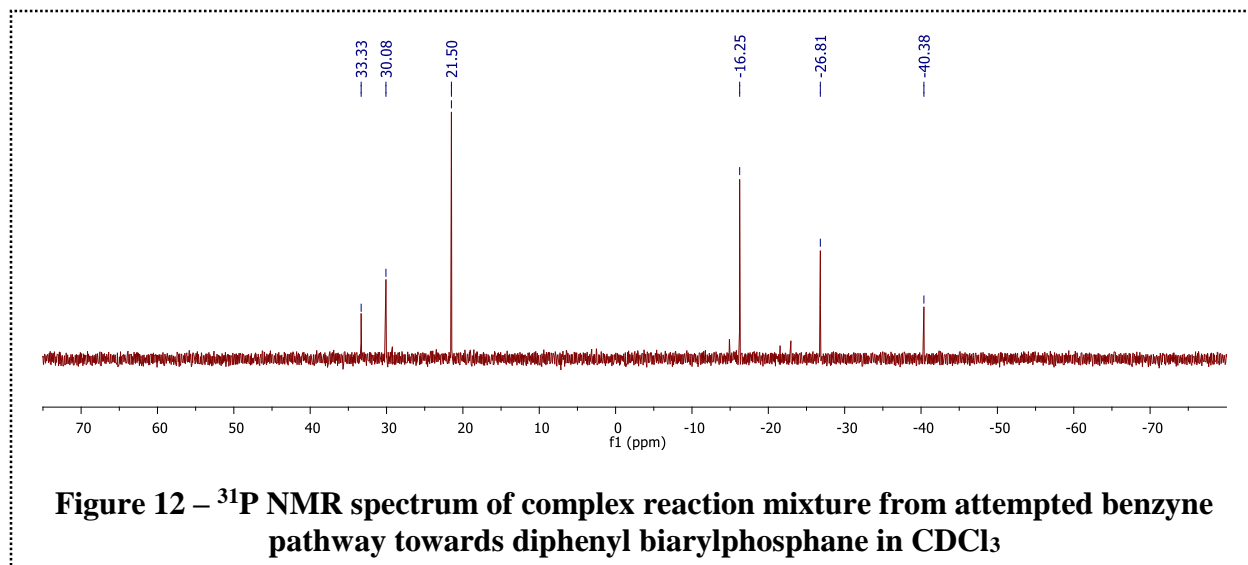
2.1.5 Modelling strategy towards phenanthrene-based dialkylbiaryl phosphane using benzene-based system

2.1.5.1 Grignard reaction strategy towards biarylphosphane

Alternative to the benzyne route attempted, the following strategy towards the target biarylphosphane relied on the formation of the aryl Grignard reagent from the synthesized *ortho*-



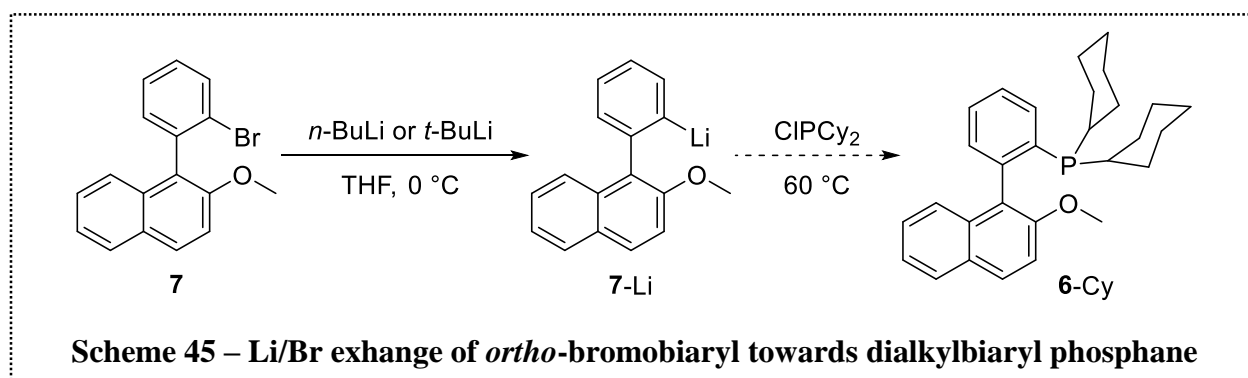
bromobiaryl **7** followed by its reaction with the desired chlorodialkylphosphane, as depicted in Scheme 44. Identical reaction conditions as those used to access the aryl Grignard of 1-bromo-2-methoxynaphthalene (**2**-MgBr) were employed towards the Grignard of **7** (**7**-MgBr), however, its formation was not clear by TLC analysis. The reaction was repeated with a greater focus on initiating the Grignard reagent formation by adding a drop of MeI, a polar short chain alkyl halide, which are known to aid in Grignard reagent formation.⁸² When these measures did not overcome the difficulties encountered, another trial was conducted with the addition of a small amount of the aryl bromide following MeI. After pre-stirring this mixture at 60 °C for 30 minutes, the bulk of the aryl halide was added. TLC analysis showed a faint spot, presumably the formed Grignard reagent, after this trial. The subsequent phosphination reaction was carried out using chlorodiphenylphosphane and this led to several products, visualized on the TLC plate and six signals were observed in the ³¹P NMR spectrum as shown in Figure 12. The ³¹P resonance signals



do not lie in the region characteristic of related types of phosphanes around δ -10 ppm. Additionally, none of the downfield signals match that of the corresponding phosphane oxide of **6-Ph** at δ 27.9 ppm.⁸⁷

2.1.5.2 Lithium halogen exchange strategy towards biarylphosphane

The difficulties encountered with efficient generation of the aryl Grignard reagent prompted the investigation of aryl lithium formation using butyllithium. Following the formation of the biaryl organolithium reagent, the intention was to react it with chlorodicyclohexylphosphane to generate the desired dialkylbiaryl phosphane (Scheme 45). The reaction was initially conducted

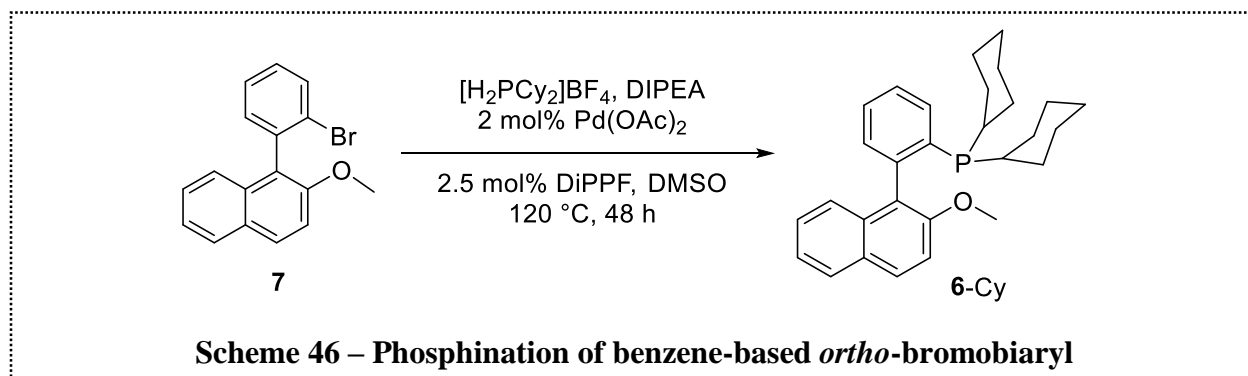


using *n*-BuLi. Formation of the aryl lithium was unclear by TLC analysis as only a faint spot with a higher R_f value than the aryl bromide **7** (TLC: 10% ethyl acetate in hexanes, R_f = 0.34), was

visible. Complete consumption of the starting material was never observed even though 1.2 equivalents of *n*-BuLi were used. The reaction outcome was not improved when *t*-BuLi was used in place of *n*-BuLi, however, visual evidence of a reaction taking place was noted and this prompted an explanation for the challenges encountered with aryl lithium formation. The methoxy group of the lower aryl moiety is Lewis basic, therefore the oxygen may interact with the Lewis acidic lithium of the BuLi reagent, directing the deprotonation of the aryl bromide at the 6-position of the bromophenyl moiety. Upon addition of methanol to quench any excess BuLi in the preparation of the TLC sample, the lithiated position would be re-protonated thereby regenerating the *ortho*-bromobiaryl **7**, which was the most intense spot observed on the TLC plate.

2.1.5.3 C-P coupling strategy towards biarylphosphane

Literature precedent revealed that a catalyst system based on Pd(OAc)₂ and the electron-donating organometallic complex, 1,1'-bis(diisopropylphosphino)ferrocene (DiPPF) was effective for the phosphination of aryl bromides and chlorides with secondary phosphanes.⁸⁸ The C-P coupling of *ortho*-bromobiaryl **7** and the desired dialkylphosphane, presented in Scheme 46, was attempted following the outlined procedure. Dialkylphosphanes are typically air-sensitive and



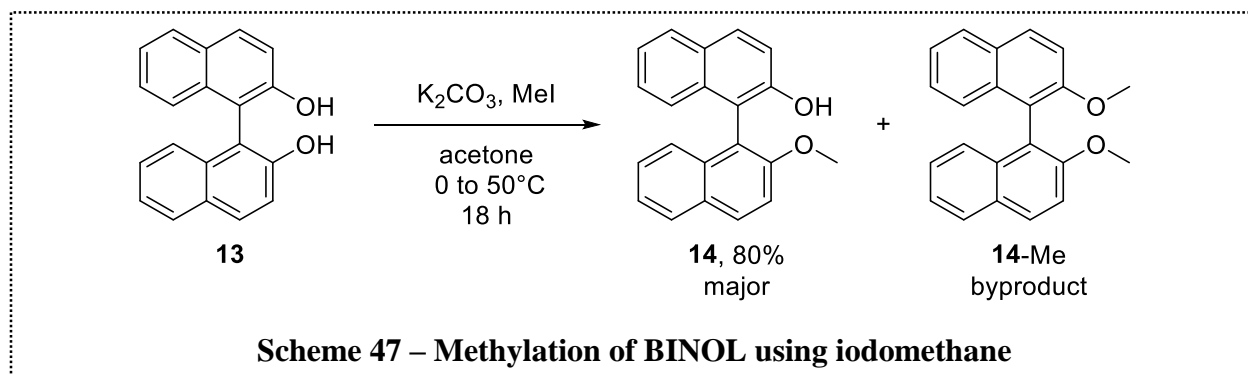
readily undergo oxidation to generate the corresponding phosphane oxide. To overcome this problem the strategy involved converting the free dicyclohexylphosphane to the air-stable phosphonium tetrafluoroborate salt.⁸⁹ The tetrafluoroborate counterion serves as a spectator in the

reaction since it is non-coordinating. This simple protection of the phosphane as the conjugate acid allows easy access to the desired phosphane *in situ* through acid-base chemistry using a weak base in the reaction mixture. Dicyclohexylphosphonium tetrafluoroborate salt, Pd(OAc)₂ (2 mol%), DiPPF (2.5 mol%) and aryl bromide **7** were added to a flame-dried Schlenk flask under inert conditions. Degassed DMSO and DIPEA were then added and the reaction mixture was heated to 120 °C, monitoring reaction progress by TLC analysis. This strategy was not successful under the described conditions, however troubleshooting was not conducted for this particular route. Due to the difficulties faced in the generation of dibromophenanthrene and the unsuccessful phosphination of the analogous benzene-based *ortho*-bromobiaryl, synthesis of the target phenanthrene-based dialkylbiaryl phosphane was found to be infeasible by the intended route.

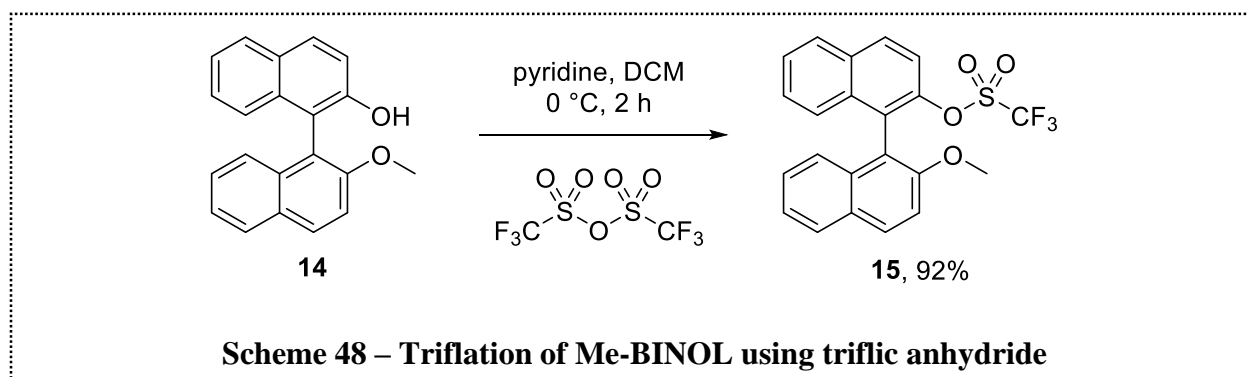
2.1.6 Synthesis of racemic and enantiopure Cy₂MOP

Encouraged by the previous success with the atropisomeric dialkylbiaryl phosphane Cy₂MOP as a supporting ligand in the palladium-catalyzed intramolecular desymmetrization of malonamides, it was the target ligand for the precatalyst complex. Since Cy₂MOP is not commercially available it was synthesized starting from either racemic or enantiopure 1,1'-bi-2-naphthol (BINOL). It has been shown that under UV irradiation BINOL and derivatives, which must contain at least one of the acidic protons, undergo photoracemization⁹⁰ thus as an added precautionary measure reaction vessels were covered with aluminum foil paper to minimize light exposure of the starting material and intermediate species.

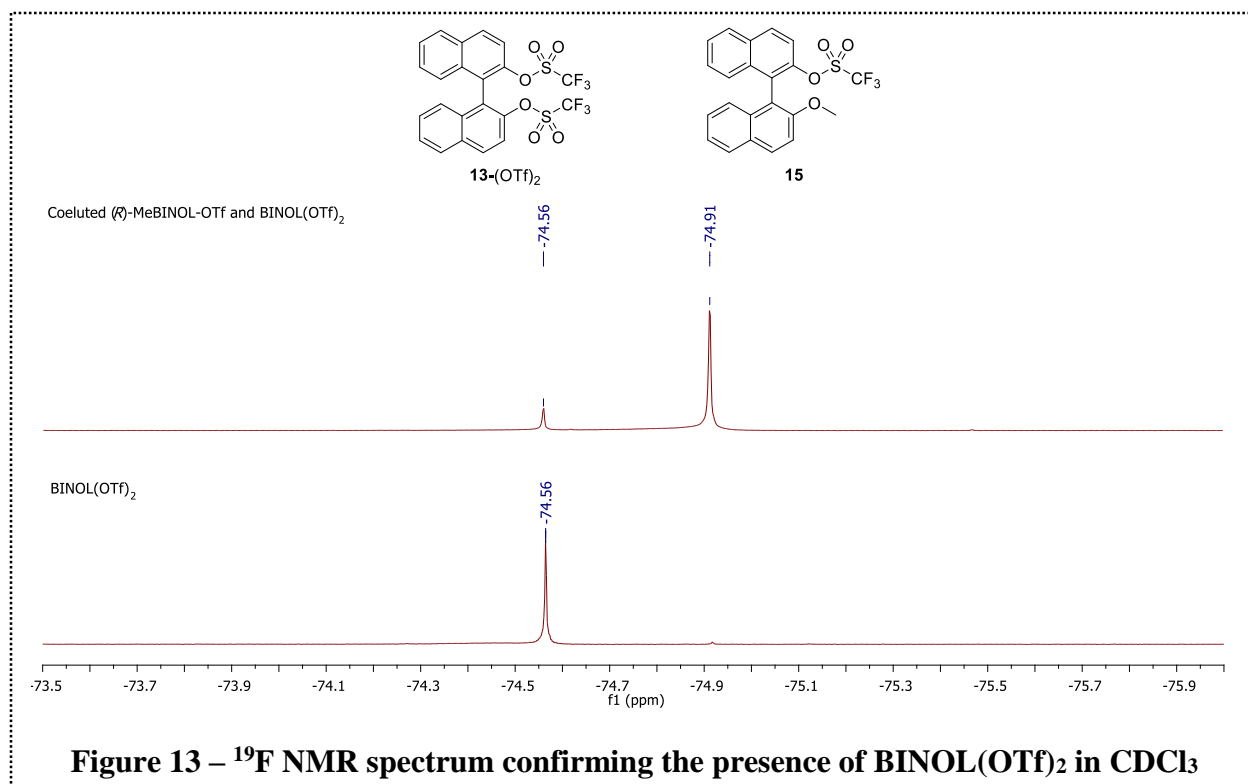
Mono-methylated BINOL (Me-BINOL) **14** was readily prepared on a 35 mmol scale *via* treatment of BINOL **13** with potassium carbonate followed by heating of the resulting aryl anion with iodomethane at 50 °C for 18 hours, as outlined in Scheme 47. Iodomethane was added



dropwise at 0 °C to minimize generation of the dimethylated byproduct which was inevitably formed. The dimethylated BINOL byproduct **14-Me** was readily separated from the desired material *via* flash column chromatography (refer to Appendix 5.1, p.109). Me-BINOL **14** was subsequently treated with pyridine then triflic anhydride to provide the corresponding triflate, Me-BINOL-OTf **15**, in high yield (92%) (Scheme 48). Efforts towards minimizing the number of

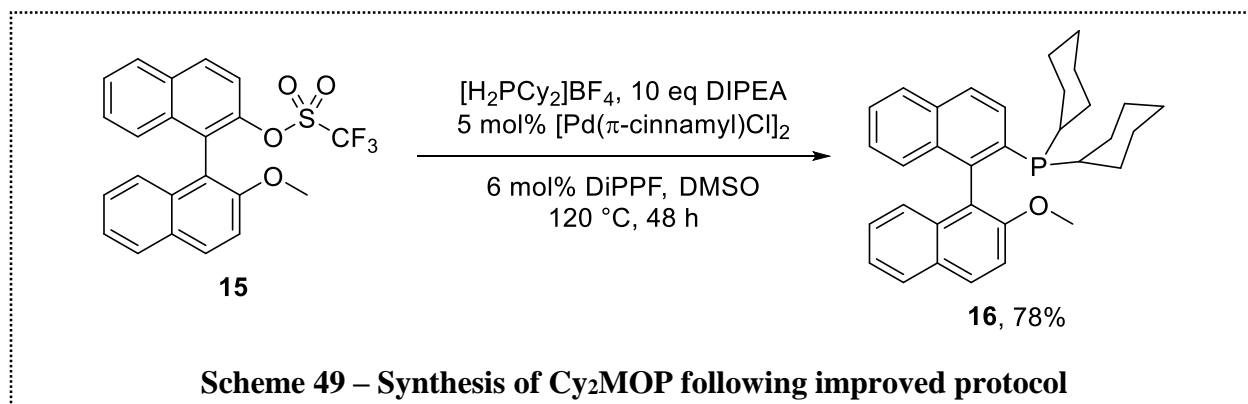


purification steps required in the synthesis of the desired phosphane involved triflating **14** directly following the methylation of **13** without purification. This led to a mixture of the desired product **15**, **14-Me**, and ditriflated BINOL (**13**-(OTf)₂), which all had similar retention factors in various solvent systems as determined *via* TLC analysis. The ¹⁹F NMR spectrum showed two signals,



confirming that the ditriflate $\mathbf{13}-(\text{OTf})_2$ was produced as a byproduct, as shown in Figure 13. Overall, avoiding the purification steps was less time effective with the introduction of an additional byproduct compared to the former side products, which were difficult to separate from the desired product $\mathbf{15}$.

Finally, the palladium-catalyzed C-P coupling shown in Scheme 49, of Me-BINOL-OTf $\mathbf{15}$ with dicyclohexylphosphane was carried out.⁷⁶ The solid reagents, $\mathbf{15}$, dicyclohexylphosphonium tetrafluoroborate, $\text{Pd}(\text{OAc})_2$, and DiPPF, were combined in a flame-

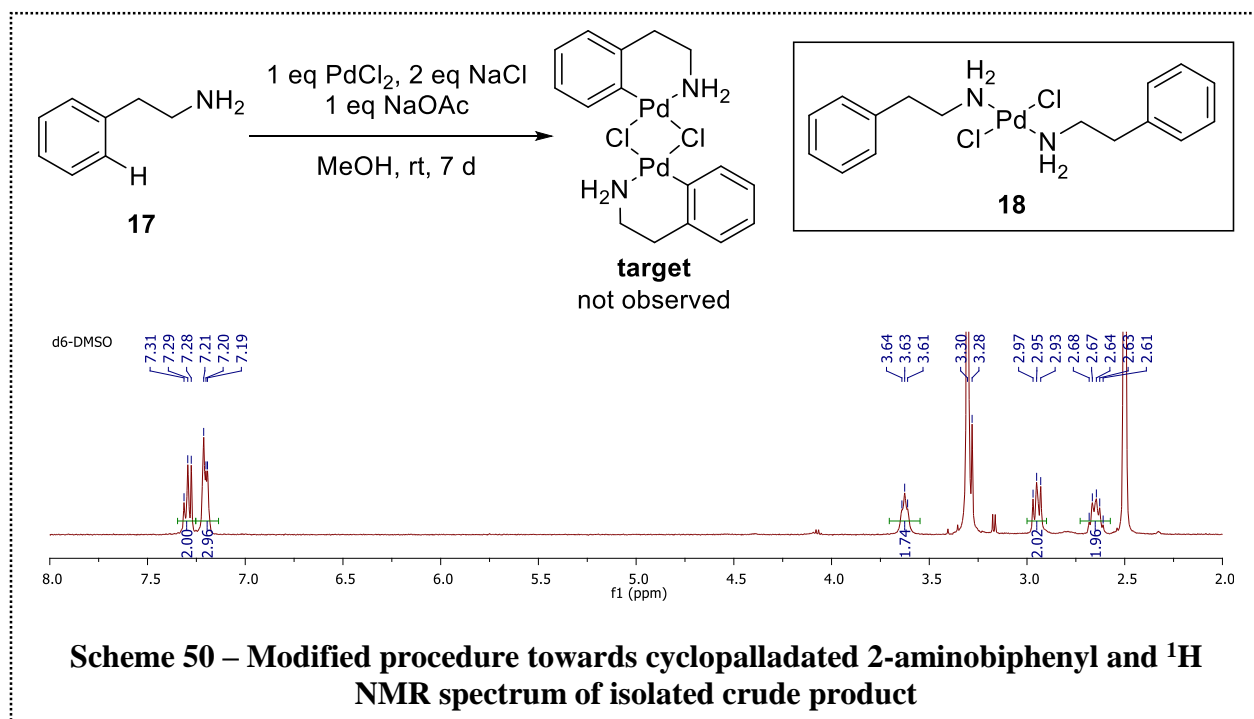


dried Schlenk flask to which degassed DMSO and DIPEA were added. DIPEA was used in a large excess as a co-solvent in order to ensure complete deprotonation of the phosphonium salt under the reaction conditions as well as to allow its use in the deprotonation step in the catalytic cycle. The palladium source employed in the C-P coupling reaction was found to have a profound effect on the performance of the ligand, with 35% yield achieved using the $\text{Pd}(\text{OAc})_2/\text{DiPPF}$ catalyst system. The activity of the $\text{Pd}(\pi\text{-cinnamyl})\text{Cl}_2/\text{DiPPF}$ catalyst proved superior with up to 78% yield achieved.

2.2 Synthesis of Buchwald-type precatalyst

2.2.1 Towards first generation Buchwald-type precatalyst

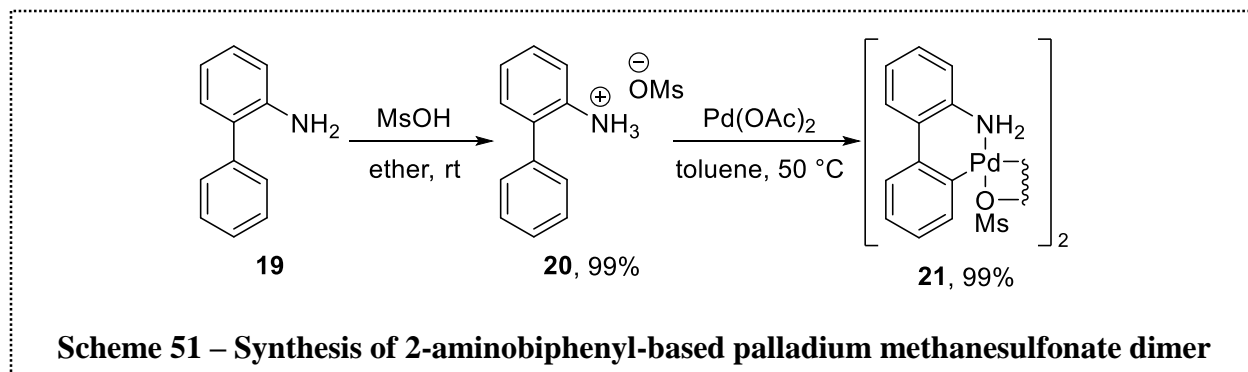
Using phenethylamine **17** as the primary amine species, the synthesis of the corresponding dimeric palladacyclic precatalyst precursor was attempted following the procedure outlined by Albert for the aromatic analog, 2-aminobiphenyl (Scheme 50).⁴⁷ Under open-air, NaCl, NaOAc were combined in a round bottom flask with methanol. Once dissolved, PdCl_2 was added followed



by dropwise addition of phenethylamine **17**. The reaction was stirred at room temperature for 7 days then the resulting grey precipitate was filtered through a frit and washed with ether and water. The experimental ^1H NMR spectrum did not match the literature spectrum of the desired compound⁴⁶ and instead showed characteristic signals supporting the proposed structure **18** shown in Scheme 50. Multiple heteroatoms and therefore multiple ligands can coordinate the palladium centre at a time leading to the formation of a stable coordination complex,³⁹ and such was found to be the case in this reaction trial.

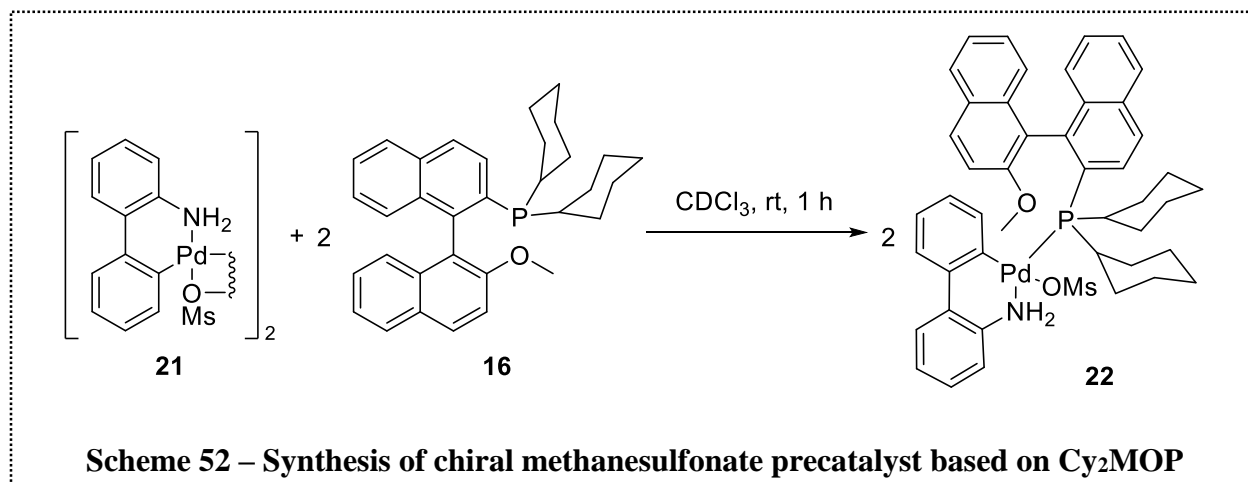
2.2.2 Synthesis of third generation Buchwald-type precatalyst

The first step towards the third generation precatalyst includes the synthesis of a methanesulfonate 2-aminobiphenyl dimeric palladacycle *via* a C-H activation/cyclopalladation sequence. As presented in Scheme 51, treatment of 2-aminobiphenyl **19** with methanesulfonic acid generates the ammonium methanesulfonate salt **20** which is then heated with $\text{Pd}(\text{OAc})_2$ to provide the methanesulfonate-bridged dimeric palladacycle **21**. Palladium acetate is used as the palladating

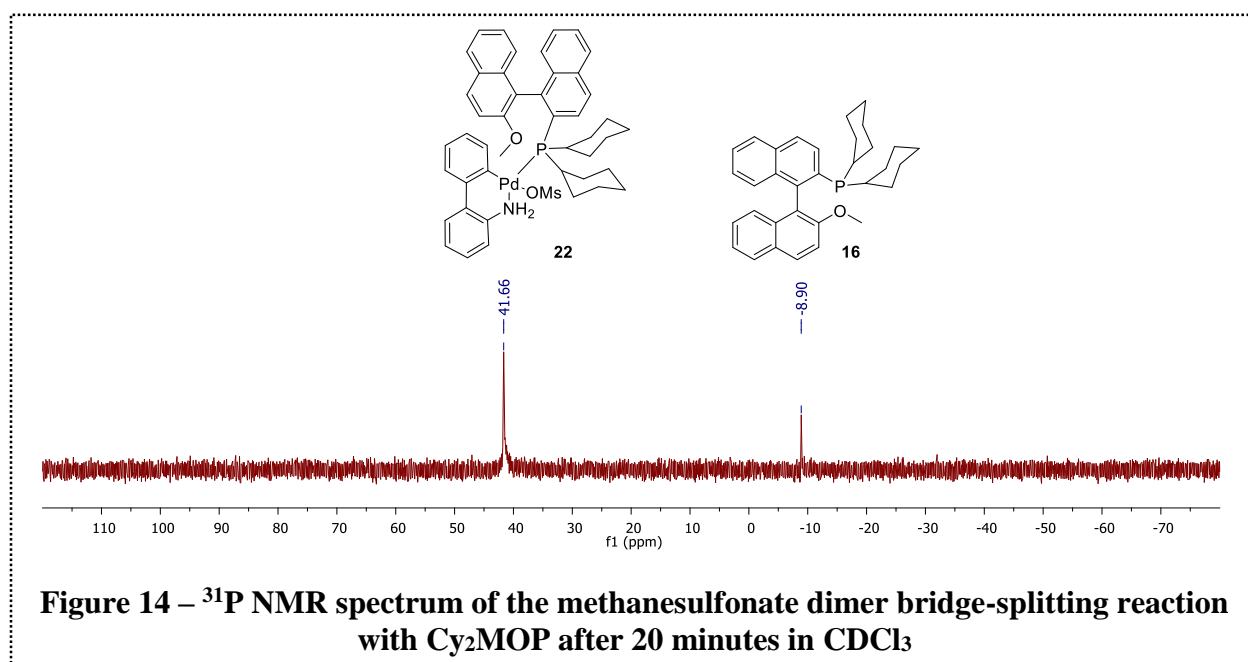


agent in a 1:1 mole ratio with the mesylate salt **20**. The acetate ligand provides an intramolecular base for deprotonation, thereby aiding in the C-H bond cleavage in the *ortho*-palladation of the 2-biphenylammonium mesylate salt **20**, forming acetic acid as a byproduct. There was evidence of this in the ^1H NMR spectrum of **21** where a minor residual solvent peak for acetic acid was present at δ 1.99 ppm (refer to Appendix 5.1, p. 120).

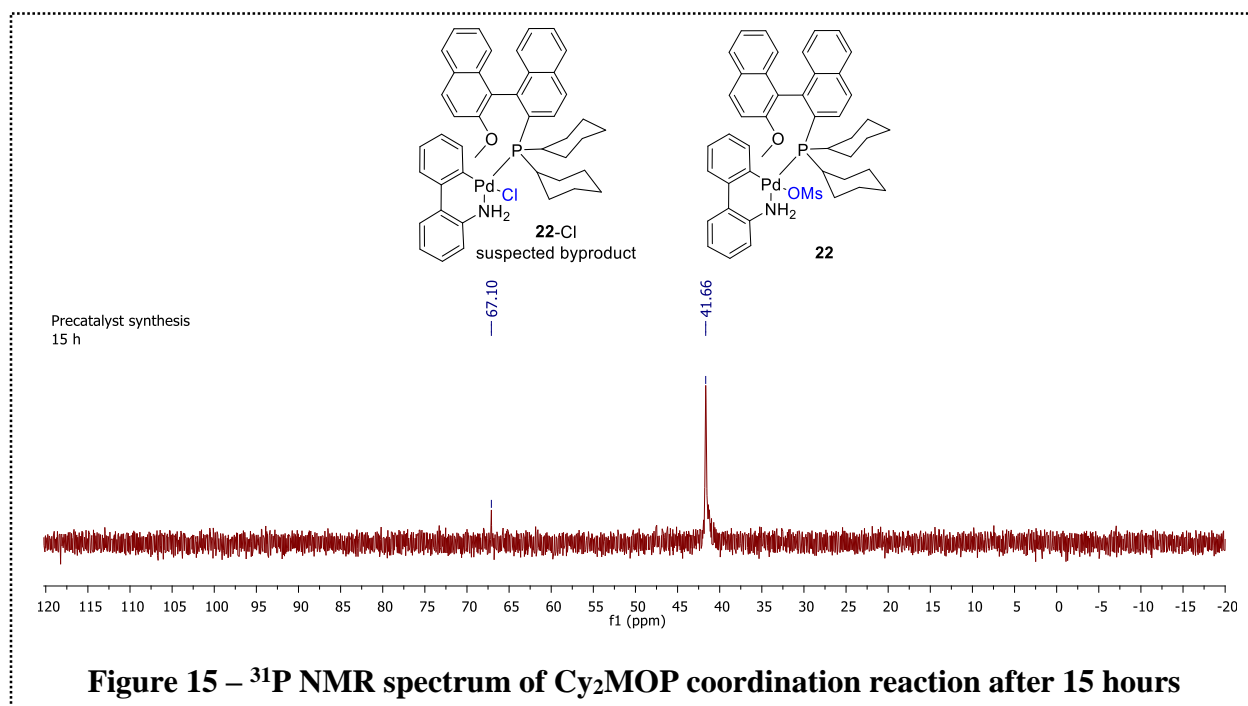
The synthesis of the Cy₂MOP-Pd precatalyst, shown in Scheme 52, was initially conducted on an analytical scale to determine whether the phosphane could be ligated onto the 2-aminobiphenyl methanesulfonate palladium backbone. The phosphane, Cy₂MOP **16**, and the



methanesulfonate dimer **21**, were transferred to an NMR tube using deuterated chloroform as the reaction solvent. The reaction progress was monitored *via* ³¹P NMR spectroscopy, observing the disappearance of the signal at δ -8.90 ppm characteristic of the free phosphane and appearance of the signal at *ca.* δ 45 ppm, in the neighbourhood of other third generation Buchwald precatalysts.⁴⁹



The ^{31}P NMR spectrum, presented in Figure 14, was obtained after 20 minutes of sonication to ensure proper mixing of the reagents. Appearance of the new signal at *ca.* δ 42 ppm supported that the $\text{Cy}_2\text{MOP-Pd}$ precatalyst had been successfully generated. When 2 hours had elapsed the reaction progress was examined again and the signal at δ -8.90 ppm was no longer present, confirming the complete consumption of Cy_2MOP . In a scaled up procedure, DCM was used as the reaction solvent and high yield of the precatalyst was obtained (up to 91%). In the initial scaled

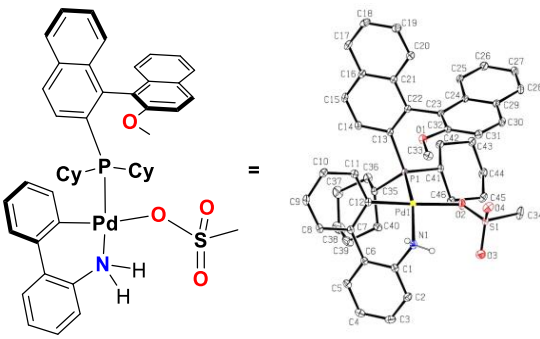


up trials, chloroform was used as the reaction solvent, attempting to replicate the analytical scale reactions as closely as possible, however it was found that prolonged storage in chloroform led to a gradual increase in a new signal which appeared downfield of the methanesulfonate palladium precatalyst at δ 67.10 ppm, as presented in Figure 15. The chemical shift of this ^{31}P NMR signal is characteristic of the chlorido-bridged second generation Buchwald-type precatalysts which are observed around δ 65 to 70 ppm. The reaction also proceeded smoothly when THF was used as the reaction solvent. The workup procedure consisted of evaporating the reaction solvent until a

minimum amount remained in the flask, then triturating the residue with pentane or ether and then isolating the precatalyst by filtration through a fritted funnel.

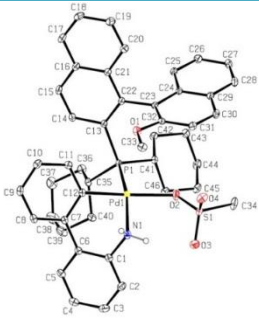
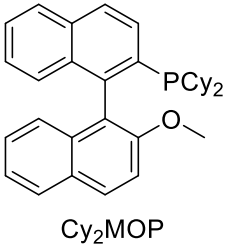
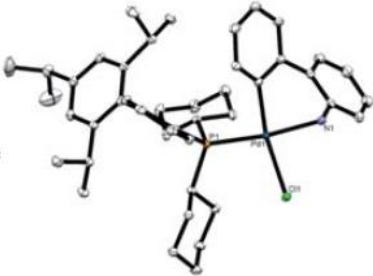
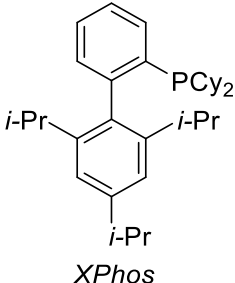
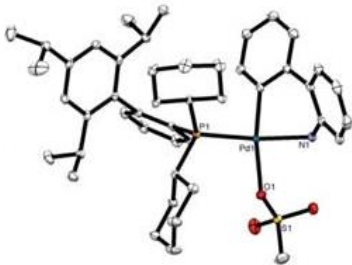
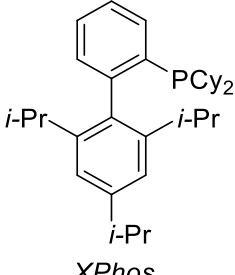
The solid state structure of the Cy₂MOP-Pd precatalyst was determined *via* X-ray crystallography. Racemic precatalyst was used towards obtaining a single crystal for X-ray structural analysis. Suitable crystals could be generated *via* slow evaporation from benzene, or by using the liquid/liquid diffusion technique (*i.e.* solvent layering technique), where the solid was dissolved in DCM and the solution was carefully covered with a layer of diethyl ether. The crystals obtained from benzene were used in the analysis and 2.5 benzene molecules per palladium complex were observed in the crystal structure. The key structural features of the complex include a coordinatively saturated palladium centre with a distorted square planar geometry, which can be inferred from the data presented in Table 4. The characteristic Pd-N, Pd-P, and Pd-C bond lengths

Table 4. X-ray structure of Cy₂MOP-Pd precatalyst and relevant bond angles

Crystal Structure of Cy ₂ MOP-Pd Precatalyst ^a	Bond Angles (°)	
	C(12)-Pd-NH ₂	85.25(7)
	C(12)-Pd-OMs	173.06(6)
	H ₂ N-Pd-OMs	92.65(6)
	C(12)-Pd-P	90.28(5)
	H ₂ N-Pd-P	161.27(5)
	MsO-Pd-P	93.74(4)
^a H atoms have been omitted from the X-ray crystal structure for clarity.		

are comparable to those of related structures reported by Buchwald,⁴⁹ as highlighted in Table 5. As observed by Buchwald in related precatalyst systems, the 2-aminobiphenyl ligand chelates the palladium centre, and the phosphane, Cy₂MOP in this case, is in the *cis*-conformation relative to the aryl moiety of the palladium-bound carbon of the 2-aminobiphenyl.

Table 5. X-ray structure of Cy₂MOP-Pd precatalyst and related structures

Precatalyst ^a	Phosphane Ligand	Bond Lengths (Å)	
	 Cy ₂ MOP	Pd-NH ₂	2.1319(15)
		Pd-OMs	2.1516(12)
		Pd-P	2.2800(5)
		Pd-C(12)	1.9852(17)
	 XPhos	Pd-NH ₂	2.1263(9)
		Pd-Cl	2.4121(3)
		Pd-P	2.2857(3)
		Pd-C	2.0170(10)
	 XPhos	Pd-NH ₂	2.1169(13)
		Pd-OMs	2.1838(11)
		Pd-P	2.2851(4)
		Pd-C	2.0078(15)

^a Crystallographically determined X-ray structures of second and third generation precatalysts based on XPhos reported by Tudge and Buchwald.⁴⁹

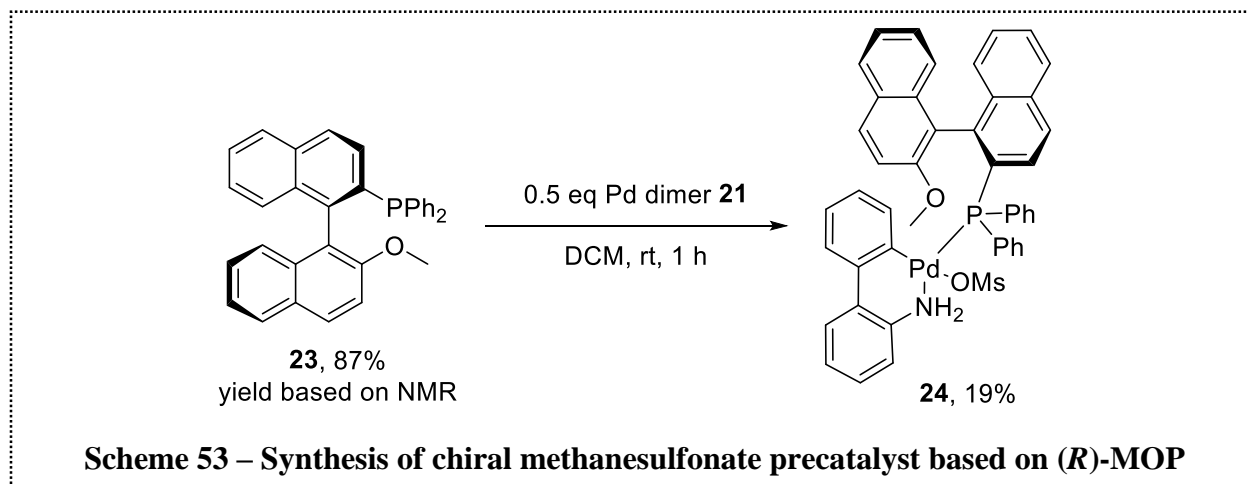
Enantioselectivities can be highly sensitive to dihedral angles of the chiral supporting ligands used.^{78,79} The dihedral angle between the naphthyl rings is directly related to the bulkiness of the substituents in the 2- and 2'-positions. The relevant dihedral angles of the biaryl moiety of the palladium-ligated phosphane ligand are highlighted in Table 6. The naphthyl rings are slightly distorted from the expected planar geometries with respect to the fused rings. The dihedral angle between the naphthyl rings, defined by C21-C22-C13 and C24-C23-C32 is 80.3°. The extended

tables of crystallographic data including the atomic coordinates, anisotropic displacement parameters and lists of bond lengths and angles are included in Appendix 5.3.

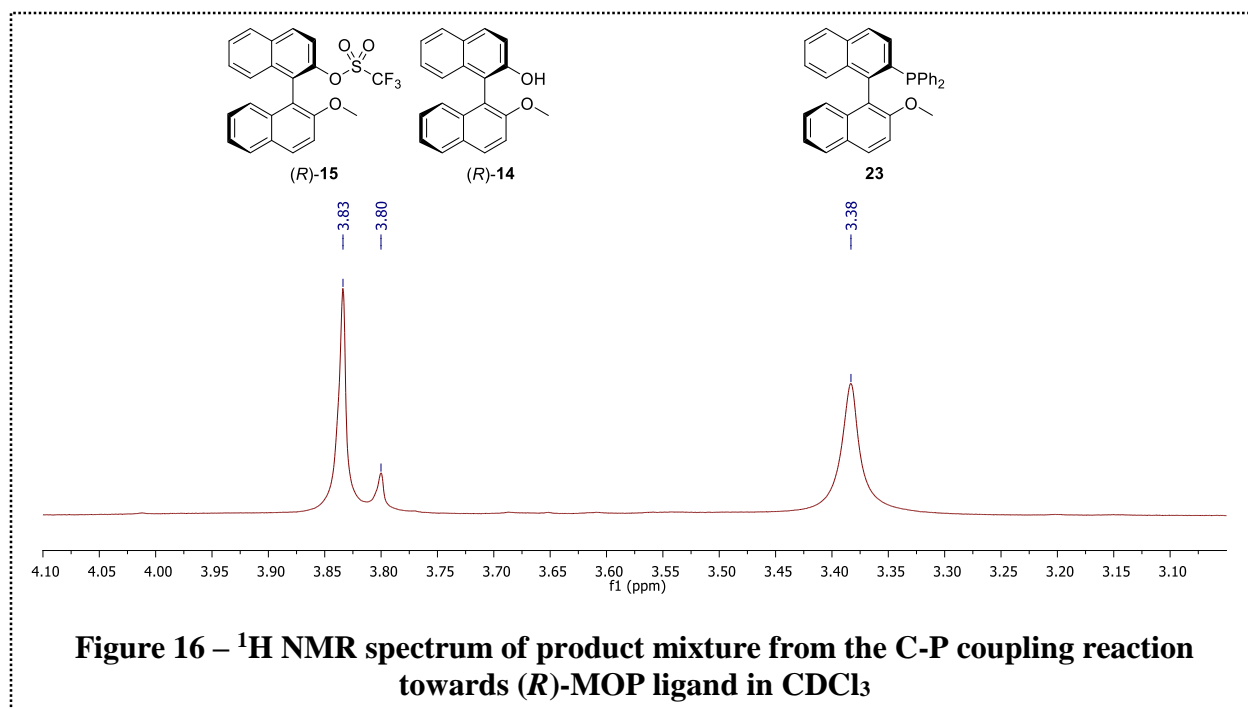
Table 6. Dihedral angles of phosphane moiety of Cy₂MOP-Pd precatalyst

Precatalyst	Phosphane Ligand	Dihedral Angles (°)	
		C(13)-C(22)-C(23)-C(32)	-80.3(2)
		C(21)-C(22)-C(23)-C(32)	96.71(19)
		C(13)-C(22)-C(23)-C(24)	105.9(2)
		C(21)-C(22)-C(23)-C(24)	-77.0(2)

Since (*R*)-MOP is versatile as a supporting ligand in asymmetric transition-metal-catalysis^{91,92} and was previously investigated in the enantioselective cross-couplings in our original report,⁶¹ the methanesulfonate 2-aminobiphenyl precatalyst containing (*R*)-MOP **23** was synthesized as well, following the route outlined in Scheme 53. (*R*)-MOP was prepared following



the pathway detailed in Section 2.1.6 (p. 53) except diphenylphosphane was employed as the coupling partner with Me-BINOL-OTf **15**. Diphenylphosphane is highly flammable and it readily oxidizes upon exposure to air, thus it was dispensed in a nitrogen atmosphere glovebox. Analysis



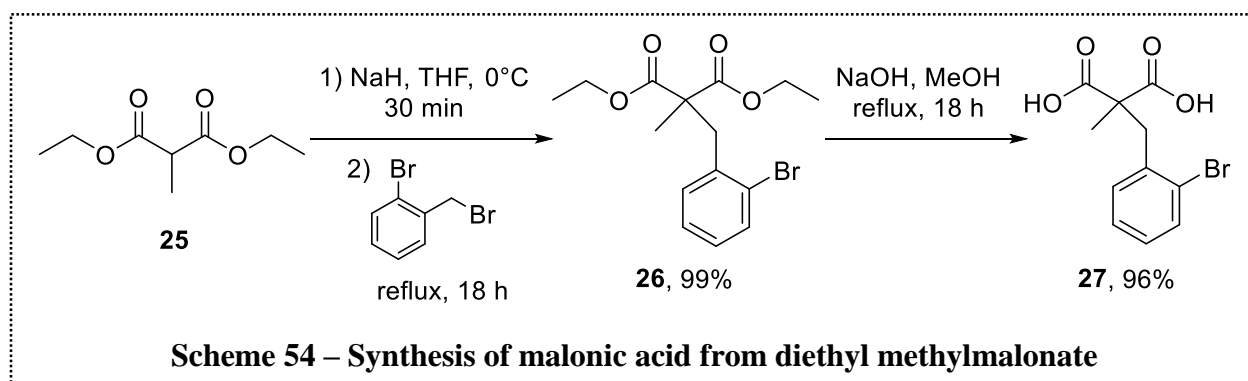
of the crude ^1H NMR spectrum (refer to Figure 16) revealed the presence of at least three compounds, as indicated by the singlets arising from unique methoxy groups. The ^{31}P NMR spectrum showed evidence of several phosphorus-containing products including two major signals for the desired product, (*R*)-MOP,⁸⁷ (δ -13.67 ppm) and diphenylphosphane oxide (δ -21.39 ppm).⁹³ Separation *via* column chromatography eluting with 1:1 DCM/hexanes was unsuccessful and further investigation of solvent systems which might provide improved separation is required. An additional byproduct from the reaction was (*R*)-**14** generated from the hydrolysis of the triflate (*R*)-**15** under the basic conditions, high temperature and prolonged time that was required for the C-P coupling. The reaction yield was estimated using the proton resonance signal integration ratio of the methoxy group in the starting material, (*R*)-**15**, to that in the desired product **23**.

The impure (*R*)-MOP **23** was used directly in the synthesis of the desired palladacyclic precatalyst. The methanesulfonate-bridged dimer **21** was treated with the triflate/phosphane mixture in DCM at room temperature for 2 h. The ligand was found to be compatible with the third

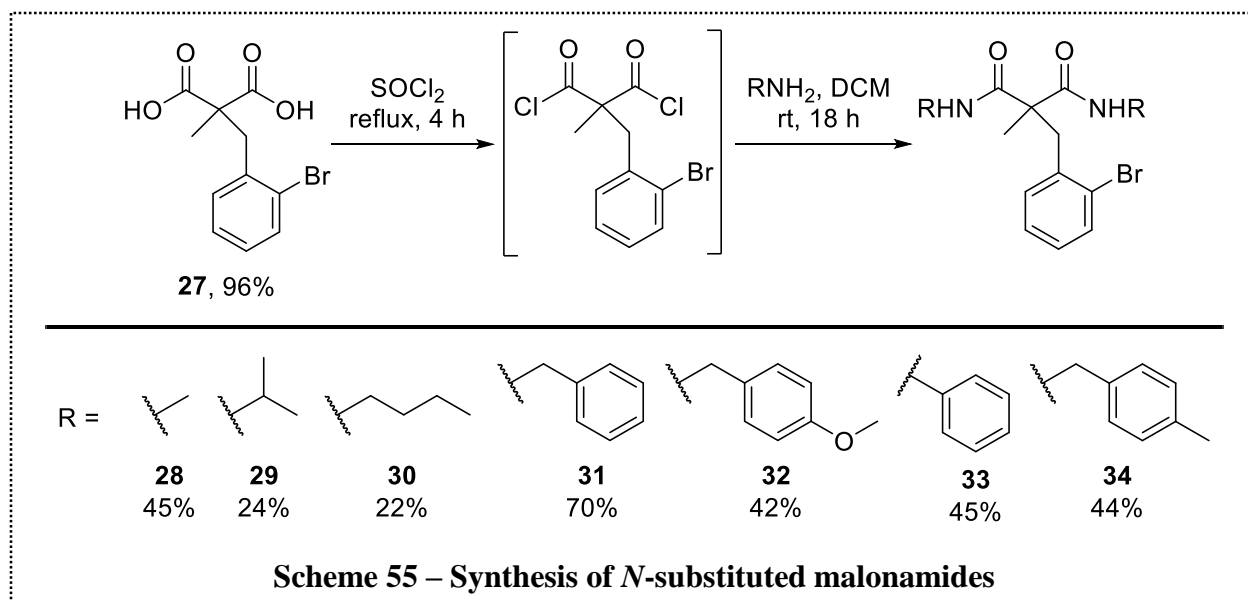
generation-type scaffold, with the precatalyst complex afforded in 19% yield. The ^{31}P NMR spectrum exhibited two signals, one at δ 37.38 ppm and the other at δ 36.40 ppm, suggesting the presence of two conformations, likely rotamers. Buchwald reported a similar effect from the second generation precatalyst complex based on *XPhos* was employed and two peaks were observed due to rotamers.⁴⁸

2.3 Synthesis of quinolinones *via* palladacycle-catalyzed Buchwald-Hartwig reaction

The prochiral α -bromobenzyl malonamides were prepared on a 2 mmol scale *via* alkylation and base catalyzed ester hydrolysis as shown in Scheme 54. Deprotonation of diethyl



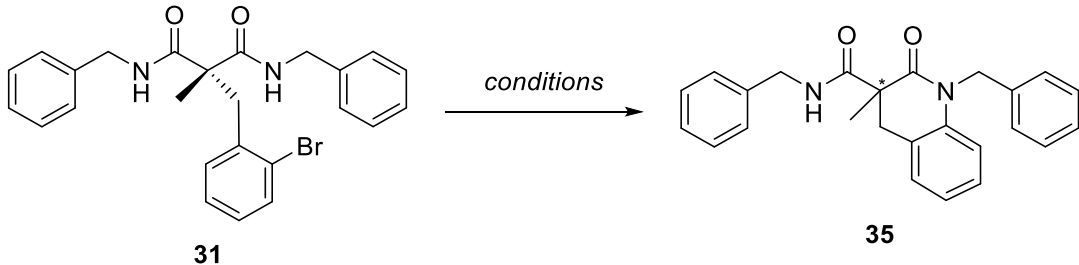
methylmalonate **25** at the α -carbon using NaH at 0°C followed by alkylation with 2-bromobenzyl bromide at reflux provided the malonate ester **26** as a colourless oil in excellent yield (99%). Following purification *via* flash column chromatography, the diester **26** was saponified followed by an acidic workup to afford the malonic acid **27** in 96% yield. The malonamides were obtained in low to moderate yields by treating **27** with thionyl chloride at reflux to generate the diacid



chloride which was used directly in the reaction with the desired amine (Scheme 55). The malonamides were purified *via* recrystallization in the appropriate solvent.

Using the palladacycle Cy₂MOP-Pd precatalyst the desymmetrization reactions of the α-(2-bromobenzyl)malonamides were carried out. In the report by Porosa and Viirre,⁶¹ a two-component palladium-catalyst system consisting of 3.3 mol% Pd(OAc)₂ and 6.6 mol% (*R*)-MOP was employed. These reaction conditions served as a starting point for the optimization of the conditions in the reaction using a single-component palladium precatalyst. Selected trials towards the optimization of the C-N cross-coupling reaction using the dibenzyl malonamide **31** as the test substrate are displayed in Table 7. While the precatalyst is air-stable, the cross-coupling reactions were still performed under inert nitrogen atmosphere to avoid destroying the generated palladium(0) species in open air over time with the application of heat.

Table 7. Optimization of malonamide cyclization reaction conditions^a

					
Entry	Catalyst loading (mol%)	Solvent	Temperature (°C)	Time (h)	Yield (%) ^b
1	3.3	Toluene	100	48	81 ^e
2	3.3	THF	60	48	96
3	3.3	THF	60	24	96
4	1.0	THF	60	24	96 ^f
5	0.1	THF	60	24	57 ^c
6	1.0	THF	45	24	40 ^{c,g}
7	1.0	THF	45	24	n.d. ^d

^a α -Bromobenzyl malonamide **31** was used in the screening of reaction conditions using 1.4 eq Cs₂CO₃. ^b Average isolated yield of two trials. ^c Yield based on a single trial. ^d Precatalyst activation procedure was used and crude product was analyzed by ¹H NMR spectroscopy. ^e The *er* determined by chiral HPLC was 51:49; ^f 54:46; ^g 54:46.

The C-N coupling reaction was initially conducted using the *rac*-Cy₂MOP-Pd precatalyst **22** (Table 7, entry 1) in order to compare the enantioselectivity achieved to that where the (*R*)-Cy₂MOP-Pd precatalyst was used. As expected, the racemic precatalyst used in this system demonstrated no asymmetric induction. Optimization of the HPLC analysis conditions for **35** was conducted using the product from this trial in order to establish conditions which provide good resolution of the peaks for either enantiomer. This was necessary to facilitate subsequent determinations of enantiomeric ratios achieved in the reactions using the (*R*)-Cy₂MOP-Pd precatalyst. The enantiopure (*R*)-Cy₂MOP-Pd precatalyst was employed in the desymmetrization reaction for all subsequent trials. An improved yield was obtained when THF was used in place of toluene (Table 7, entry 2). There was starting material remaining in the reaction mixture after 24 hours, as revealed in the ¹H NMR spectrum of the crude product, however, the yield was not

negatively affected when the reaction was stopped after 24 hours rather than 48 hours. Next, experiments towards lowering the catalyst loading were investigated. The loading was decreased from 3.3 mol% to 1.0 mol% (Table 7, entry 4), then to 0.1 mol% (Table 7, entry 5). The reaction using 1.0 mol% (*R*)-Cy₂MOP-Pd precatalyst at 60 °C was found to be most efficient with 96% yield obtained. However, the enantiomeric ratio observed in the cyclized product **35** was only 54:46. The trial conducted using 0.1 mol% was unsuccessful, with a significant decrease in yield to 57%.

Towards investigating the lower temperature limits of the reaction with the goal of improving enantioselectivity, the reaction was carried out at 45 °C. Lowering the temperature resulted in a dramatic decrease in the yield with only 40% of the quinolinone product isolated and there was no improvement in the enantiomeric ratio observed (Table 7, entry 6). It was suspected that at the lower temperature the precatalyst activation was not proceeding as effectively as at the standard temperature (60 °C) trials, resulting in the low conversion. To address this, an activation procedure was carried prior to completing the reaction setup for the cyclization. The precatalyst activation procedure involved pre-stirring the malonamide and precatalyst with 10 mol% of Cs₂CO₃ at 60 °C for 30 minutes, then cooling the mixture to 45 °C and adding the remainder of the base (Table 7, entry 7). The crude product was analyzed by ¹H NMR spectroscopy and was found to consist mainly of starting material.

The aim was to compare the effectiveness of the two-component catalyst system based on (*R*)-MOP and the single-component (*R*)-Cy₂MOP-Pd precatalyst **22**. The activity of the precatalyst was inferior in the studied reaction system with no conversion observed in the cases of the methyl, isopropyl, and *n*-butyl malonamides **28** – **30**, respectively. Incomplete conversion to the corresponding quinolinone was observed in the case of malonamides **32** and **33**. The

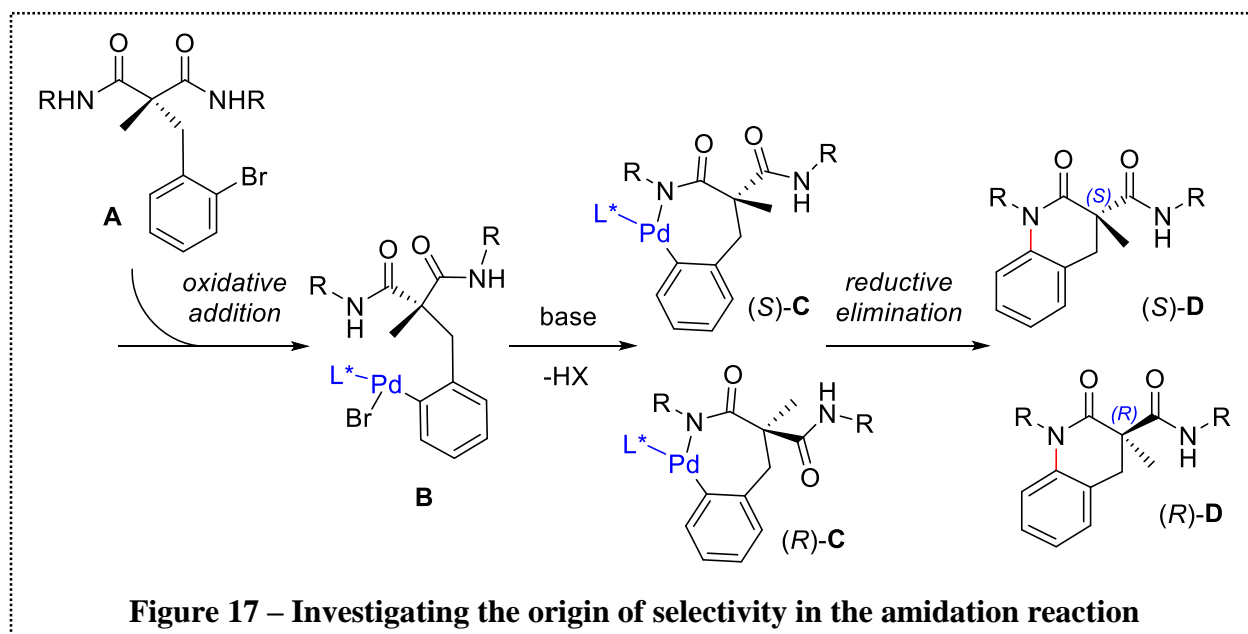
enantioselectivity was not determined from these reactions. The discrepancy between the results presented in the 2009 report⁶¹ and those obtained with the new catalyst system **22** could possibly arise from a combination of various factors. The activity of the catalyst species might be affected by the mode of delivery or the activation pathway of the catalyst which differ between the single-component versus the two-component systems.

More significantly however, the chiral phosphane was modified between the two sets of reactions, with (*R*)-MOP having been employed in the two-component system and (*R*)-Cy₂MOP in the current work. The electronic and steric properties of the ligands likely played a major role in the efficacy of the cross-coupling reaction. It was assumed that the dialkylbiaryl phosphane, Cy₂MOP **16**, would have a positive effect on the activity of the catalyst system since it is electron-rich and this aids in the oxidative addition step of the aryl halide. In addition, the cyclohexyl groups provide a fair amount of steric bulk which enhances the rate of reductive elimination. However, it was observed that the catalyst containing the comparatively electron-poor ligand, (*R*)-MOP, outperformed the (*R*)-Cy₂MOP-Pd precatalyst in terms of activity. The enantioselectivity achieved using the (*R*)-Cy₂MOP-Pd precatalyst was not impressive in the case of **35** where negligible asymmetric induction was observed. Insight regarding the origin of selectivity in the reaction might explain why the two systems differed so greatly in terms of enantioselectivity as well. To investigate which factor led to the low activity of the precatalyst, experiments must be conducted using the analogous (*R*)-MOP-Pd precatalyst to determine whether the precatalyst palladacycle itself and its mode of delivery are what influence the activity. In addition, experiments using a two-component system based on (*R*)-Cy₂MOP and a palladium source should be conducted to assess the influence of the phosphane ligands on the catalytic activity in this reaction. Overall, the

electronic and steric variability between the (*R*)-Cy₂MOP and (*R*)-MOP phosphane ligands were found to be extremely important in the desymmetrization reaction.

2.4 Investigating the origin of selectivity in the desymmetrization of malonamides

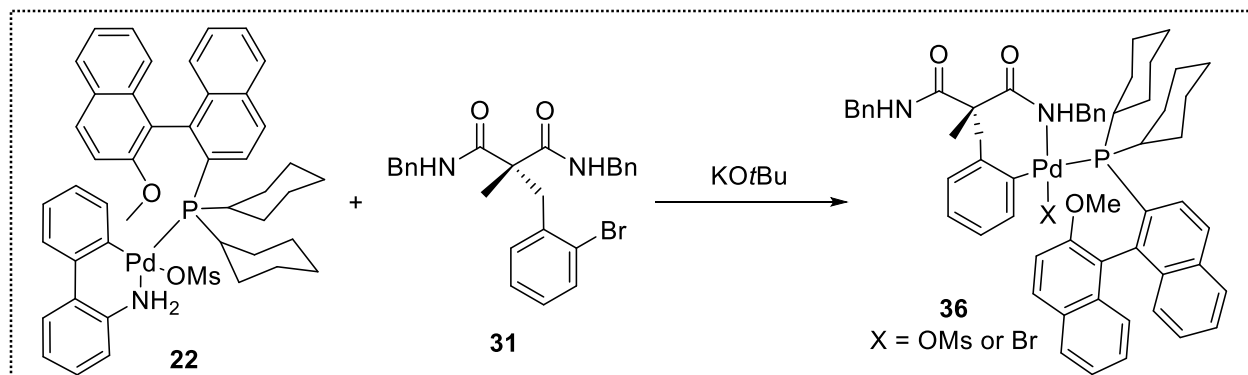
Structural information of specific reaction intermediates within the catalytic cycle in the palladium-catalyzed desymmetrization of malonamides remains elusive to a certain extent. The atropisomeric ligand, Cy₂MOP, was employed to provide the chiral discrimination motif for asymmetric induction. Following oxidative addition of the aryl bromide to the phosphane-ligated palladium(0) source, the two amide protons of the palladium(II) oxidative addition complex **B** are diastereotopic. Stereochemical control of the reaction likely results from the steric bias presented by the methyl on the α -carbon versus the *N*-substituent of the malonamide, as shown in Figure 17.



The *N*-substituent points away from the sterically encumbered space of the amide-bound palladium complex leaving only one of the amide NH nucleophiles accessible to react. The absolute configuration of the quinolinone products would need to be determined in order to propose the exact structure of the reaction intermediate accessed in the amidation reaction.

One of the research objectives was to study the individual steps in the catalytic cycle mechanism, mainly the “transmetallation” step, which is the coordination of the amide nucleophile to the palladium(II) centre of the intermediate complex **B** and subsequent deprotonation, forming a palladium-amido species **C**. This might provide insight regarding the origin of enantioselectivity. In a kinetic study of intermolecular aryl amidation of primary amides in the presence of a monodentate phosphane ligand, the results suggested that transmetallation step constitutes the rate determining step.^{94,95} The challenges associated with this step are likely more pronounced in the malonamide substrates since the NH nucleophiles are larger secondary amides. Isolating a crystal of a palladium-amido intermediate complex *via* treatment of the test malonamide substrate **31** with a stoichiometric amount of the enantiopure precatalyst was desired. Following the synthesis and characterization of this reaction species, it would be subjected to basic conditions in the appropriate solvent under inert conditions to confirm that the products observed are consistent with those in the catalytic system.

The propensity of this system to undergo reductive elimination was a foreseeable challenge which was expected to potentially limit this strategy. The measure taken to prevent catalytic turnover involved adding small aliquots of the base at a time and monitoring the precatalyst consumption and conversion by ³¹P NMR spectroscopy. A series of reactions were conducted on an analytical scale reacting the dibenzyl malonamide **31** with the precatalyst in the presence of KO^tBu in deuterated benzene as shown in Scheme 56. A ratio of 1:1 of malonamide to precatalyst was used while titrating base equivalents. The ³¹P NMR signal for the precatalyst complex



Scheme 56 – Towards the synthesis of a palladium-amido species of the catalytic cycle

appeared at *ca.* δ 43 ppm in deuterated benzene. Following the addition of 0.25 equivalents of KO^tBu , the sample was gently warmed and sonicated to dissolve the starting reagents. The reaction was monitored periodically and two new weak signals and disappearance of the signal corresponding to the precatalyst were observed after 1 hour of sonication (Figure 18). The poor

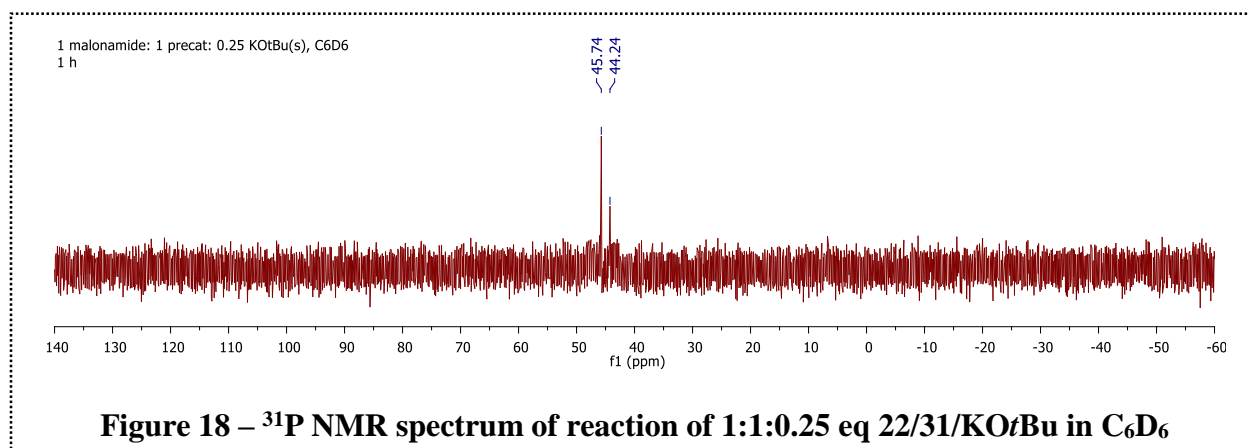
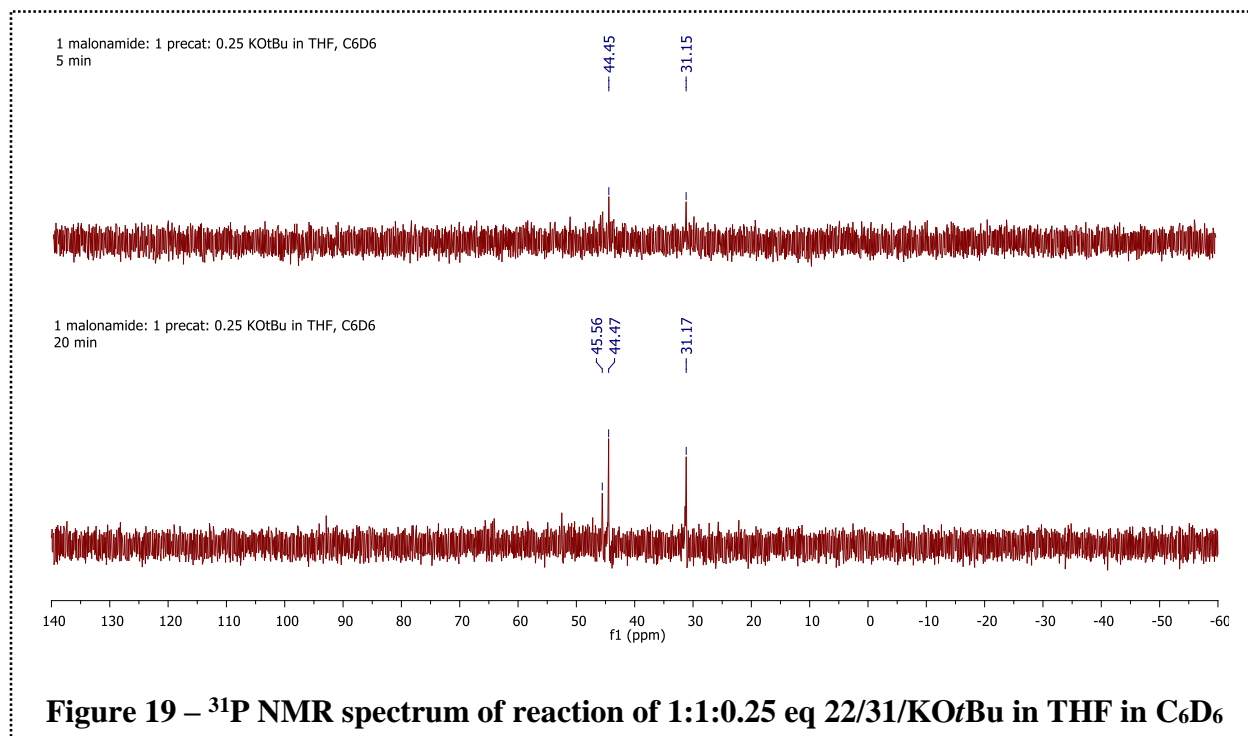


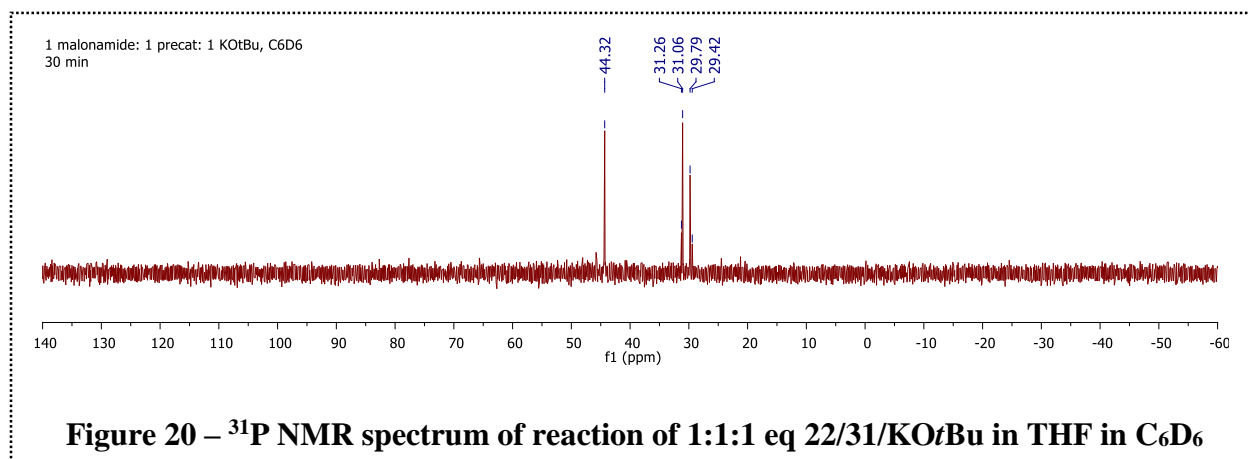
Figure 18 – ^{31}P NMR spectrum of reaction of 1:1:0.25 eq 22/31/ KO^tBu in C_6D_6

solubility of the base in deuterated benzene precluded quantification of base consumed in the reaction and made it difficult to determine qualitatively what was occurring during the reaction (*i.e.* whether or not a precipitate was formed). To overcome this issue a stock solution of KO^tBu

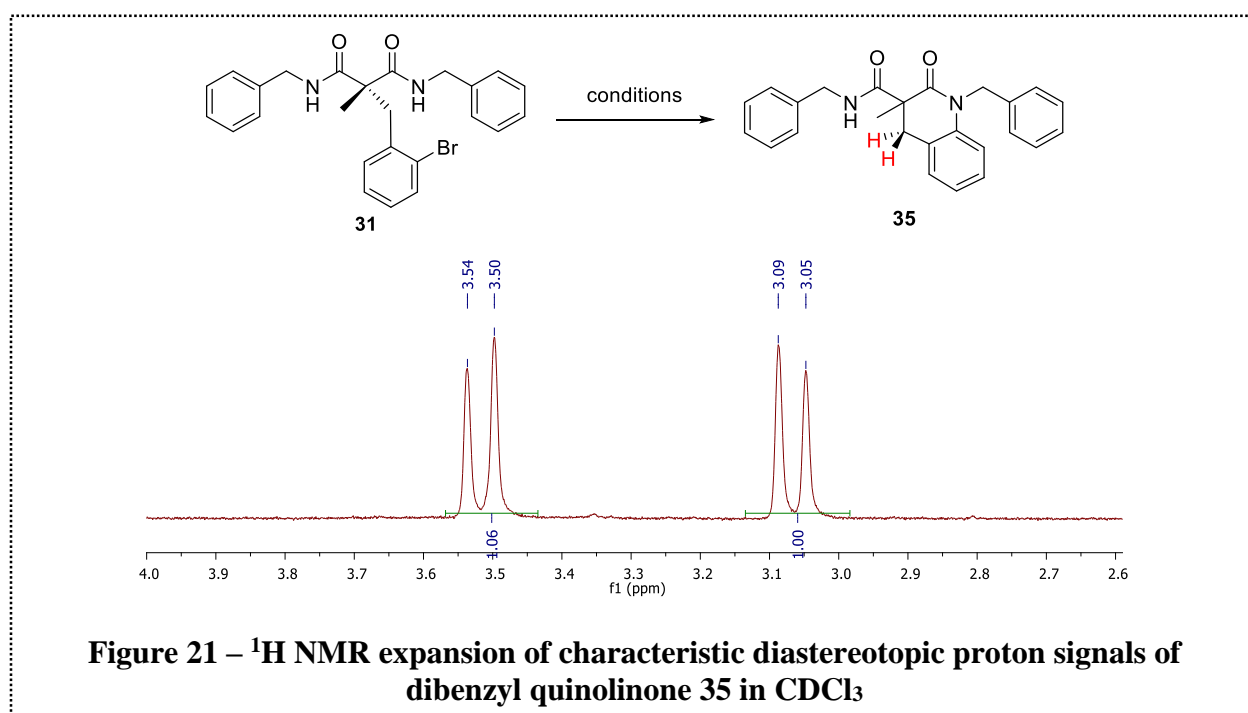
in THF was used to dispense 0.25 equivalents (Figure 19). After 5 minutes the signal characteristic of the precatalyst complex disappeared and two new signals were observed, one in the same region of the spectrum at δ 44.47 ppm, and the other further upfield at δ 31.17 ppm. After 20 minutes an additional signal was observed at δ 45.56 ppm. The results from reacting a full equivalent of



KOtBu at once was tested next and four new signals in the ^{31}P NMR spectrum appeared, as shown in Figure 20, with only the proportions of these products changing over 2 hours.



The reaction was scaled up from the analytical scale in order to workup the reaction to isolate and identify the compounds which gave rise to the observed ^{31}P NMR signals. The workup procedure consisted of the removal of insoluble salts *via* filtration, evaporation of about 90% of reaction solvent followed by trituration of the product mixture using pentane with the aid of sonication. The resulting solid was then filtered and dried *in vacuo*. All attempts led to a signal in the ^{31}P NMR spectrum around δ 47 ppm which is consistent with the signal of the phosphane oxide of Cy₂MOP.⁹⁶ Also noteworthy, the coupled product was not observed in the product mixture according to the ^1H NMR spectrum determined by the absence of the diastereotopic proton signals (refer to Figure 21). Successfully determining how the different structural features of the catalyst



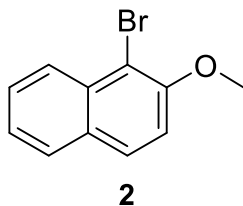
system influence the geometry of the reaction intermediates could improve our understanding of the origin of selectivity which in turn could lead to the development of more effective catalysts for this class of reactions. Further work towards this objective is required.

3 Experimental

3.1 General information

All reagents were purchased from commercial suppliers and used without further purification. Dry solvents were obtained from a solvent purification system and used directly as reaction solvents. Microwave reactions were performed on a Biotage® Initiator Microwave Synthesizer (2.45 GHz) using sealed glass reaction vials. Silicycle SiliaFlash® P60 Academic Silica gel (particle size 40–63 μm) was used for flash column chromatography. Analytical TLC was performed on silica gel 60 F254 aluminum-backed plates and visualized by ultraviolet fluorescence quenching and fluorescence with the aid of an ultraviolet lamp ($\lambda = 254$ and 365 nm, respectively). Nuclear magnetic resonance spectroscopy was conducted on a Bruker Avance 400 MHz instrument. ^1H NMR spectra were measured relative to residual protiated solvent signals which in turn were referenced to the methyl resonance signal of TMS at δ 0 ppm. $^{13}\text{C}\{^1\text{H}\}$ NMR spectra were measured relative to the carbon signals of the respective deuterated solvent. $^{19}\text{F}\{^1\text{H}\}$ and $^{31}\text{P}\{^1\text{H}\}$ NMR spectra were recorded relative to external references, CFCl_3 and 85% H_3PO_4 , respectively. Melting points were determined using a Fisher-Johns melting point apparatus and are uncorrected. HPLC analyses were performed on an Agilent 1260 Infinity instrument with a diode array and multiple-wavelength detector using a $4.6\text{ mm} \times 250\text{ mm}$ Chiralpak OD-H column with cellulose tris(3,5-dimethylphenylcarbamate) coated on $5\text{ }\mu\text{m}$ silica gel as the stationary phase. Crystallographic X-ray diffraction data were collected using a Bruker-Nonius Kappa-CCD diffractometer with monochromated Mo-K α radiation ($\lambda = 0.71073\text{ }\text{\AA}$) at the University of Toronto by Dr. Alan Lough.

3.2 Towards benzene-based *ortho*-bromobiaryl

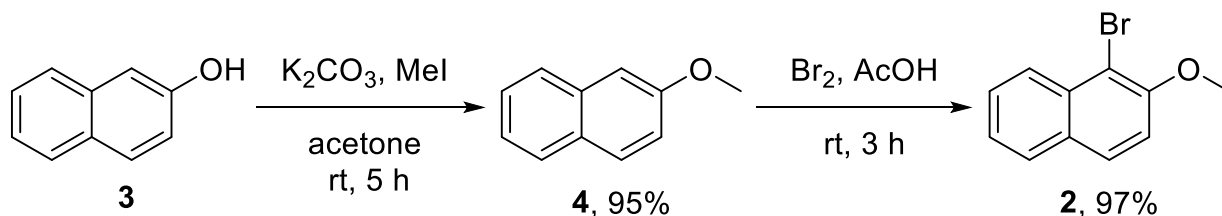


Synthesis of 1-Bromo-2-methoxynaphthalene (2)

Method 1. Methylation of bromo-2-naphthol

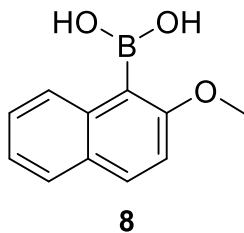
A solution of bromo-2-naphthol (6.06 g, 26 mmol) in acetone (40 mL) was prepared in an oven-dried 250-mL round-bottom flask equipped with a magnetic stir bar. Potassium carbonate (7.19 g, 52 mmol) was added while stirring and after 20 minutes, iodomethane (3.24 mL, 52 mmol) was added dropwise. The mixture was stirred for 22 hours at room temperature and the reaction progress was monitored periodically by TLC (10% ethyl acetate in hexanes) until there was no evidence of starting material present. The reaction mixture was concentrated under reduced pressure, then re-dissolved in diethyl ether (50 mL). The organic layer was washed with distilled water (3×50 mL), dried over anhydrous MgSO_4 , filtered, and concentrated under reduced pressure. The resulting product was dried *in vacuo* to afford the title compound as colourless crystals. Yield 86% (5.30 g).

Method 2. Bromination of 2-methoxynaphthalene

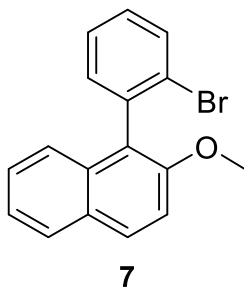


In a 2-L round-bottom flask equipped with a magnetic stir bar, 2-naphthol (100.0 g, 0.6936 mol) was dissolved in acetone (1300 mL). Potassium carbonate (191.7 g, 1.387 mol) was added and stirred for 20 minutes after which, iodomethane (86.3 mL, 1.387 mmol) was added dropwise. The

mixture was stirred at room temperature for 5 hours and the reaction progress was monitored by TLC (10% ethyl acetate in hexanes) until there was no evidence of starting material present in the reaction mixture. The reaction mixture was filtered through a pad of celite. The precursor **4** was afforded as a white solid. Yield 95% (104.4 g); Melting point: 73 – 74 °C; TLC: 10% ethyl acetate in hexanes, R_f = 0.44; ^1H NMR (400 MHz, CDCl_3) δ 7.81 – 7.73 (m, 3H), 7.49 – 7.42 (m, 1H), 7.39 – 7.32 (m, 1H), 7.21 – 7.12 (m, 2H), 3.94 (s, 3H) ppm; ^{13}C NMR (101 MHz, CDCl_3) δ 157.62, 134.59, 129.39, 128.98, 127.66, 126.74, 126.37, 123.59, 118.71, 105.79, 55.30 ppm. Spectroscopic data are consistent with the literature data.⁹⁷ A solution of 2-methoxynaphthalene **4** (10.000 g, 63.2 mmol) in acetic acid (50 mL) was prepared in an oven-dried 250-mL round-bottom flask equipped with a magnetic stir bar. Bromine (3.2 mL, 63.2 mmol) diluted with 15 mL acetic acid was added to the flask slowly *via* addition funnel and the reaction mixture was stirred for 3 hours at room temperature. The formed precipitate was filtered and washed with cold distilled water then dried *in vacuo* to provide the title compound as a white solid. Yield 97% (14.531 g); Melting point: 82 – 83 °C; TLC: 10% ethyl acetate in hexanes, R_f = 0.42; ^1H NMR (400 MHz, CDCl_3) δ 8.23 (d, J = 8.6 Hz, 1H), 7.83 (d, J = 9.0 Hz, 1H), 7.79 (d, J = 8.2 Hz, 1H), 7.57 (ddd, J = 8.4, 6.8, 1.2 Hz, 1H), 7.40 (ddd, J = 8.0, 6.9, 1.1 Hz, 1H), 7.29 (d, J = 9.0 Hz, 1H), 4.04 (s, 3H) ppm; ^{13}C NMR (101 MHz, CDCl_3) δ 153.88, 133.25, 129.94, 129.10, 128.17, 127.88, 126.25, 124.45, 113.73, 108.78, 57.19 ppm. Spectroscopic data are consistent with the literature data.⁹⁷

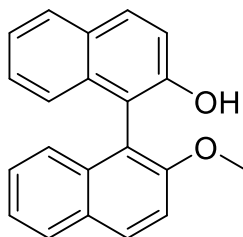


2-Methoxy-1-naphthylboronic acid (8). A flame-dried 250-mL Schlenk flask equipped with a magnetic stir bar was flushed with nitrogen gas. The flask was charged with magnesium turnings (1.8631 g, 76.67 mmol), THF (50 mL) and a crystal of iodine. Following the activation of the magnesium indicated by the disappearance of yellow colour from the solution, 1-bromo-2-methoxynaphthalene **2** (15.0001 g, 63.2671 mmol) dissolved in THF (50 mL), was added dropwise to the reaction mixture. The reaction mixture was heated at 60 °C and progress was monitored periodically by TLC (1:4 ethyl acetate to hexanes), quenching a drop of the reaction mixture with methanol. Upon complete disappearance of **2**, the reaction mixture was cooled to -84 °C and trimethylborate (14.1 mL, 126.5 mmol) slowly added. After 30 minutes at -84 °C, the mixture was allowed to warm to room temperature and stirred for 18 hours. Distilled water (20 mL) was added and the reaction mixture was left stirring until a homogeneous mixture resulted. The volatiles were removed under reduced pressure and the remaining aqueous solution was extracted using DCM (3×50 mL). The organic layer was dried over anhydrous MgSO₄, filtered, and concentrated, and the resulting solid was re-suspended in cold DCM. The mixture was stirred for 10 minutes, filtered and washed with cold DCM to afford the title compound as a white solid. Yield 85% (10.8808 g); Melting point: 117 – 119 °C; ¹H NMR (400 MHz, CDCl₃) δ 8.84 (d, *J* = 8.5 Hz, 1H), 7.94 (d, *J* = 8.9 Hz, 1H), 7.78 (d, *J* = 8.1 Hz, 1H), 7.56 – 7.45 (m, 1H), 7.42 – 7.33 (m, 1H), 7.28 (d, *J* = 9.0 Hz, 1H), 6.11 (s, 2H), 4.03 (s, 3H) ppm; ¹³C NMR (101 MHz, (CD₃)₂SO) δ 159.01, 136.17, 129.79, 128.95, 128.34, 127.80, 126.30, 123.51, 114.18, 56.60 ppm. The carbon attached to the boron was not observed due to quadrupole broadening caused by the ¹¹B nucleus. Spectroscopic data are consistent with the literature data.⁹⁸



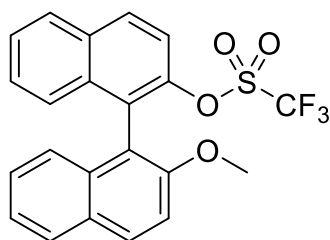
1-(2-Bromophenyl)-2-methoxynaphthalene (7). A flame-dried 50 mL Schlenk flask equipped with a magnetic stir bar, was flushed with nitrogen gas then charged with 2-methoxy-1-naphthylboronic acid **8** (2.0201 g, 1.000 mmol) and dioxane (72 mL). The mixture was degassed for 10 minutes before adding 1,2-dibromobenzene (4.82 mL, 40.00 mmol) followed by 2.5 mol% Pd(PPh₃)₄ under inert atmosphere. A 7.5 M solution of potassium carbonate (8.0 mL) was degassed and added to the reaction mixture which was stirred at 100 °C for 72 hours. The reaction mixture was cooled to room temperature then diluted with ethyl acetate (50 mL) and washed with distilled water (4×50 mL). The organic layer was dried over anhydrous MgSO₄, filtered, and concentrated then purified by column chromatography, eluting with 10% ethyl acetate in hexanes, to provide the title compound as colourless crystals. Yield 45% (2.8187 g); Melting point: 120 – 122 °C; TLC: 10% ethyl acetate in hexanes, R_f = 0.34; ¹H NMR (400 MHz, CDCl₃) δ 7.94 (d, *J* = 9.0 Hz, 1H), 7.88 – 7.81 (m, 1H), 7.76 (dd, *J* = 8.4, 1.2 Hz, 1H), 7.47 – 7.41 (m, 1H), 7.38 (d, *J* = 9.0 Hz, 1H), 7.37 – 7.33 (m, 2H), 7.33 – 7.28 (m, 2H), 7.26 – 7.22 (m, 1H), 3.88 (s, 3H) ppm; ¹³C NMR (101 MHz, CDCl₃) δ 153.88, 137.81, 133.00, 132.72, 132.49, 129.78, 128.96, 128.86, 127.96, 127.29, 126.62, 125.42, 124.67, 124.24, 123.65, 113.67, 56.76 ppm. Spectroscopic data are consistent with the literature data.⁹⁹

3.3 Synthesis of binaphthyl-based chiral phosphanes



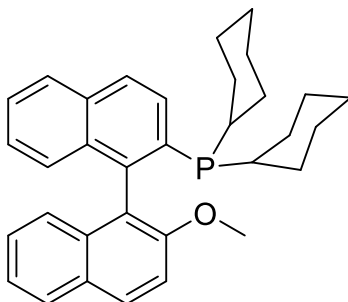
14

2'-Methoxy-[1,1'-binaphthalen]-2-ol (14). An oven-dried 250-mL round bottom flask equipped with a magnetic stir bar was charged with 1,1'-bi-(2-naphthol) (5.0000 g, 17.46 mmol) and acetone (70 mL). Potassium carbonate (2.6547 g, 19.21 mmol) was added and the mixture was stirred at room temperature for 30 minutes. The reaction was then cooled to 0 °C in an ice bath then iodomethane (1.2 mL, 19.21 mmol) was slowly added dropwise to the mixture followed by stirring at 50 °C for 18 hours. The reaction was cooled to room temperature then diluted with ethyl acetate and filtered through a pad of celite. The crude product was concentrated under reduced pressure and purified by column chromatography, eluting with DCM, to provide the title compound as colourless crystals. Yield 86 % (4.5156 g); Melting point: 152 – 154 °C for racemic-**14**; TLC: neat DCM, R_f = 0.32; ^1H NMR (400 MHz, CDCl_3) δ 8.06 (d, J = 9.1 Hz, 1H), 7.91 (d, J = 9.0 Hz, 2H), 7.87 (d, J = 8.1 Hz, 1H), 7.49 (d, J = 9.1 Hz, 1H), 7.43 – 7.27 (m, 4H), 7.25 – 7.15 (m, 2H), 7.05 (d, J = 8.2 Hz, 1H), 4.91 (s, 1H), 3.81 (s, 3H) ppm; ^{13}C NMR (101 MHz, CDCl_3) δ 156.01, 151.24, 134.04, 133.77, 131.08, 129.80, 129.45, 129.15, 128.15, 128.13, 127.33, 126.40, 124.91, 124.83, 124.19, 123.23, 117.46, 115.34, 115.02, 113.83, 56.70 ppm. Spectroscopic data are consistent with the literature data.^{76,97}



15

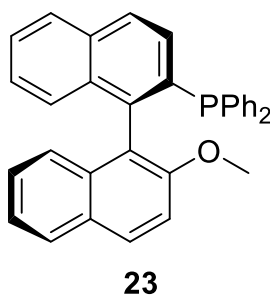
2'-Methoxy-[1,1'-binaphthalen]-2-yl trifluoromethanesulfonate (15). A solution of 2'-methoxy-[1,1'-binaphthalen]-2-ol **14** (1.3656 g, 4.5467 mmol) and pyridine (0.44 mL, 5.4560 mmol) in DCM (50 mL) was prepared in an oven-dried 100-mL round-bottom flask equipped with a magnetic stir bar, then cooled to 0 °C in an ice bath. Triflic anhydride (0.92 mL, 5.4560 mmol) was added dropwise over 10 minutes, then the mixture was stirred for 1 hour and allowed to warm to room temperature. The reaction mixture was quenched with 1M HCl (25 mL) and extracted with DCM (3×25 mL). The organic layers were combined and washed with saturated sodium bicarbonate solution (25 mL), then saturated sodium chloride solution (25 mL). The organic layer was then dried over anhydrous MgSO₄, filtered, and concentrated under reduced pressure. The crude product was purified by column chromatography, eluting with 1:1 DCM/hexanes, to provide the title compound as colourless crystals. Yield 86 % (4.5156 g); Melting point: 107 – 108 °C for racemic-**15**; TLC: 1:1 DCM/hexanes, R_f = 0.45; ¹H NMR (400 MHz, CDCl₃) δ 8.05 (dd, *J* = 9.0, 7.1 Hz, 2H), 7.98 (d, *J* = 8.3 Hz, 1H), 7.90 (d, *J* = 8.1 Hz, 1H), 7.60 – 7.51 (m, 2H), 7.46 (d, *J* = 9.1 Hz, 1H), 7.40 – 7.30 (m, 3H), 7.29 – 7.22 (m, 1H), 7.02 (d, *J* = 8.5 Hz, 1H), 3.83 (s, 3H) ppm; ¹³C NMR (101 MHz, CDCl₃) δ 155.18, 145.63, 133.66, 133.57, 132.56, 131.05, 130.19, 128.84, 128.23, 128.09, 127.37, 127.27, 126.93, 126.86, 126.82, 124.81, 123.68, 119.54, 118.26 (q, *J* = 320.0 Hz, 1C), 115.14, 112.93, 56.20 ppm; ¹⁹F NMR (376 MHz, CDCl₃) δ -74.88 ppm. Spectroscopic data are consistent with the literature data.^{76,100}



16

Dicyclohexyl(2'-methoxy-[1,1'-binaphthalen]-2-yl)phosphane (16). A flame-dried 50-mL Schlenk flask equipped with a magnetic stir bar was charged with 2'-methoxy-[1,1'-binaphthalen]-2-yl triflate **15** (1.0810 g, 2.5000 mmol), dicyclohexylphosphonium tetrafluoroborate (0.7868 g, 2.750 mmol), palladium(π -cinnamyl) chloride dimer (32.4 mg, 0.0625 mmol) and 1,1'-bis(diisopropylphosphino)ferrocene palladium dichloride (62.7 mg, 0.150 mmol). The flask was evacuated and backfilled with nitrogen several times between additions. Degassed DMSO (20 mL) was then added followed by degassed DIPEA (4.4 mL, 25 mmol). The reaction mixture was stirred at 120 °C for 48 hours. The reaction was cooled to room temperature then diluted with ethyl acetate (10 mL) and washed with distilled water (4×100 mL). The organic layer was dried over anhydrous MgSO₄, and concentrated under reduced pressure. The crude product was purified by column chromatography, eluting with 10% ethyl acetate in hexanes, to provide the title compound as colourless crystals. Yield 78% (0.9372 g); Melting point: 177 – 179 °C for (*R*)-**16**; TLC: 10% ethyl acetate in hexanes, *R_f* = 0.39; ¹H NMR (400 MHz, CDCl₃) δ 7.99 (d, *J* = 9.0 Hz, 1H), 7.91 – 7.88 (m, 2H), 7.83 (d, *J* = 8.1 Hz, 1H), 7.77 (d, *J* = 8.7 Hz, 1H), 7.46 – 7.37 (m, 2H), 7.29 – 7.27 (m, 1H), 7.25 – 7.10 (m, 3H), 6.90 (d, *J* = 8.7 Hz, 1H), 3.74 (s, 3H), 1.88 – 1.43 (m, 11H), 1.29 – 0.82 (m, 11H) ppm; ¹³C NMR (101 MHz, CDCl₃; No doublets arising from coupling to ³¹P have been deconvoluted) δ 154.37, 154.36, 143.57, 143.25, 135.23, 135.04, 134.27, 133.56, 133.33, 133.26, 129.60, 129.18, 128.53, 127.87, 127.81, 126.97, 126.70, 126.23, 126.16, 125.96, 125.78, 123.18,

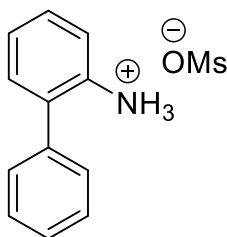
122.58, 122.49, 112.28, 55.52, 35.44, 35.29, 34.41, 30.66, 30.58, 30.49, 30.42, 29.98, 29.89, 27.63, 27.57, 27.50, 27.37, 27.29, 27.19, 26.55, 26.38 ppm; ^{31}P NMR (162 MHz, CDCl_3) δ -8.88 ppm. Spectroscopic data are consistent with the literature data.⁹⁶ Analytical HPLC was carried out using a Chiralpak OD-H column with a flow rate of 1.000 mL/min eluting with 0.1% 2-propanol in hexanes, t_{R} = 14.132 and 16.220 min.



(R)-(2'-Methoxy-[1,1'-binaphthalen]-2-yl)diphenylphosphane (23). A flame-dried 100-mL Schlenk flask equipped with a magnetic stir bar was charged with 2'-methoxy-[1,1'-binaphthalen]-2-yl triflate **15** (2.1620 g, 5.0000 mmol), palladium(π -cinnamyl) chloride dimer (64.8 mg, 0.125 mmol) and 1,1'-bis(diisopropylphosphino)ferrocene palladium dichloride (125.4 mg, 0.3000 mmol). The flask was evacuated and backfilled with nitrogen several times between additions. Degassed DMSO (20 mL) was then added followed by degassed DIPEA (8.71 mL, 50.0 mmol). Diphenylphosphane (0.96 mL, 5.5 mmol) was dispensed in an inert nitrogen atmosphere glovebox and transferred to the reaction flask. The reaction mixture was stirred at 120 °C for 48 hours. The reaction was cooled to room temperature then poured into a 1000-mL separatory funnel containing distilled water (200 mL) and ethyl acetate (50 mL). The reaction flask was rinsed with ethyl acetate (2×50 mL) and distilled water (2×50 mL) and transferred to the separatory funnel. The organic layer was washed a total of three times (3×100 mL) then the aqueous layer was extracted using ethyl acetate (2×50 mL). The organic layers were combined and washed with a saturated sodium

chloride solution (2×100 mL), then dried over anhydrous MgSO₄, and concentrated under reduced pressure. Purification of the crude product by column chromatography, eluting with 1:1 DCM/hexanes, was unsuccessful. A mixture consisting of the triflate **15**, Me-BINOL **14** and the desired phosphane resulted. Yield calculated based on ¹H NMR spectrum, 16% (0.1581 g); 1:1 DCM/hexanes, R_f = 0.32; ¹H NMR (400 MHz, CDCl₃) A crude spectrum is included in Appendix 5.1; ³¹P NMR (162 MHz, CDCl₃) δ -13.63 ppm. The ³¹P NMR spectrum was consistent with the literature spectrum.⁹¹

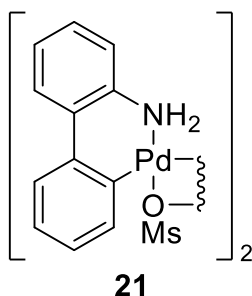
3.4 Synthesis of 2-aminobiphenyl-based palladium methanesulfonate dimer⁴⁹



20

2-Biphenylammonium mesylate (20). To a 100-mL round-bottom flask equipped with a magnetic stir bar, 2-aminobiphenyl[‡] (1.6923 g, 10 mmol) was dissolved in 30 mL of diethyl ether. A 1M solution of methanesulfonic acid (0.65 mL, 10 mmol) in diethyl ether was prepared and added dropwise to the 2-aminobiphenyl solution. After stirring for 30 minutes the reaction mixture was filtered and washed with diethyl ether (3×5 mL), then dried *in vacuo*. Yield 99% (2.6253 g); ¹H NMR (400 MHz, CD₃OD) δ 7.62 – 7.38 (m, 9H), 2.69 (s, 3H) ppm; ¹³C NMR (101 MHz, CDCl₃) δ 137.30, 136.38, 131.73, 129.42, 129.10, 129.06, 128.94, 128.63, 127.75, 123.84, 38.30 ppm. Spectroscopic data are consistent with the literature data.⁴⁹

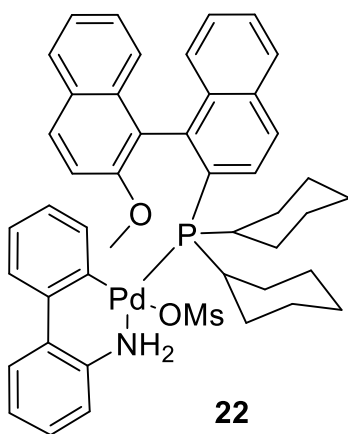
[‡] The MSDS for 2-aminobiphenyl should be read carefully prior to its use due to toxicity concerns.¹⁰⁵



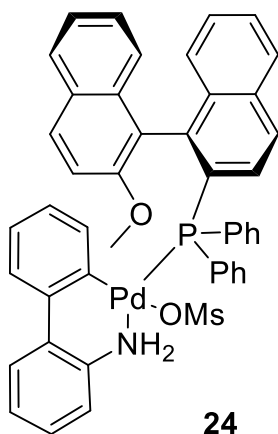
Methanesulfonate-bridged palladacyclic dimer (21). To a 50-mL round-bottom flask equipped with a magnetic stir bar, 2-ammoniumbiphenyl mesylate **20** (1.3267 g, 5 mmol) and Pd(OAc)₂ (1.1226 g, 5 mmol) were added. The flask was evacuated and backfilled with nitrogen several times prior to adding toluene (20 mL) and stirring the reaction mixture at 50 °C for 1 hour. The suspended solid was isolated by filtration through a frit, rinsing with toluene (5 mL) followed by diethyl ether (5 mL) then dried *in vacuo*. The title compound was afforded as a light brown solid. Yield 99% (1.8146 g); ¹H NMR (400 MHz, CD₃OD) δ 7.63 (dd, *J* = 7.4, 1.5 Hz, 1H), 7.47 (d, *J* = 7.6 Hz, 1H), 7.32 – 7.18 (m, 3H), 7.16 – 7.03 (m, 3H), 6.68 (bs, 1H), 2.71 (s, 3H) ppm; ¹³C NMR (101 MHz, CD₃OD) δ 138.57, 138.16, 136.84, 136.32, 133.19, 127.45, 127.33, 126.41, 125.71, 125.63, 124.21, 119.35, 38.16 ppm.

3.5 General procedure for the synthesis of third generation palladium precatalysts

The methanesulfonate dimer **21** (92.4 mg, 0.1250 mmol) and biarylphosphane (0.2500 mmol) were added to a 10-mL round bottom flask equipped with a magnetic stir bar. The flask was evacuated and backfilled with nitrogen several times prior to adding DCM (5 mL) and stirring the reaction mixture for 2 hours. Following completion of the reaction, evidenced by the disappearance of the signal for free phosphane and appearance of the downfield precatalyst signal at *ca.* δ 45 ppm in the ³¹P NMR spectrum, the residue was triturated from diethyl ether with the aid of sonication. The solid was isolated by filtration through a frit then dried *in vacuo*.

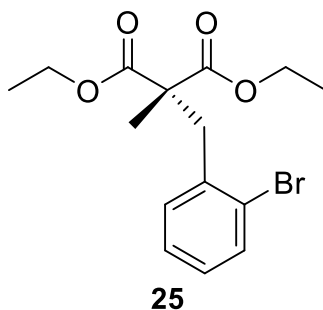


Cy₂MOP-Pd precatalyst (22). Recrystallization from benzene *via* slow evaporation yielded diffraction quality tan crystals. Yield 91% (193.4 mg). ¹H NMR (400 MHz, CD₃OD) The spectrum is highly complicated due to the likely presence of diastereomeric complexes in solution, as well as ³¹P coupling (see Appendix 5.1, p.122). ¹³C NMR (101 MHz, CDCl₃; No doublets arising from coupling to ³¹P have been deconvoluted) δ 142.35, 139.90, 139.48, 138.48, 137.50, 136.74, 135.94, 135.13, 130.03, 129.20, 129.11, 128.80, 128.09, 127.87, 127.54, 126.86, 126.66, 126.57, 126.10, 125.60, 125.55, 125.42, 125.19, 124.95, 124.43, 121.16, 119.69, 115.94, 114.27, 56.74, 55.88, 39.55, 35.08, 31.22, 30.25, 29.22, 27.91, 27.77, 26.70, 26.18, 26.06, 25.81, 25.48, 22.32, 14.05 ppm. ³¹P NMR (162 MHz, CDCl₃) δ 41.71 ppm; ³¹P NMR (162 MHz, CD₃OD) δ 42.78, 42.49 ppm.



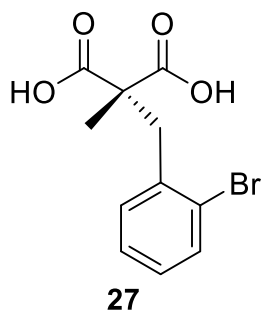
(R)-MOP-Pd precatalyst (24). The impure (R)-(2'-methoxy-[1,1'-binaphthalen]-2-yl)diphenylphosphane **23** was weighed, accounting for true mass contribution of the desired compound calculated based on the ^1H NMR spectrum of impure material (200.0 mg, 0.4288 mmol) and transferred to a 10-mL round bottom flask equipped with a magnetic stir bar. The methanesulfonate dimer **21** (157.8 mg, 0.2134 mmol) was added to the reaction flask which was then evacuated and backfilled with nitrogen several times prior to adding DCM (5 mL) and stirring the reaction mixture for 2 hours. Following completion of the reaction, evidenced by the disappearance of the signal for free phosphane (δ -13.63 ppm) and appearance of the downfield precatalyst signal (*ca.* δ 40 ppm) in the ^{31}P NMR spectrum, the residue was triturated from diethyl ether with the aid of sonication. The solid was isolated by filtration through a frit then dried *in vacuo*. Yield 19% (69.4 mg); ^{31}P NMR (162 MHz, CDCl_3) 37.38, 36.40 ppm. The two peaks observed are likely due to the presence of rotamers.⁴⁸

3.6 General procedure for the synthesis of α -(2-bromobenzyl)malonamides⁶¹



Diethyl 2-(2-bromobenzyl)-2-methylmalonate (25). A flame-dried 50-mL Schlenk flask equipped with a magnetic stir bar was charged with NaH (60% dispersion in mineral oil, 1.2904 g, 32.26 mmol) and THF (30.0 mL), then cooled to 0 °C in an ice bath. Diethyl methylmalonate (5.0 mL, 29.33 mmol) was slowly added dropwise to the mixture which was stirred for approximately 30 minutes. Once the evolution of hydrogen gas ceased, 2-bromobenzyl bromide

(9.5298 g, 38.13 mmol) was added to the reaction flask and the solution turned milky white. The reaction mixture was heated to reflux for 18 hours. The reaction mixture was cooled to room temperature and the solvent was evaporated under reduced pressure. The crude mixture was re-dissolved in ethyl acetate (60 mL) then washed with distilled water (3×60 mL), dried over anhydrous MgSO_4 , and concentrated under reduced pressure. The crude product was purified by column chromatography, eluting with 10% ethyl acetate in hexanes, to provide the title compound as a pale yellow oil. Yield (10.000 g, 99%); TLC: $R_f = 0.31$ (10% ethyl acetate in hexanes); ^1H NMR (400 MHz, CDCl_3) δ 7.54 (d, $J = 7.9$ Hz, 1H), 7.23 – 7.13 (m, 2H), 7.11 – 7.02 (m, 1H), 4.30 – 4.12 (m, 4H), 3.51 (s, 2H), 1.38 (s, 3H), 1.25 (t, $J = 7.1$ Hz, 6H) ppm; ^{13}C NMR (101 MHz, CDCl_3) δ 171.86, 136.43, 133.08, 131.37, 128.44, 127.26, 126.27, 61.46, 55.08, 39.35, 19.36, 13.98 ppm. Spectroscopic data are consistent with the literature data.⁶¹

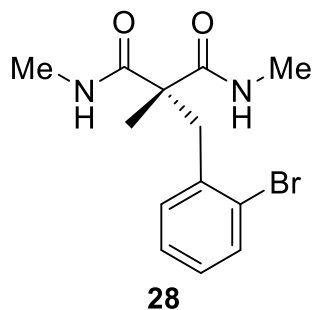


2-(2-Bromobenzyl)-2-methylmalonic acid (27). An oven-dried 250-mL round-bottom flask equipped with a magnetic stir bar was charged with diester **25** (9.885 g, 28.80 mmol) dissolved in methanol (90 mL) and 4 M aqueous NaOH (29.1 mL), and the reaction mixture was heated to reflux for 18 hours. The mixture was cooled to room temperature then diluted with distilled water and extracted with ether (3×30 mL). The aqueous layer was cooled to 0 °C in an ice bath and acidified to pH 3 by dropwise addition of 6 M HCl. A white precipitate formed and was extracted using ethyl acetate (3×30 mL). The organic layers were combined and dried over anhydrous

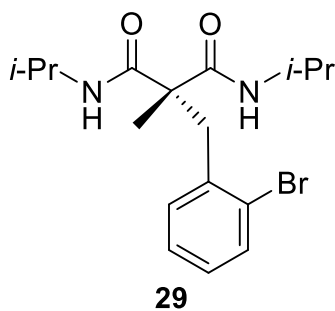
MgSO₄, filtered, and concentrated under reduced pressure then dried *in vacuo* to yield the title compound as a white solid. Yield 96% (7.9740 g); Melting point: 164 – 166 °C; ¹H NMR (400 MHz, (CD₃)₂CO) δ 7.65 – 7.58 (m, 1H), 7.40 – 7.34 (m, 1H), 7.32 – 7.24 (m, 1H), 7.21 – 7.12 (m, 1H), 3.53 (s, 2H), 1.34 (s, 3H) ppm; ¹³C NMR (101 MHz, (CD₃)₂CO) δ 172.30, 136.72, 132.94, 131.42, 128.64, 127.54, 125.89, 54.34, 38.98, 18.58 ppm. Spectroscopic data are consistent with the literature data.⁶¹

Synthesis of α -(2-bromobenzyl)malonamides

An oven-dried round-bottom flask equipped with a magnetic stir bar was charged with 2-(2-bromobenzyl)-2-methylmalonic acid **27** (1 eq) and thionyl chloride (~ 0.2 M) and heated to reflux for 4 hours. The reaction mixture was cooled to room temperature then concentrated under reduced pressure. The malonic acid chloride was dissolved in chloroform (1×reaction volume) then concentrated under reduced pressure three times to remove residual thionyl chloride. An oven-dried round-bottom flask equipped with a magnetic stir bar was charged with the appropriate amine (2.2 eq), triethylamine (2.2 eq) and DCM (~ 0.8 M). The mixture was cooled to 0 °C in an ice bath and a solution of the diacid chloride in DCM (~ 0.2 M) was added dropwise *via* addition funnel. The reaction was allowed to warm to room temperature and then heated to reflux for 18 hours. The reaction mixture was cooled to room temperature then washed with 1 M HCl (4× reaction volume), dried over anhydrous MgSO₄, filtered, and concentrated under reduced pressure.

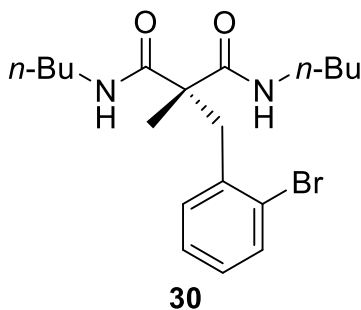


2-(2-Bromobenzyl)-N,N',2-trimethylmalonamide (28). The crude product was purified *via* recrystallization from ethyl acetate to afford the title compound as a white solid. Yield 45% (1.7415 mmol scale, 0.2456 g); Melting point: 132 – 134 °C; TLC: neat ethyl acetate, R_f = 0.23; ^1H NMR (400 MHz, CDCl_3) δ 7.50 (d, J = 8.1 Hz, 1H), 7.06 – 7.10 (m, 2H), 7.06 – 6.88 (m, 3H), 3.39 (s, 2H), 2.77 (d, J = 4.8 Hz, 6H), 1.34 (s, 3H) ppm; ^{13}C NMR (101 MHz, CDCl_3) δ 173.24, 136.49, 132.97, 130.99, 128.42, 127.24, 126.02, 54.38, 43.15, 26.70, 18.15 ppm. Spectroscopic data are consistent with the literature data.⁶¹

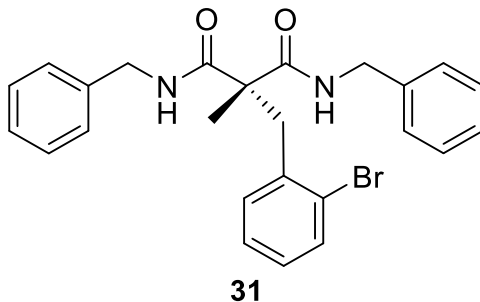


2-(2-Bromobenzyl)-N,N'-diisopropyl-2-methylmalonamide (29). The crude product was purified *via* recrystallization from hexanes to afford the title compound as white needle-like crystals. Yield 24% (3.4830 mmol scale, 0.314 g,); Melting point: 167 – 169 °C; TLC: 45% ethyl acetate in hexanes, R_f = 0.41; ^1H NMR (400 MHz, CDCl_3) δ 7.53 (dd, J = 8.0, 1.1 Hz, 1H), 7.25 – 7.14 (m, 2H), 7.09 – 7.02 (m, 1H), 6.62 (d, J = 6.7 Hz, 2H), 4.12 – 3.98 (m, 2H), 3.43 (s, 2H), 1.34 (s, 3H), 1.15 (d, J = 6.6 Hz, 6H), 1.10 (d, J = 6.6 Hz, 6H) ppm; ^{13}C NMR (101 MHz, CDCl_3)

δ 171.75, 136.70, 132.98, 131.08, 128.37, 127.28, 126.07, 54.22, 42.66, 41.85, 22.45, 22.38, 18.47 ppm. Spectroscopic data are consistent with the literature data.⁶¹

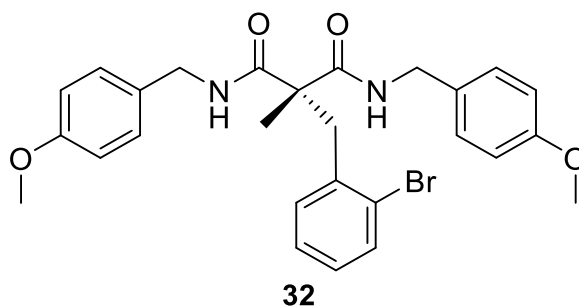


2-(2-Bromobenzyl)-N,N'-dibutyl-2-methylmalonamide (30). The crude product was purified *via* recrystallization from hexanes to afford the title compound as white needle-like crystals. Yield 22% (1.7415 mmol scale, 0.1546 g); Melting point: 134 – 137 °C; TLC: 45% ethyl acetate in hexanes, R_f = 0.44; ^1H NMR (400 MHz, CDCl_3) δ 7.53 (d, J = 7.9 Hz, 1H), 7.24 – 7.13 (m, 2H), 7.09 – 7.02 (m, 1H), 6.89 – 6.80 (m, 2H), 3.44 (s, 2H), 3.25 (dd, J = 12.9, 6.0 Hz, 4H), 1.52 – 1.41 (m, 4H), 1.37 (s, 3H), 1.30 (dq, J = 14.4, 7.2 Hz, 4H), 0.91 (t, J = 7.3 Hz, 6H) ppm; ^{13}C NMR (101 MHz, CDCl_3) δ 172.59, 136.61, 133.00, 131.05, 128.39, 127.29, 126.04, 54.39, 42.93, 39.70, 31.30, 20.05, 18.44, 13.71 ppm. Spectroscopic data are consistent with the literature data.⁶¹

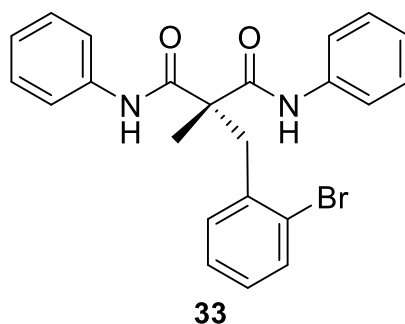


N,N'-Dibenzyl-2-(2-bromobenzyl)-2-methylmalonamide (31). The crude product was purified *via* recrystallization from 2-propanol to afford the title compound as a fluffy white solid. Yield

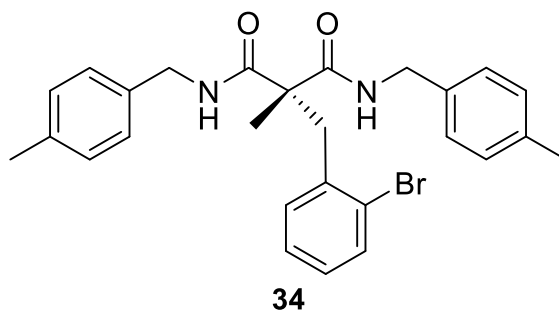
70% (3.4830 mmol scale, 1.1269 g); Melting point: 173 – 174 °C; TLC: 45% ethyl acetate in hexanes, R_f = 0.34; ^1H NMR (400 MHz, CDCl_3) δ 7.52 (dd, J = 7.2, 2.0 Hz, 1H), 7.36 – 7.27 (m, 6H), 7.24 – 7.18 (m, 5H), 7.14 – 7.01 (m, 3H), 4.45 (m, 4H), 3.50 (s, 2H), 1.43 (s, 3H) ppm; ^{13}C NMR (101 MHz, CDCl_3) δ 172.48, 137.73, 136.33, 133.05, 131.13, 128.73, 128.47, 127.71, 127.54, 127.39, 126.02, 54.59, 44.04, 42.97, 18.52 ppm. Spectroscopic data are consistent with the literature data.⁶¹



2-(2-Bromobenzyl)-N,N'-bis(4-methoxybenzyl)-2-methylmalonamide (32). The crude product was purified *via* recrystallization from ethyl acetate to afford the title compound as white cubic crystals. Yield 42% (6.9660 mmol scale, 1.5379 g); Melting point: 147 – 149 °C; TLC: 45% ethyl acetate in hexanes, R_f = 0.33; ^1H NMR (400 MHz, CDCl_3) δ 7.57 – 7.44 (m, 1H), 7.14 – 7.04 (m, 9H), 6.84 – 6.82 (m, 4H), 4.36 (m, 4H), 3.79 (s, 6H), 3.48 (s, 2H), 1.39 (s, 3H) ppm; ^{13}C NMR (101 MHz, CDCl_3) δ 172.37, 159.05, 136.40, 133.03, 131.13, 129.87, 129.08, 128.43, 127.36, 126.03, 114.11, 55.30, 54.53, 43.52, 42.93, 18.43 ppm. Spectroscopic data are consistent with the literature data.⁶¹



2-(2-Bromobenzyl)-2-methyl-*N,N'*-diphenylmalonamide (33). The crude product was purified *via* recrystallization from 2-propanol to afford the title compound as a white solid. Yield 45% (3.4830 mmol scale, 0.6855 g); Melting point: 217 – 218 °C; TLC: 30% ethyl acetate in hexanes, $R_f = 0.41$; ^1H NMR (400 MHz, CDCl_3) δ 8.74 (s, 2H), 7.60 – 7.55 (m, 1H), 7.55 – 7.47 (m, 4H), 7.39 – 7.31 (m, 4H), 7.22 – 7.13 (m, 3H), 7.12 – 7.05 (m, 1H), 3.66 (s, 2H), 1.65 (s, 3H) ppm; ^{13}C NMR (101 MHz, CDCl_3) δ 170.66, 137.17, 135.90, 133.23, 131.08, 129.07, 128.83, 127.64, 126.05, 125.03, 120.65, 55.76, 43.56, 18.76 ppm. Spectroscopic data are consistent with the literature data.⁶¹

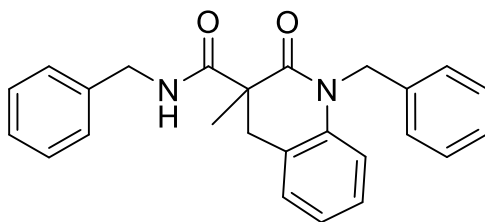


2-(2-Bromobenzyl)-2-methyl-*N,N'*-bis(4-methylbenzyl)malonamide (34). The crude product was purified *via* recrystallization from 2-propanol to afford the title compound as a white needle-like crystals. Yield 44% (3.4830 mmol scale, 0.7525 g); Melting point: 169 – 171 °C; TLC: 45% ethyl acetate in hexanes, $R_f = 0.52$; ^1H NMR (400 MHz, CDCl_3) δ 7.52 (dd, $J = 7.5, 1.7$ Hz, 1H), 7.18 – 7.01 (m, 12H), 4.47 – 4.32 (m, 4H), 3.49 (s, 2H), 2.34 (s, 6H), 1.40 (s, 3H) ppm.; ^{13}C NMR

(101 MHz, CDCl₃) δ 172.53, 137.33, 136.54, 134.84, 133.16, 131.29, 129.51, 128.56, 127.84, 127.49, 126.16, 54.70, 43.94, 43.09, 21.23, 18.53 ppm.

3.7 General procedure for the *N*-arylation of α -(2-bromobenzyl)malonamides

A flame-dried 10-mL Schlenk flask equipped with a magnetic stir bar was charged with the appropriate α -(2-bromobenzyl)malonamide (0.1074 mmol) and base, either Cs₂CO₃ (49.0 mg, 0.1504 mmol) or K₃PO₄ (31.9 mg, 0.1504 mmol). The flask was evacuated and backfilled with nitrogen prior to the addition of THF (0.88 mL) followed by a solution of (*R*)-Cy₂MOP-Pd precatalyst in THF (1.27 mL of 0.847 mM). The reaction was stirred at 60 °C for 24 hours. The reaction mixture was cooled to room temperature then diluted with ethyl acetate (10 mL) and filtered through a pad of celite. The crude product was purified by flash column chromatography. The enantiomeric excess for each reaction was determined *via* chiral HPLC analysis.



35

***N*,1-Dibenzyl-3-methyl-2-oxo-1,2,3,4-tetrahydroquinoline-3-carboxamide (35).** The product was purified by flash column chromatography, eluting with 45% ethyl acetate in hexanes to afford the title compound as a white solid. Yield 96% (0.2578 mmol scale, 99.4 mg); Melting point: 135 – 137 °C; TLC: 45% ethyl acetate in hexanes, *R*_f = 0.34; ¹H NMR (400 MHz, CDCl₃) δ 7.37 – 7.27 (m, 2H), 7.25 – 7.01 (m, 10H), 6.85 (d, *J* = 8.2 Hz, 1H), 5.27 – 5.02 (m, 2H), 4.39 (d, *J* = 5.7 Hz, 2H), 3.52 (d, *J* = 15.6 Hz, 1H), 3.07 (d, *J* = 16.0 Hz, 1H), 1.57 (s, 1H) ppm; ¹³C NMR (101 MHz, CDCl₃) δ 172.44, 170.94, 138.61, 138.05, 136.55, 128.86, 128.81, 128.64, 127.58, 127.51,

127.34, 127.17, 125.98, 124.71, 123.96, 115.28, 48.64, 47.34, 43.63, 35.46, 23.28 ppm. Analytical HPLC was carried out using a Chiralpak OD-H column with a flow rate of 1.000 mL/min eluting with 20% 2-propanol in hexanes, $t_R = 12.097$ and 16.300 min. Spectroscopic data are consistent with the literature data.⁶¹

4 Conclusion

A third generation precatalyst, integrating a chiral element through (*R*)-Cy₂MOP, was successfully synthesized and characterized *via* ¹H, ¹³C{¹H}, and ³¹P{¹H} NMR, and X-ray crystallography. The precatalyst was employed in a Buchwald-Hartwig amination, specifically, the desymmetrization of α-(2-bromobenzyl) malonamides *via* intramolecular *N*-arylation in the presence of a base at moderate temperatures. Negligible enantioselectivity was observed in the synthesis of the dibenzyl quinolinone product using the (*R*)-Cy₂MOP-Pd precatalyst.

Currently, work on modifying the *O*- and *P*-substituents of (*R*)-Cy₂MOP towards enhancing the activity and enantioselectivity achieved by the corresponding precatalysts is underway. Preliminary work towards a chiral (*R*)-MOP-Pd precatalyst was conducted and (*R*)-MOP was found to be compatible with the third generation precatalyst system. Strategies to optimize the reaction conditions to synthesize (*R*)-MOP are being reviewed. In addition, other candidate substrates for enantioselective Buchwald-Hartwig reactions are being developed after which the performance of the (*R*)-Cy₂MOP-Pd precatalyst and related precatalyst complexes in these reaction systems will be investigated. Further research is still required towards isolating a palladium-amido intermediate structure.

5 Appendix

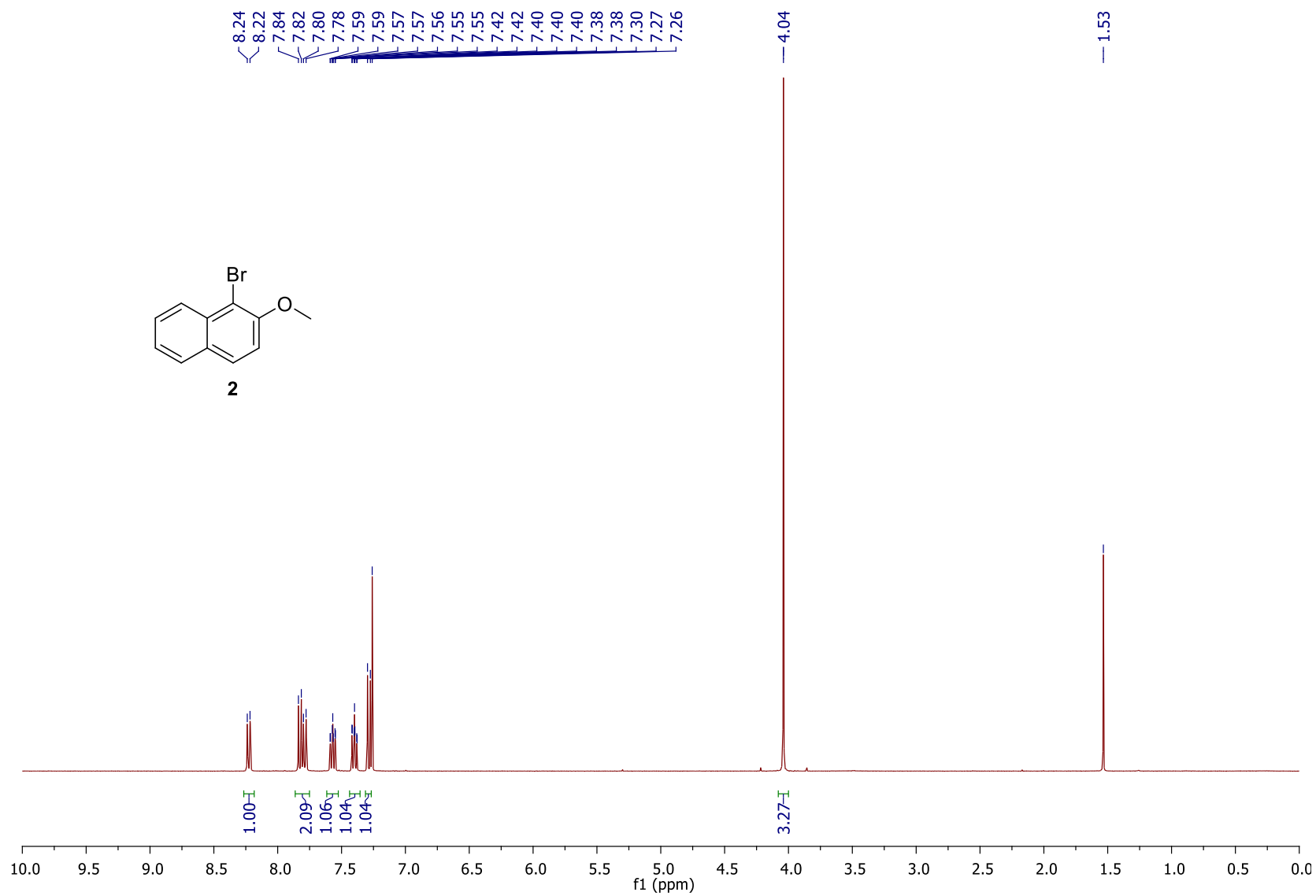
5.1 NMR spectroscopy data

¹ H NMR spectrum of 1-bromo-2-methoxynaphthalene 2 in CDCl ₃	99
¹³ C NMR spectrum of 1-bromo-2-methoxynaphthalene 2 in CDCl ₃	100
¹ H NMR spectrum of 2-methoxynaphthalene 4 in CDCl ₃	101
¹³ C NMR spectrum of 2-methoxynaphthalene 4 in CDCl ₃	102
¹ H NMR spectrum of 2-methoxy-1-naphthylboronic acid 8 in CDCl ₃	103
¹³ C NMR spectrum of 2-methoxy-1-naphthylboronic acid 8 in (CD ₃) ₂ SO	104
¹ H NMR spectrum of 1-(2-bromophenyl)naphthalene 7 in CDCl ₃	105
¹³ C NMR spectrum of 1-(2-bromophenyl)naphthalene 7 in CDCl ₃	106
¹ H NMR spectrum of 2'-methoxy-[1,1'-binaphthalen]-2-ol 14 in CDCl ₃	107
¹³ C NMR spectrum of 2'-methoxy-[1,1'-binaphthalen]-2-ol 14 in CDCl ₃	108
¹ H NMR spectrum of 2,2'-dimethoxy-1,1'-binaphthalene 14 -Me in CDCl ₃	109
¹ H NMR spectrum of 2'-methoxy-[1,1'-binaphthalen]-2-yl triflate 15 in CDCl ₃	110
¹³ C NMR spectrum of 2'-methoxy-[1,1'-binaphthalen]-2-yl triflate 15 in CDCl ₃	111
¹⁹ F NMR spectrum of 2'-methoxy-[1,1'-binaphthalen]-2-yl triflate 15 in CDCl ₃	112
¹ H NMR spectrum of dicyclohexyl(2'-methoxy-[1,1'-binaphth-2-yl])phosphane 16 in CDCl ₃ .	113
¹³ C NMR spectrum of dicyclohexyl(2'-methoxy-[1,1'-binaphth-2-yl])phosphane 16 in CDCl ₃	114
³¹ P NMR spectrum of dicyclohexyl(2'-methoxy-[1,1'-binaphth-2-yl])phosphane 16 in CDCl ₃	115
¹ H NMR spectrum of impure (<i>R</i>)-(2'-methoxy-[1,1'-binaphthalen]-2-yl)diphenylphosphane 23 from purification attempt in CDCl ₃	116
³¹ P NMR spectrum of (<i>R</i>)-(2'-methoxy-[1,1'-binaphthalen]-2-yl)diphenylphosphane 23 in CDCl ₃	117
¹ H NMR spectrum of 2-ammoniumbiphenyl mesylate 20 in CD ₃ OD.....	118

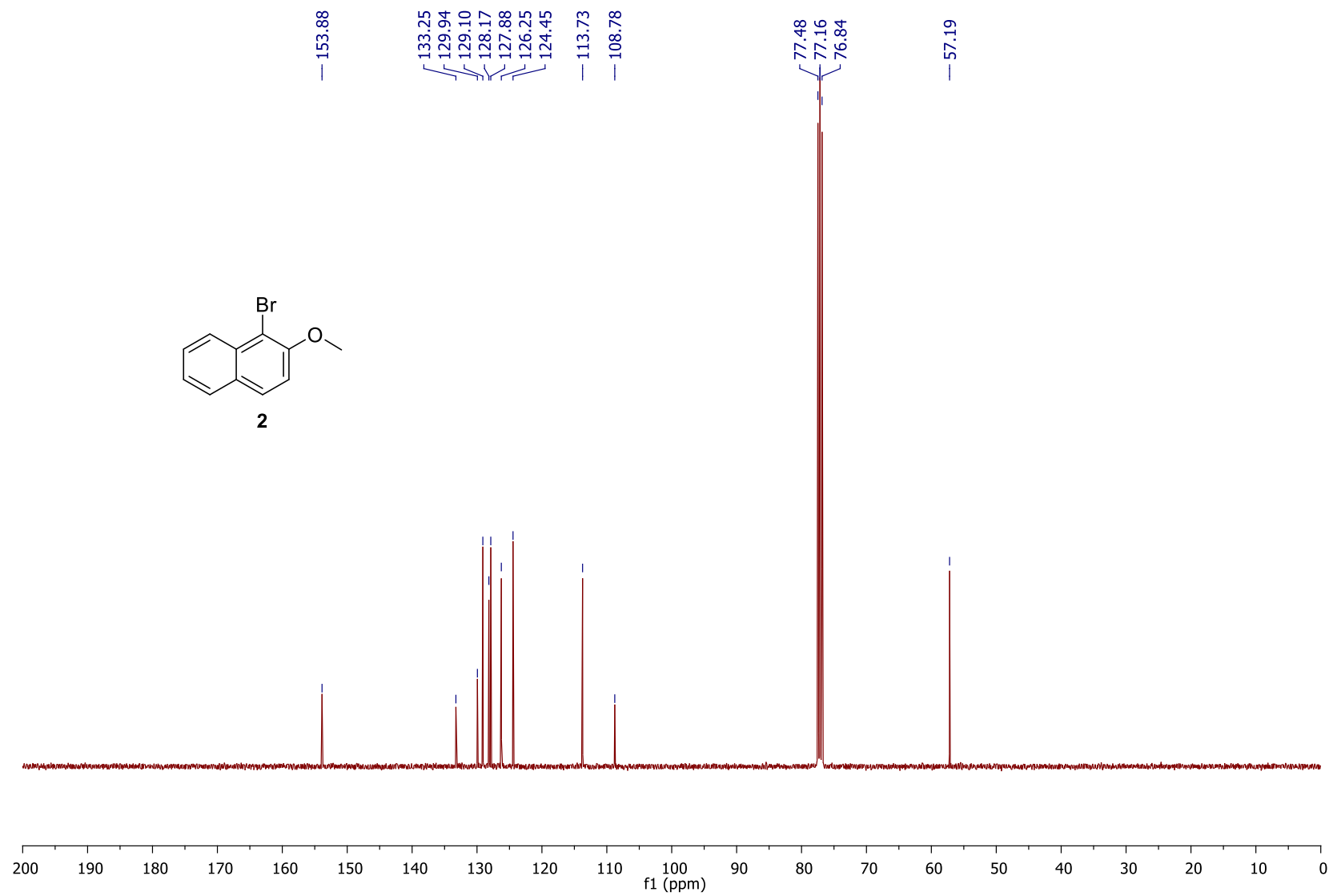
¹³ C NMR spectrum of 2-ammoniumbiphenyl mesylate 20 in CD ₃ OD.....	119
¹ H NMR spectrum of 2-aminobiphenyl-based mesylate-bridged dimer 21 in CD ₃ OD.....	120
¹³ C NMR spectrum of 2-aminobiphenyl-based mesylate-bridged dimer 21 in CD ₃ OD	121
¹ H NMR spectrum of 2-aminobiphenyl methanesulfonate precatalyst 22 in CDCl ₃	122
¹³ C NMR spectrum of 2-aminobiphenyl methanesulfonate precatalyst 22 in CDCl ₃	123
³¹ P NMR spectrum of 2-aminobiphenyl methanesulfonate precatalyst 22 in CDCl ₃ (top) and CD ₃ OD (bottom).....	124
³¹ P NMR spectrum of 2-aminobiphenyl methanesulfonate precatalyst 24 in CDCl ₃	125
¹ H NMR spectrum of diethyl 2-(2-bromobenzyl)-2-methylmalonate 25 in CDCl ₃	126
¹³ C NMR spectrum of diethyl 2-(2-bromobenzyl)-2-methylmalonate 25 in CDCl ₃	127
¹ H NMR spectrum of 2-(2-bromobenzyl)-2-methylmalonic acid 27 in (CD ₃) ₂ CO.....	128
¹³ C NMR spectrum of 2-(2-bromobenzyl)-2-methylmalonic acid 27 in (CD ₃) ₂ CO.....	129
¹ H NMR spectrum of 2-(2-bromobenzyl)- <i>N,N'</i> -2-trimethylmalonamide 28 in CDCl ₃	130
¹³ C NMR spectrum of 2-(2-bromobenzyl)- <i>N,N'</i> -2-trimethylmalonamide 28 in CDCl ₃	131
¹ H NMR spectrum of 2-(2-bromobenzyl)- <i>N,N'</i> -diisopropyl-2-methylmalonamide 29 in CDCl ₃	132
¹³ C NMR spectrum of 2-(2-bromobenzyl)- <i>N,N'</i> -diisopropyl-2-methylmalonamide 29 in CDCl ₃	133
¹ H NMR spectrum of 2-(2-bromobenzyl)- <i>N,N'</i> -dibutyl-2-methylmalonamide 30 in CDCl ₃	134
¹³ C NMR spectrum of 2-(2-bromobenzyl)- <i>N,N'</i> -dibutyl-2-methylmalonamide 30 in CDCl ₃	135
¹ H NMR spectrum of <i>N,N'</i> -dibenzyl-2-(2-bromobenzyl)-2-methylmalonamide 31 in CDCl ₃ ...	136
¹³ C NMR spectrum of <i>N,N'</i> -dibenzyl-2-(2-bromobenzyl)-2-methylmalonamide 31 in CDCl ₃ ..	137
¹ H NMR spectrum of 2-(2'-bromobenzyl)- <i>N,N'</i> -bis(4-methoxybenzyl)-2-methylpropanediamide 32 in CDCl ₃	138
¹³ C NMR spectrum of 2-(2'-bromobenzyl)- <i>N,N'</i> -bis(4-methoxybenzyl)-2-methylpropanediamide 32 in CDCl ₃	139

¹ H NMR spectrum of 2-(2-bromobenzyl)-2-methyl- <i>N,N'</i> -diphenylmalonamide 33 in CDCl ₃ ...	140
¹³ C NMR spectrum of 2-(2-bromobenzyl)-2-methyl- <i>N,N'</i> -diphenylmalonamide 33 in CDCl ₃ .	141
¹ H NMR spectrum of 2-(2-bromobenzyl)-2-methyl- <i>N,N'</i> -bis(4-methylbenzyl)malonamide 34 in CDCl ₃	142
¹³ C NMR spectrum of 2-(2-bromobenzyl)-2-methyl- <i>N,N'</i> -bis(4-methylbenzyl)malonamide 34 in CDCl ₃	143
¹ H NMR spectrum of <i>N</i> ,1-dibenzyl-3-methyl-2-oxo-1,2,3,4-tetrahydroquinoline-3-carboxamide 35 in CDCl ₃	144
¹³ C NMR spectrum of <i>N</i> ,1-dibenzyl-3-methyl-2-oxo-1,2,3,4-tetrahydroquinoline-3-carboxamide 35 in CDCl ₃	145

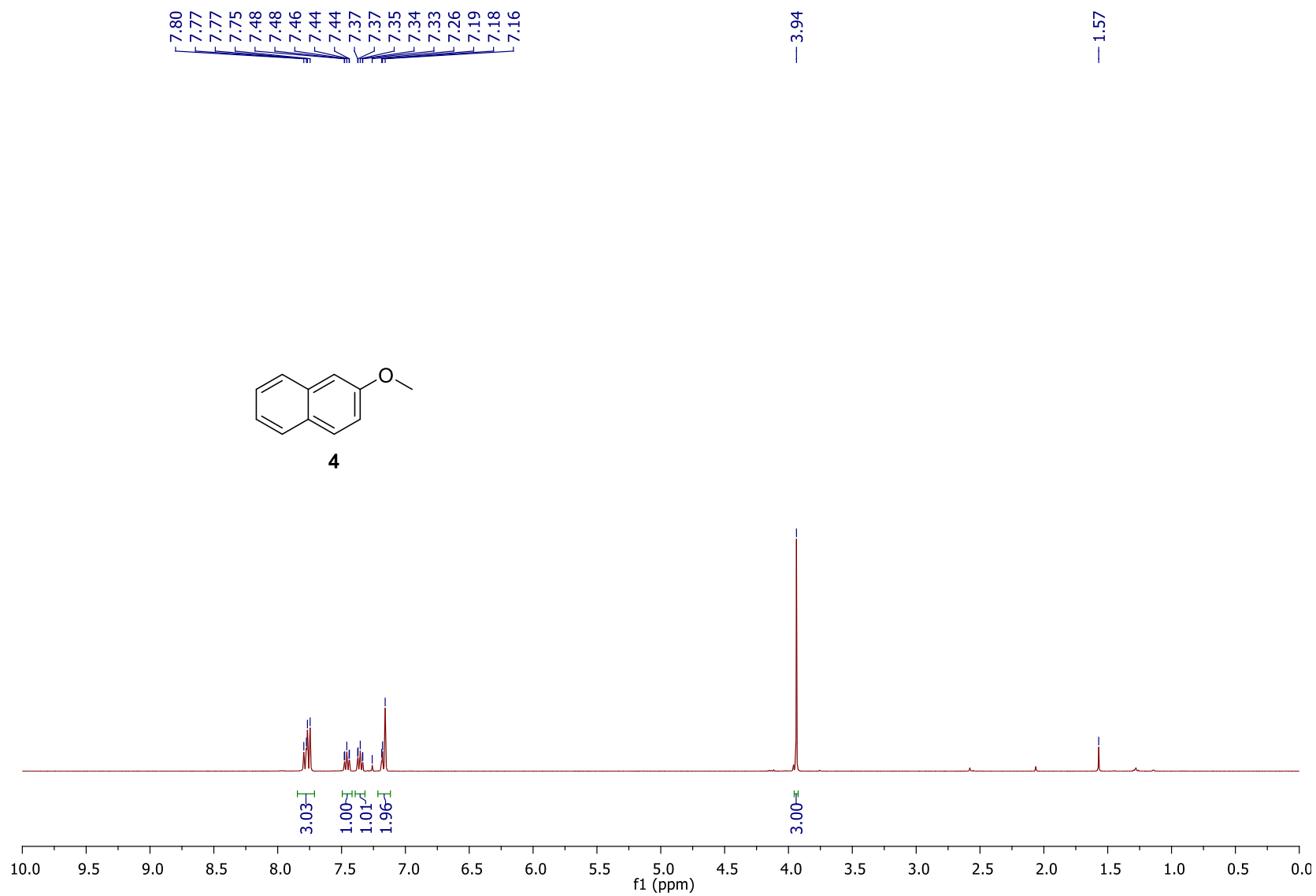
¹H NMR spectrum of 2 in CDCl₃



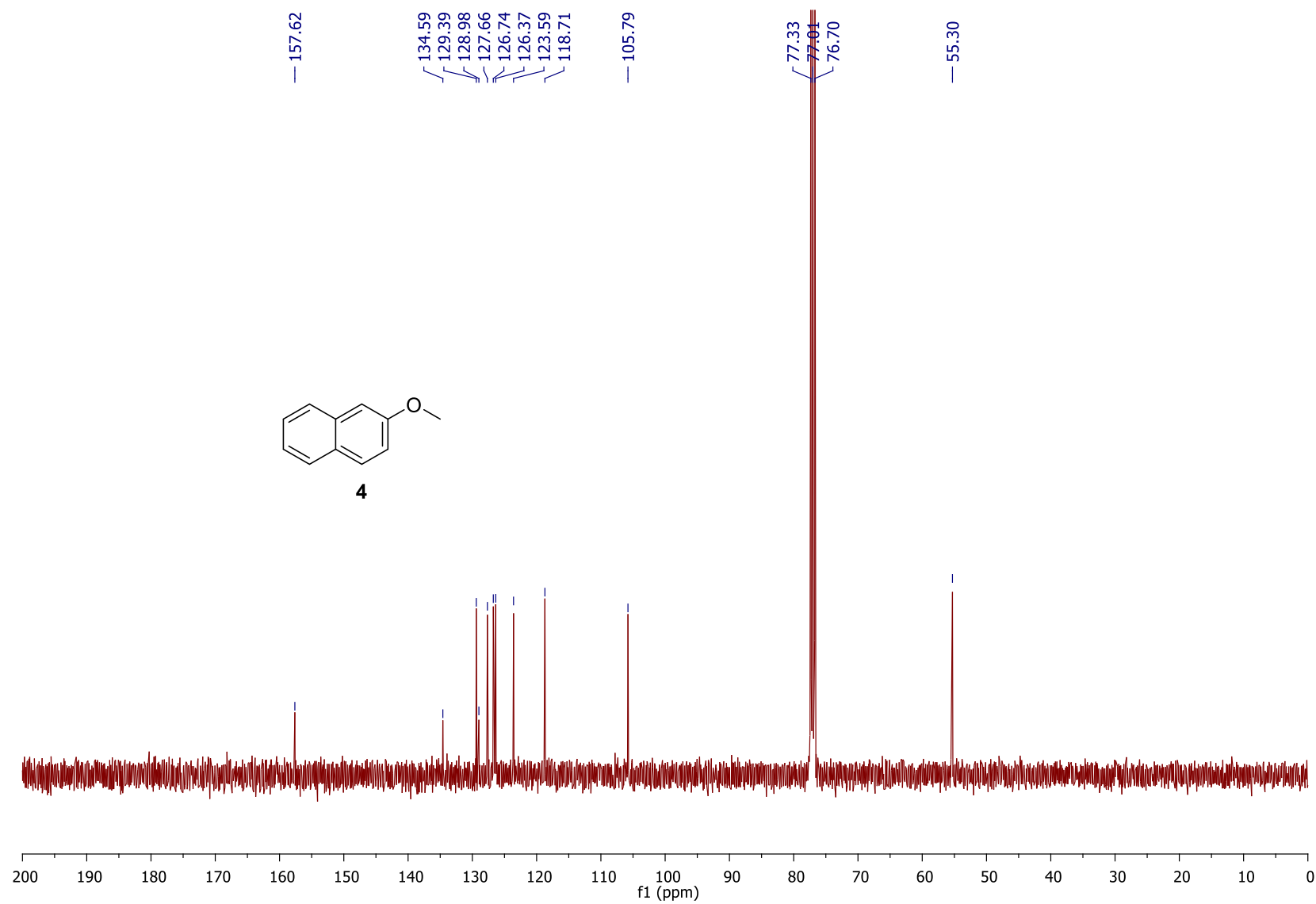
^{13}C NMR spectrum of 2 in CDCl_3



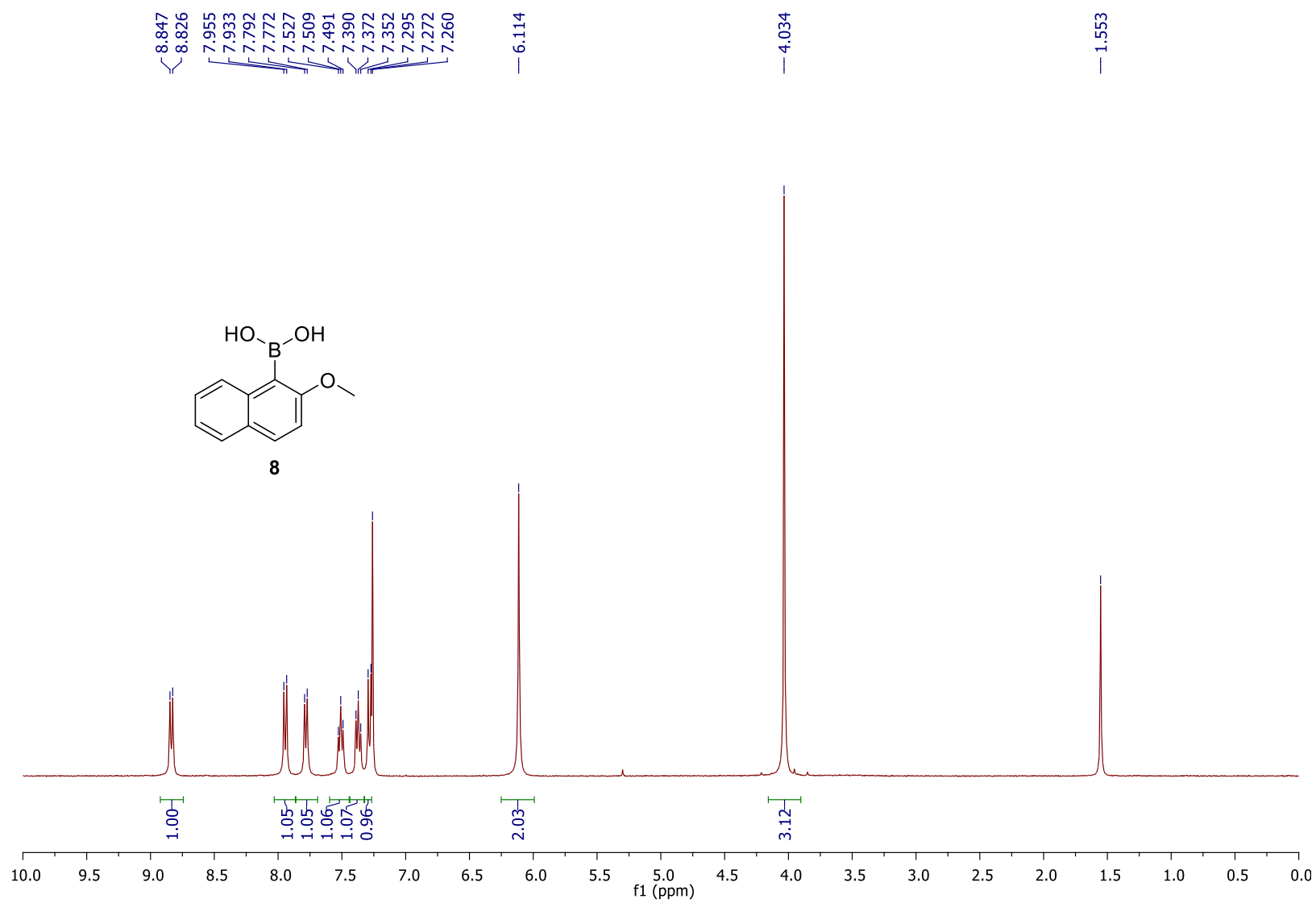
^1H NMR spectrum of 4 in CDCl_3



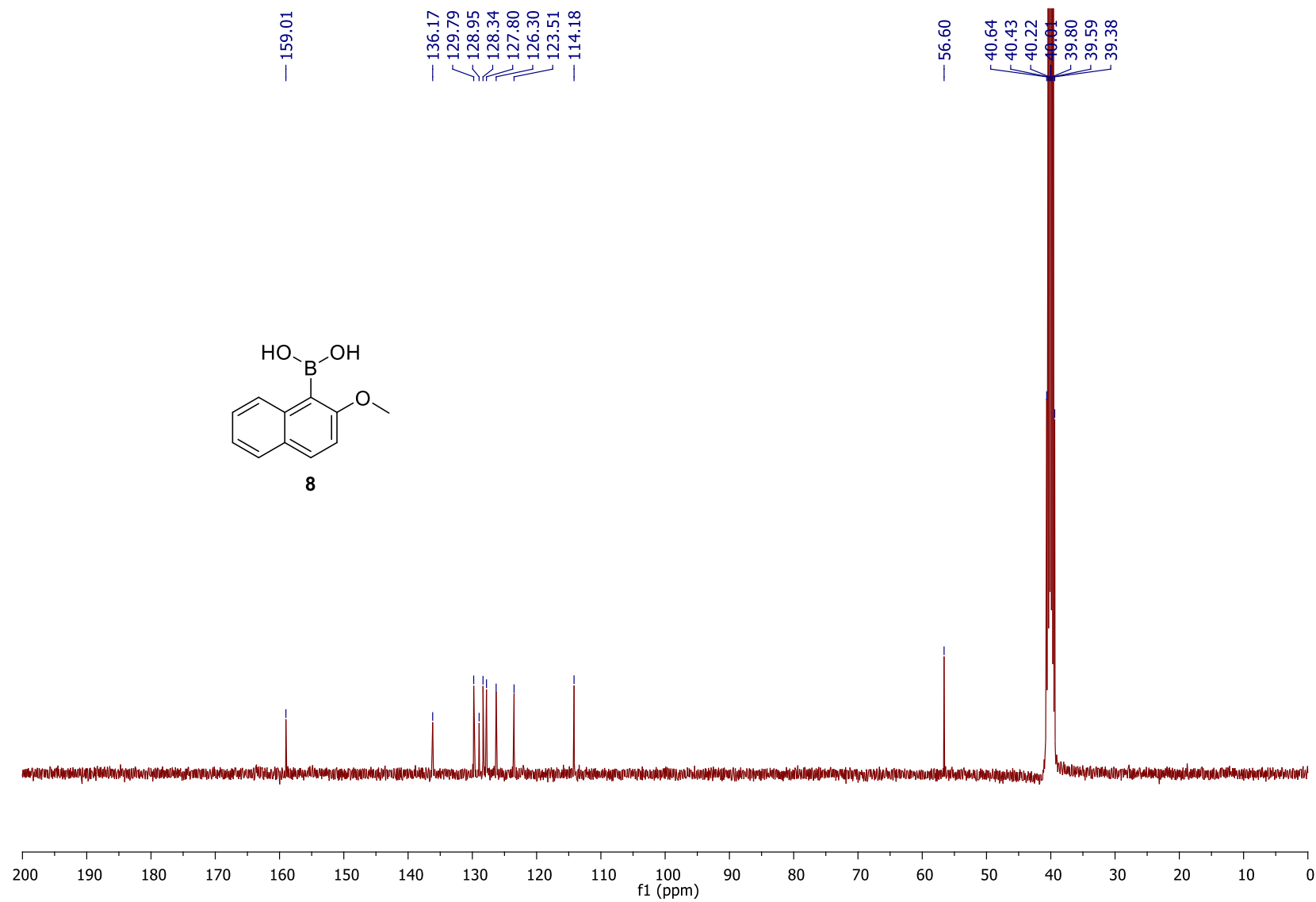
^{13}C NMR spectrum of 4 in CDCl_3



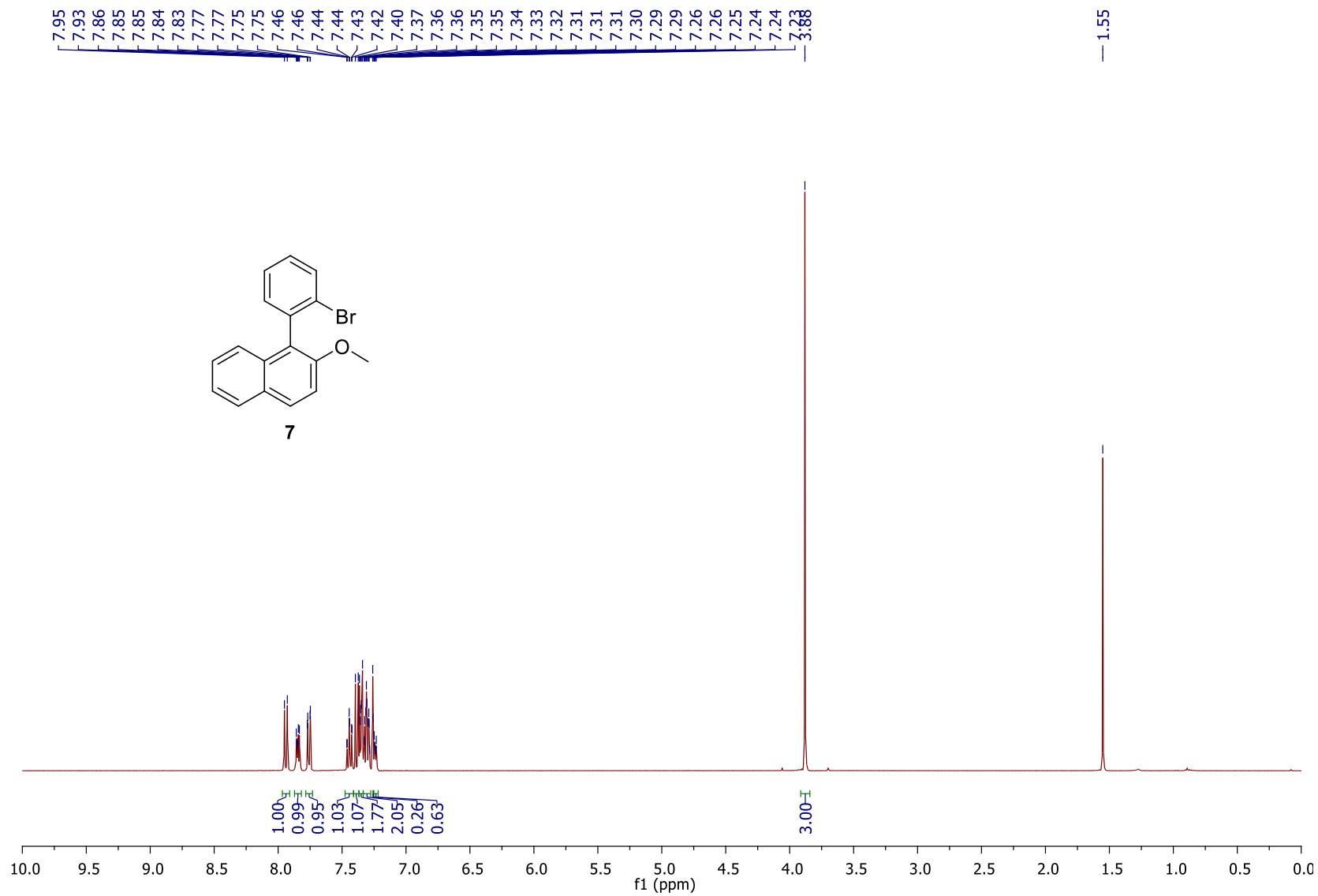
¹H NMR spectrum of 8 in CDCl₃



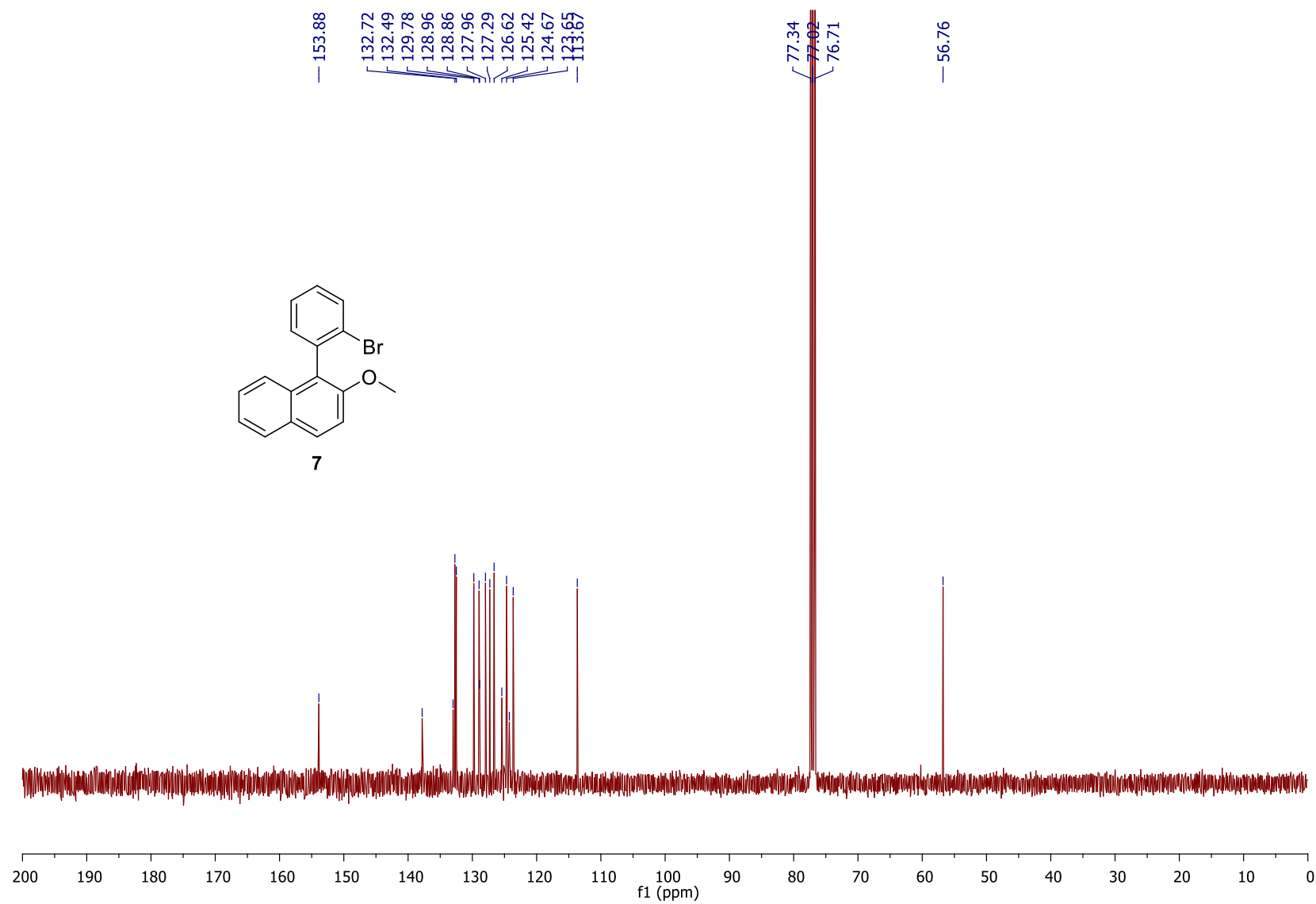
^{13}C NMR spectrum of 8 in $(\text{CD}_3)_2\text{SO}$



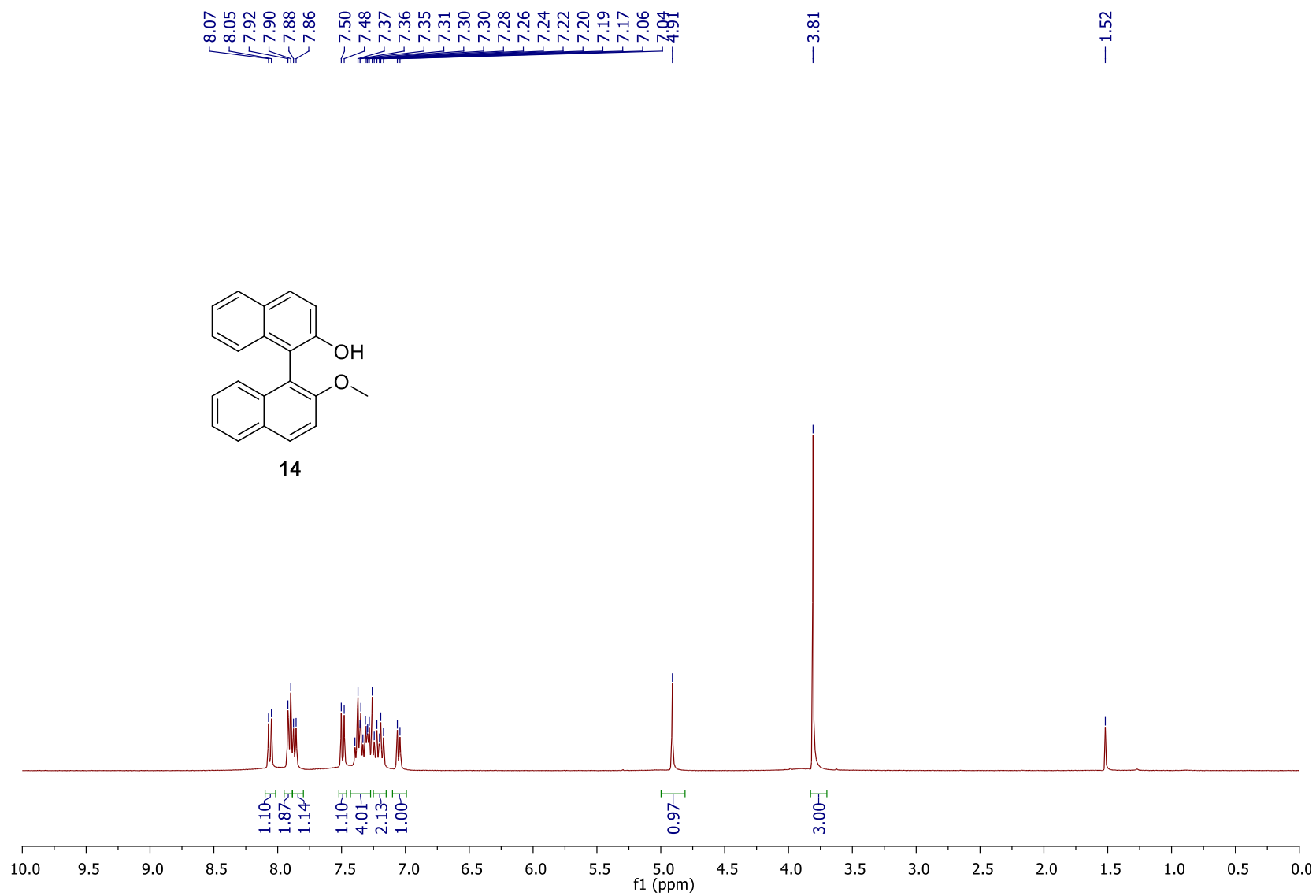
¹H NMR spectrum of **7** in CDCl₃



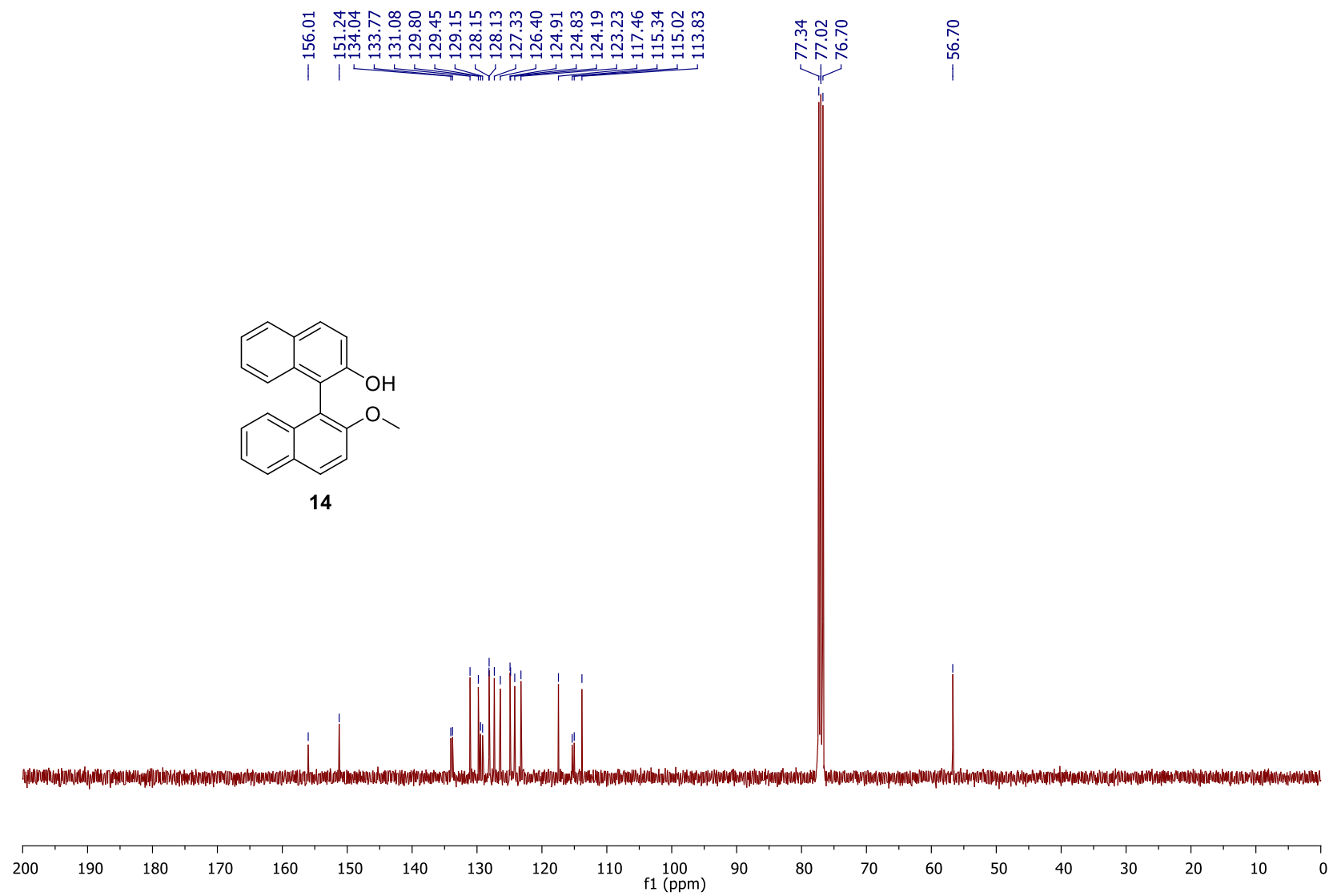
^{13}C NMR spectrum of 7 in CDCl_3



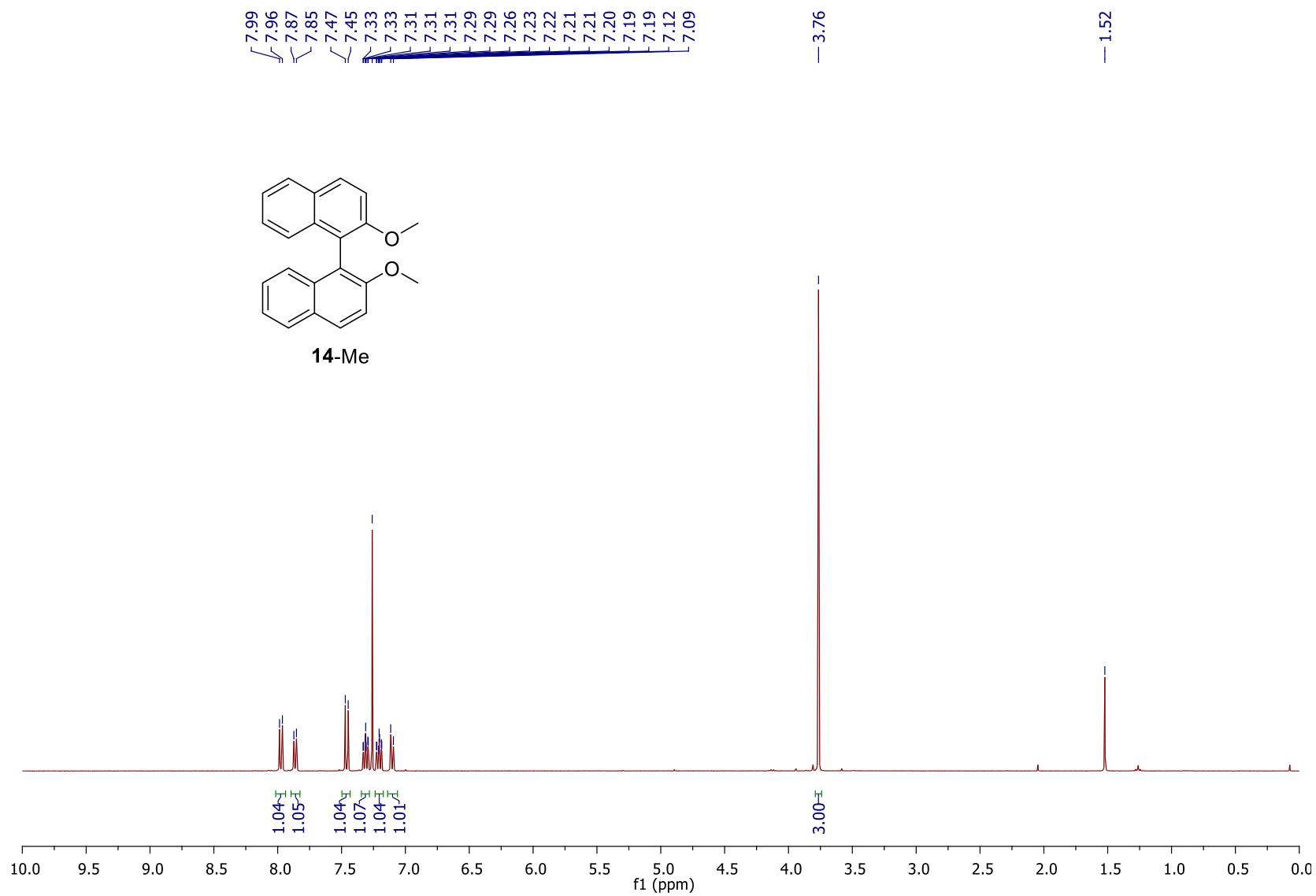
^1H NMR spectrum of 14 in CDCl_3



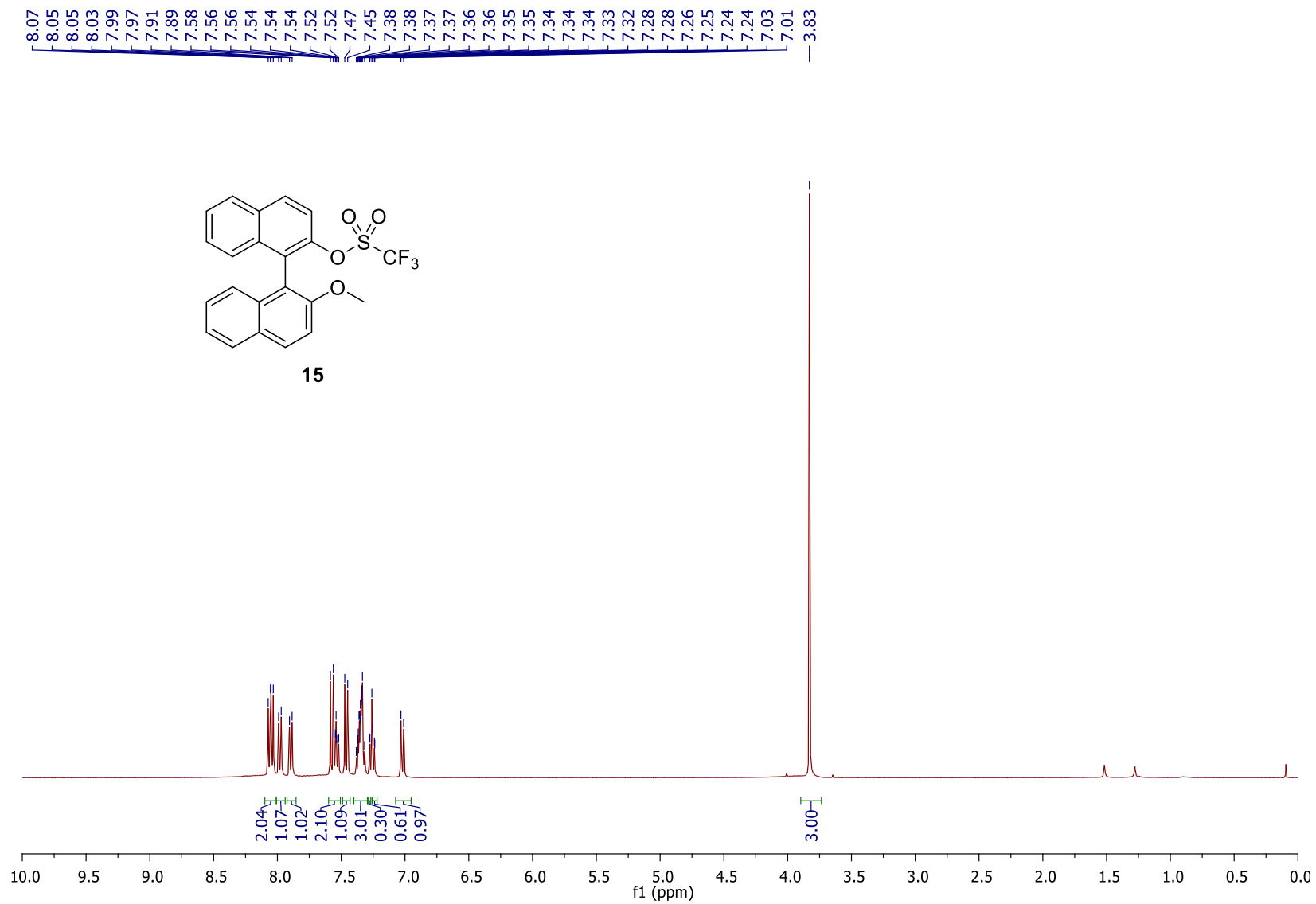
^{13}C NMR spectrum of 14 in CDCl_3



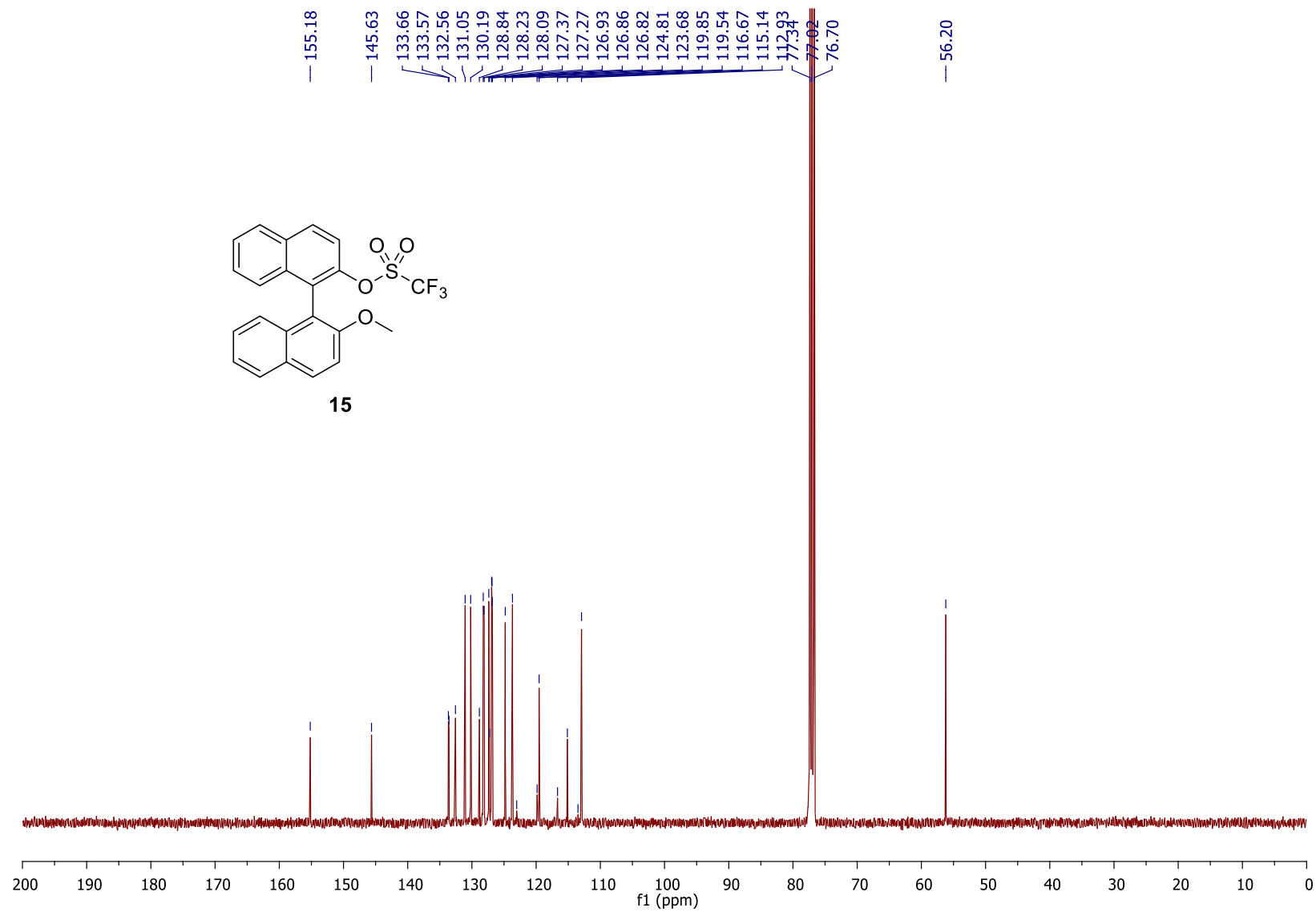
^1H NMR spectrum of 14-Me in CDCl_3



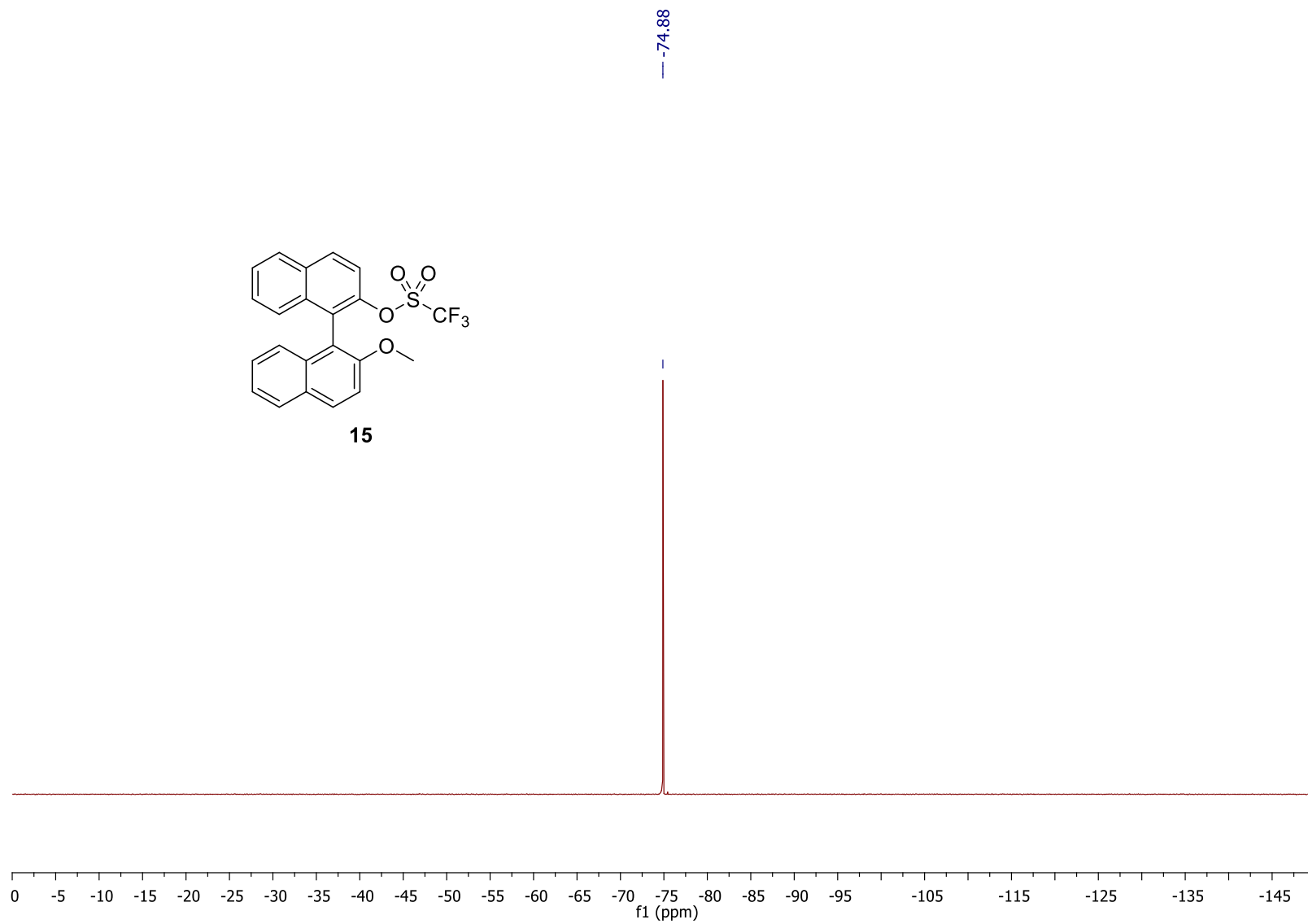
¹H NMR spectrum of 15 in CDCl₃



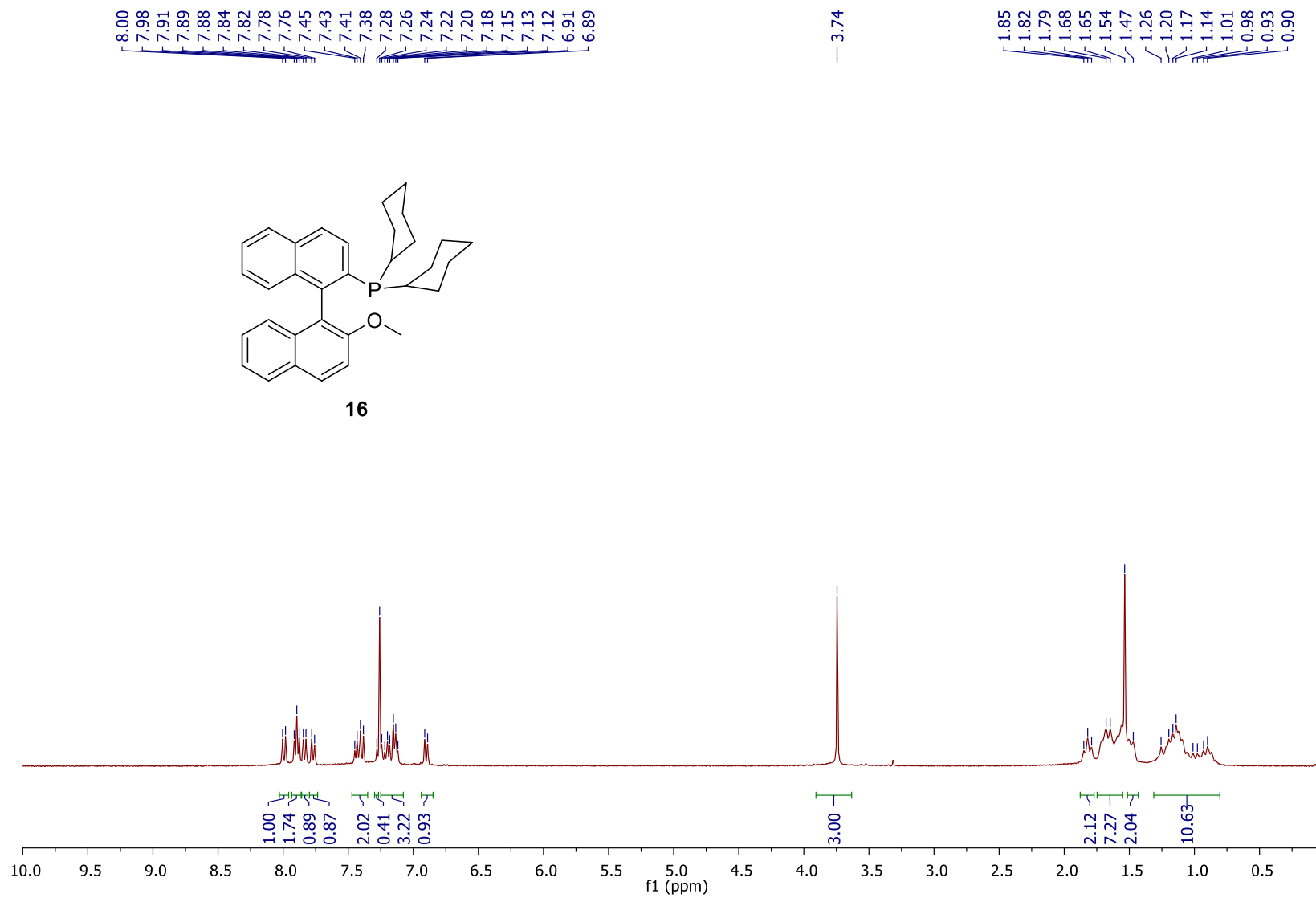
^{13}C NMR spectrum of 15 in CDCl_3



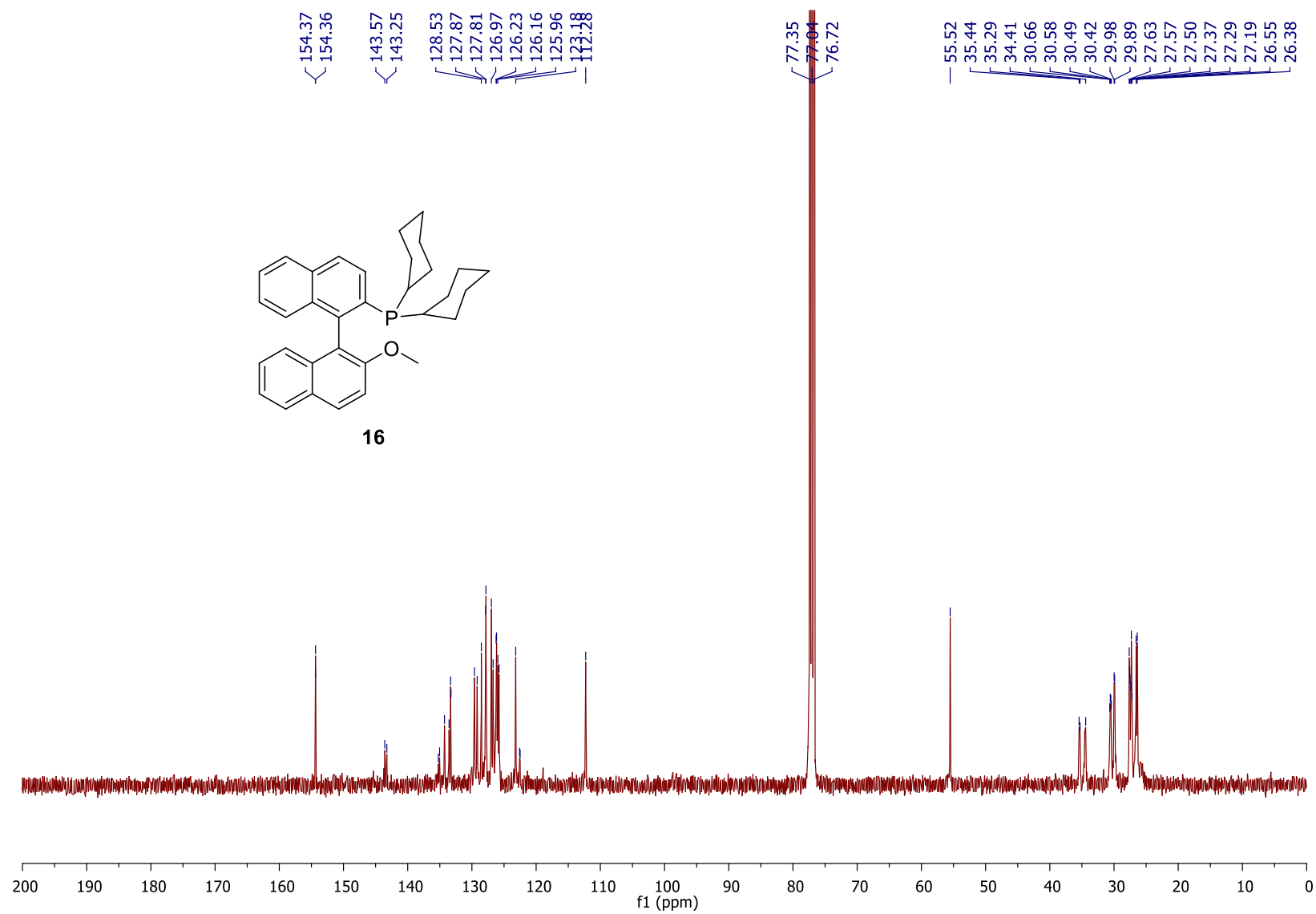
^{19}F NMR spectrum of 15 in CDCl_3



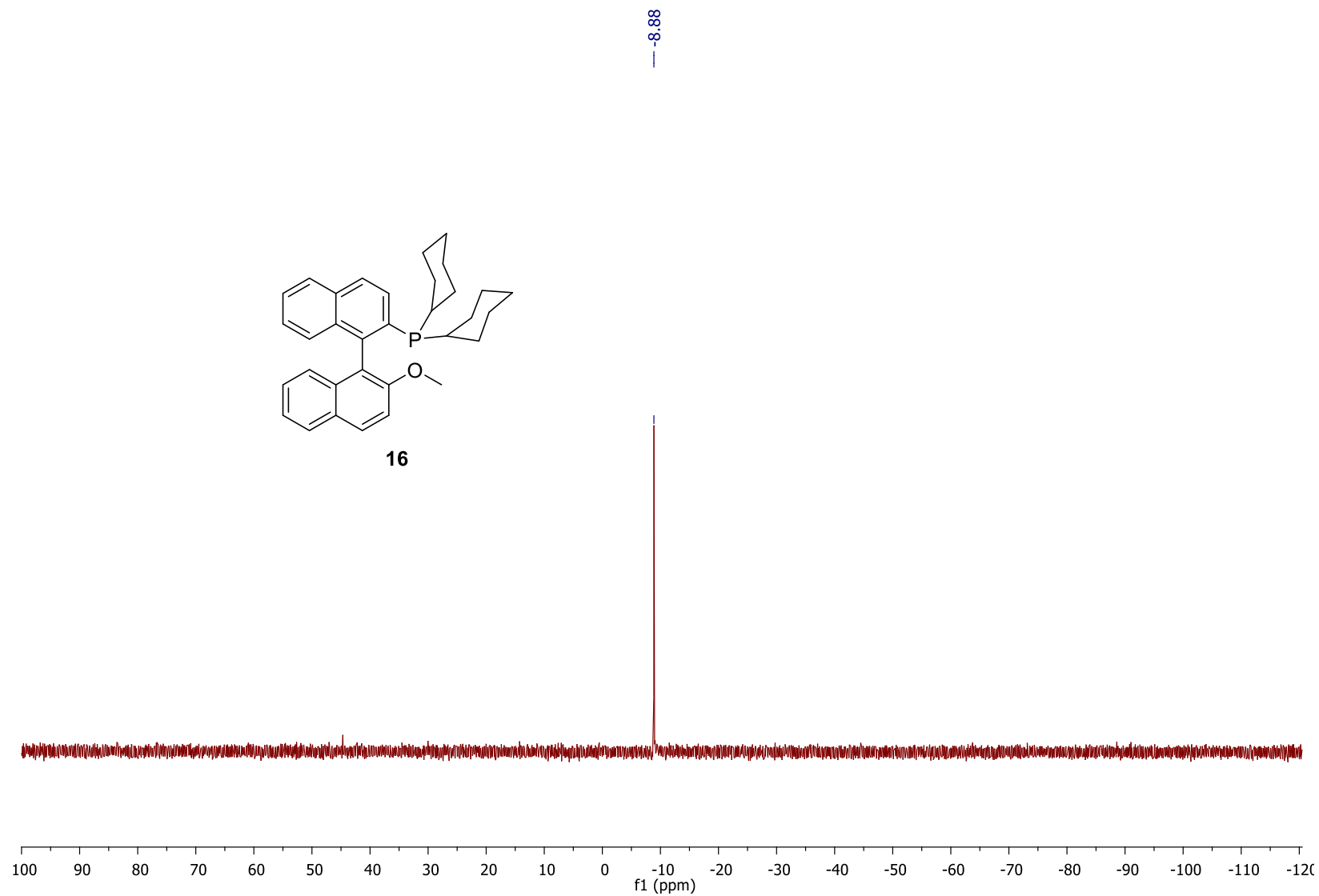
^1H NMR spectrum of 16 in CDCl_3



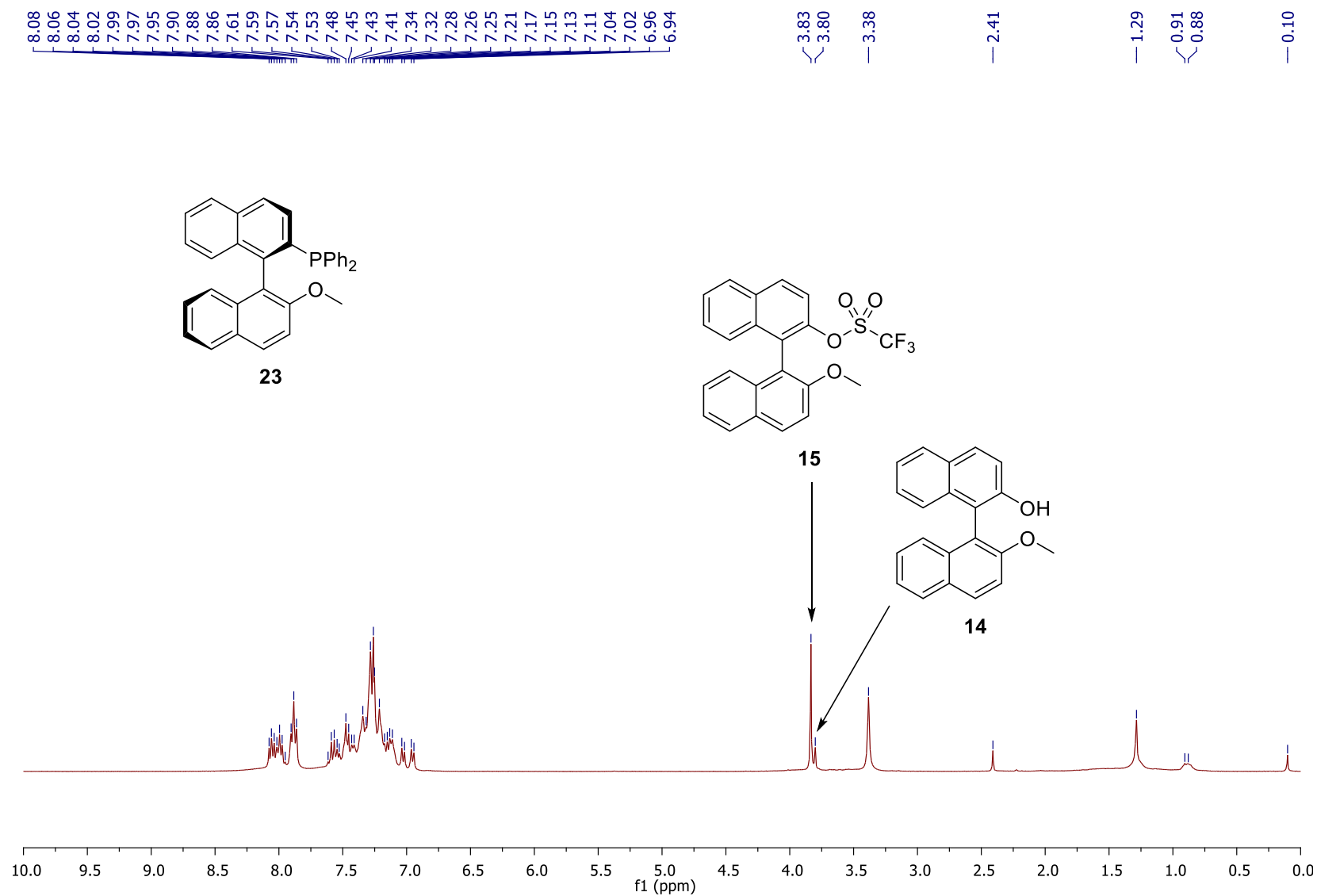
^{13}C NMR spectrum of 16 in CDCl_3



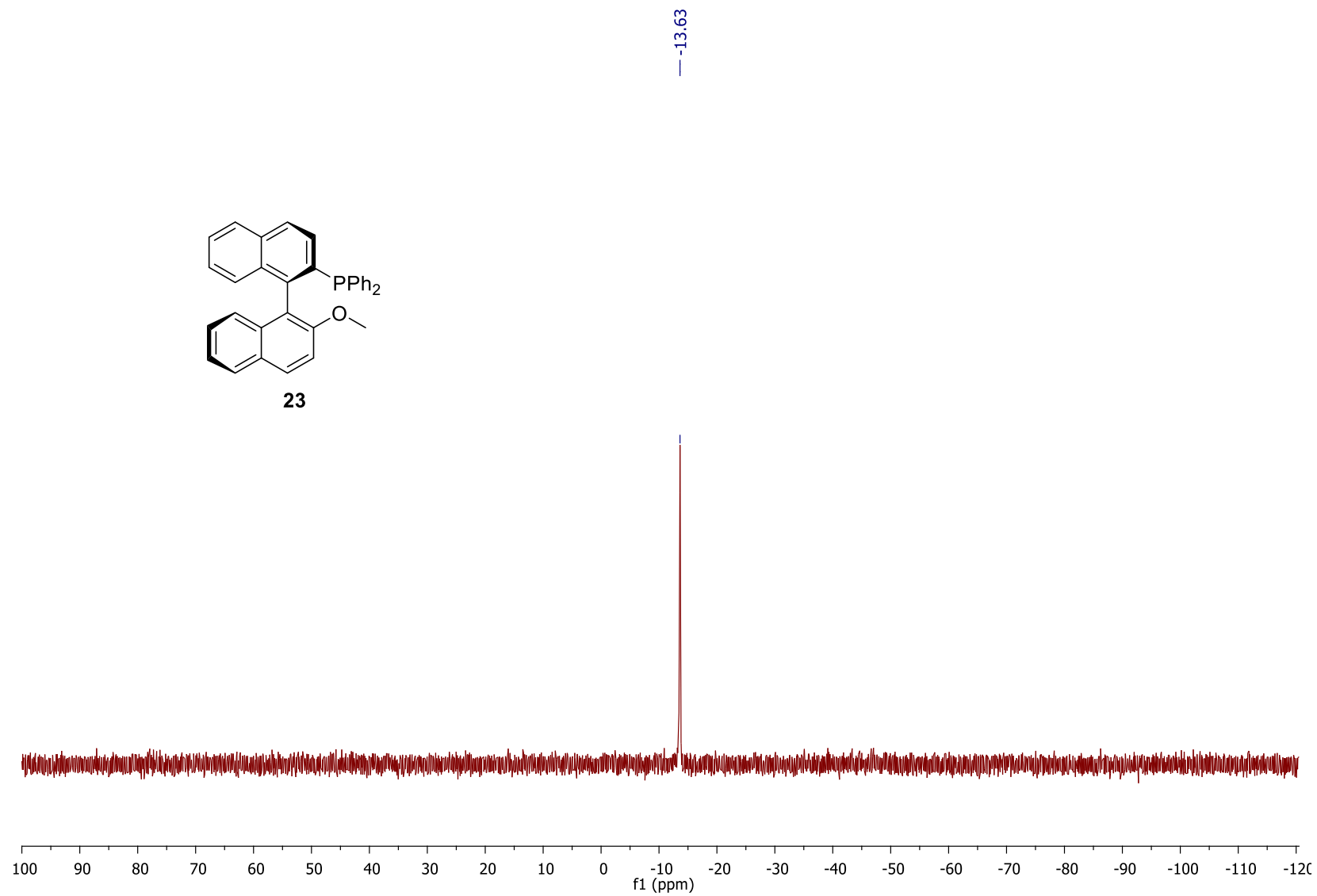
^{31}P NMR spectrum of 16 in CDCl_3



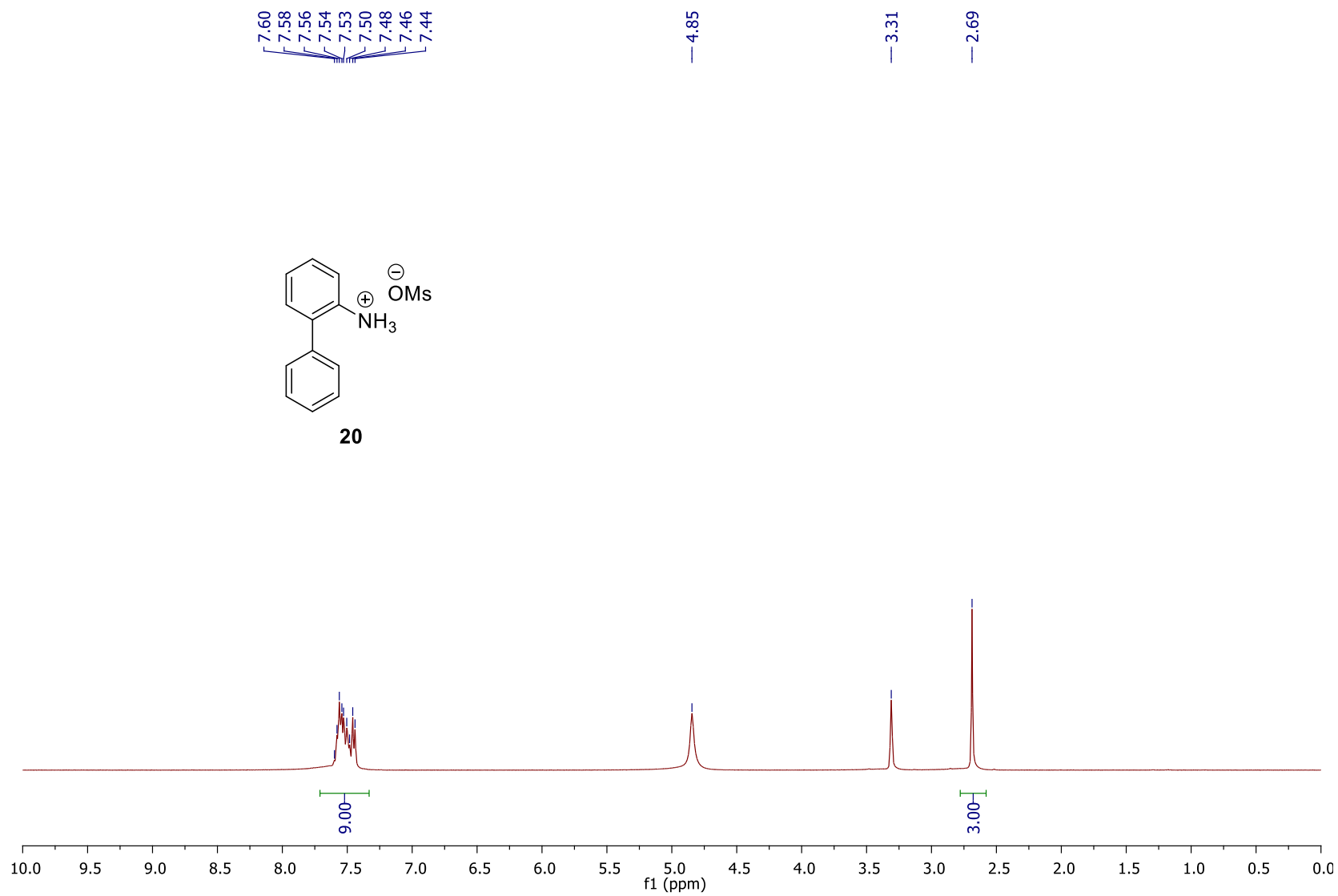
¹H NMR spectrum of impure 23 in CDCl₃



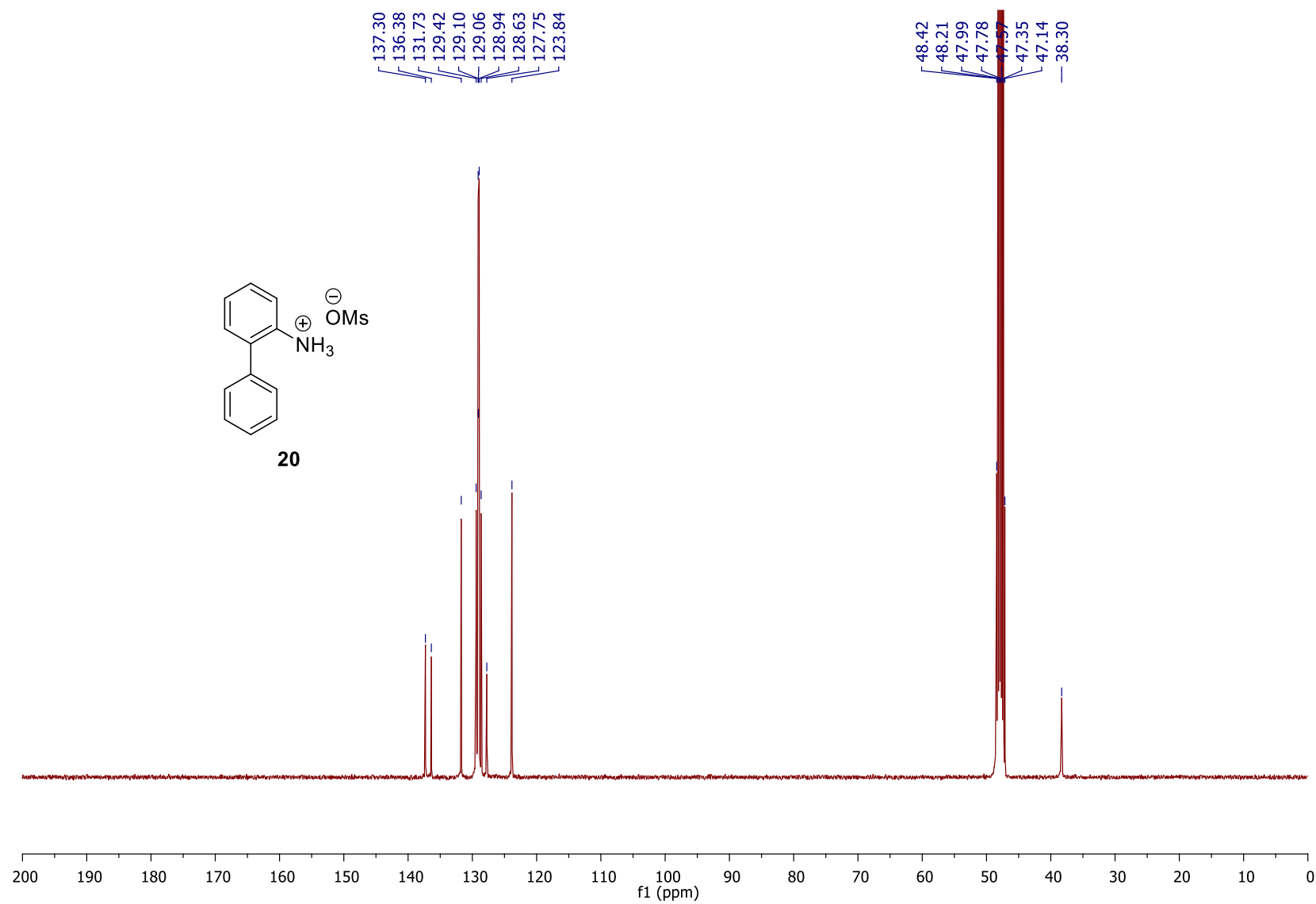
^{31}P NMR spectrum of 23 in CDCl_3



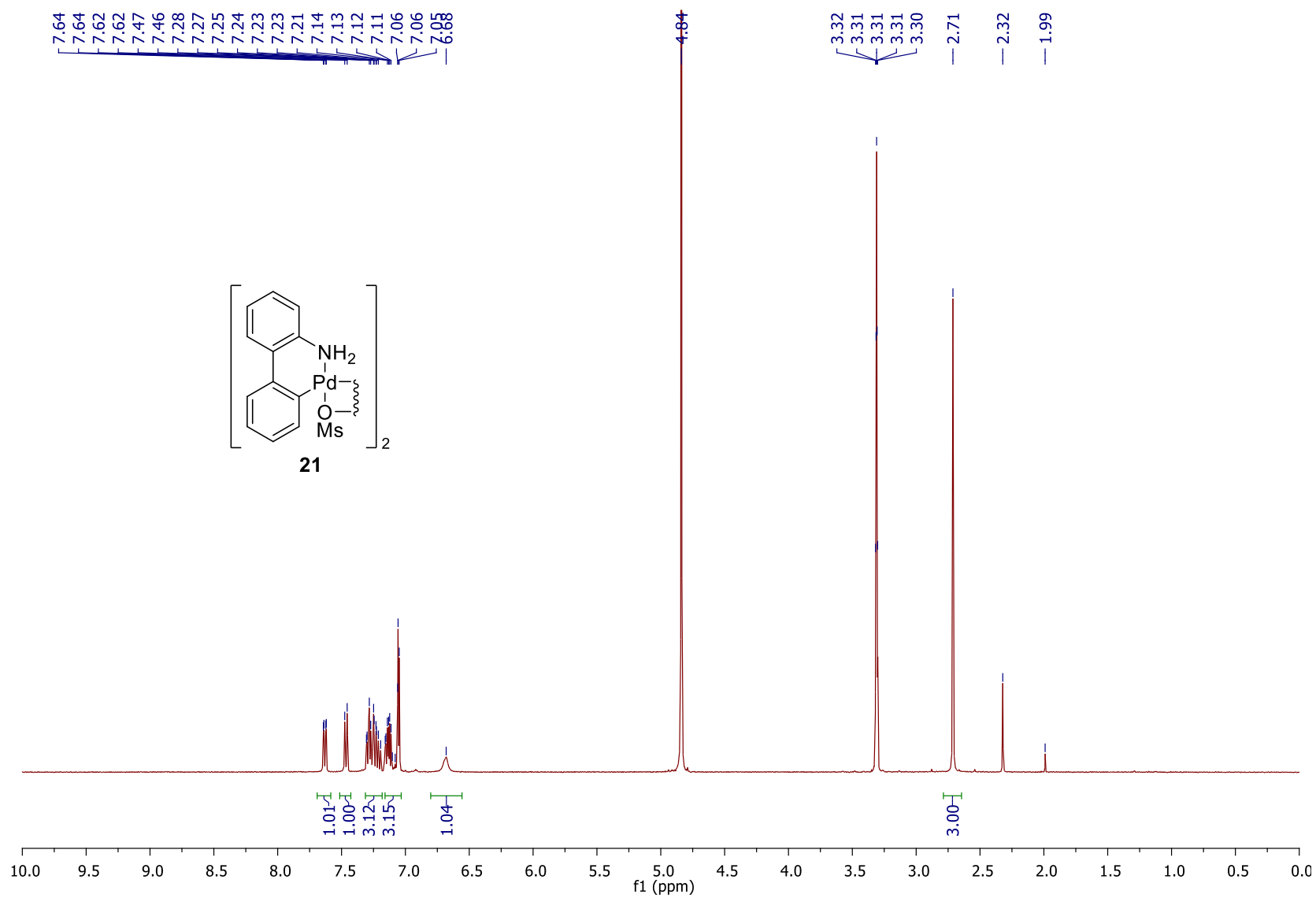
^1H NMR spectrum of 20 in CD_3OD



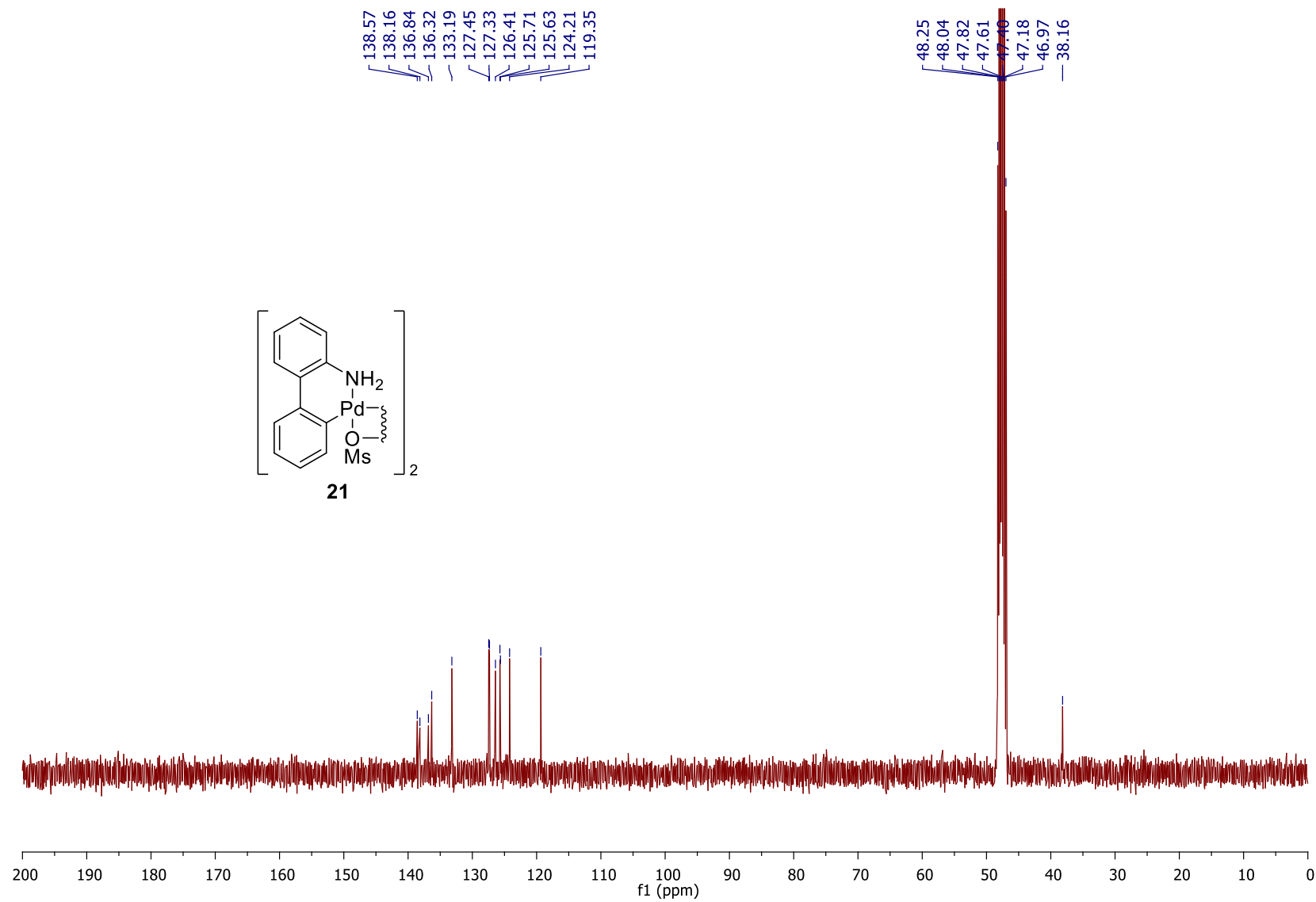
^{13}C NMR spectrum of 20 in CD_3OD



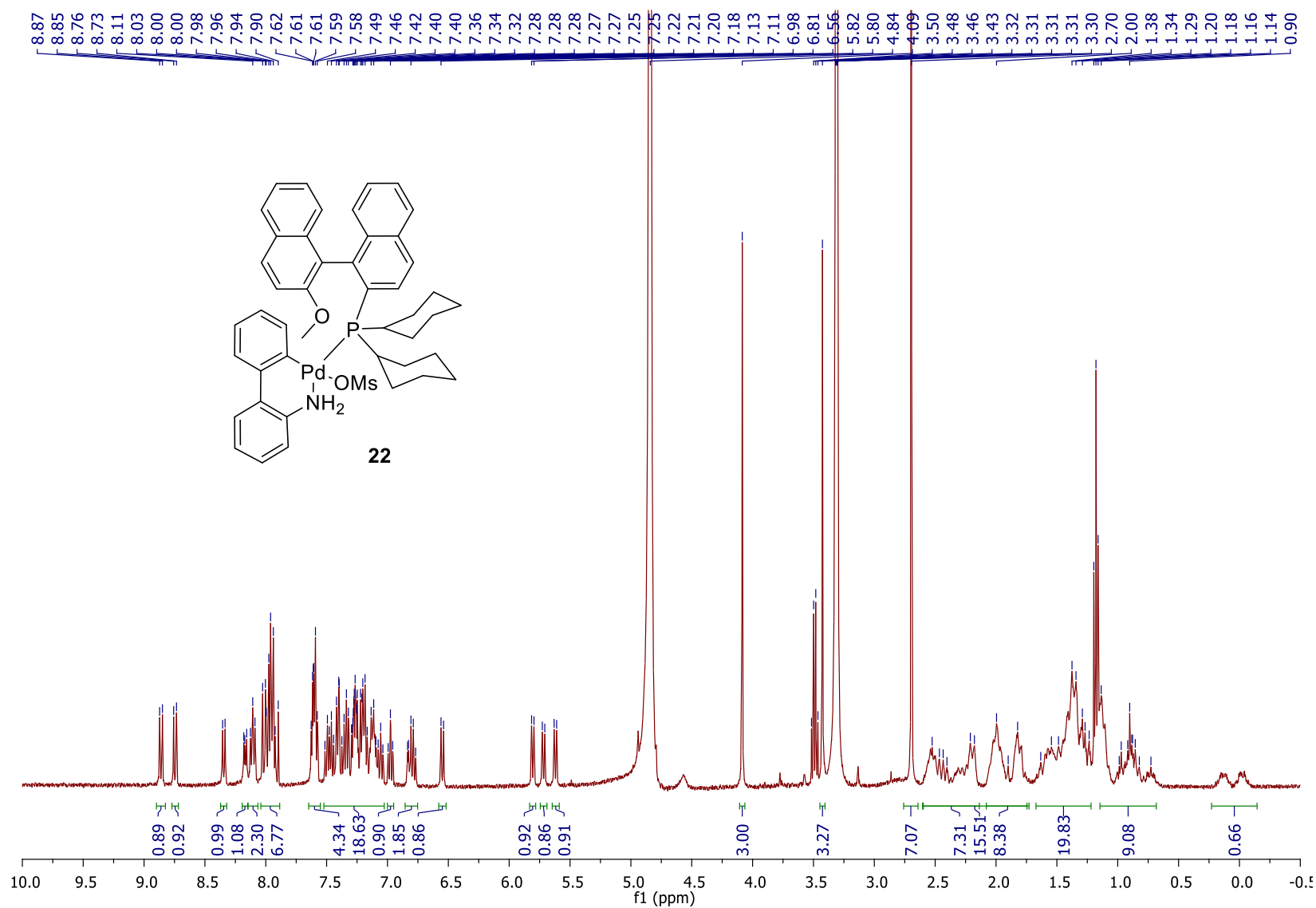
¹H NMR spectrum of 21 in CD₃OD



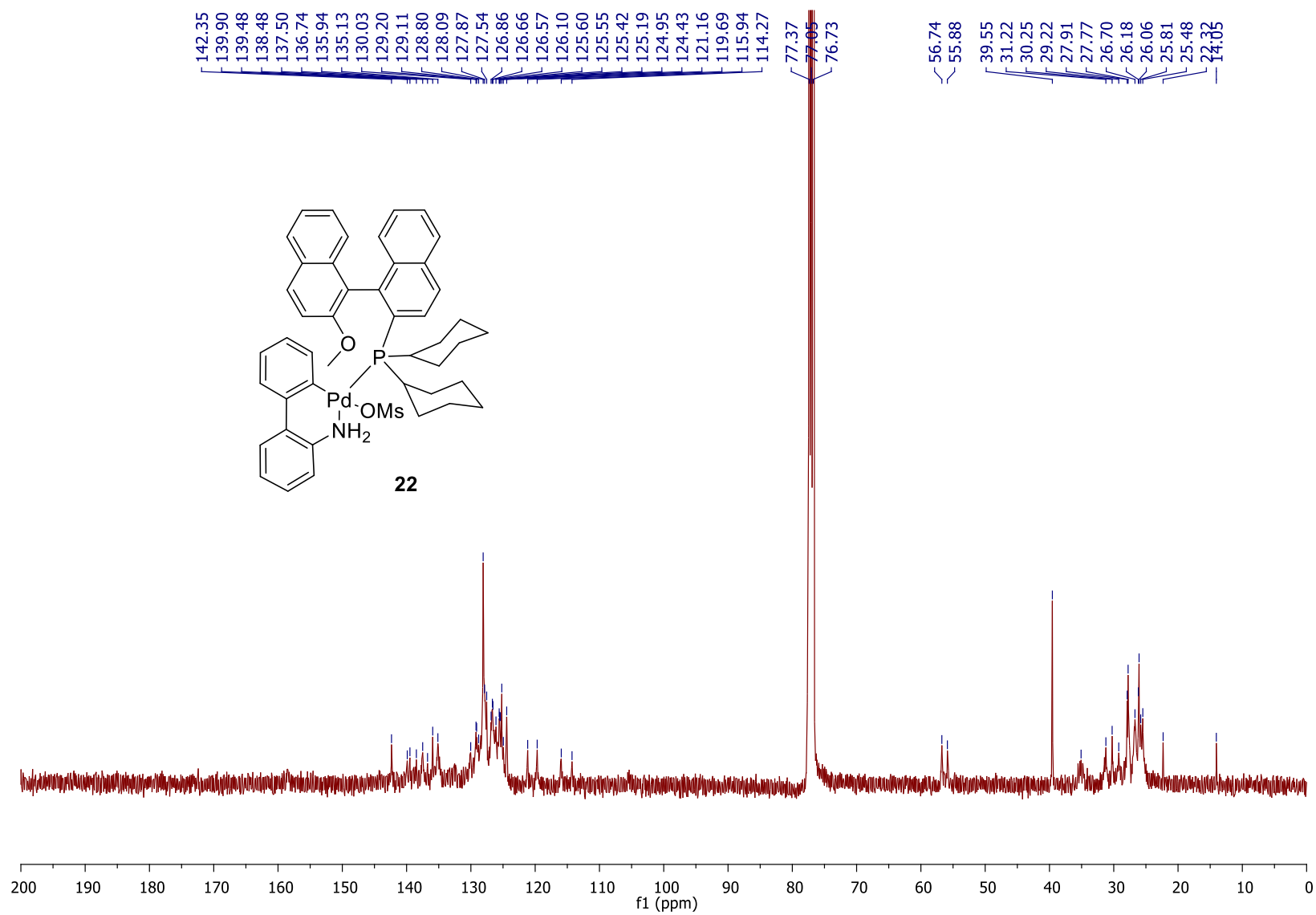
^{13}C NMR spectrum of 21 in CD_3OD



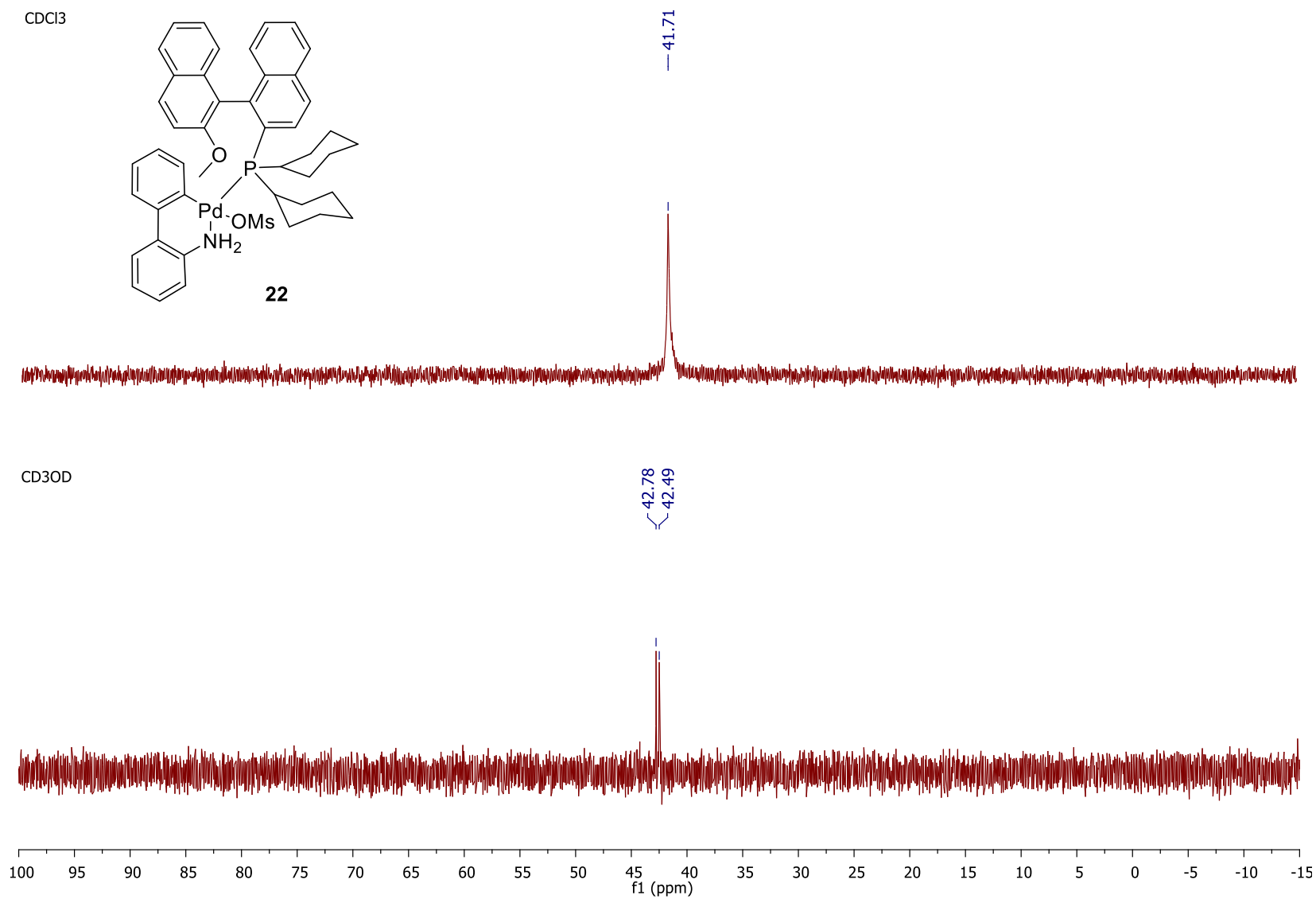
¹H NMR spectrum of 22 in CD₃OD



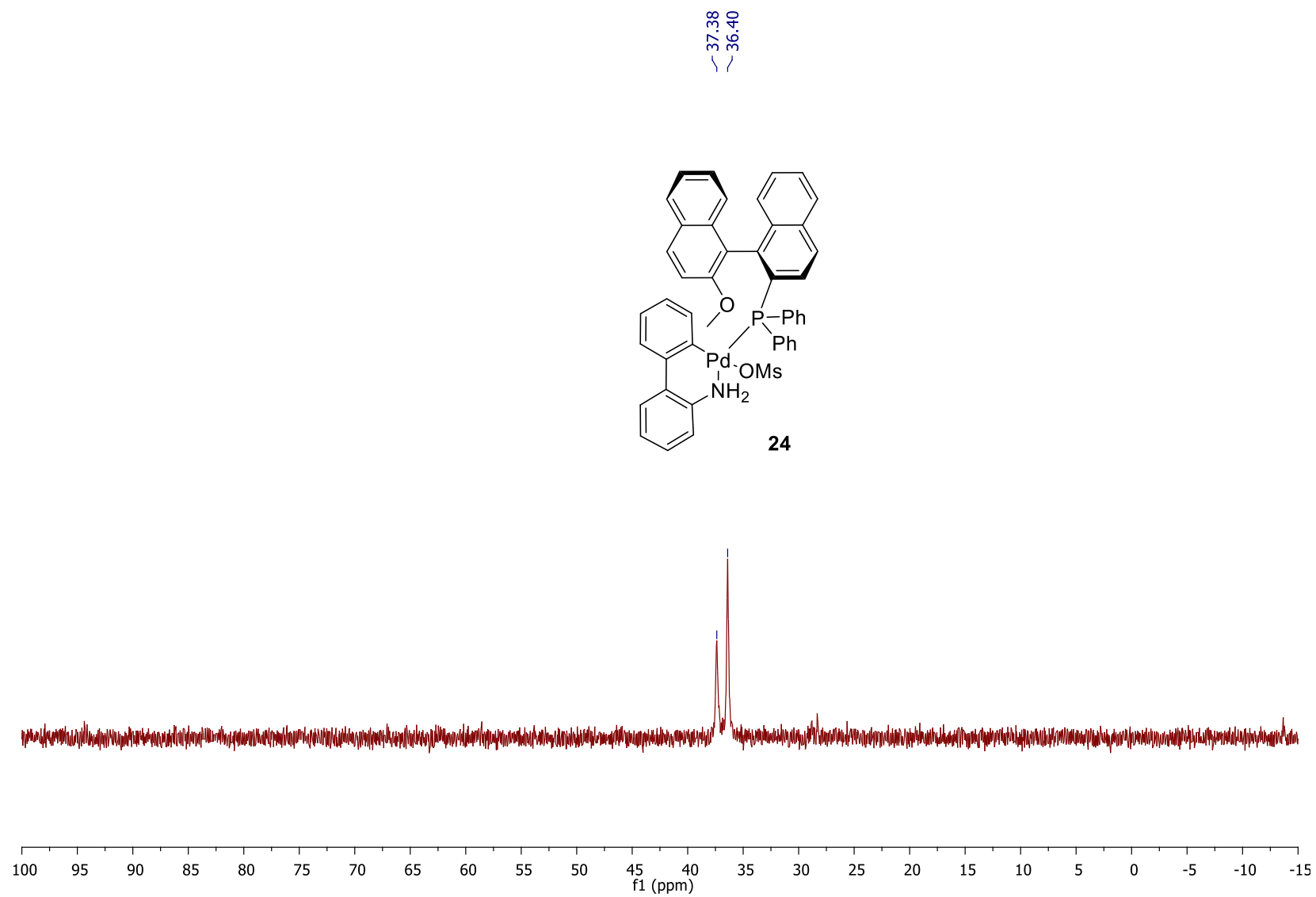
^{13}C NMR spectrum of 22 in CDCl_3



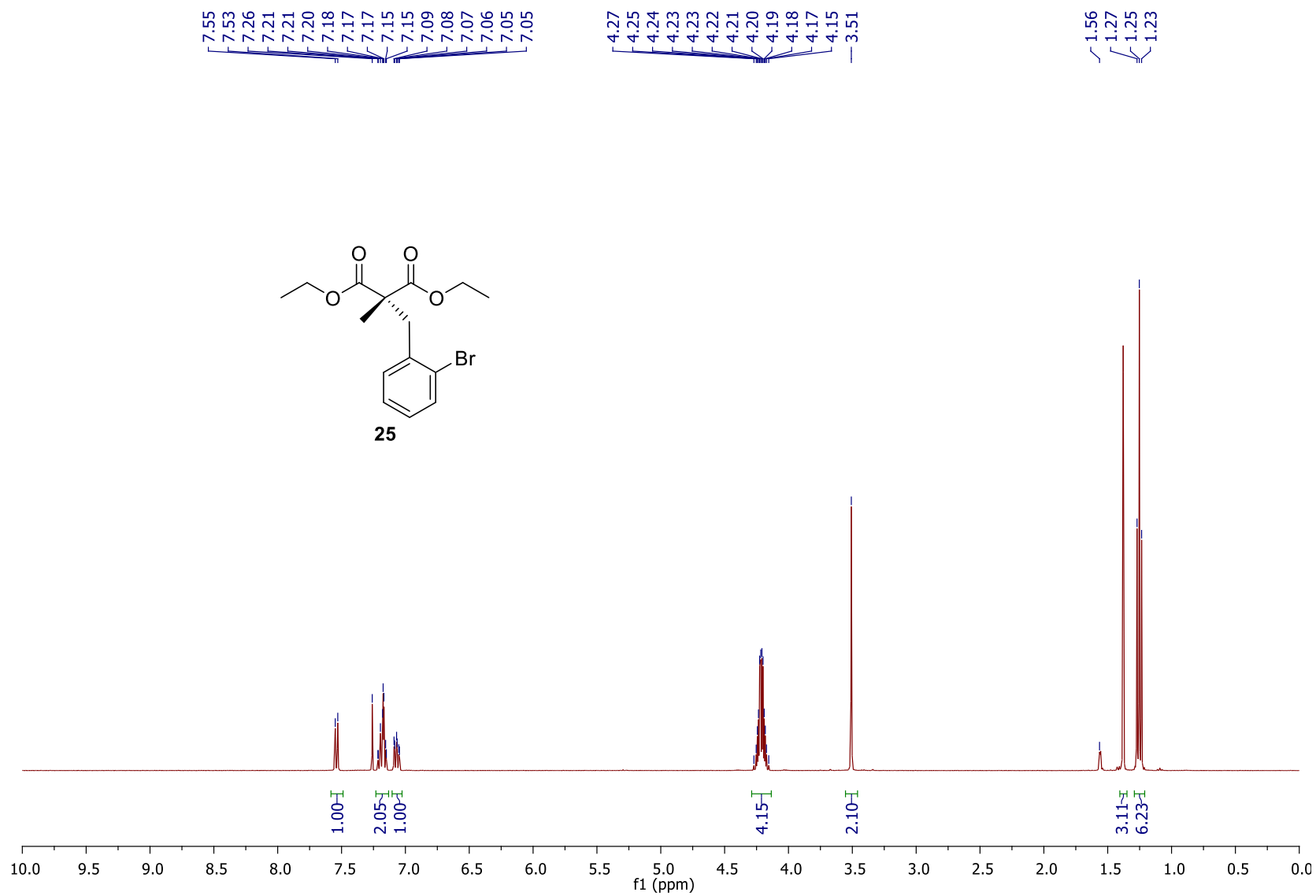
^{31}P NMR spectrum of 22 in CDCl_3 (top) and CD_3OD (bottom)



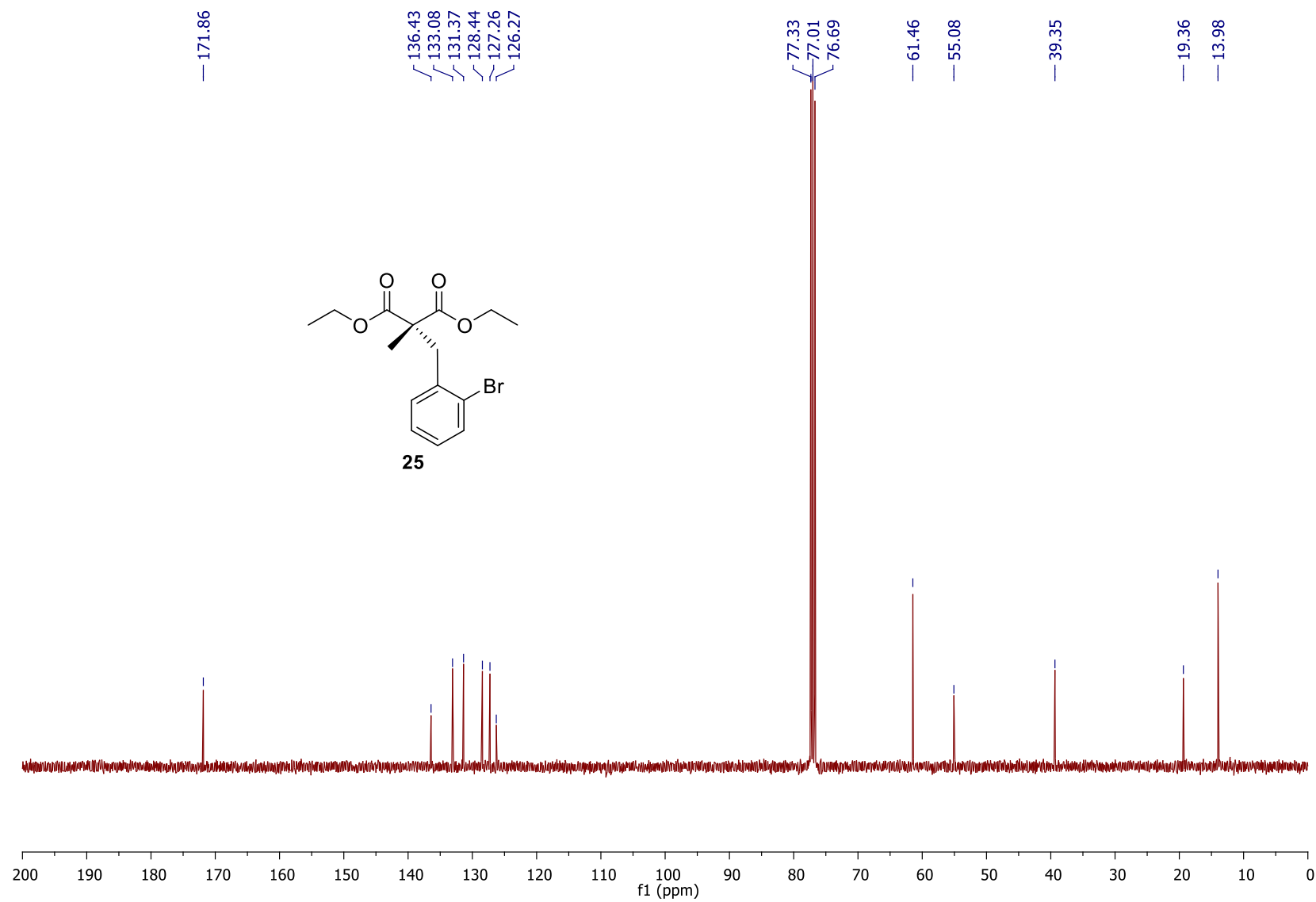
^{31}P NMR spectrum of 24 in CDCl_3



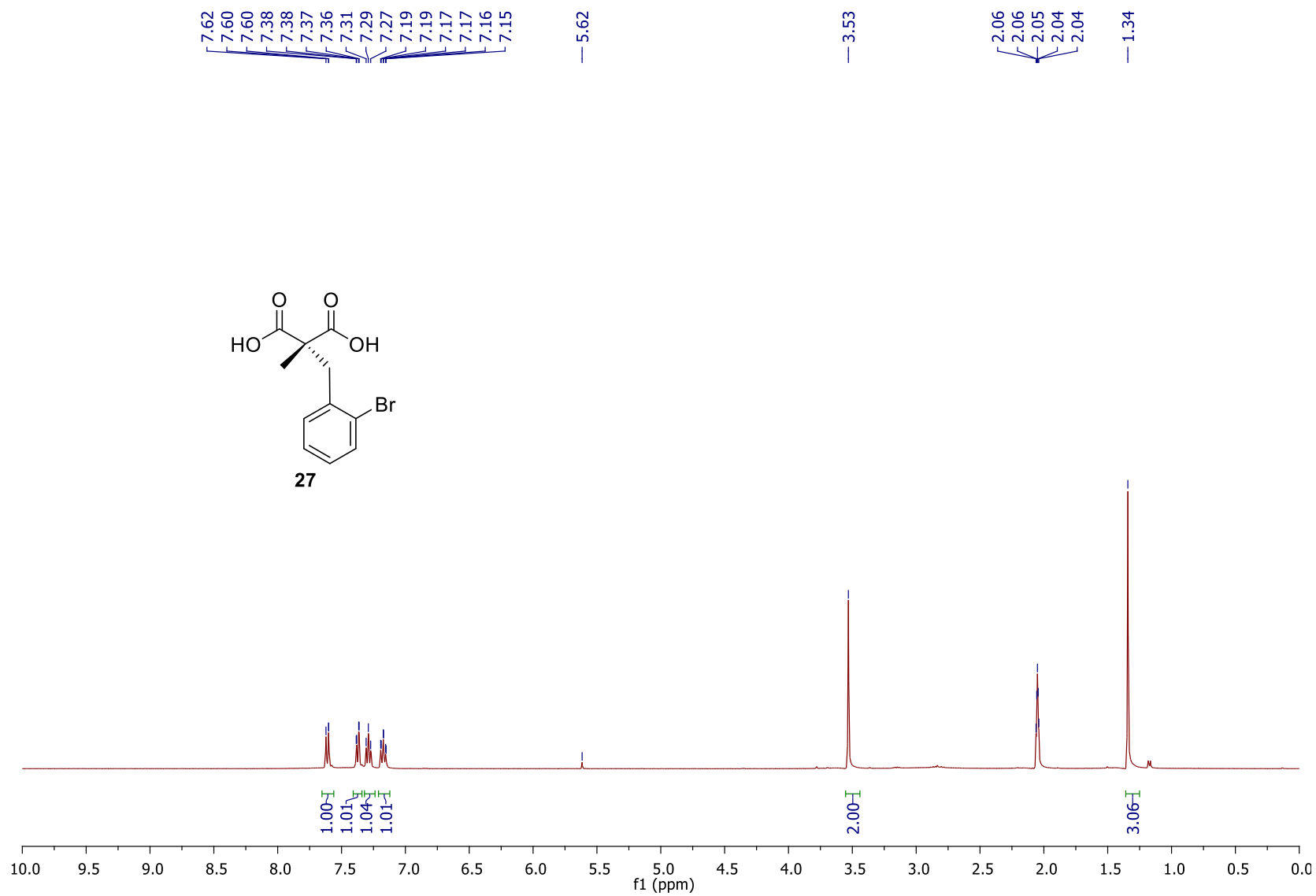
^1H NMR spectrum of 25 in CDCl_3



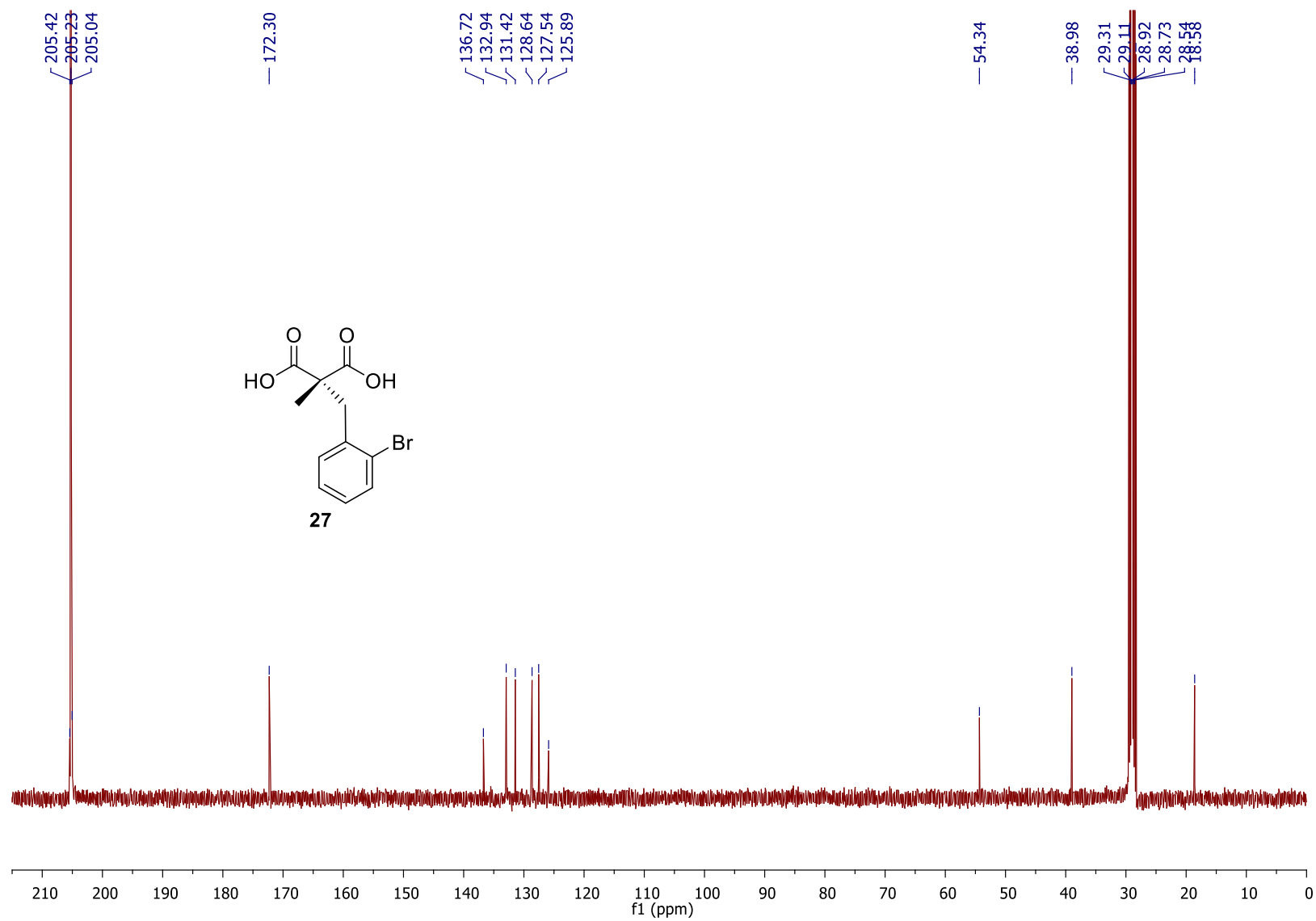
^{13}C NMR spectrum of 25 in CDCl_3



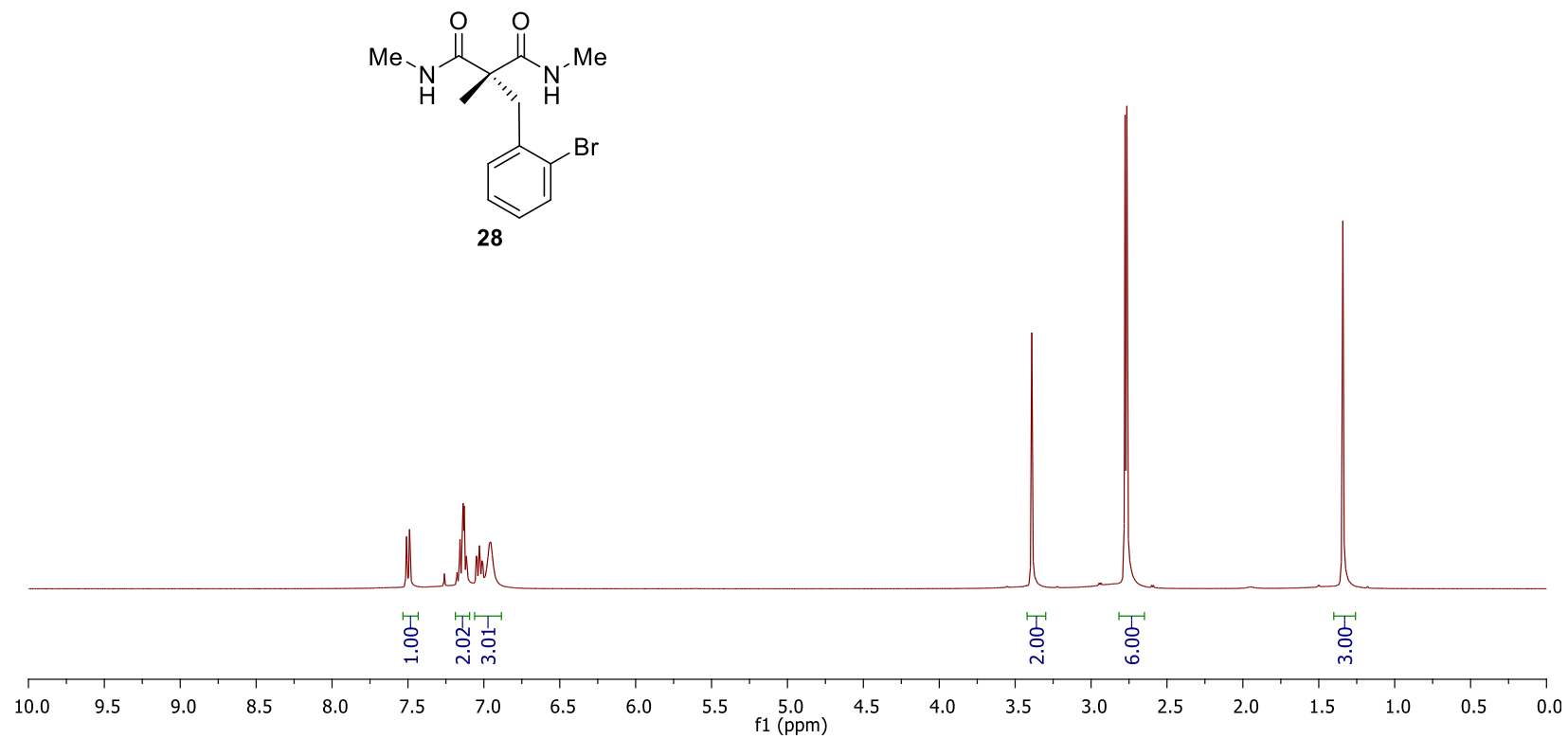
^1H NMR spectrum of 27 in CDCl_3



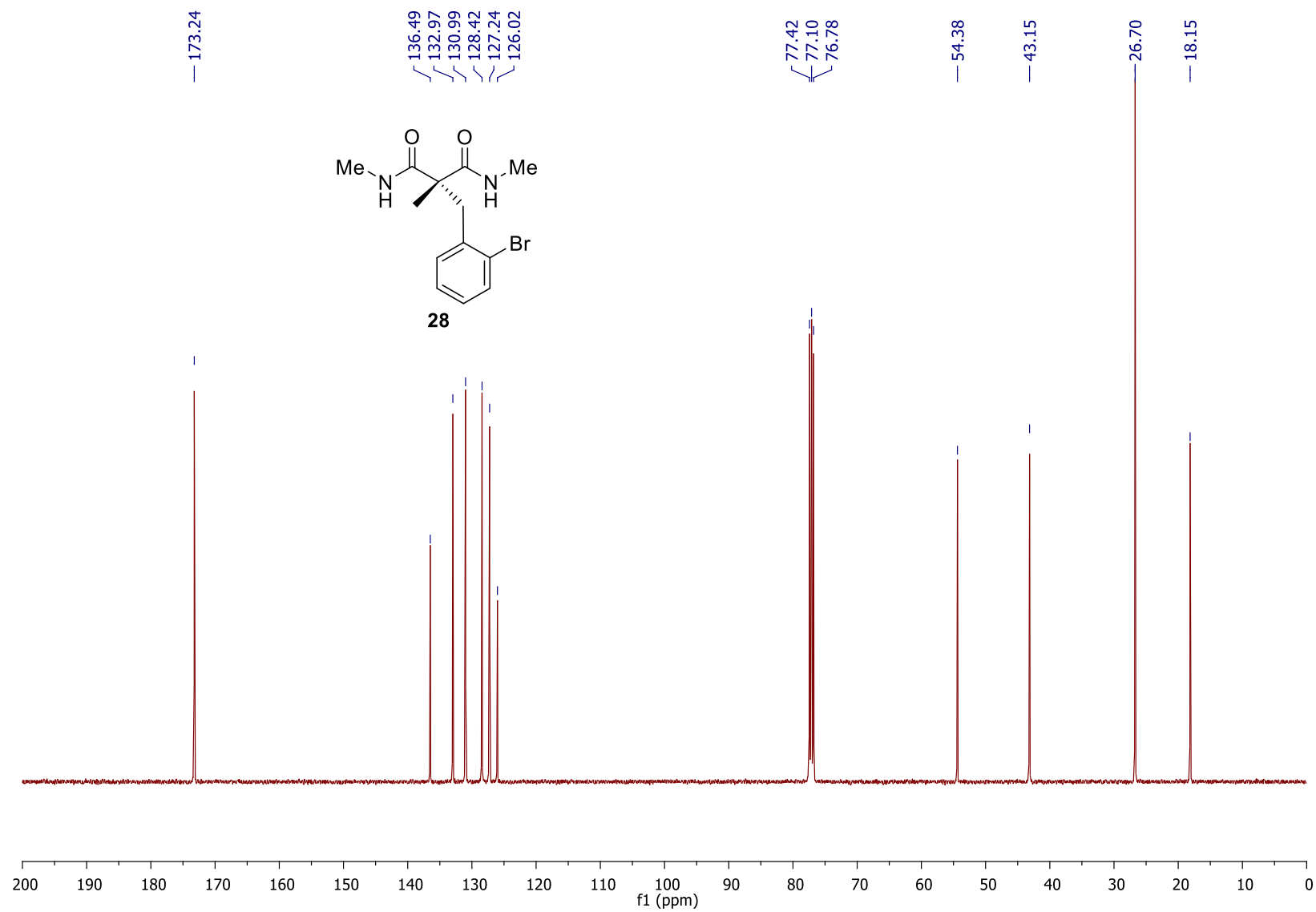
^{13}C NMR spectrum of 27 in CDCl_3



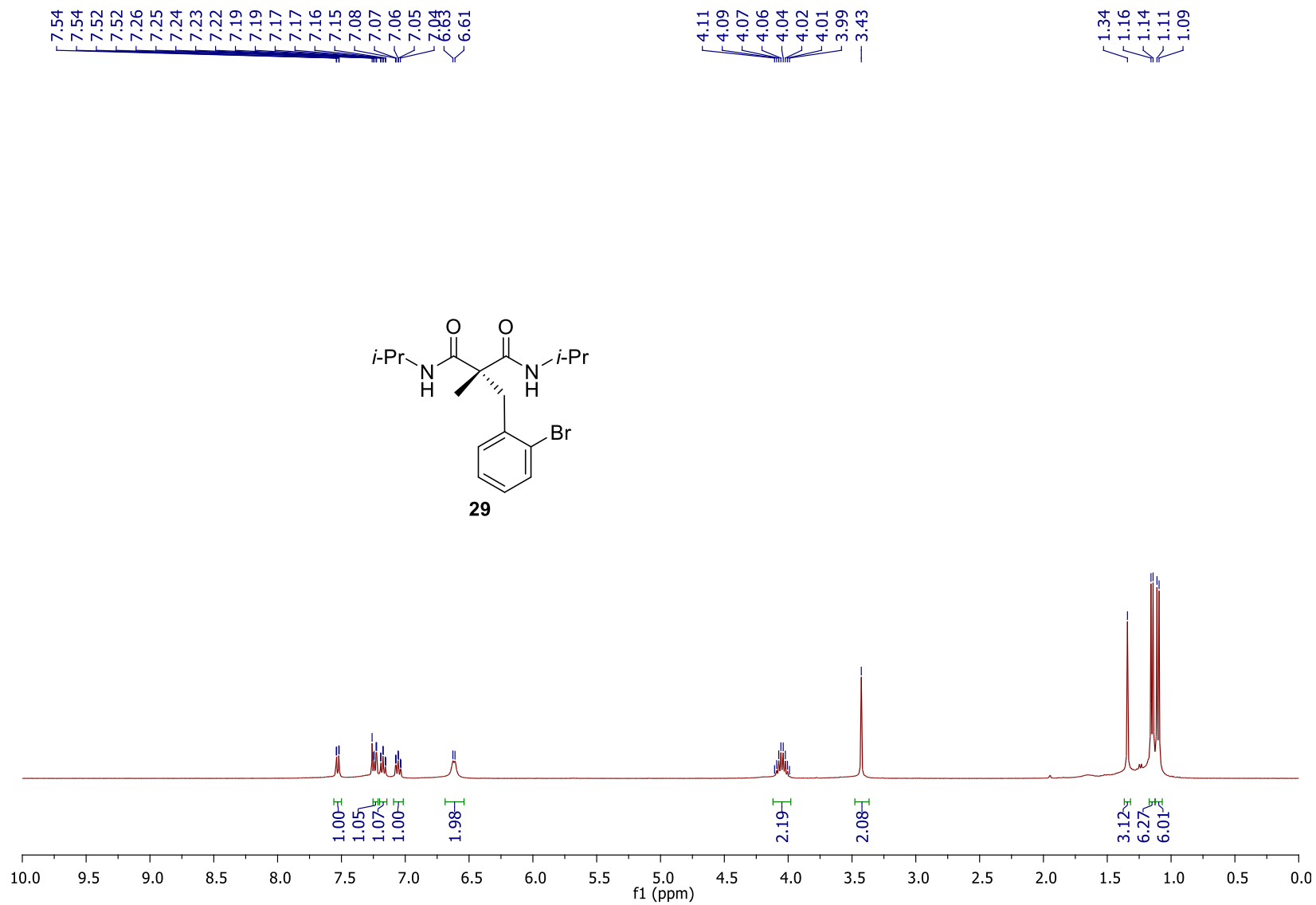
^1H NMR spectrum of 28 in CDCl_3



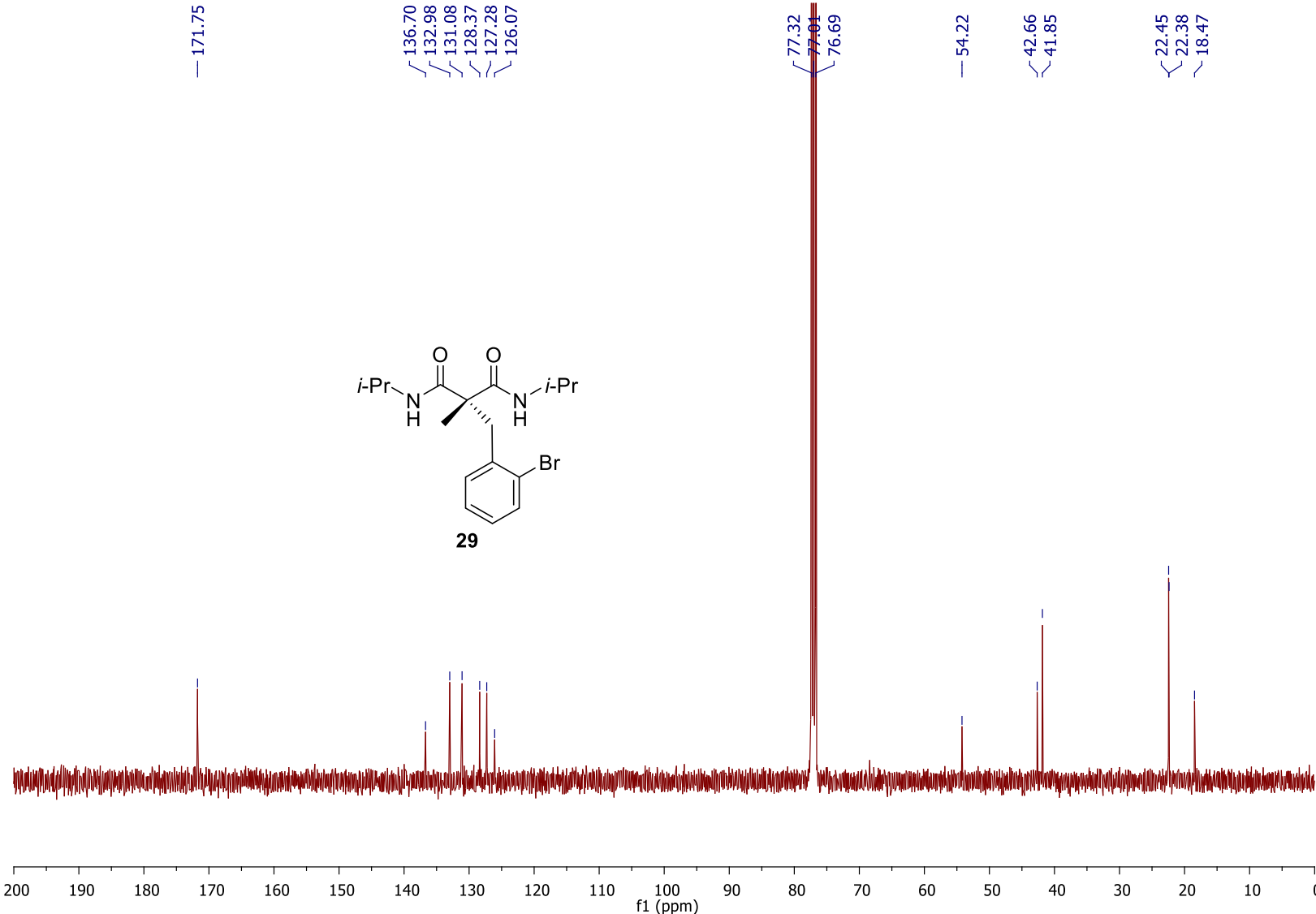
^{13}C NMR spectrum of 28 in CDCl_3



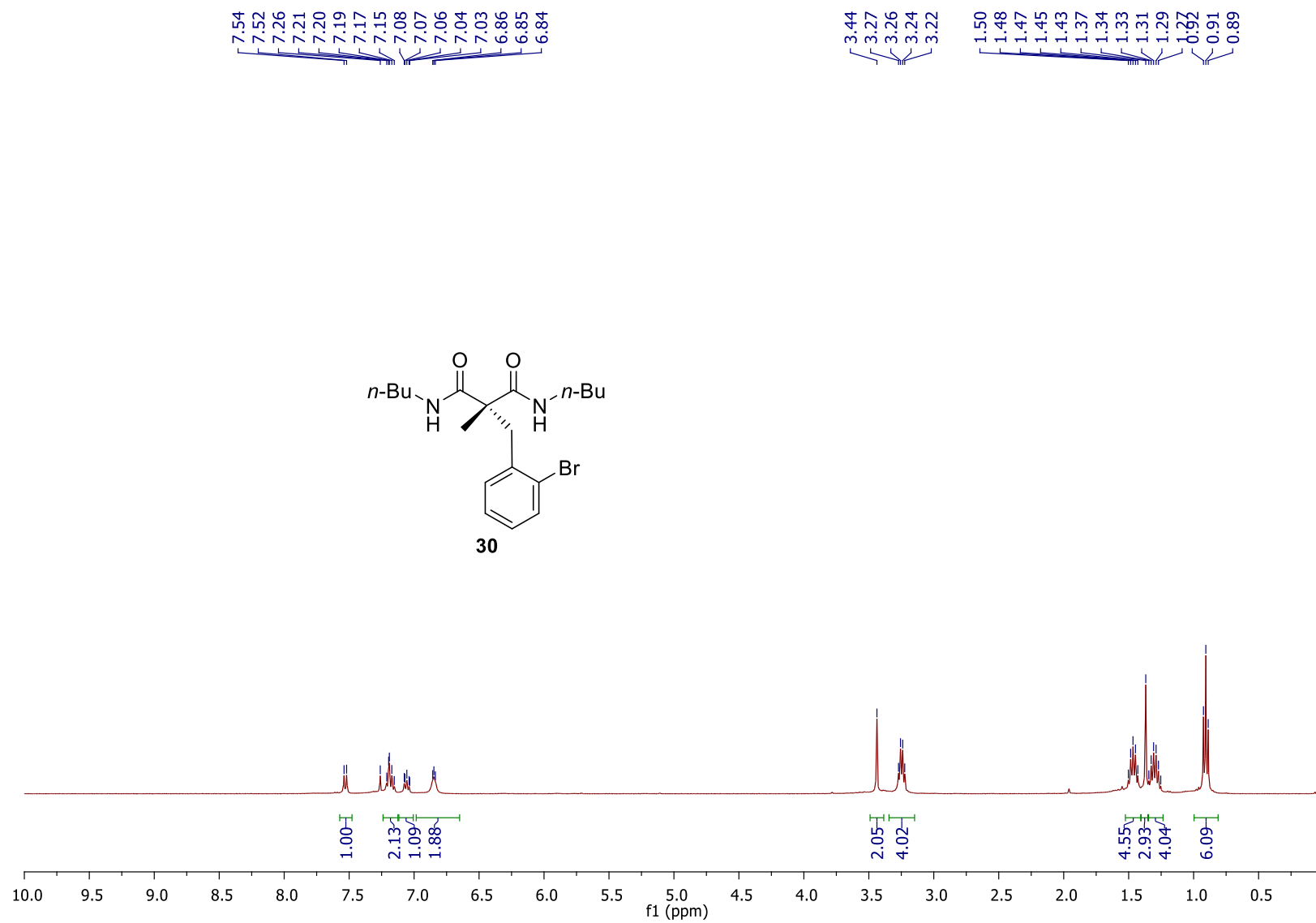
¹H NMR spectrum of 29 in CDCl₃



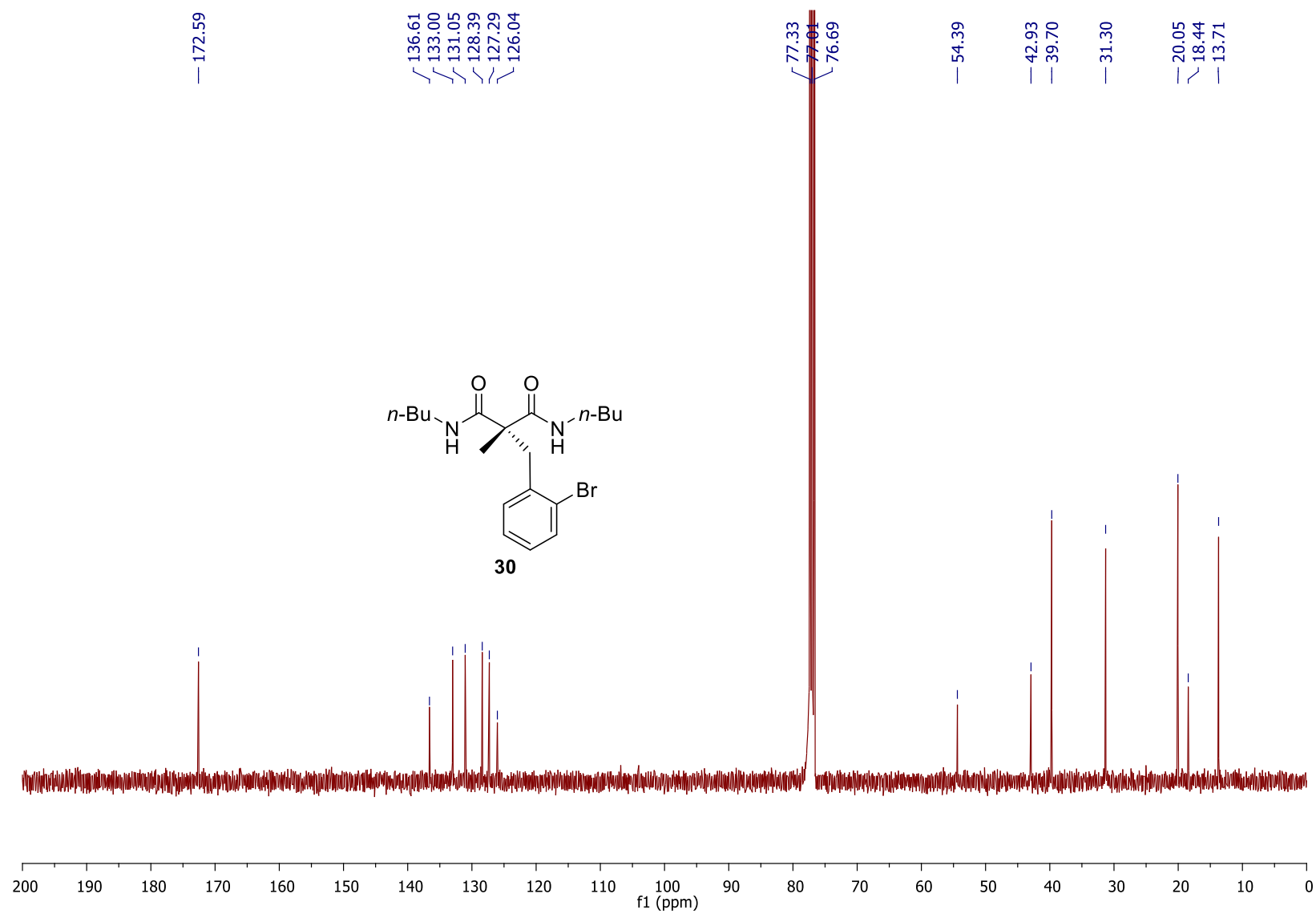
^{13}C NMR spectrum of 29 in CDCl_3



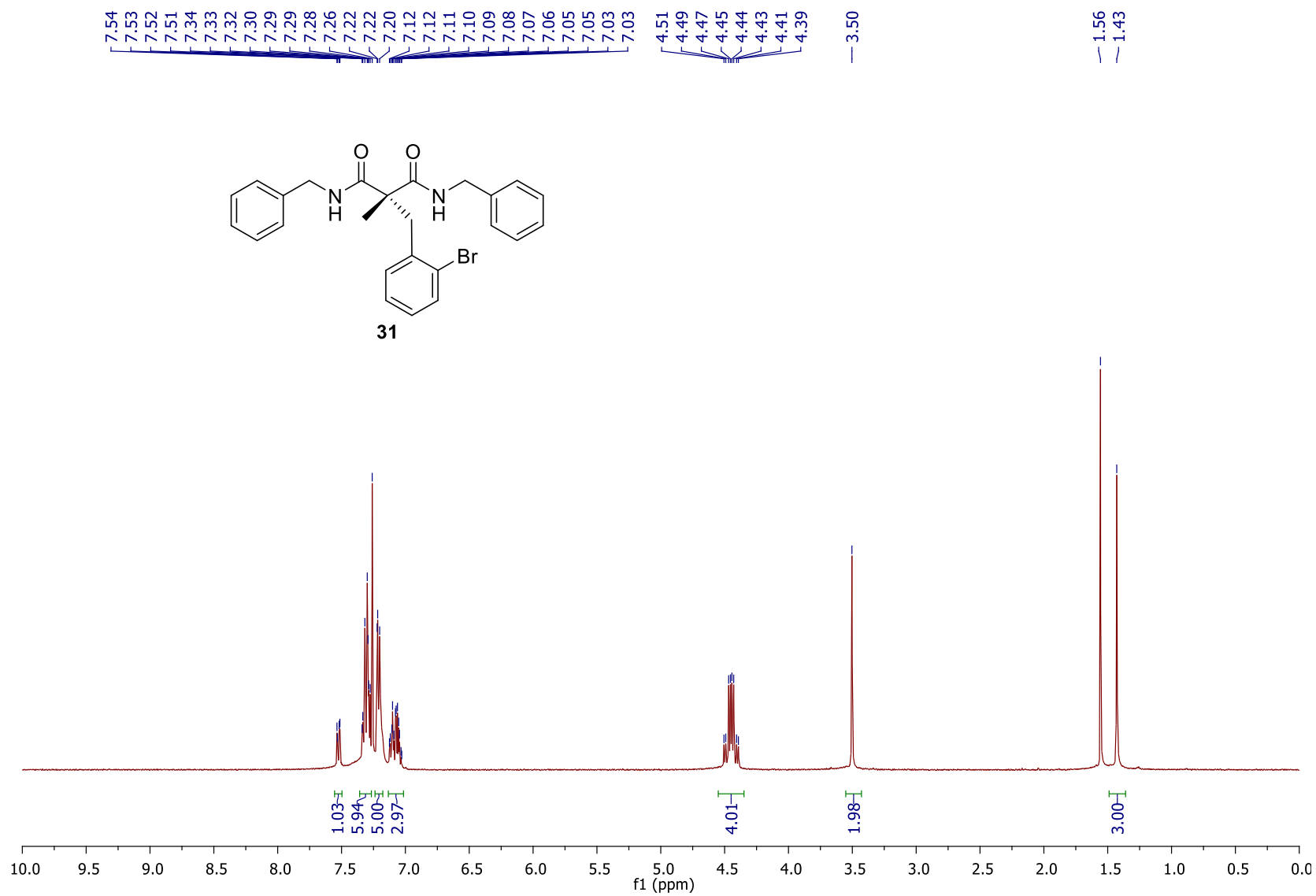
^1H NMR spectrum of 30 in CDCl_3



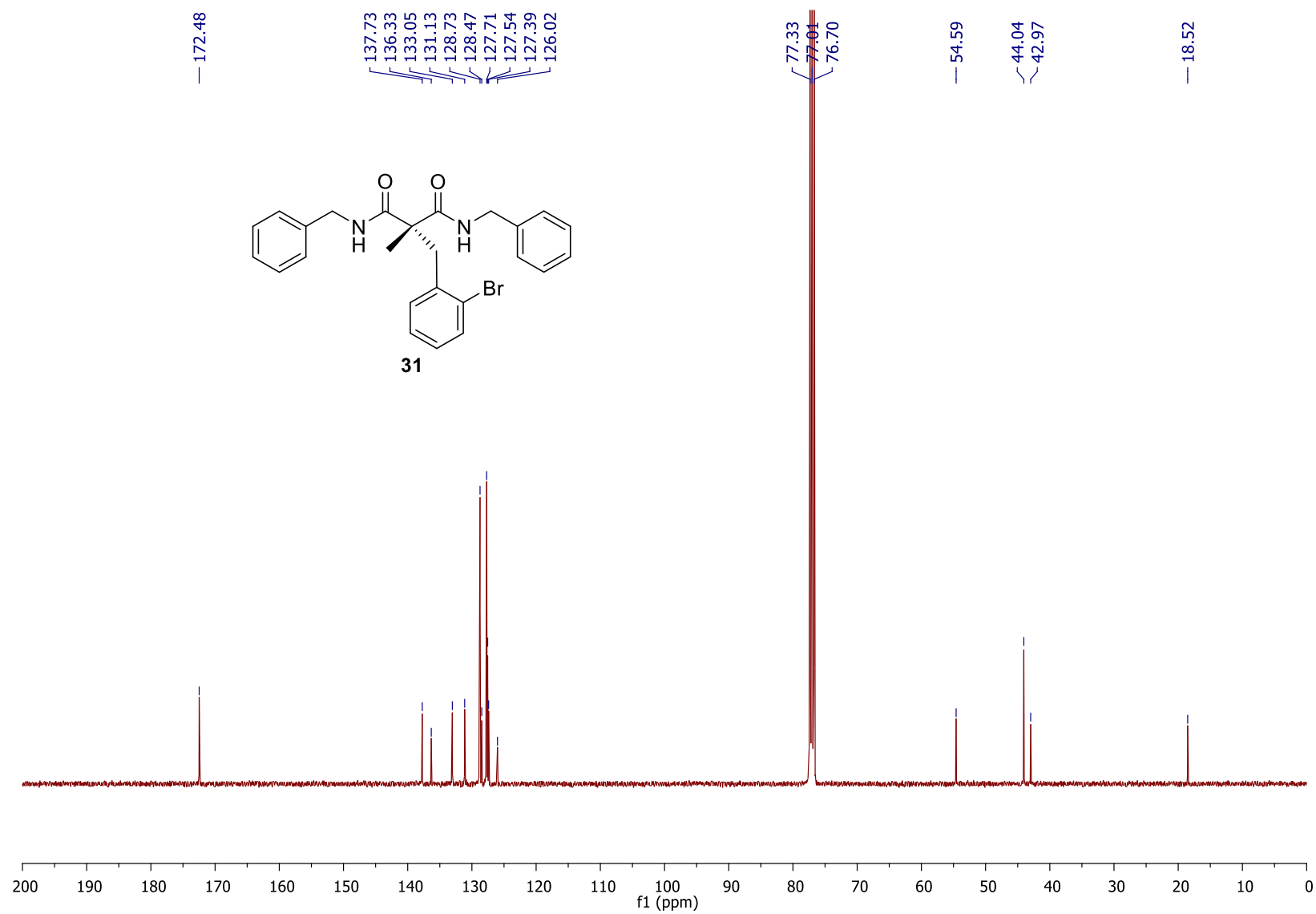
^{13}C NMR spectrum of 30 in CDCl_3



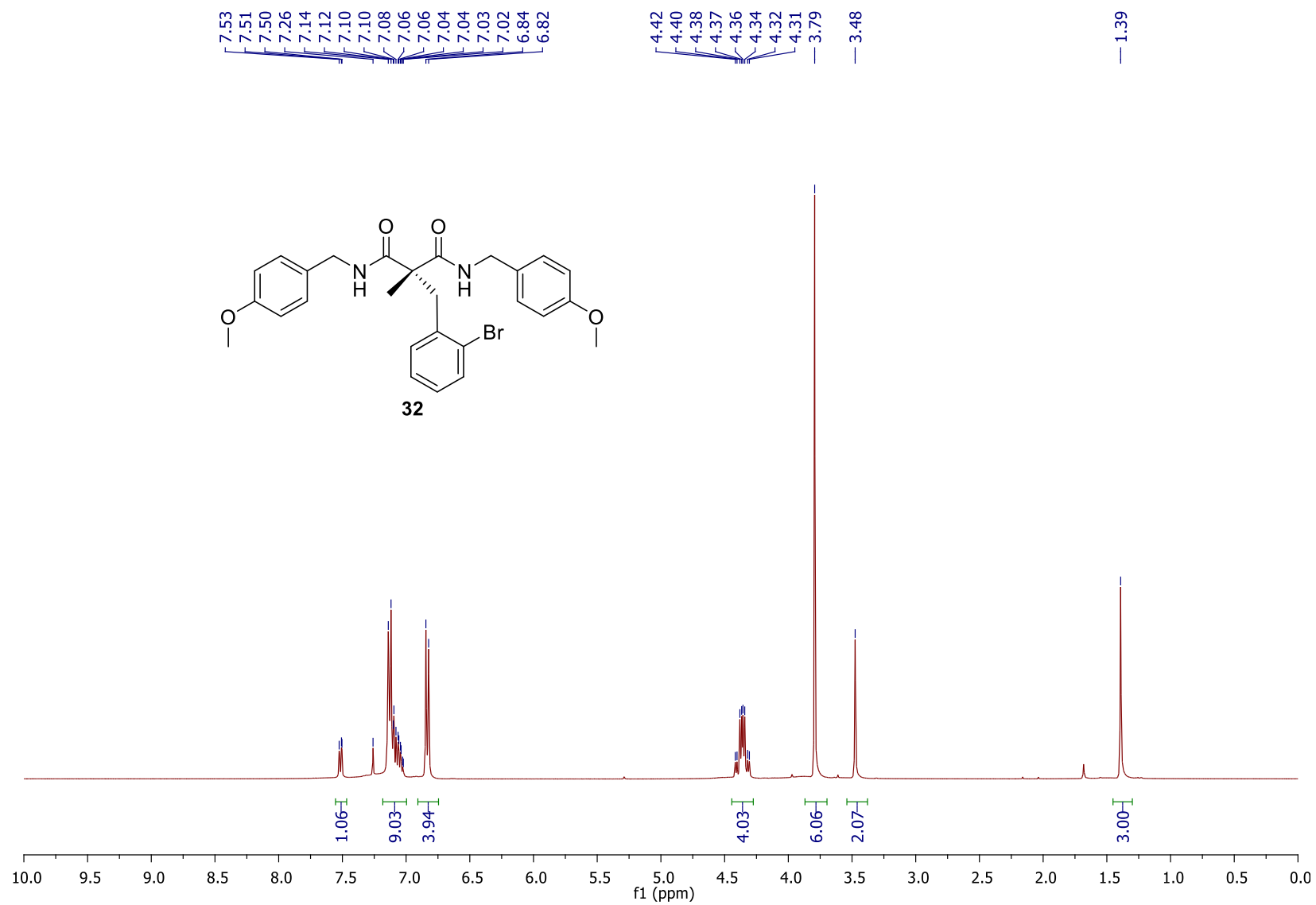
¹H NMR spectrum of 31 in CDCl₃



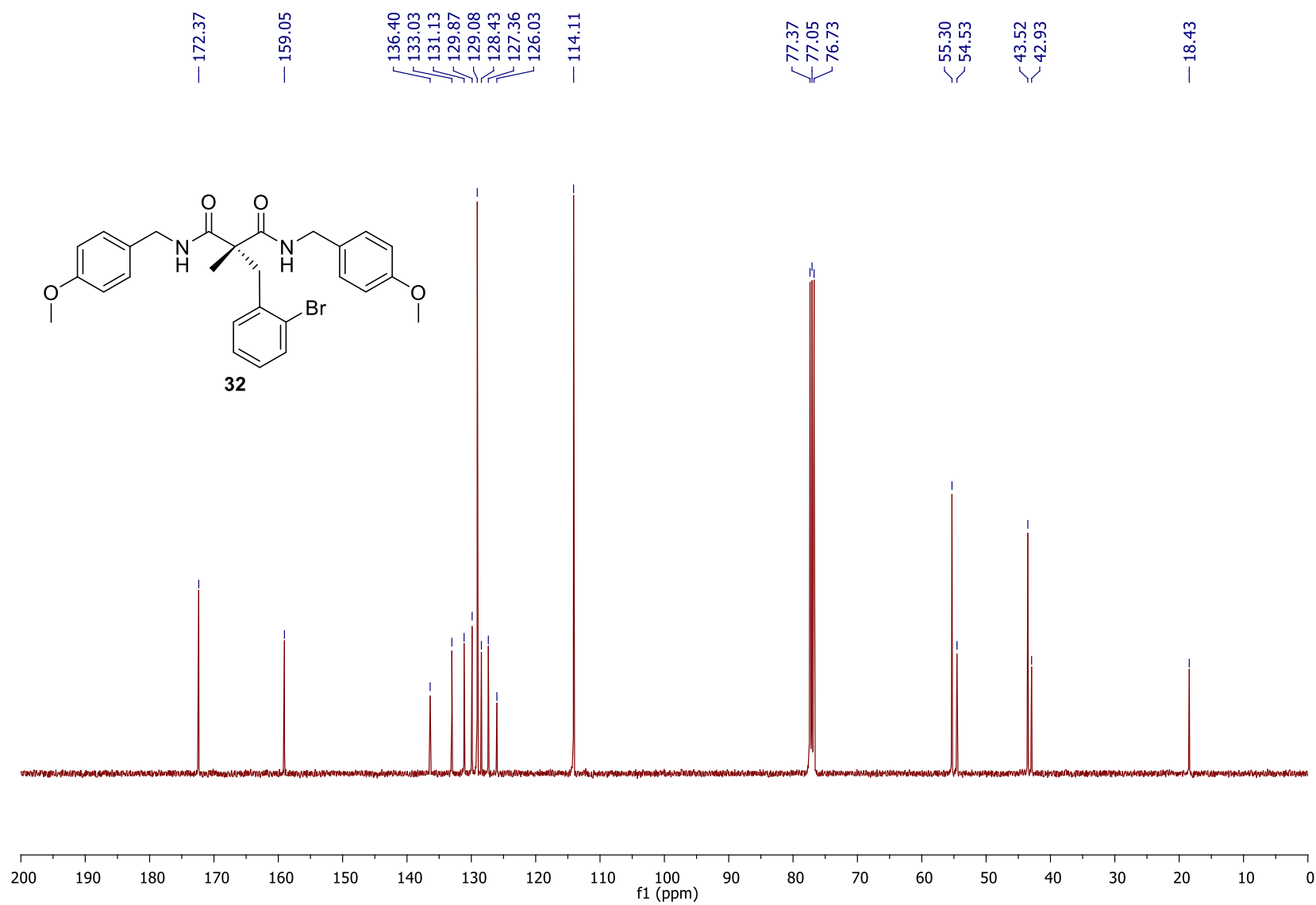
¹³C NMR spectrum of 31 in CDCl₃



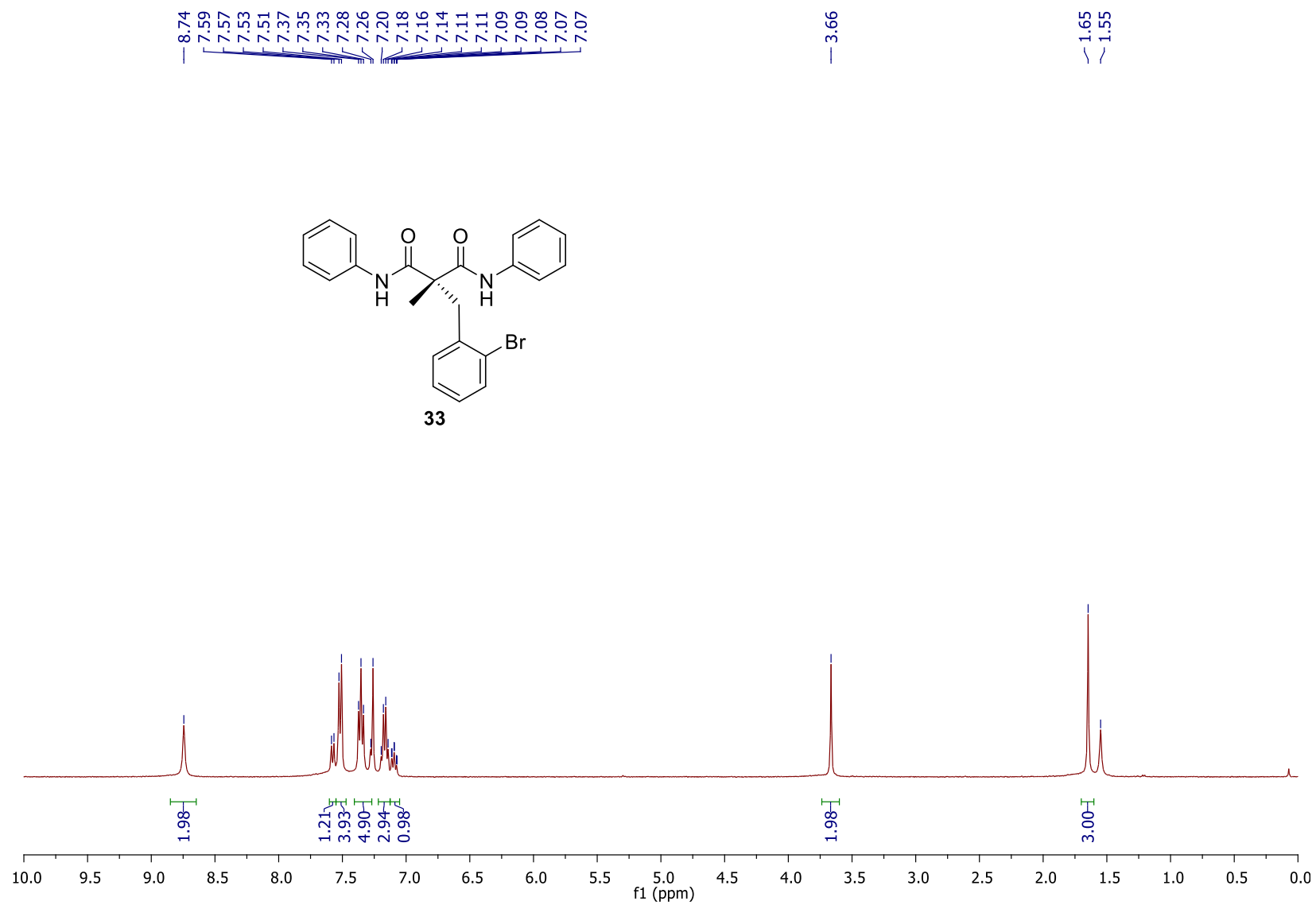
¹H NMR spectrum of 32 in CDCl₃



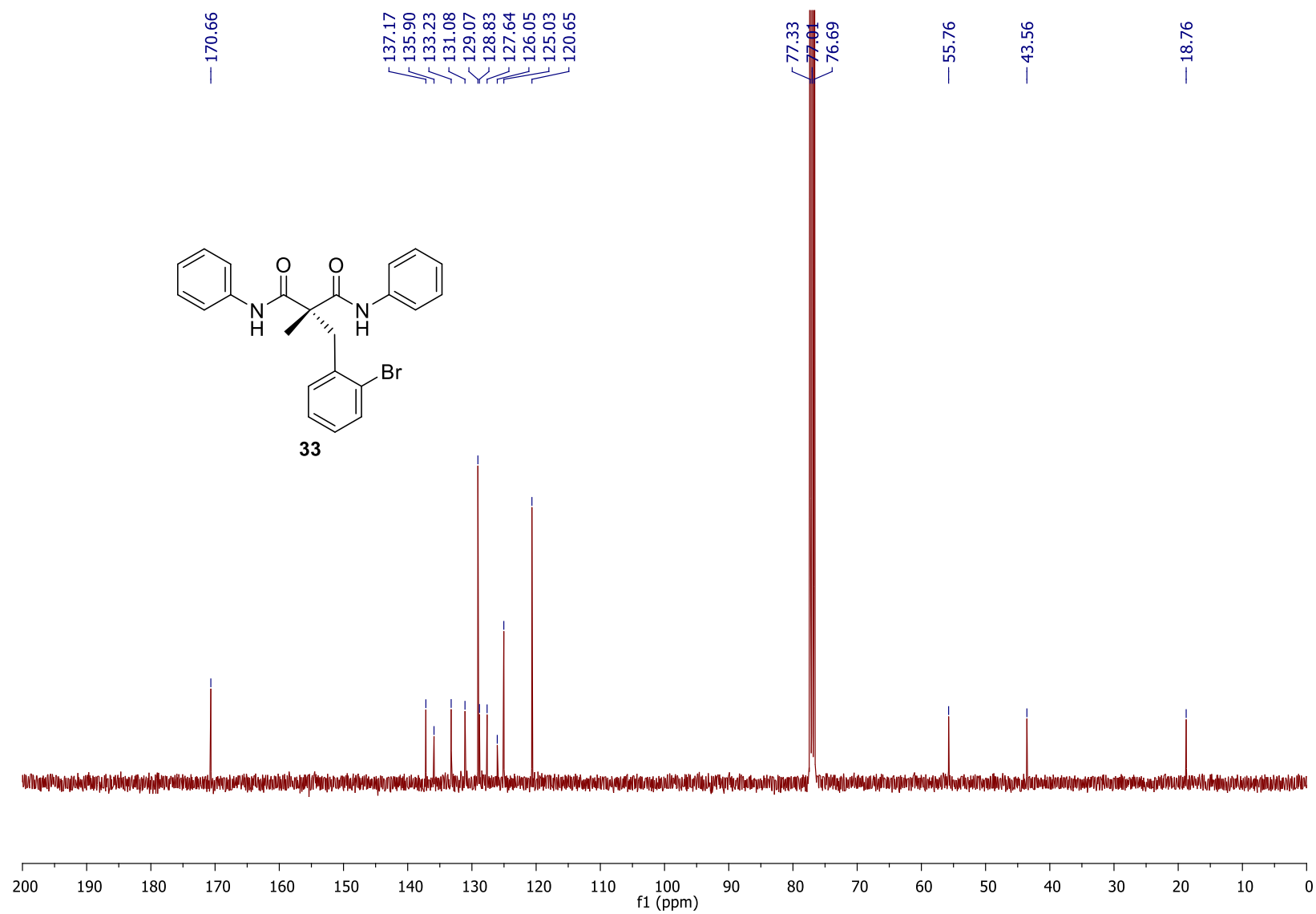
^{13}C NMR spectrum of 32 in CDCl_3



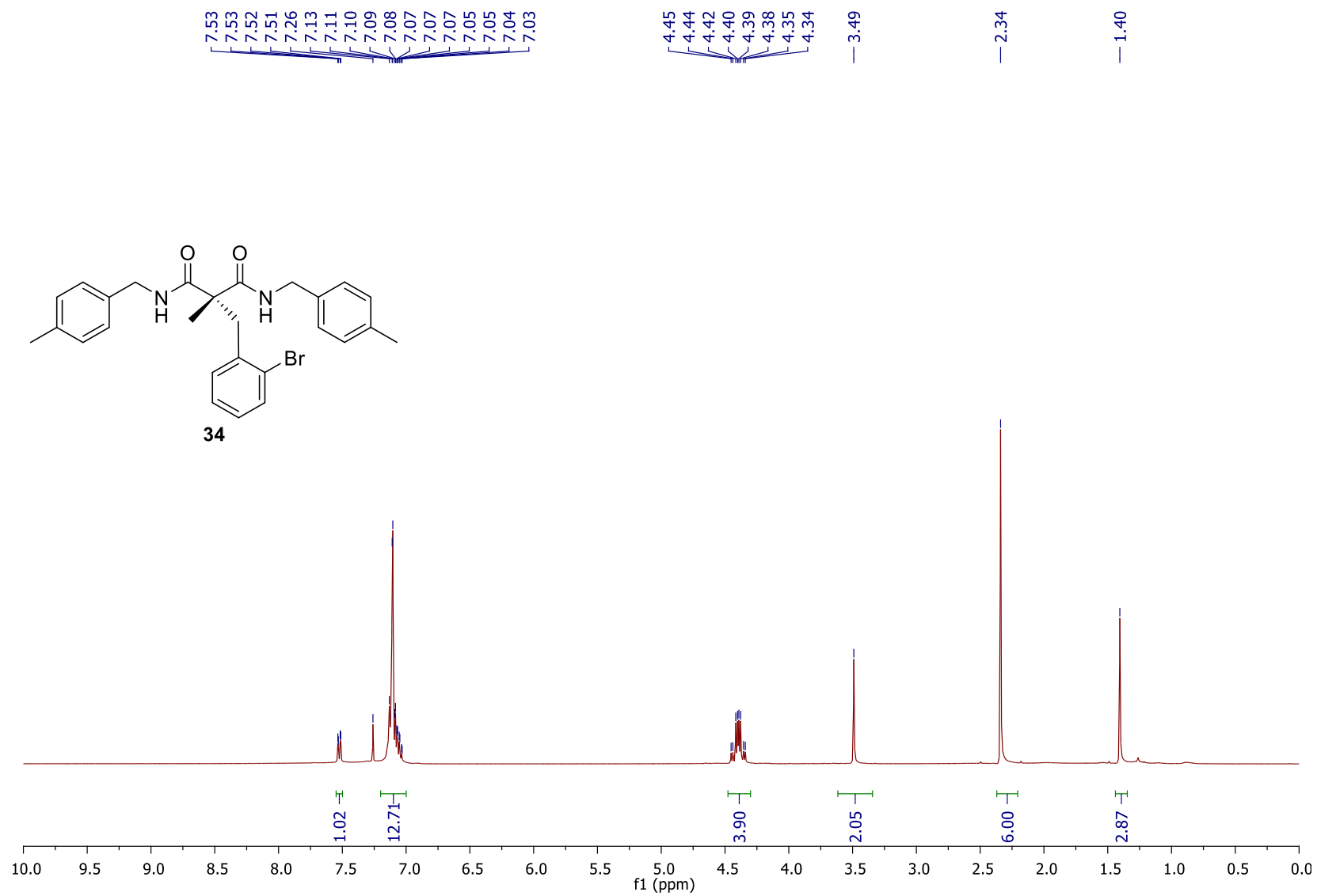
^1H NMR spectrum of 33 in CDCl_3



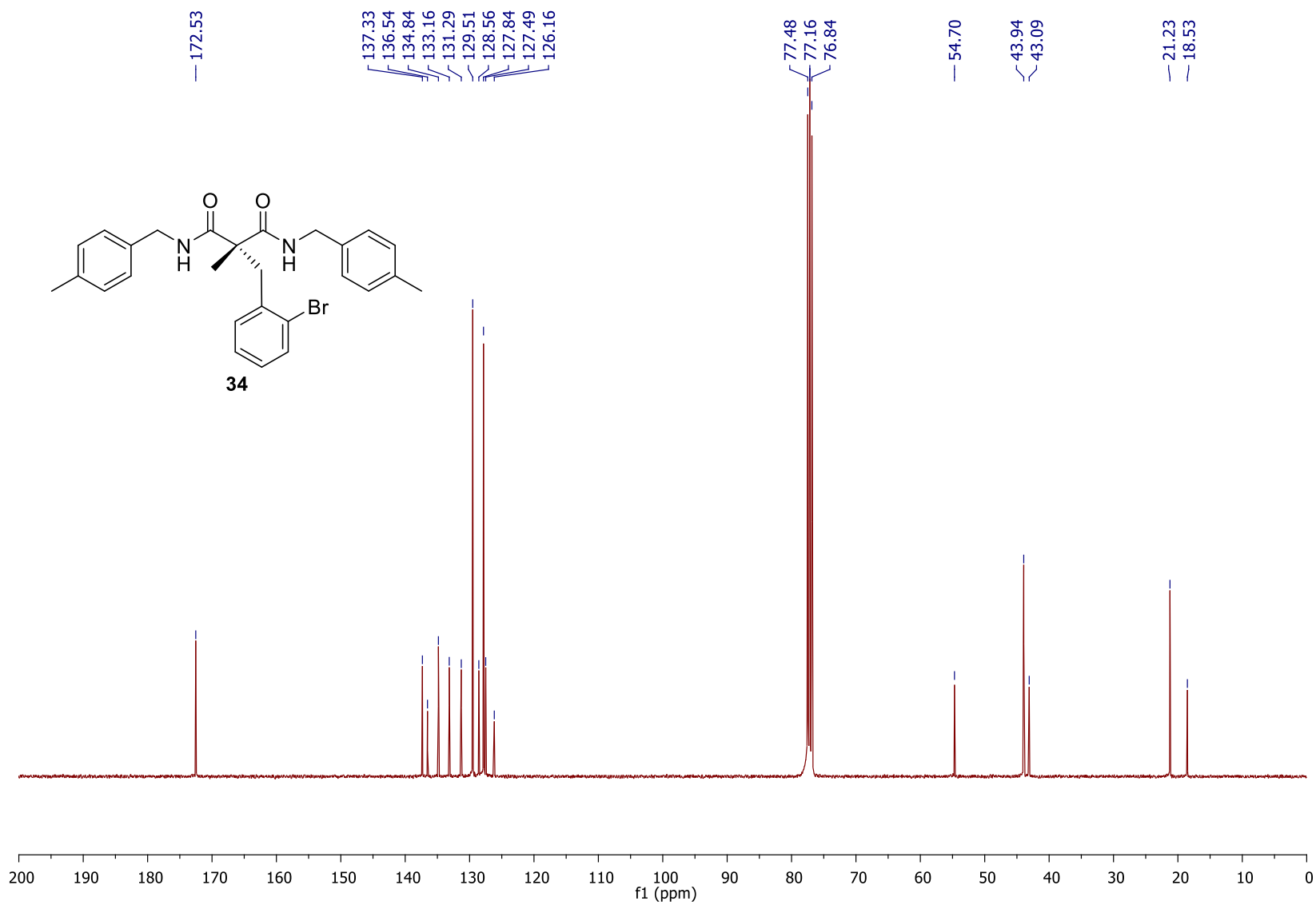
^{13}C NMR spectrum of 33 in CDCl_3



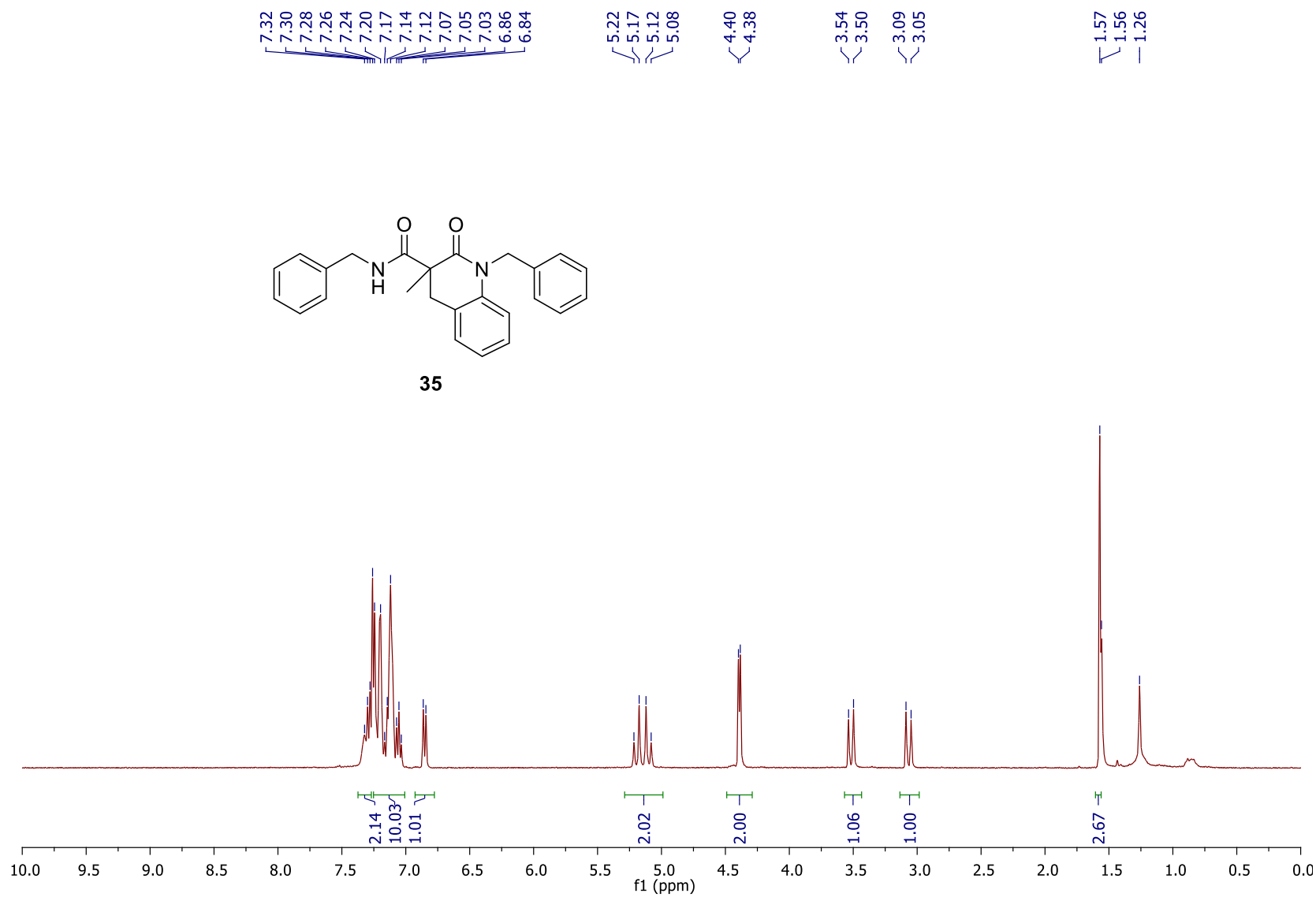
^1H NMR spectrum of 34 in CDCl_3



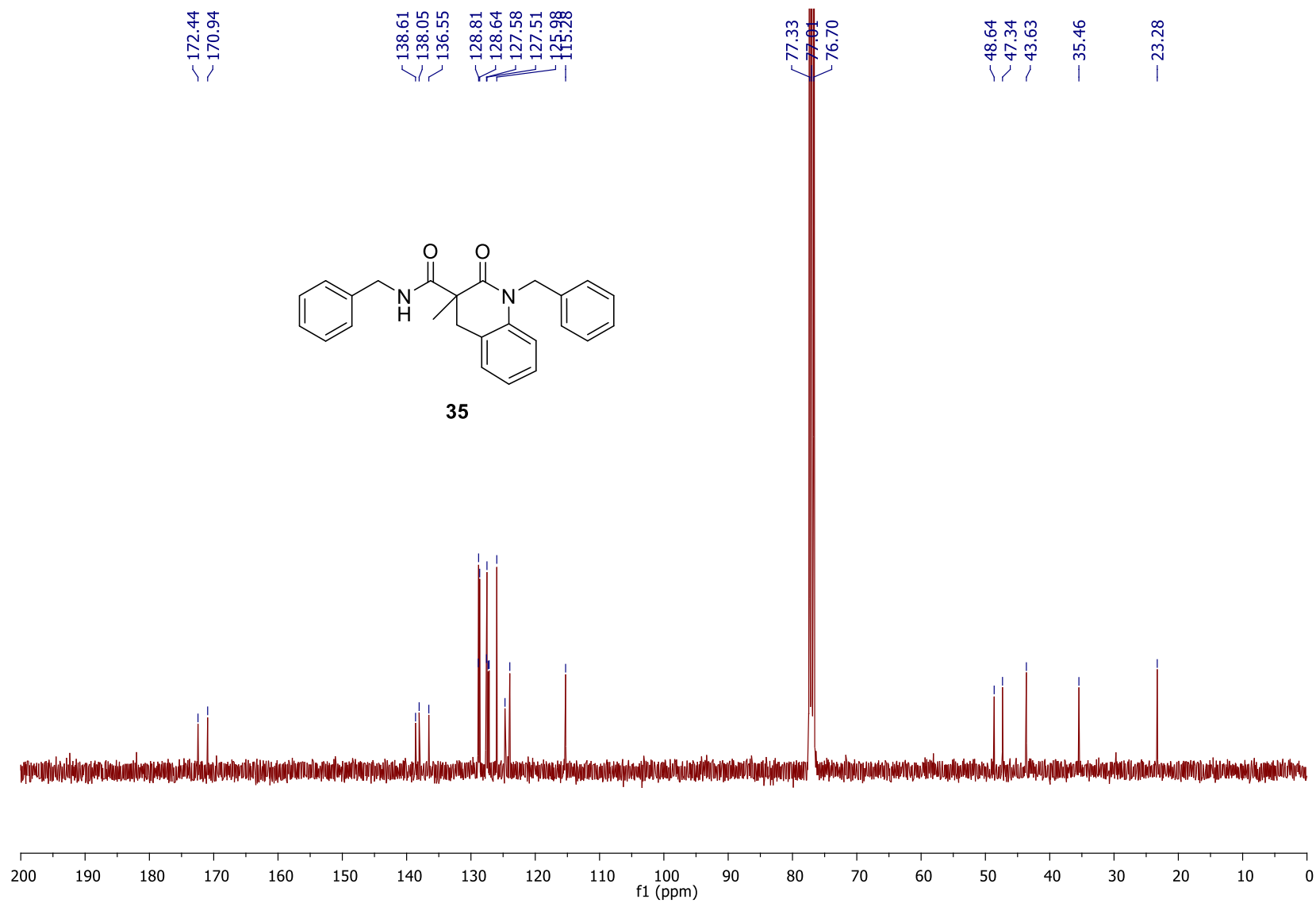
^{13}C NMR spectrum of 34 in CDCl_3



¹H NMR spectrum of 35 in CDCl₃



^{13}C NMR spectrum of 35 in CDCl_3



5.2 HPLC chromatograms

HPLC chromatogram of <i>rac</i> -Cy ₂ MOP 16	147
HPLC chromatogram of (<i>R</i>)-Cy ₂ MOP 16	148
HPLC chromatogram of 35 from the cyclization of 31 using <i>rac</i> -Cy ₂ MOP-Pd precatalyst	149
HPLC chromatogram of 35 from the cyclization of 31 using (<i>R</i>)-Cy ₂ MOP-Pd precatalyst	150
HPLC chromatogram from the cyclization of 31 using (<i>R</i>)-Cy ₂ MOP-Pd precatalyst at 45° C..	151

HPLC chromatogram of *rac*-Cy₂MOP 16

Print of window 38: Current Chromatogram(s)

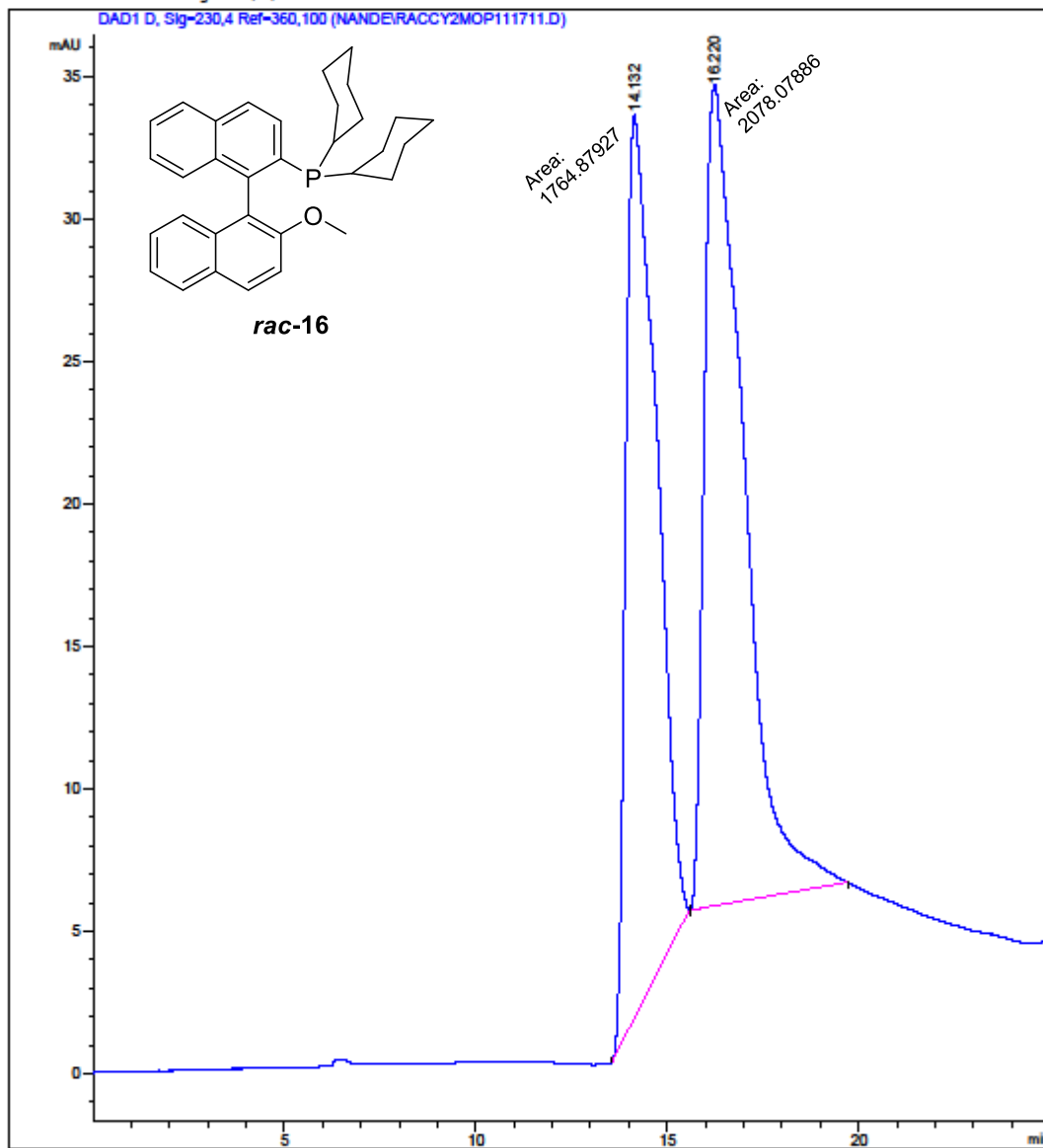
Data File : C:\CHEM32\1\DATA\NANDE\RACCY2MOP111711.D

Sample Name : RACCY2MOP

```
=====
Acq. Operator   : SYSTEM                      Seq. Line :    1
Acq. Instrument : Instrument 1                 Location  : Vial 31
Injection Date  : 11/17/2015 6:06:28 PM        Inj       :    1
                                           Inj Volume: 2.000 µl

Acq. Method     : C:\CHEM32\1\METHODS\NWCY2MOP2.M
Last changed    : 11/17/2015 6:05:38 PM by SYSTEM
Analysis Method : C:\CHEM32\1\METHODS\NWCY2MOP2.M
Last changed    : 11/19/2015 6:05:45 PM by SYSTEM
=====
```

Current Chromatogram(s)



HPLC chromatogram of (R)-Cy₂MOP 16

Print of window 38: Current Chromatogram(s)

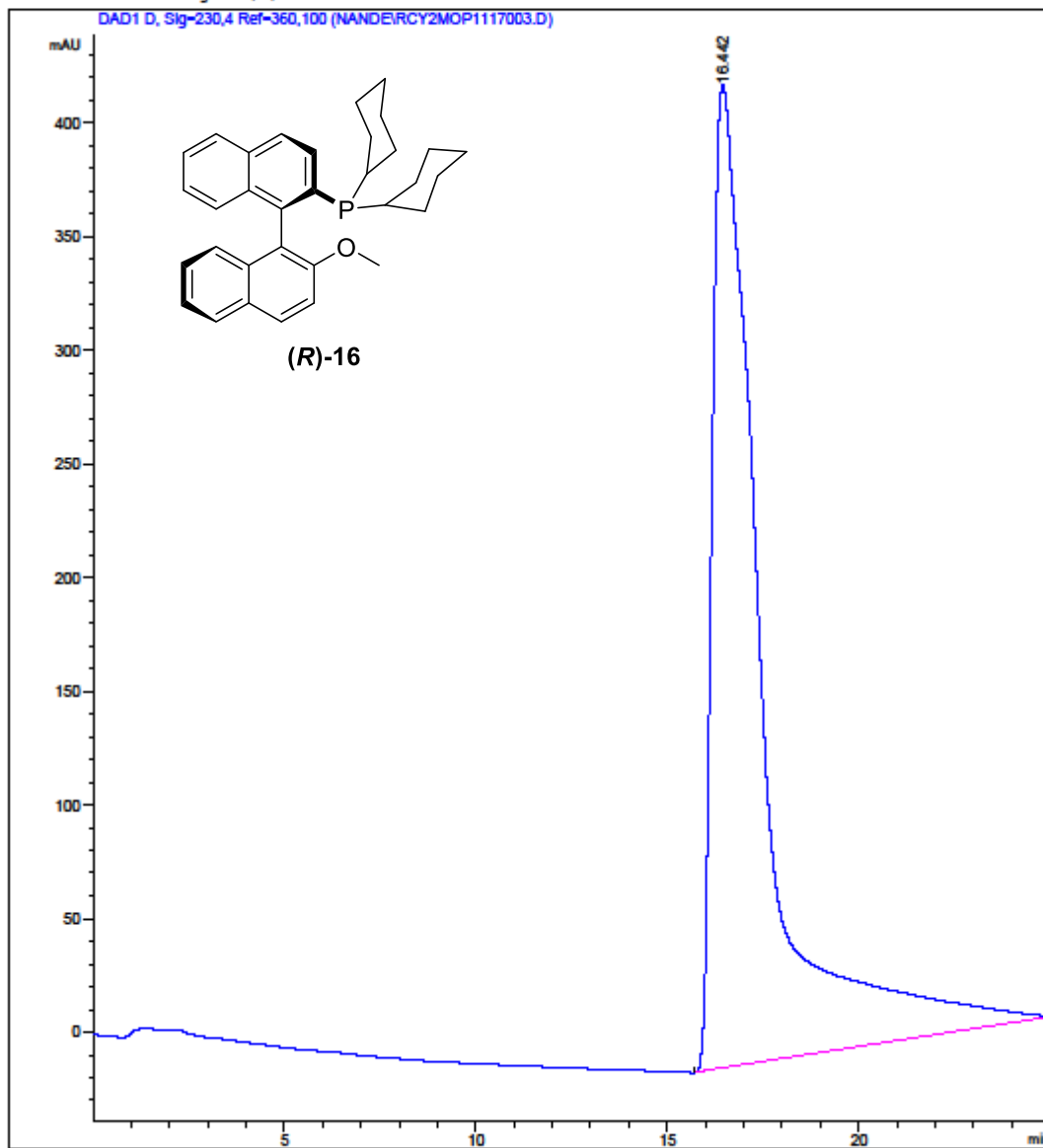
Data File : C:\CHEM32\1\DATA\NANDE\RCY2MOP1117003.D

Sample Name : RCY2MOP

```
=====
Acq. Operator   : SYSTEM                      Seq. Line :    1
Acq. Instrument : Instrument 1                 Location  : Vial 32
Injection Date  : 11/17/2015 7:38:04 PM        Inj       :    3
                                           Inj Volume: 2.000 µl

Acq. Method     : C:\CHEM32\1\METHODS\NWCY2MOP2.M
Last changed    : 11/17/2015 6:05:38 PM by SYSTEM
Analysis Method : C:\CHEM32\1\METHODS\NWCY2MOP2.M
Last changed    : 11/19/2015 6:05:45 PM by SYSTEM
=====
```

Current Chromatogram(s)



Instrument 1 4/23/2016 3:08:00 PM SYSTEM

Page 1 of 1

HPLC chromatogram of 35 from the cyclization of 31 using *rac*-Cy₂MOP-Pd precatalyst

Print of window 38: Current Chromatogram(s)

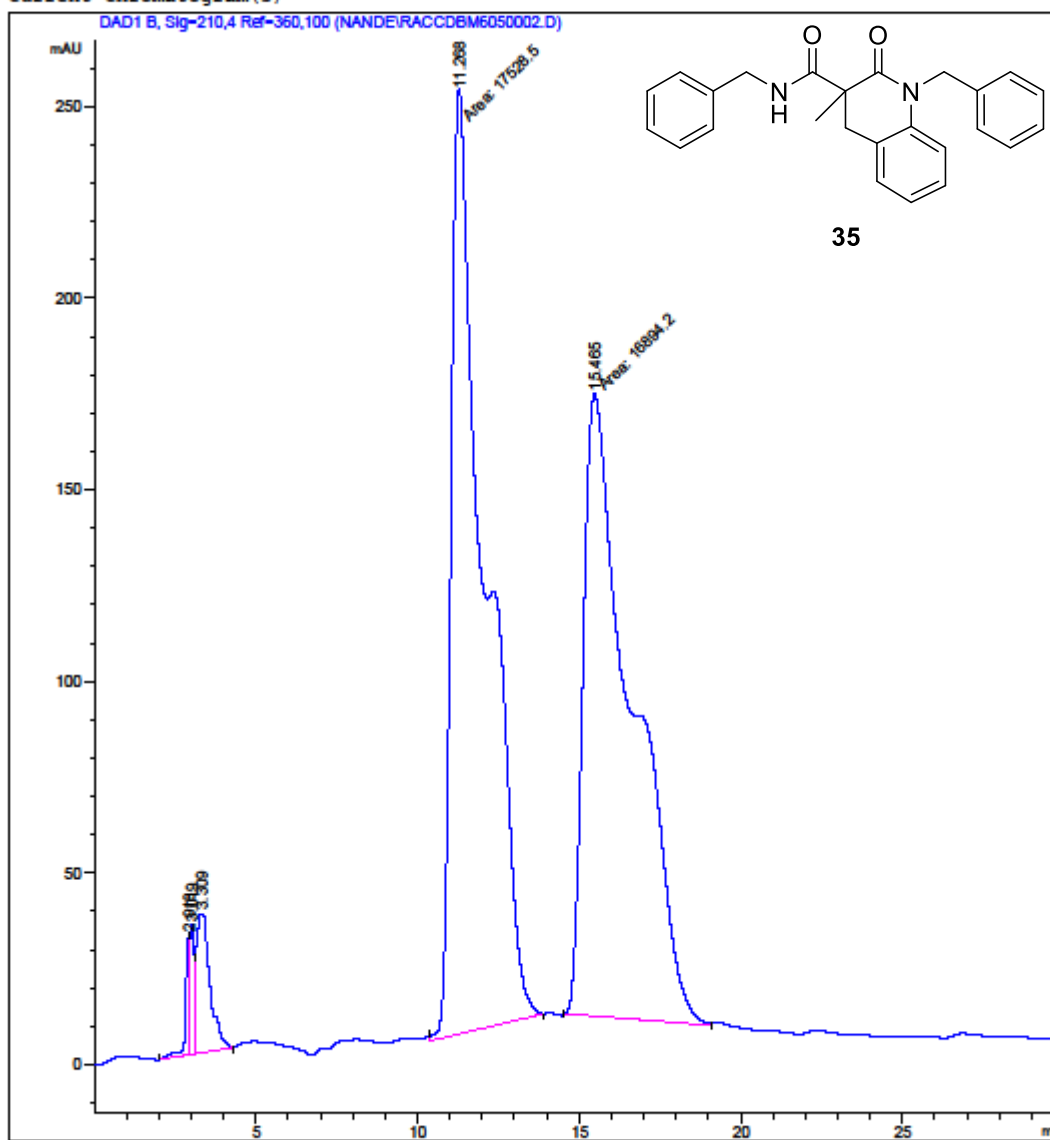
Data File : C:\CHEM32\1\DATA\NANDE\RACCD6M6050002.D

Sample Name : CDBM (+/-)-PRECATALYST

```
=====
Acq. Operator   : SYSTEM                      Seq. Line :    1
Acq. Instrument : Instrument 1                Location  : Vial 31
Injection Date  : 6/5/2015 12:58:11 PM        Inj       :    1
                                           Inj Volume: 20.000 µl

Acq. Method     : C:\CHEM32\1\METHODS\NWSTD8020.M
Last changed    : 6/5/2015 12:40:04 PM by SYSTEM
Analysis Method : C:\CHEM32\1\METHODS\NWSTD8020.M
Last changed    : 4/23/2016 1:48:01 PM by SYSTEM
Additional Info  : Peak(s) manually integrated
=====
```

Current Chromatogram(s)



Instrument 1 4/23/2016 2:59:23 PM SYSTEM

Page 1 of 1

HPLC chromatogram of 35 from the cyclization of 31 using (R)-Cy₂MOP-Pd precatalyst

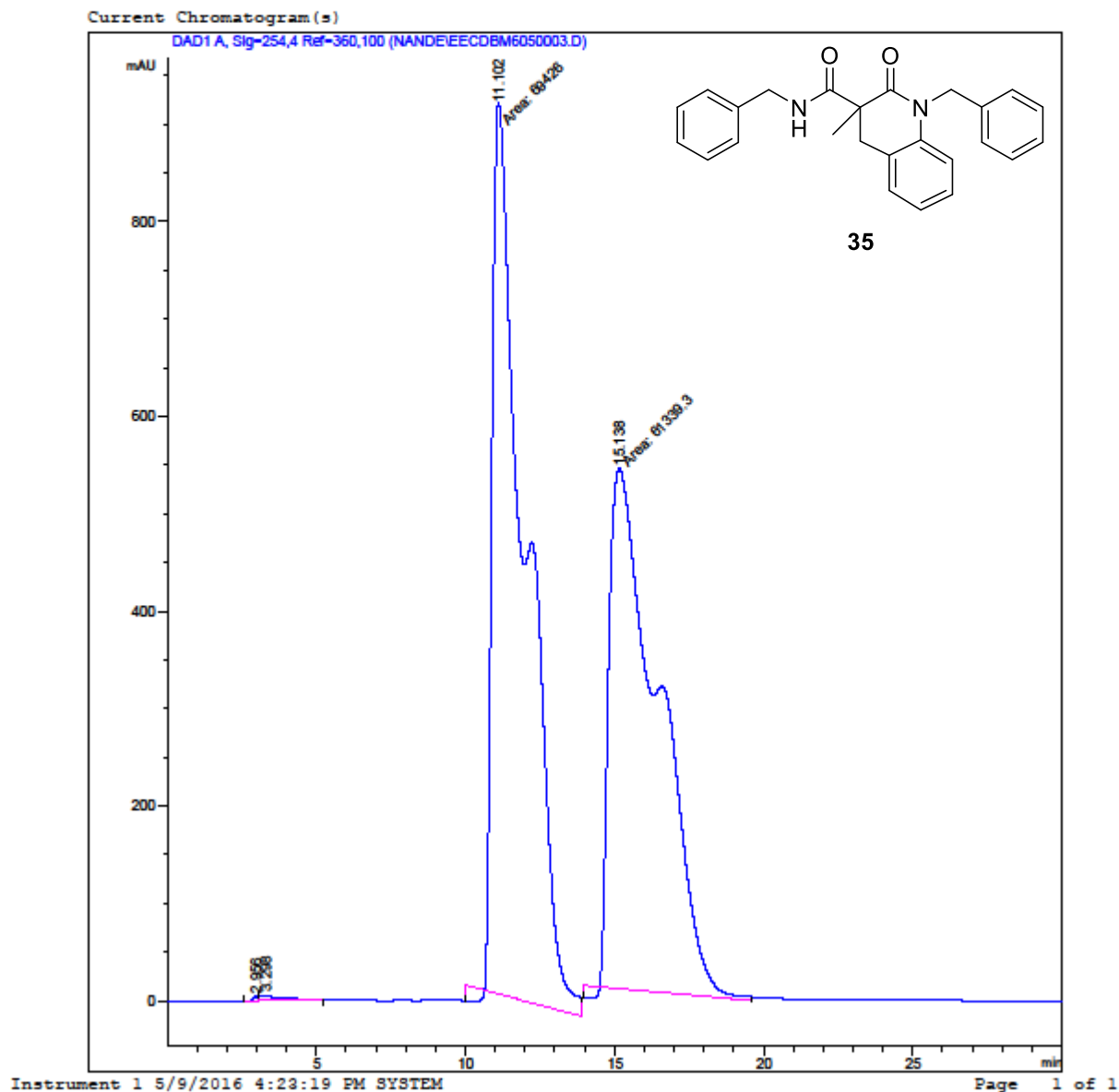
Print of window 38: Current Chromatogram(s)

Data File : C:\CHEM32\1\DATA\NANDE\EECD6M6050003.D

Sample Name : CDBM (R)-PRECATALYST

```
=====
Acq. Operator   : SYSTEM                      Seq. Line :    1
Acq. Instrument : Instrument 1                 Location  : Vial 32
Injection Date  : 6/5/2015 4:05:06 PM          Inj       :    2
                                           Inj Volume: 20.000 µl

Acq. Method     : C:\CHEM32\1\METHODS\NWSTD8020.M
Last changed    : 6/5/2015 12:40:04 PM by SYSTEM
Analysis Method : C:\CHEM32\1\METHODS\NWSTD9010.M
Last changed    : 5/8/2016 4:18:27 PM by SYSTEM
Additional Info  : Peak(s) manually integrated
=====
```



HPLC chromatogram of 35 using (R)-Cy₂MOP-Pd precatalyst at 45° C

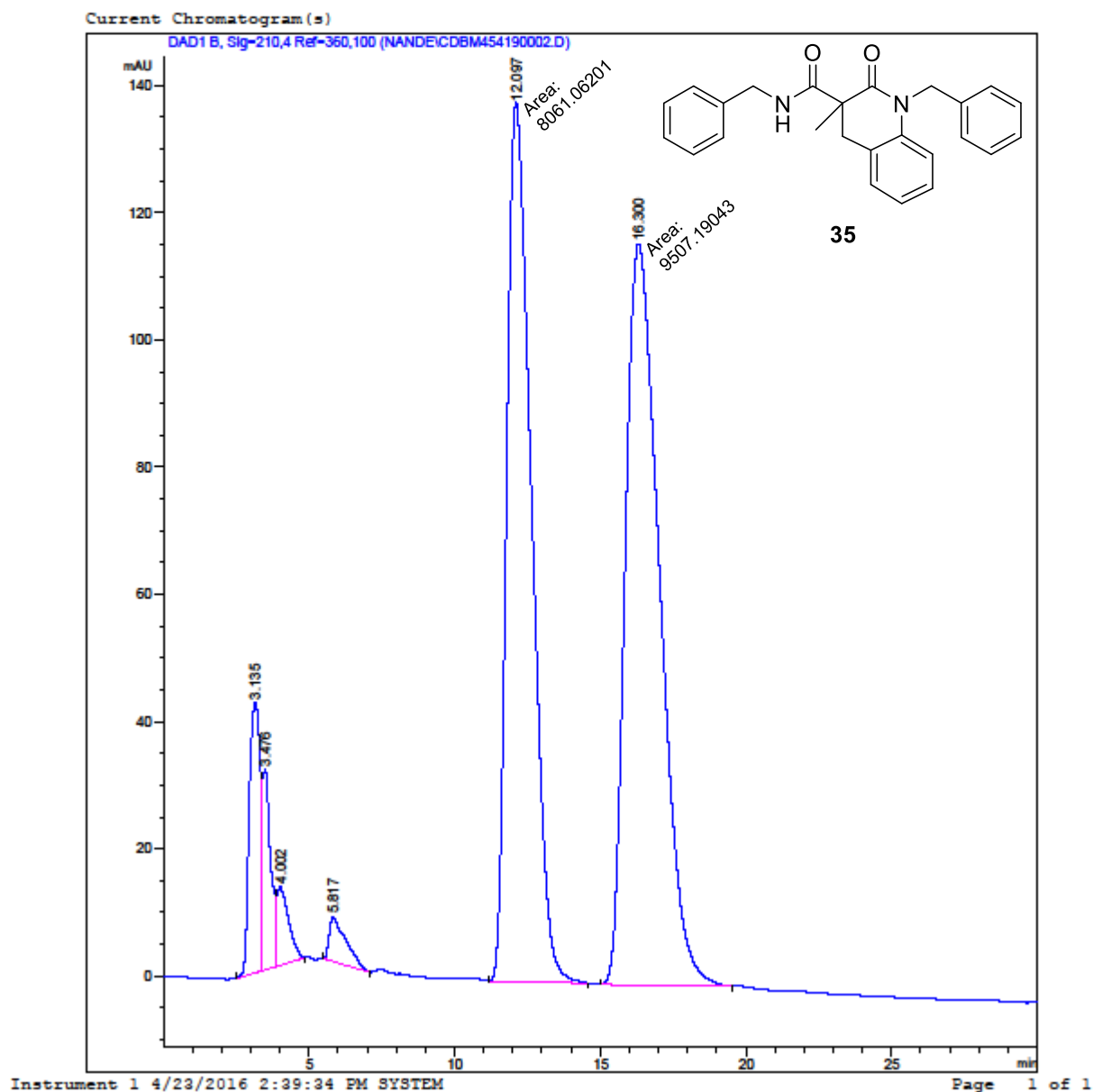
Print of window 38: Current Chromatogram(s)

Data File : C:\CHEM32\1\DATA\NANDE\CDBM454190002.D

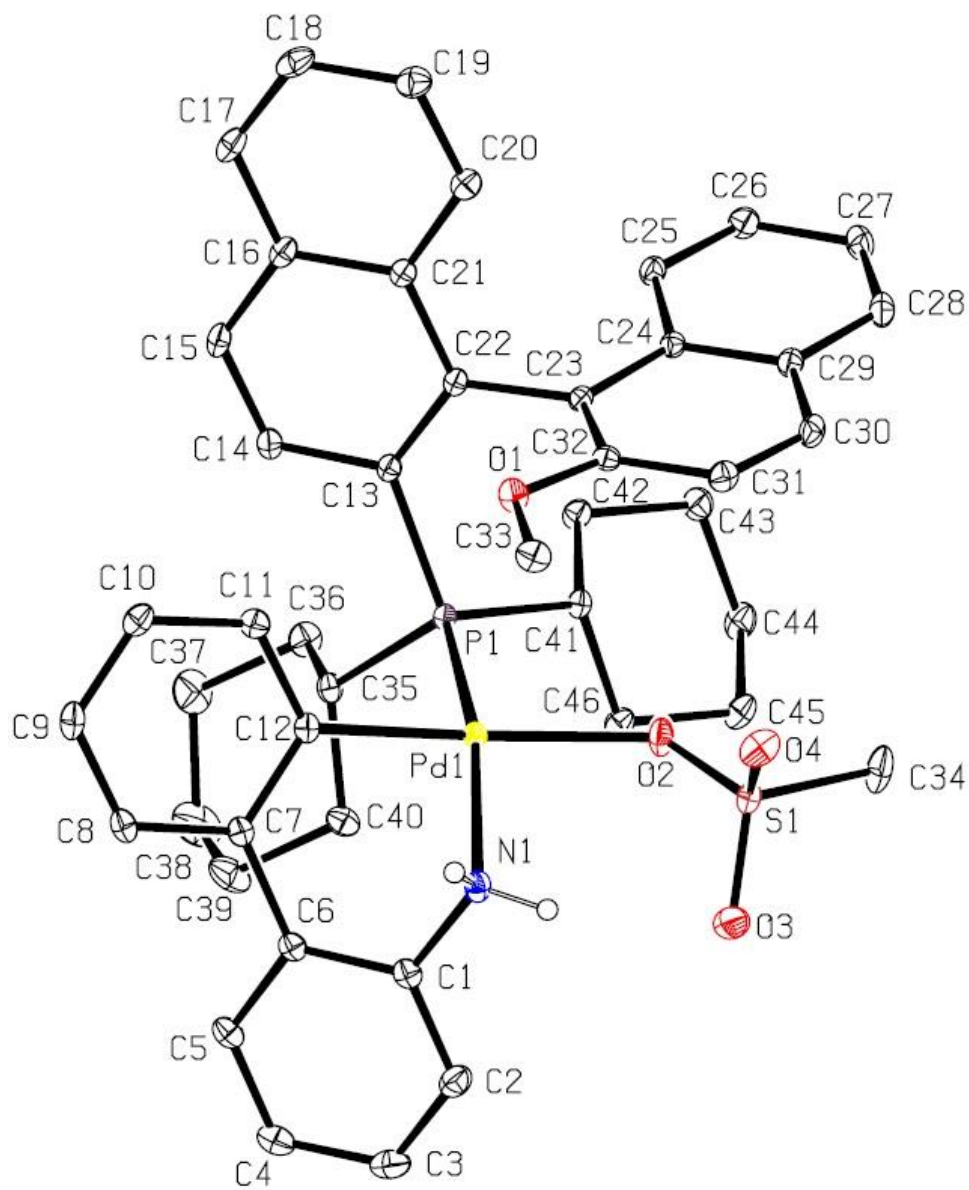
Sample Name : CDBM45

```
=====
Acq. Operator   : SYSTEM                      Seq. Line :    1
Acq. Instrument : Instrument 1                 Location  : Vial 31
Injection Date  : 4/19/2016 4:06:01 PM        Inj       :    1
                                                Inj Volume: 20.000 µl

Acq. Method     : C:\CHEM32\1\METHODS\NWSTD8020.M
Last changed    : 4/19/2016 4:04:59 PM by SYSTEM
Analysis Method : C:\CHEM32\1\METHODS\NWSTD8020.M
Last changed    : 4/23/2016 1:48:01 PM by SYSTEM
=====
```



5.3 X-ray crystallography data for Cy₂MOP-Pd precatalyst[§]



[§] There are 2.5 benzene molecules per Cy₂MOP-Pd precatalyst complex. Hydrogen atoms and solvent molecules are omitted from the crystal structure for clarity.

Table A1. Crystal data and structure refinement for d1567_a.

Identification code	d1567_a	
Empirical formula	C ₆₁ H ₆₅ NO ₄ PPdS	
Formula weight	1045.57	
Temperature	147(2) K	
Wavelength	0.71073 Å	
Crystal system	Triclinic	
Space group	P-1	
Unit cell dimensions	a = 12.8117(8) Å	α = 68.066(2)°.
	b = 13.5771(9) Å	β = 78.551(2)°.
	c = 17.4499(12) Å	γ = 66.979(2)°.
Volume	2586.5(3) Å ³	
Z	2	
Density (calculated)	1.343 Mg/m ³	
Absorption coefficient	0.479 mm ⁻¹	
F(000)	1094	
Crystal size	0.180 x 0.170 x 0.050 mm ³	
Theta range for data collection	1.725 to 27.632°.	
Index ranges	-16 ≤ h ≤ 16, -17 ≤ k ≤ 17, -22 ≤ l ≤ 22	
Reflections collected	65261	
Independent reflections	11986 [R(int) = 0.0429]	
Completeness to theta = 25.242°	100.0 %	
Absorption correction	Semi-empirical from equivalents	
Max. and min. transmission	0.7456 and 0.7166	
Refinement method	Full-matrix least-squares on F ²	
Data / restraints / parameters	11986 / 0 / 663	
Goodness-of-fit on F ²	1.025	
Final R indices [I > 2σ(I)]	R1 = 0.0285, wR2 = 0.0594	
R indices (all data)	R1 = 0.0433, wR2 = 0.0649	
Extinction coefficient	n/a	
Largest diff. peak and hole	0.436 and -0.489 e.Å ⁻³	

Table A2. Atomic coordinates ($\times 10^4$) and equivalent isotropic displacement parameters ($\text{\AA}^2 \times 10^3$) for d1567_a. U(eq) is defined as one third of the trace of the orthogonalized U^{ij} tensor.

	x	y	z	U(eq)
Pd(1)	5727(1)	5630(1)	3046(1)	14(1)
S(1)	4038(1)	4817(1)	2429(1)	18(1)
P(1)	7038(1)	6165(1)	2056(1)	13(1)
O(1)	7596(1)	3238(1)	3249(1)	21(1)
O(2)	4990(1)	5250(1)	2233(1)	24(1)
O(3)	2999(1)	5578(1)	2698(1)	31(1)
O(4)	4336(1)	3665(1)	2984(1)	29(1)
N(1)	4285(1)	5708(1)	3907(1)	18(1)
C(1)	3844(2)	6836(2)	3965(1)	18(1)
C(2)	2721(2)	7504(2)	3804(1)	25(1)
C(3)	2299(2)	8597(2)	3834(1)	29(1)
C(4)	2996(2)	9019(2)	4034(1)	25(1)
C(5)	4115(2)	8348(2)	4199(1)	20(1)
C(6)	4569(2)	7249(2)	4161(1)	16(1)
C(7)	5773(2)	6540(1)	4330(1)	16(1)
C(8)	6263(2)	6600(2)	4955(1)	20(1)
C(9)	7372(2)	5929(2)	5155(1)	24(1)
C(10)	8003(2)	5166(2)	4742(1)	24(1)
C(11)	7536(2)	5092(2)	4118(1)	19(1)
C(12)	6432(2)	5791(2)	3887(1)	15(1)
C(13)	8555(1)	5270(2)	2188(1)	14(1)
C(14)	9269(2)	5661(2)	2445(1)	18(1)
C(15)	10365(2)	5004(2)	2638(1)	20(1)
C(16)	10837(2)	3894(2)	2597(1)	18(1)
C(17)	11966(2)	3180(2)	2821(1)	23(1)
C(18)	12392(2)	2107(2)	2787(1)	26(1)
C(19)	11719(2)	1691(2)	2529(1)	25(1)
C(20)	10633(2)	2354(2)	2312(1)	20(1)
C(21)	10153(1)	3480(2)	2336(1)	16(1)
C(22)	9004(1)	4187(2)	2126(1)	14(1)
C(23)	8328(1)	3672(1)	1884(1)	14(1)

C(24)	8495(1)	3555(1)	1085(1)	15(1)
C(25)	9313(2)	3891(2)	474(1)	18(1)
C(26)	9428(2)	3787(2)	-292(1)	23(1)
C(27)	8758(2)	3312(2)	-488(1)	25(1)
C(28)	7993(2)	2938(2)	96(1)	23(1)
C(29)	7835(2)	3051(2)	890(1)	18(1)
C(30)	7057(2)	2659(2)	1503(1)	21(1)
C(31)	6951(2)	2713(2)	2280(1)	20(1)
C(32)	7609(1)	3206(1)	2477(1)	16(1)
C(33)	6886(2)	2751(2)	3899(1)	22(1)
C(34)	3835(2)	4805(2)	1469(1)	34(1)
C(35)	6946(2)	7556(2)	2071(1)	17(1)
C(36)	7580(2)	8236(2)	1368(1)	24(1)
C(37)	7607(2)	9216(2)	1588(2)	36(1)
C(38)	6416(2)	9978(2)	1771(2)	45(1)
C(39)	5739(2)	9311(2)	2422(1)	34(1)
C(40)	5718(2)	8350(2)	2182(1)	21(1)
C(41)	6692(1)	6331(2)	1023(1)	16(1)
C(42)	7582(2)	6539(2)	310(1)	20(1)
C(43)	7239(2)	6528(2)	-478(1)	24(1)
C(44)	6068(2)	7407(2)	-715(1)	26(1)
C(45)	5184(2)	7219(2)	-2(1)	24(1)
C(46)	5520(2)	7241(2)	782(1)	20(1)
C(1S)	2327(4)	10020(4)	1165(2)	80(1)
C(2S)	1306(4)	10668(3)	832(2)	76(1)
C(3S)	552(3)	10197(3)	865(2)	63(1)
C(4S)	794(2)	9066(2)	1229(2)	57(1)
C(5S)	1803(2)	8392(2)	1578(2)	49(1)
C(6S)	2581(2)	8859(3)	1552(2)	61(1)
C(7S)	4933(2)	824(2)	4234(2)	37(1)
C(8S)	4040(2)	23(2)	5527(2)	37(1)
C(9S)	3979(2)	844(2)	4758(2)	36(1)
C(10S)	736(6)	10927(12)	6629(5)	73(3)
C(11S)	613(7)	12007(10)	6073(9)	88(4)
C(12S)	626(7)	12214(3)	5229(8)	74(4)
C(13S)	763(5)	11342(5)	4941(3)	55(2)

C(14S)	887(5)	10263(3)	5497(4)	48(2)
C(15S)	873(6)	10055(7)	6341(3)	51(3)
C(16S)	727(9)	10445(8)	6690(9)	82(5)
C(17S)	599(8)	11571(9)	6512(5)	76(4)
C(18S)	565(9)	12285(6)	5696(8)	68(4)
C(19S)	659(12)	11873(19)	5057(4)	91(7)
C(20S)	787(11)	10750(20)	5234(12)	128(9)
C(21S)	822(9)	10032(10)	6051(16)	97(7)

Table A3. Bond lengths [Å] and angles [°] for d1567_a.

Pd(1)-C(12)	1.9852(17)
Pd(1)-N(1)	2.1319(15)
Pd(1)-O(2)	2.1516(12)
Pd(1)-P(1)	2.2800(5)
S(1)-O(4)	1.4416(14)
S(1)-O(3)	1.4489(14)
S(1)-O(2)	1.4807(13)
S(1)-C(34)	1.753(2)
P(1)-C(13)	1.8515(18)
P(1)-C(41)	1.8524(17)
P(1)-C(35)	1.8556(18)
O(1)-C(32)	1.362(2)
O(1)-C(33)	1.432(2)
N(1)-C(1)	1.446(2)
N(1)-H(1N)	0.84(2)
N(1)-H(2N)	0.85(2)
C(1)-C(2)	1.386(3)
C(1)-C(6)	1.404(2)
C(2)-C(3)	1.384(3)
C(2)-H(2A)	0.9500
C(3)-C(4)	1.386(3)
C(3)-H(3A)	0.9500
C(4)-C(5)	1.385(3)
C(4)-H(4A)	0.9500
C(5)-C(6)	1.396(2)
C(5)-H(5A)	0.9500
C(6)-C(7)	1.484(2)
C(7)-C(8)	1.403(2)
C(7)-C(12)	1.414(2)
C(8)-C(9)	1.385(3)
C(8)-H(8A)	0.9500
C(9)-C(10)	1.383(3)
C(9)-H(9A)	0.9500
C(10)-C(11)	1.394(3)

C(10)-H(10A)	0.9500
C(11)-C(12)	1.397(2)
C(11)-H(11A)	0.9500
C(13)-C(22)	1.392(2)
C(13)-C(14)	1.429(2)
C(14)-C(15)	1.365(3)
C(14)-H(14A)	0.9500
C(15)-C(16)	1.412(3)
C(15)-H(15A)	0.9500
C(16)-C(21)	1.424(2)
C(16)-C(17)	1.425(3)
C(17)-C(18)	1.362(3)
C(17)-H(17A)	0.9500
C(18)-C(19)	1.411(3)
C(18)-H(18A)	0.9500
C(19)-C(20)	1.365(3)
C(19)-H(19A)	0.9500
C(20)-C(21)	1.421(3)
C(20)-H(20A)	0.9500
C(21)-C(22)	1.438(2)
C(22)-C(23)	1.501(2)
C(23)-C(32)	1.382(2)
C(23)-C(24)	1.427(2)
C(24)-C(25)	1.417(2)
C(24)-C(29)	1.428(2)
C(25)-C(26)	1.371(3)
C(25)-H(25A)	0.9500
C(26)-C(27)	1.409(3)
C(26)-H(26A)	0.9500
C(27)-C(28)	1.365(3)
C(27)-H(27A)	0.9500
C(28)-C(29)	1.416(3)
C(28)-H(28A)	0.9500
C(29)-C(30)	1.411(3)
C(30)-C(31)	1.363(3)
C(30)-H(30A)	0.9500

C(31)-C(32)	1.415(2)
C(31)-H(31A)	0.9500
C(33)-H(33A)	0.9800
C(33)-H(33B)	0.9800
C(33)-H(33C)	0.9800
C(34)-H(34A)	0.9800
C(34)-H(34B)	0.9800
C(34)-H(34C)	0.9800
C(35)-C(36)	1.537(2)
C(35)-C(40)	1.543(2)
C(35)-H(35A)	1.0000
C(36)-C(37)	1.531(3)
C(36)-H(36A)	0.9900
C(36)-H(36B)	0.9900
C(37)-C(38)	1.523(3)
C(37)-H(37A)	0.9900
C(37)-H(37B)	0.9900
C(38)-C(39)	1.522(3)
C(38)-H(38A)	0.9900
C(38)-H(38B)	0.9900
C(39)-C(40)	1.524(3)
C(39)-H(39A)	0.9900
C(39)-H(39B)	0.9900
C(40)-H(40A)	0.9900
C(40)-H(40B)	0.9900
C(41)-C(42)	1.535(2)
C(41)-C(46)	1.540(2)
C(41)-H(41A)	1.0000
C(42)-C(43)	1.531(2)
C(42)-H(42A)	0.9900
C(42)-H(42B)	0.9900
C(43)-C(44)	1.524(3)
C(43)-H(43A)	0.9900
C(43)-H(43B)	0.9900
C(44)-C(45)	1.525(3)
C(44)-H(44A)	0.9900

C(44)-H(44B)	0.9900
C(45)-C(46)	1.527(3)
C(45)-H(45A)	0.9900
C(45)-H(45B)	0.9900
C(46)-H(46A)	0.9900
C(46)-H(46B)	0.9900
C(1S)-C(2S)	1.357(5)
C(1S)-C(6S)	1.391(5)
C(1S)-H(1S)	0.9500
C(2S)-C(3S)	1.334(5)
C(2S)-H(2S)	0.9500
C(3S)-C(4S)	1.354(4)
C(3S)-H(3S)	0.9500
C(4S)-C(5S)	1.360(4)
C(4S)-H(4S)	0.9500
C(5S)-C(6S)	1.361(4)
C(5S)-H(5S)	0.9500
C(6S)-H(6S)	0.9500
C(7S)-C(9S)	1.371(3)
C(7S)-C(8S)#1	1.380(3)
C(7S)-H(7S)	0.9500
C(8S)-C(7S)#1	1.380(3)
C(8S)-C(9S)	1.381(3)
C(8S)-H(8S)	0.9500
C(9S)-H(9S)	0.9500
C(10S)-C(11S)	1.3900
C(10S)-C(15S)	1.3900
C(10S)-H(10S)	0.9500
C(11S)-C(12S)	1.3900
C(11S)-H(11S)	0.9500
C(12S)-C(13S)	1.3900
C(12S)-H(12S)	0.9500
C(13S)-C(14S)	1.3900
C(13S)-H(13S)	0.9500
C(14S)-C(15S)	1.3900
C(14S)-H(14S)	0.9500

C(15S)-H(15S)	0.9500
C(16S)-C(17S)	1.3900
C(16S)-C(21S)	1.3900
C(16S)-H(16S)	0.9500
C(17S)-C(18S)	1.3900
C(17S)-H(17S)	0.9500
C(18S)-C(19S)	1.3900
C(18S)-H(18S)	0.9500
C(19S)-C(20S)	1.3900
C(19S)-H(19S)	0.9500
C(20S)-C(21S)	1.3900
C(20S)-H(20S)	0.9500
C(21S)-H(21S)	0.9500
C(12)-Pd(1)-N(1)	85.25(7)
C(12)-Pd(1)-O(2)	173.06(6)
N(1)-Pd(1)-O(2)	92.65(6)
C(12)-Pd(1)-P(1)	90.28(5)
N(1)-Pd(1)-P(1)	161.27(5)
O(2)-Pd(1)-P(1)	93.74(4)
O(4)-S(1)-O(3)	113.11(9)
O(4)-S(1)-O(2)	112.69(8)
O(3)-S(1)-O(2)	112.36(8)
O(4)-S(1)-C(34)	107.14(10)
O(3)-S(1)-C(34)	107.99(10)
O(2)-S(1)-C(34)	102.77(9)
C(13)-P(1)-C(41)	107.77(8)
C(13)-P(1)-C(35)	104.73(8)
C(41)-P(1)-C(35)	109.33(8)
C(13)-P(1)-Pd(1)	118.18(6)
C(41)-P(1)-Pd(1)	110.38(6)
C(35)-P(1)-Pd(1)	106.08(6)
C(32)-O(1)-C(33)	118.88(14)
S(1)-O(2)-Pd(1)	127.90(8)
C(1)-N(1)-Pd(1)	106.70(11)
C(1)-N(1)-H(1N)	112.2(15)

Pd(1)-N(1)-H(1N)	112.3(14)
C(1)-N(1)-H(2N)	110.7(15)
Pd(1)-N(1)-H(2N)	108.7(15)
H(1N)-N(1)-H(2N)	106(2)
C(2)-C(1)-C(6)	120.93(17)
C(2)-C(1)-N(1)	119.55(17)
C(6)-C(1)-N(1)	119.50(16)
C(3)-C(2)-C(1)	120.10(18)
C(3)-C(2)-H(2A)	120.0
C(1)-C(2)-H(2A)	120.0
C(2)-C(3)-C(4)	119.97(18)
C(2)-C(3)-H(3A)	120.0
C(4)-C(3)-H(3A)	120.0
C(5)-C(4)-C(3)	119.84(18)
C(5)-C(4)-H(4A)	120.1
C(3)-C(4)-H(4A)	120.1
C(4)-C(5)-C(6)	121.39(18)
C(4)-C(5)-H(5A)	119.3
C(6)-C(5)-H(5A)	119.3
C(5)-C(6)-C(1)	117.76(17)
C(5)-C(6)-C(7)	121.01(16)
C(1)-C(6)-C(7)	121.23(16)
C(8)-C(7)-C(12)	119.23(16)
C(8)-C(7)-C(6)	119.12(16)
C(12)-C(7)-C(6)	121.65(15)
C(9)-C(8)-C(7)	121.32(17)
C(9)-C(8)-H(8A)	119.3
C(7)-C(8)-H(8A)	119.3
C(10)-C(9)-C(8)	119.45(17)
C(10)-C(9)-H(9A)	120.3
C(8)-C(9)-H(9A)	120.3
C(9)-C(10)-C(11)	120.29(18)
C(9)-C(10)-H(10A)	119.9
C(11)-C(10)-H(10A)	119.9
C(10)-C(11)-C(12)	121.08(17)
C(10)-C(11)-H(11A)	119.5

C(12)-C(11)-H(11A)	119.5
C(11)-C(12)-C(7)	118.53(16)
C(11)-C(12)-Pd(1)	121.35(13)
C(7)-C(12)-Pd(1)	119.76(13)
C(22)-C(13)-C(14)	118.41(16)
C(22)-C(13)-P(1)	122.82(13)
C(14)-C(13)-P(1)	118.48(13)
C(15)-C(14)-C(13)	122.17(17)
C(15)-C(14)-H(14A)	118.9
C(13)-C(14)-H(14A)	118.9
C(14)-C(15)-C(16)	120.71(16)
C(14)-C(15)-H(15A)	119.6
C(16)-C(15)-H(15A)	119.6
C(15)-C(16)-C(21)	118.65(16)
C(15)-C(16)-C(17)	121.74(17)
C(21)-C(16)-C(17)	119.60(17)
C(18)-C(17)-C(16)	120.41(18)
C(18)-C(17)-H(17A)	119.8
C(16)-C(17)-H(17A)	119.8
C(17)-C(18)-C(19)	120.29(18)
C(17)-C(18)-H(18A)	119.9
C(19)-C(18)-H(18A)	119.9
C(20)-C(19)-C(18)	120.68(19)
C(20)-C(19)-H(19A)	119.7
C(18)-C(19)-H(19A)	119.7
C(19)-C(20)-C(21)	121.05(18)
C(19)-C(20)-H(20A)	119.5
C(21)-C(20)-H(20A)	119.5
C(20)-C(21)-C(16)	117.97(16)
C(20)-C(21)-C(22)	122.07(16)
C(16)-C(21)-C(22)	119.95(16)
C(13)-C(22)-C(21)	120.10(15)
C(13)-C(22)-C(23)	123.25(15)
C(21)-C(22)-C(23)	116.59(15)
C(32)-C(23)-C(24)	119.29(15)
C(32)-C(23)-C(22)	118.86(15)

C(24)-C(23)-C(22)	121.55(15)
C(25)-C(24)-C(23)	122.94(15)
C(25)-C(24)-C(29)	117.78(16)
C(23)-C(24)-C(29)	119.26(16)
C(26)-C(25)-C(24)	121.10(16)
C(26)-C(25)-H(25A)	119.4
C(24)-C(25)-H(25A)	119.4
C(25)-C(26)-C(27)	120.86(17)
C(25)-C(26)-H(26A)	119.6
C(27)-C(26)-H(26A)	119.6
C(28)-C(27)-C(26)	119.57(17)
C(28)-C(27)-H(27A)	120.2
C(26)-C(27)-H(27A)	120.2
C(27)-C(28)-C(29)	121.15(17)
C(27)-C(28)-H(28A)	119.4
C(29)-C(28)-H(28A)	119.4
C(30)-C(29)-C(28)	121.83(16)
C(30)-C(29)-C(24)	118.70(16)
C(28)-C(29)-C(24)	119.46(16)
C(31)-C(30)-C(29)	121.67(17)
C(31)-C(30)-H(30A)	119.2
C(29)-C(30)-H(30A)	119.2
C(30)-C(31)-C(32)	119.67(17)
C(30)-C(31)-H(31A)	120.2
C(32)-C(31)-H(31A)	120.2
O(1)-C(32)-C(23)	115.72(15)
O(1)-C(32)-C(31)	123.17(16)
C(23)-C(32)-C(31)	121.10(16)
O(1)-C(33)-H(33A)	109.5
O(1)-C(33)-H(33B)	109.5
H(33A)-C(33)-H(33B)	109.5
O(1)-C(33)-H(33C)	109.5
H(33A)-C(33)-H(33C)	109.5
H(33B)-C(33)-H(33C)	109.5
S(1)-C(34)-H(34A)	109.5
S(1)-C(34)-H(34B)	109.5

H(34A)-C(34)-H(34B)	109.5
S(1)-C(34)-H(34C)	109.5
H(34A)-C(34)-H(34C)	109.5
H(34B)-C(34)-H(34C)	109.5
C(36)-C(35)-C(40)	108.67(15)
C(36)-C(35)-P(1)	118.22(13)
C(40)-C(35)-P(1)	113.64(12)
C(36)-C(35)-H(35A)	105.0
C(40)-C(35)-H(35A)	105.0
P(1)-C(35)-H(35A)	105.0
C(37)-C(36)-C(35)	109.77(16)
C(37)-C(36)-H(36A)	109.7
C(35)-C(36)-H(36A)	109.7
C(37)-C(36)-H(36B)	109.7
C(35)-C(36)-H(36B)	109.7
H(36A)-C(36)-H(36B)	108.2
C(38)-C(37)-C(36)	111.61(18)
C(38)-C(37)-H(37A)	109.3
C(36)-C(37)-H(37A)	109.3
C(38)-C(37)-H(37B)	109.3
C(36)-C(37)-H(37B)	109.3
H(37A)-C(37)-H(37B)	108.0
C(39)-C(38)-C(37)	112.10(18)
C(39)-C(38)-H(38A)	109.2
C(37)-C(38)-H(38A)	109.2
C(39)-C(38)-H(38B)	109.2
C(37)-C(38)-H(38B)	109.2
H(38A)-C(38)-H(38B)	107.9
C(38)-C(39)-C(40)	111.06(18)
C(38)-C(39)-H(39A)	109.4
C(40)-C(39)-H(39A)	109.4
C(38)-C(39)-H(39B)	109.4
C(40)-C(39)-H(39B)	109.4
H(39A)-C(39)-H(39B)	108.0
C(39)-C(40)-C(35)	109.55(16)
C(39)-C(40)-H(40A)	109.8

C(35)-C(40)-H(40A)	109.8
C(39)-C(40)-H(40B)	109.8
C(35)-C(40)-H(40B)	109.8
H(40A)-C(40)-H(40B)	108.2
C(42)-C(41)-C(46)	109.74(14)
C(42)-C(41)-P(1)	116.30(12)
C(46)-C(41)-P(1)	111.84(12)
C(42)-C(41)-H(41A)	106.1
C(46)-C(41)-H(41A)	106.1
P(1)-C(41)-H(41A)	106.1
C(43)-C(42)-C(41)	110.15(15)
C(43)-C(42)-H(42A)	109.6
C(41)-C(42)-H(42A)	109.6
C(43)-C(42)-H(42B)	109.6
C(41)-C(42)-H(42B)	109.6
H(42A)-C(42)-H(42B)	108.1
C(44)-C(43)-C(42)	111.29(16)
C(44)-C(43)-H(43A)	109.4
C(42)-C(43)-H(43A)	109.4
C(44)-C(43)-H(43B)	109.4
C(42)-C(43)-H(43B)	109.4
H(43A)-C(43)-H(43B)	108.0
C(43)-C(44)-C(45)	110.60(16)
C(43)-C(44)-H(44A)	109.5
C(45)-C(44)-H(44A)	109.5
C(43)-C(44)-H(44B)	109.5
C(45)-C(44)-H(44B)	109.5
H(44A)-C(44)-H(44B)	108.1
C(44)-C(45)-C(46)	110.95(15)
C(44)-C(45)-H(45A)	109.4
C(46)-C(45)-H(45A)	109.4
C(44)-C(45)-H(45B)	109.4
C(46)-C(45)-H(45B)	109.4
H(45A)-C(45)-H(45B)	108.0
C(45)-C(46)-C(41)	110.16(15)
C(45)-C(46)-H(46A)	109.6

C(41)-C(46)-H(46A)	109.6
C(45)-C(46)-H(46B)	109.6
C(41)-C(46)-H(46B)	109.6
H(46A)-C(46)-H(46B)	108.1
C(2S)-C(1S)-C(6S)	119.7(3)
C(2S)-C(1S)-H(1S)	120.1
C(6S)-C(1S)-H(1S)	120.1
C(3S)-C(2S)-C(1S)	120.4(3)
C(3S)-C(2S)-H(2S)	119.8
C(1S)-C(2S)-H(2S)	119.8
C(2S)-C(3S)-C(4S)	120.6(3)
C(2S)-C(3S)-H(3S)	119.7
C(4S)-C(3S)-H(3S)	119.7
C(3S)-C(4S)-C(5S)	120.7(3)
C(3S)-C(4S)-H(4S)	119.7
C(5S)-C(4S)-H(4S)	119.7
C(4S)-C(5S)-C(6S)	119.5(3)
C(4S)-C(5S)-H(5S)	120.2
C(6S)-C(5S)-H(5S)	120.2
C(5S)-C(6S)-C(1S)	119.1(3)
C(5S)-C(6S)-H(6S)	120.5
C(1S)-C(6S)-H(6S)	120.5
C(9S)-C(7S)-C(8S)#1	120.0(2)
C(9S)-C(7S)-H(7S)	120.0
C(8S)#1-C(7S)-H(7S)	120.0
C(7S)#1-C(8S)-C(9S)	119.7(2)
C(7S)#1-C(8S)-H(8S)	120.2
C(9S)-C(8S)-H(8S)	120.2
C(7S)-C(9S)-C(8S)	120.4(2)
C(7S)-C(9S)-H(9S)	119.8
C(8S)-C(9S)-H(9S)	119.8
C(11S)-C(10S)-C(15S)	120.0
C(11S)-C(10S)-H(10S)	120.0
C(15S)-C(10S)-H(10S)	120.0
C(12S)-C(11S)-C(10S)	120.0
C(12S)-C(11S)-H(11S)	120.0

C(10S)-C(11S)-H(11S)	120.0
C(13S)-C(12S)-C(11S)	120.0
C(13S)-C(12S)-H(12S)	120.0
C(11S)-C(12S)-H(12S)	120.0
C(12S)-C(13S)-C(14S)	120.0
C(12S)-C(13S)-H(13S)	120.0
C(14S)-C(13S)-H(13S)	120.0
C(15S)-C(14S)-C(13S)	120.0
C(15S)-C(14S)-H(14S)	120.0
C(13S)-C(14S)-H(14S)	120.0
C(14S)-C(15S)-C(10S)	120.0
C(14S)-C(15S)-H(15S)	120.0
C(10S)-C(15S)-H(15S)	120.0
C(17S)-C(16S)-C(21S)	120.0
C(17S)-C(16S)-H(16S)	120.0
C(21S)-C(16S)-H(16S)	120.0
C(18S)-C(17S)-C(16S)	120.0
C(18S)-C(17S)-H(17S)	120.0
C(16S)-C(17S)-H(17S)	120.0
C(17S)-C(18S)-C(19S)	120.0
C(17S)-C(18S)-H(18S)	120.0
C(19S)-C(18S)-H(18S)	120.0
C(18S)-C(19S)-C(20S)	120.0
C(18S)-C(19S)-H(19S)	120.0
C(20S)-C(19S)-H(19S)	120.0
C(21S)-C(20S)-C(19S)	120.0
C(21S)-C(20S)-H(20S)	120.0
C(19S)-C(20S)-H(20S)	120.0
C(20S)-C(21S)-C(16S)	120.0
C(20S)-C(21S)-H(21S)	120.0
C(16S)-C(21S)-H(21S)	120.0

Symmetry transformations used to generate equivalent atoms:

#1 -x+1,-y,-z+1

Table A4. Anisotropic displacement parameters ($\text{\AA}^2 \times 10^3$) for d1567_a. The anisotropic displacement factor exponent takes the form: $-2\pi^2 [h^2 a^{*2} U^{11} + \dots + 2 h k a^* b^* U^{12}]$

	U ¹¹	U ²²	U ³³	U ²³	U ¹³	U ¹²
Pd(1)	15(1)	14(1)	13(1)	-5(1)	0(1)	-7(1)
S(1)	19(1)	22(1)	17(1)	-5(1)	-4(1)	-10(1)
P(1)	14(1)	15(1)	13(1)	-4(1)	-1(1)	-7(1)
O(1)	26(1)	25(1)	15(1)	-6(1)	4(1)	-16(1)
O(2)	28(1)	35(1)	21(1)	-12(1)	2(1)	-21(1)
O(3)	23(1)	31(1)	42(1)	-16(1)	0(1)	-9(1)
O(4)	26(1)	25(1)	28(1)	2(1)	-5(1)	-11(1)
N(1)	20(1)	22(1)	17(1)	-7(1)	2(1)	-13(1)
C(1)	21(1)	20(1)	13(1)	-5(1)	3(1)	-10(1)
C(2)	19(1)	33(1)	24(1)	-9(1)	-1(1)	-11(1)
C(3)	21(1)	30(1)	26(1)	-8(1)	-1(1)	-1(1)
C(4)	28(1)	19(1)	21(1)	-6(1)	2(1)	-4(1)
C(5)	26(1)	19(1)	15(1)	-6(1)	4(1)	-10(1)
C(6)	20(1)	18(1)	11(1)	-4(1)	2(1)	-8(1)
C(7)	20(1)	14(1)	13(1)	-3(1)	0(1)	-9(1)
C(8)	27(1)	20(1)	18(1)	-8(1)	1(1)	-13(1)
C(9)	29(1)	30(1)	19(1)	-8(1)	-5(1)	-16(1)
C(10)	20(1)	27(1)	22(1)	-5(1)	-6(1)	-8(1)
C(11)	21(1)	20(1)	15(1)	-4(1)	0(1)	-7(1)
C(12)	19(1)	16(1)	12(1)	-2(1)	-1(1)	-10(1)
C(13)	15(1)	19(1)	10(1)	-4(1)	0(1)	-8(1)
C(14)	21(1)	21(1)	17(1)	-7(1)	0(1)	-10(1)
C(15)	21(1)	28(1)	16(1)	-6(1)	-2(1)	-15(1)
C(16)	17(1)	25(1)	12(1)	-2(1)	-1(1)	-10(1)
C(17)	18(1)	34(1)	17(1)	-3(1)	-4(1)	-13(1)
C(18)	16(1)	32(1)	21(1)	-1(1)	-5(1)	-3(1)
C(19)	23(1)	22(1)	24(1)	-4(1)	-5(1)	-4(1)
C(20)	20(1)	21(1)	18(1)	-4(1)	-2(1)	-8(1)
C(21)	16(1)	20(1)	11(1)	-3(1)	0(1)	-8(1)
C(22)	15(1)	19(1)	8(1)	-3(1)	1(1)	-9(1)
C(23)	13(1)	14(1)	16(1)	-4(1)	-2(1)	-5(1)

C(24)	15(1)	13(1)	15(1)	-4(1)	-3(1)	-4(1)
C(25)	17(1)	22(1)	19(1)	-7(1)	-1(1)	-9(1)
C(26)	21(1)	29(1)	19(1)	-8(1)	1(1)	-10(1)
C(27)	29(1)	32(1)	18(1)	-13(1)	-2(1)	-11(1)
C(28)	26(1)	26(1)	24(1)	-11(1)	-5(1)	-12(1)
C(29)	18(1)	17(1)	20(1)	-6(1)	-4(1)	-6(1)
C(30)	21(1)	19(1)	26(1)	-7(1)	-4(1)	-12(1)
C(31)	20(1)	18(1)	24(1)	-5(1)	1(1)	-11(1)
C(32)	16(1)	14(1)	15(1)	-4(1)	-1(1)	-4(1)
C(33)	25(1)	24(1)	17(1)	-4(1)	5(1)	-12(1)
C(34)	38(1)	52(1)	22(1)	-9(1)	-7(1)	-28(1)
C(35)	21(1)	16(1)	18(1)	-5(1)	-1(1)	-9(1)
C(36)	27(1)	22(1)	24(1)	-5(1)	2(1)	-14(1)
C(37)	45(1)	30(1)	42(1)	-10(1)	5(1)	-26(1)
C(38)	57(2)	21(1)	59(2)	-14(1)	10(1)	-22(1)
C(39)	42(1)	20(1)	40(1)	-15(1)	6(1)	-11(1)
C(40)	24(1)	16(1)	21(1)	-6(1)	2(1)	-7(1)
C(41)	18(1)	18(1)	14(1)	-4(1)	-3(1)	-8(1)
C(42)	18(1)	25(1)	16(1)	-6(1)	0(1)	-9(1)
C(43)	24(1)	35(1)	16(1)	-11(1)	1(1)	-11(1)
C(44)	28(1)	34(1)	16(1)	-4(1)	-6(1)	-12(1)
C(45)	21(1)	29(1)	22(1)	-3(1)	-7(1)	-10(1)
C(46)	18(1)	21(1)	18(1)	-4(1)	-3(1)	-6(1)
C(1S)	92(3)	118(3)	82(3)	-66(3)	47(2)	-83(3)
C(2S)	129(3)	41(2)	50(2)	-16(2)	25(2)	-35(2)
C(3S)	67(2)	45(2)	58(2)	-16(2)	-22(2)	10(2)
C(4S)	48(2)	51(2)	83(2)	-29(2)	-15(2)	-14(1)
C(5S)	61(2)	29(1)	48(2)	-13(1)	-13(1)	-1(1)
C(6S)	28(1)	102(3)	61(2)	-55(2)	-4(1)	-4(2)
C(7S)	52(2)	33(1)	34(1)	-6(1)	-15(1)	-22(1)
C(8S)	35(1)	48(2)	46(1)	-29(1)	4(1)	-22(1)
C(9S)	34(1)	26(1)	56(2)	-19(1)	-20(1)	-4(1)
C(10S)	62(5)	110(10)	75(6)	-50(6)	-6(4)	-40(6)
C(11S)	79(6)	96(9)	109(12)	-54(9)	-6(8)	-32(7)
C(12S)	61(5)	72(5)	90(11)	-43(7)	15(6)	-17(4)
C(13S)	38(4)	55(5)	53(4)	-20(3)	18(3)	-7(3)

C(14S)	31(3)	61(4)	38(4)	-17(3)	7(3)	-5(3)
C(15S)	28(3)	78(7)	47(3)	-21(3)	-10(3)	-14(3)
C(16S)	56(6)	61(8)	141(14)	-20(7)	-56(8)	-21(6)
C(17S)	77(7)	50(7)	91(9)	21(6)	-59(7)	-28(6)
C(18S)	46(6)	90(8)	41(7)	9(7)	-22(6)	-16(5)
C(19S)	65(9)	160(20)	73(7)	-68(12)	31(6)	-50(13)
C(20S)	71(12)	170(20)	170(20)	-110(20)	85(13)	-68(16)
C(21S)	20(5)	87(12)	190(20)	-75(15)	14(10)	-2(6)

Table A5. Hydrogen coordinates ($\times 10^4$) and isotropic displacement parameters ($\text{\AA}^2 \times 10^{-3}$) for d1567_a.

	x	y	z	U(eq)
H(1N)	4444(18)	5201(19)	4372(14)	26(6)
H(2N)	3797(19)	5589(19)	3725(14)	30(6)
H(2A)	2241	7212	3674	30
H(3A)	1532	9058	3716	35
H(4A)	2705	9767	4059	30
H(5A)	4585	8641	4340	24
H(8A)	5825	7112	5247	24
H(9A)	7696	5991	5572	29
H(10A)	8759	4692	4885	28
H(11A)	7975	4558	3845	23
H(14A)	8972	6403	2482	22
H(15A)	10815	5298	2802	24
H(17A)	12424	3454	2995	27
H(18A)	13146	1636	2937	32
H(19A)	12024	942	2506	30
H(20A)	10191	2057	2143	24
H(25A)	9789	4193	599	22
H(26A)	9967	4039	-697	27
H(27A)	8839	3251	-1024	30
H(28A)	7559	2597	-32	28
H(30A)	6595	2348	1371	25
H(31A)	6438	2422	2688	24
H(33A)	6959	2848	4413	34
H(33B)	7120	1942	3980	34
H(33C)	6094	3130	3750	34
H(34A)	3209	4534	1529	51
H(34B)	4532	4301	1271	51
H(34C)	3652	5574	1069	51
H(35A)	7313	7378	2585	21
H(36A)	8366	7735	1281	29

H(36B)	7193	8538	847	29
H(37A)	8057	8907	2079	44
H(37B)	7986	9670	1122	44
H(38A)	6472	10551	1967	54
H(38B)	6008	10383	1255	54
H(39A)	4951	9825	2485	41
H(39B)	6083	8995	2962	41
H(40A)	5335	8664	1658	25
H(40B)	5288	7918	2618	25
H(41A)	6630	5596	1075	19
H(42A)	7648	7281	209	24
H(42B)	8332	5943	460	24
H(43A)	7806	6687	-938	29
H(43B)	7232	5766	-389	29
H(44A)	5851	7354	-1208	31
H(44B)	6092	8176	-858	31
H(45A)	5110	6479	107	29
H(45B)	4436	7818	-157	29
H(46A)	4945	7100	1240	24
H(46B)	5545	7998	687	24
H(1S)	2865	10357	1134	96
H(2S)	1127	11462	575	91
H(3S)	-160	10658	631	76
H(4S)	254	8740	1241	69
H(5S)	1963	7601	1839	59
H(6S)	3289	8399	1794	73
H(7S)	4888	1394	3707	44
H(8S)	3378	42	5890	45
H(9S)	3272	1426	4591	44
H(10S)	727	10786	7206	87
H(11S)	519	12603	6269	105
H(12S)	541	12952	4849	89
H(13S)	772	11484	4364	66
H(14S)	980	9667	5300	58
H(15S)	958	9317	6721	61
H(16S)	751	9957	7248	99

H(17S)	534	11853	6949	91
H(18S)	477	13055	5574	81
H(19S)	635	12361	4498	109
H(20S)	852	10464	4797	153
H(21S)	909	9262	6172	116

Table A6. Torsion angles [°] for d1567_a.

O(4)-S(1)-O(2)-Pd(1)	-69.03(12)
O(3)-S(1)-O(2)-Pd(1)	60.17(13)
C(34)-S(1)-O(2)-Pd(1)	175.99(11)
Pd(1)-N(1)-C(1)-C(2)	123.84(15)
Pd(1)-N(1)-C(1)-C(6)	-54.39(18)
C(6)-C(1)-C(2)-C(3)	0.2(3)
N(1)-C(1)-C(2)-C(3)	-178.04(17)
C(1)-C(2)-C(3)-C(4)	-0.8(3)
C(2)-C(3)-C(4)-C(5)	0.5(3)
C(3)-C(4)-C(5)-C(6)	0.5(3)
C(4)-C(5)-C(6)-C(1)	-1.2(3)
C(4)-C(5)-C(6)-C(7)	179.39(16)
C(2)-C(1)-C(6)-C(5)	0.8(3)
N(1)-C(1)-C(6)-C(5)	179.04(15)
C(2)-C(1)-C(6)-C(7)	-179.74(16)
N(1)-C(1)-C(6)-C(7)	-1.5(2)
C(5)-C(6)-C(7)-C(8)	37.7(2)
C(1)-C(6)-C(7)-C(8)	-141.69(17)
C(5)-C(6)-C(7)-C(12)	-143.43(17)
C(1)-C(6)-C(7)-C(12)	37.2(2)
C(12)-C(7)-C(8)-C(9)	-1.0(3)
C(6)-C(7)-C(8)-C(9)	177.86(16)
C(7)-C(8)-C(9)-C(10)	-1.3(3)
C(8)-C(9)-C(10)-C(11)	1.4(3)
C(9)-C(10)-C(11)-C(12)	0.9(3)
C(10)-C(11)-C(12)-C(7)	-3.2(3)
C(10)-C(11)-C(12)-Pd(1)	-176.34(14)
C(8)-C(7)-C(12)-C(11)	3.2(2)
C(6)-C(7)-C(12)-C(11)	-175.63(16)
C(8)-C(7)-C(12)-Pd(1)	176.49(13)
C(6)-C(7)-C(12)-Pd(1)	-2.4(2)
C(41)-P(1)-C(13)-C(22)	-56.91(16)
C(35)-P(1)-C(13)-C(22)	-173.24(14)
Pd(1)-P(1)-C(13)-C(22)	69.00(15)

C(41)-P(1)-C(13)-C(14)	129.44(14)
C(35)-P(1)-C(13)-C(14)	13.11(15)
Pd(1)-P(1)-C(13)-C(14)	-104.66(13)
C(22)-C(13)-C(14)-C(15)	-0.8(3)
P(1)-C(13)-C(14)-C(15)	173.17(14)
C(13)-C(14)-C(15)-C(16)	-0.5(3)
C(14)-C(15)-C(16)-C(21)	1.1(3)
C(14)-C(15)-C(16)-C(17)	-177.99(17)
C(15)-C(16)-C(17)-C(18)	179.02(17)
C(21)-C(16)-C(17)-C(18)	-0.1(3)
C(16)-C(17)-C(18)-C(19)	0.0(3)
C(17)-C(18)-C(19)-C(20)	-0.2(3)
C(18)-C(19)-C(20)-C(21)	0.4(3)
C(19)-C(20)-C(21)-C(16)	-0.4(3)
C(19)-C(20)-C(21)-C(22)	-178.77(17)
C(15)-C(16)-C(21)-C(20)	-178.85(16)
C(17)-C(16)-C(21)-C(20)	0.3(2)
C(15)-C(16)-C(21)-C(22)	-0.5(2)
C(17)-C(16)-C(21)-C(22)	178.65(16)
C(14)-C(13)-C(22)-C(21)	1.4(2)
P(1)-C(13)-C(22)-C(21)	-172.26(12)
C(14)-C(13)-C(22)-C(23)	178.35(15)
P(1)-C(13)-C(22)-C(23)	4.7(2)
C(20)-C(21)-C(22)-C(13)	177.51(16)
C(16)-C(21)-C(22)-C(13)	-0.8(2)
C(20)-C(21)-C(22)-C(23)	0.4(2)
C(16)-C(21)-C(22)-C(23)	-177.95(15)
C(13)-C(22)-C(23)-C(32)	-80.3(2)
C(21)-C(22)-C(23)-C(32)	96.71(19)
C(13)-C(22)-C(23)-C(24)	105.9(2)
C(21)-C(22)-C(23)-C(24)	-77.0(2)
C(32)-C(23)-C(24)-C(25)	-172.51(16)
C(22)-C(23)-C(24)-C(25)	1.2(3)
C(32)-C(23)-C(24)-C(29)	5.8(2)
C(22)-C(23)-C(24)-C(29)	179.49(16)
C(23)-C(24)-C(25)-C(26)	-178.51(17)

C(29)-C(24)-C(25)-C(26)	3.2(3)
C(24)-C(25)-C(26)-C(27)	-1.9(3)
C(25)-C(26)-C(27)-C(28)	-0.7(3)
C(26)-C(27)-C(28)-C(29)	1.9(3)
C(27)-C(28)-C(29)-C(30)	-179.30(18)
C(27)-C(28)-C(29)-C(24)	-0.5(3)
C(25)-C(24)-C(29)-C(30)	176.85(16)
C(23)-C(24)-C(29)-C(30)	-1.6(3)
C(25)-C(24)-C(29)-C(28)	-1.9(3)
C(23)-C(24)-C(29)-C(28)	179.66(16)
C(28)-C(29)-C(30)-C(31)	176.42(18)
C(24)-C(29)-C(30)-C(31)	-2.3(3)
C(29)-C(30)-C(31)-C(32)	2.0(3)
C(33)-O(1)-C(32)-C(23)	-178.87(15)
C(33)-O(1)-C(32)-C(31)	0.1(2)
C(24)-C(23)-C(32)-O(1)	172.66(15)
C(22)-C(23)-C(32)-O(1)	-1.2(2)
C(24)-C(23)-C(32)-C(31)	-6.3(3)
C(22)-C(23)-C(32)-C(31)	179.81(16)
C(30)-C(31)-C(32)-O(1)	-176.42(17)
C(30)-C(31)-C(32)-C(23)	2.5(3)
C(13)-P(1)-C(35)-C(36)	64.82(15)
C(41)-P(1)-C(35)-C(36)	-50.43(16)
Pd(1)-P(1)-C(35)-C(36)	-169.45(13)
C(13)-P(1)-C(35)-C(40)	-166.01(13)
C(41)-P(1)-C(35)-C(40)	78.74(14)
Pd(1)-P(1)-C(35)-C(40)	-40.28(14)
C(40)-C(35)-C(36)-C(37)	60.5(2)
P(1)-C(35)-C(36)-C(37)	-168.06(14)
C(35)-C(36)-C(37)-C(38)	-56.4(2)
C(36)-C(37)-C(38)-C(39)	53.0(3)
C(37)-C(38)-C(39)-C(40)	-53.9(3)
C(38)-C(39)-C(40)-C(35)	58.3(2)
C(36)-C(35)-C(40)-C(39)	-61.6(2)
P(1)-C(35)-C(40)-C(39)	164.52(14)
C(13)-P(1)-C(41)-C(42)	-41.99(15)

C(35)-P(1)-C(41)-C(42)	71.29(15)
Pd(1)-P(1)-C(41)-C(42)	-172.38(12)
C(13)-P(1)-C(41)-C(46)	-169.14(12)
C(35)-P(1)-C(41)-C(46)	-55.86(14)
Pd(1)-P(1)-C(41)-C(46)	60.47(13)
C(46)-C(41)-C(42)-C(43)	-58.0(2)
P(1)-C(41)-C(42)-C(43)	173.81(13)
C(41)-C(42)-C(43)-C(44)	57.3(2)
C(42)-C(43)-C(44)-C(45)	-56.2(2)
C(43)-C(44)-C(45)-C(46)	56.5(2)
C(44)-C(45)-C(46)-C(41)	-57.9(2)
C(42)-C(41)-C(46)-C(45)	58.53(19)
P(1)-C(41)-C(46)-C(45)	-170.87(12)
C(6S)-C(1S)-C(2S)-C(3S)	-0.9(5)
C(1S)-C(2S)-C(3S)-C(4S)	0.0(5)
C(2S)-C(3S)-C(4S)-C(5S)	0.9(5)
C(3S)-C(4S)-C(5S)-C(6S)	-0.8(4)
C(4S)-C(5S)-C(6S)-C(1S)	-0.1(4)
C(2S)-C(1S)-C(6S)-C(5S)	0.9(4)
C(8S)#1-C(7S)-C(9S)-C(8S)	0.4(3)
C(7S)#1-C(8S)-C(9S)-C(7S)	-0.4(3)
C(15S)-C(10S)-C(11S)-C(12S)	0.0
C(10S)-C(11S)-C(12S)-C(13S)	0.0
C(11S)-C(12S)-C(13S)-C(14S)	0.0
C(12S)-C(13S)-C(14S)-C(15S)	0.0
C(13S)-C(14S)-C(15S)-C(10S)	0.0
C(11S)-C(10S)-C(15S)-C(14S)	0.0
C(21S)-C(16S)-C(17S)-C(18S)	0.0
C(16S)-C(17S)-C(18S)-C(19S)	0.0
C(17S)-C(18S)-C(19S)-C(20S)	0.0
C(18S)-C(19S)-C(20S)-C(21S)	0.0
C(19S)-C(20S)-C(21S)-C(16S)	0.0
C(17S)-C(16S)-C(21S)-C(20S)	0.0

Symmetry transformations used to generate equivalent atoms:

#1 -x+1,-y,-z+1

Table A7. Hydrogen bonds for d1567_a [\AA and $^\circ$].

D-H...A	d(D-H)	d(H...A)	d(D...A)	<(DHA)
N(1)-H(2N)...S(1)	0.85(2)	2.75(2)	3.3407(17)	128.8(18)
N(1)-H(2N)...O(3)	0.85(2)	2.24(2)	3.013(2)	152(2)

Symmetry transformations used to generate equivalent atoms:

#1 -x+1,-y,-z+1

References

1. Johansson Seechurn, C. C. C.; Kitching, M. O.; Colacot, T. J.; Snieckus, V. Palladium-Catalyzed Cross-Coupling: A Historical Contextual Perspective to the 2010 Nobel Prize. *Angew. Chem. Int. Ed.* **2012**, *51*, 5062–5085.
2. Melchor, M. G. General Introduction. In *A Theoretical Study of Pd-Catalyzed C-C Cross-Coupling Reactions*; Springer Science and Business Media: Barcelona, 2013; pp. 1–28.
3. Paradies, J. Palladium-Catalyzed Aromatic Carbon-Nitrogen Bond Formation. In *Metal-Catalyzed Cross-Coupling Reactions and More*; de Meijere, A.; Bräse, S.; Oestreich, M., Eds.; John Wiley & Sons: Weinheim, 2014; pp. 995–1066.
4. Kosugi, M.; Kameyama, M.; Migita, T. Palladium-Catalyzed Aromatic Amination of Aryl Bromides with *N,N*-Di-Ethylamino-Tributyltin. *Chem. Lett.* **1983**, 927–928.
5. Guram, A. S.; Buchwald, S. L. Palladium-Catalyzed Aromatic Aminations with *in Situ* Generated Aminostannanes. *J. Am. Chem. Soc.* **1994**, *116*, 7901–7902.
6. Paul, F.; Patt, J.; Hartwig, J. F. Palladium-Catalyzed Formation of Carbon-Nitrogen Bonds. Reaction Intermediates and Catalyst Improvements in the Hetero Cross-Coupling of Aryl Halides and Tin Amides. *J. Am. Chem. Soc.* **1994**, *116*, 5969–5970.
7. Guram, A. S.; Rennels, R. A.; Buchwald, S. L. A Simple Catalytic Method for the Conversion of Aryl Bromides to Arylamines. *Angew. Chem. Int. Ed. Engl.* **1995**, *34*, 1348–1350.
8. Louie, J.; Hartwig, J. F. Palladium-Catalyzed Synthesis of Arylamines from Aryl Halides. Mechanistic Studies Lead to Coupling in the Absence of Tin Reagents. *Tetrahedron Lett.* **1995**, *36*, 3609–3612.
9. Muci, A. R.; Buchwald, S. L. Practical Palladium Catalysts for C-N and C-O Bond Formation. *Top. Curr. Chem.* **2002**, *219*, 131.
10. Driver, M. S.; Hartwig, J. F. A Rare, Low-Valent Alkylamido Complex, a Diphenylamido Complex, and Their Reductive Elimination of Amines by Three-Coordinate Intermediates. *J. Am. Chem. Soc.* **1995**, *117*, 4708–4709.
11. Driver, M. S.; Hartwig, J. F. Carbon-Nitrogen-Bond-Forming Reductive Elimination of Arylamines from Palladium(II) Phosphine Complexes. *J. Am. Chem. Soc.* **1997**, *119*, 8232–8245.
12. Hamann, B. C.; Hartwig, J. F. Systematic Variation of Bidentate Ligands Used in Aryl Halide Amination. Unexpected Effects of Steric, Electronic, and Geometric Perturbations. *J. Am. Chem. Soc.* **1998**, *120*, 3694–3703.
13. Shekhar, S.; Ryberg, P.; Hartwig, J. F.; Mathew, J. S.; Blackmond, D. G.; Strieter, E. R.; Buchwald, S. L. Reevaluation of the Mechanism of the Amination of Aryl Halides Catalyzed by BINAP-Ligated Palladium Complexes. *J. Am. Chem. Soc.* **2006**, *128*, 3584–3591.

14. Muzart, J. On the Behavior of Amines in the Presence of Pd⁰ and Pd^{II} Species. *J. Mol. Catal. A: Chem.* **2009**, *308*, 15–24.
15. Strieter, E. R.; Blackmond, D. G.; Buchwald, S. L. Insights into the Origin of High Activity and Stability of Catalysts Derived from Bulky, Electron-Rich Monophosphinobiaryl Ligands in the Pd-Catalyzed C-N Bond Formation. *J. Am. Chem. Soc.* **2003**, *125*, 13978–13980.
16. Amatore, C.; Carré, E.; Jutand, A.; M'Barki, M. A. Rates and Mechanism of the Formation of Zerovalent Palladium Complexes from Mixtures of Pd(OAc)₂ and Tertiary Phosphines and Their Reactivity in Oxidative Additions. *Organometallics* **1995**, *14*, 1818–1826.
17. Alcazar-Roman, L. M.; Hartwig, J. F.; Rheingold, A. L.; Liable-Sands, L. M.; Guzei, I. A. Mechanistic Studies of the Palladium-Catalyzed Amination of Aryl Halides and the Oxidative Addition of Aryl Bromides to Pd(BINAP)₂ and Pd(DPPF)₂: An Unusual Case of Zero-Order Kinetic Behavior and Product Inhibition. *J. Am. Chem. Soc.* **2000**, *122*, 4618–4630.
18. Zalesskiy, S. S.; Ananikov, V. P. Pd₂(dba)₃ as a Precursor of Soluble Metal Complexes and Nanoparticles: Determination of Palladium Active Species for Catalysis and Synthesis. *Organometallics* **2012**, *31*, 2302–2309.
19. Amatore, C.; Broeker, G.; Jutand, A.; Khalil, F. Identification of the Effective palladium(0) Catalytic Species Generated *in Situ* from Mixtures of Pd(dba)₂ and Bidentate Phosphine Ligands. Determination of Their Rates and Mechanism in Oxidative Addition. *J. Am. Chem. Soc.* **1997**, *119*, 5176–5185.
20. Littke, A. F.; Dai, C.; Fu, G. C. Versatile Catalysts for the Suzuki Cross-Coupling of Arylboronic Acids with Aryl and Vinyl Halides and Triflates under Mild Conditions. **2000**, *122*, 4020–4028.
21. Surry, D. S.; Buchwald, S. L. Dialkylbiaryl Phosphines in Pd-Catalyzed Amination: A User's Guide. *Chem. Sci.* **2011**, *2*, 27–50.
22. Hayashi, T.; Konishi, M.; Kobori, Y.; Kumada, M.; Higuchi, T.; Hirotsu, K. Dichloro[1,1'-bis(diphenylphosphino)ferrocene]palladium(II): An Effective Catalyst for Cross-Coupling of Secondary and Primary Alkyl Grignard and Alkylzinc Reagents with Organic Halides. *J. Am. Chem. Soc.* **1984**, *106*, 158–163.
23. Kranenburg, M.; Kamer, P. C. J.; van Leeuwen, P. W. N. M. The Effect of the Bite Angle of Diphosphane Ligands on Activity and Selectivity in Palladium-Catalyzed Cross-Coupling. *Eur. J. Inorg. Chem.* **1998**, *1998*, 155–157.
24. Old, D. W.; Wolfe, J. P.; Buchwald, S. L. A Highly Active Catalyst for Palladium-Catalyzed Cross-Coupling Reactions: Room-Temperature Suzuki Couplings and Amination of Unactivated Aryl Chlorides. *J. Am. Chem. Soc.* **1998**, *120*, 9722–9723.
25. Tomori, H.; Fox, J. M.; Buchwald, S. L. An Improved Synthesis of Functionalized Biphenyl-Based Phosphine Ligands. *J. Org. Chem.* **2000**, *65*, 5334–5341.
26. Kaye, S.; Fox, J. M.; Hicks, F. A.; Buchwald, S. L. The Use of Catalytic Amounts of CuCl

- and Other Improvements in the Benzyne Route to Biphenyl-Based Phosphine Ligands. *Adv. Synth. Catal.* **2001**, *343*, 789–794.
27. Barder, T. E.; Buchwald, S. L. Insights into Amine Binding to Biaryl Phosphine Palladium Oxidative Addition Complexes and Reductive Elimination from Biaryl Phosphine Arylpalladium Amido Complexes *via* Density Functional Theory. *J. Am. Chem. Soc.* **2007**, *129*, 12003–12010.
 28. Hamann, B. C.; Hartwig, J. F. Sterically Hindered Chelating Alkyl Phosphines Provide Large Rate Accelerations in Palladium-Catalyzed Amination of Aryl Iodides, Bromides, and Chlorides, and the First Amination of Aryl Tosylates. *J. Am. Chem. Soc.* **1998**, *120*, 7369–7370.
 29. Li, H.; Johansson Seechurn, C. C. C.; Colacot, T. J. Development of Preformed Pd Catalysts for Cross-Coupling Reactions, Beyond the 2010 Nobel Prize. *ACS Catal.* **2012**, *2*, 1147–1164.
 30. Hill, L. L.; Crowell, J. L.; Tutwiler, S. L.; Massie, N. L.; Hines, C. C.; Griffin, S. T.; Rogers, R. D.; Shaughnessy, K. H.; Grasa, G. A.; Johansson Seechurn, C. C. C.; Li, H.; Colacot, T. J.; Chou, J.; Woltermann, C. J. Synthesis and X-ray Structure Determination of Highly Active Pd(II), Pd(I), and Pd(0) Complexes of Di(*tert*-Butyl)neopentylphosphine (DTBNpP) in the Arylation of Amines and Ketones. *J. Org. Chem.* **2010**, *75*, 6477–6488.
 31. Fortman, G. C.; Nolan, S. P. *N*-Heterocyclic Carbene (NHC) Ligands and Palladium in Homogeneous Cross-Coupling Catalysis: A Perfect Union. *Chem. Soc. Rev.* **2011**, *40*, 5151–5169.
 32. Littke, A. F.; Fu, G. C. A Convenient and General Method for Pd-Catalyzed Suzuki Cross-Couplings of Aryl Chlorides and Arylboronic Acids. *Angew. Chem. Int. Ed.* **1998**, *37*, 3387–3388.
 33. Nishiyama, M.; Yamamoto, T.; Koie, Y. Synthesis of *N*-Arylpiperazines from Aryl Halides and Piperazine under a Palladium Tri-*tert*-Butylphosphine Catalyst. *Tetrahedron Lett.* **1998**, *39*, 617–620.
 34. Mario, G. A.; Zapf, A.; Beller, M. Molecularly Defined palladium(0) Monophosphine Complexes as Catalysts for Efficient Cross-Coupling of Aryl Chlorides and Phenylboronic Acid. *Chem. Commun.* **2000**, *2*, 2475–2476.
 35. Viciu, M. S.; Kissling, R. M.; Stevens, E. D.; Nolan, S. P. An Air-Stable Palladium/*N*-Heterocyclic Carbene Complex and Its Reactivity in Aryl Amination. *Org. Lett.* **2002**, *4*, 2229–2231.
 36. O'Brien, C. J.; Kantchev, E. A. B.; Valente, C.; Hadei, N.; Chass, G. A.; Lough, A.; Hopkinson, A. C.; Organ, M. G. Easily Prepared Air- and Moisture-Stable Pd-NHC (NHC=*N*-Heterocyclic Carbene) Complexes: A Reliable, User-Friendly, Highly Active Palladium Precatalyst for the Suzuki-Miyaura Reaction. *Chem. Eur. J.* **2006**, *12*, 4743–4748.
 37. Pompeo, M.; Farmer, J. L.; Froese, R. D. J.; Organ, M. G. Room-Temperature Amination of Deactivated Aniline and Aryl Halide Partners with Carbonate Base Using a Pd-PEPSI-IPent^{Cl}-*o*-Picoline Catalyst. *Angew. Chem. Int. Ed.* **2014**, *53*, 3223–3226.

38. Zhang, Y.; César, V.; Lavigne, G. Efficient and Versatile Buchwald-Hartwig Amination of (Hetero)aryl Chlorides Using the Pd-PEPPSI-IPr^{(NMe₂)₂} Precatalyst in the Presence of Carbonate Base. *Eur. J. Org. Chem.* **2015**, 2015, 2042–2050.
39. Albrecht, M. C-H Bond Activation. In *Palladacycles: Synthesis, Characterization and Applications*; Dupont, J.; Pfeffer, M., Eds.; John Wiley & Sons: Weinheim, 2008; pp. 13–35.
40. Herrmann, W. A.; Brossmer, C.; Öfele, K.; Reisinger, Claus-Peter Priermeier, T.; Beller, M.; Fischer, H. Palladacycles as Structurally Defined Catalysts for the Heck Olefination of Chloro- and Bromoarenes. *Angew. Chem. Int. Ed. Engl.* **1995**, 34, 1844–1848.
41. Beller, M.; Hartmut, F.; Herrmann, W. A.; Öfele, K.; Brossmer, C. Palladacycles as Efficient Catalysts for Aryl Coupling Reactions. *Angew. Chem. Int. Ed. Engl.* **1995**, 34, 1848–1849.
42. Louie, J.; Hartwig, J. F. A Route to Pd⁰ from Pd^{II} Metallacycles in Animation and Cross-Coupling Chemistry. *Angew. Chem. Int. Ed.* **1996**, 35, 2359–2360.
43. Beller, M.; Riermeier, T. H.; Reisinger, C.-P.; Herrmann, W. A. First Palladium-Catalyzed Aminations of Aryl Chlorides. *Tetrahedron Lett.* **1997**, 38, 2073–2074.
44. Zim, D.; Buchwald, S. L. An Air and Thermally Stable One-Component Catalyst for the Amination of Aryl Chlorides. *Org. Lett.* **2003**, 5, 2413–2415.
45. Biscoe, M. R.; Fors, B. P.; Buchwald, S. L. A New Class of Easily Activated Palladium Precatalysts for Facile C-N Cross-Coupling Reactions and the Low Temperature Oxidative Addition of Aryl Chlorides. *J. Am. Chem. Soc.* **2008**, 130, 6686–6687.
46. Vicente, J.; Saura-Llamas, I.; Oliva-Madrid, M.-J.; García-López, J.-A.; Bautista, D. A New Method for High-Yield Cyclopalladation of Primary and Secondary Amines. Atom-Efficient Open-to-Air Inexpensive Synthesis of Buchwald-Type Precatalysts. *Organometallics* **2011**, 30, 4624–4631.
47. Albert, J.; Granell, J.; Zafrilla, J.; Font-Bardia, M.; Solans, X. The Cyclopalladation Reaction of 2-Phenylaniline Revisited. *J. Organomet. Chem.* **2005**, 690, 422–429.
48. Kinzel, T.; Zhang, Y.; Buchwald, S. L. A New Palladium Precatalyst Allows for the Fast Suzuki-Miyaura Coupling Reactions of Unstable Polyfluorophenyl and 2-Heteroaryl Boronic Acids. *J. Am. Chem. Soc.* **2010**, 132, 14073–14075.
49. Bruno, N. C.; Tudge, M. T.; Buchwald, S. L. Design and Preparation of New Palladium Precatalysts for C-C and C-N Cross-Coupling Reactions. *Chem. Sci.* **2013**, 4, 916–920.
50. Bruno, N. C.; Buchwald, S. L. Synthesis and Application of Palladium Precatalysts That Accommodate Extremely Bulky Di-*Tert*-Butylphosphino Biaryl Ligands. *Org. Lett.* **2013**, 15, 2876–2879.
51. Rossen, K.; Pye, P. J.; Maliakal, A.; Volante, R. P. Kinetic Resolution of *Rac*-4,12-dibromo[2.2]paracyclophane in a Palladium [2.2]PHANEPHOS Catalyzed Amination. *J. Org. Chem.* **1997**, 62, 6462–6463.
52. Vyskočil, Š.; Smrčina, M.; Kočovský, P. Synthesis of 2-Amino-2'-Diphenylphosphino-

- 1,1'-Binaphthyl (MAP) and Its Accelerating Effect on the Pd(0)-Catalyzed *N*-Arylation. *Tetrahedron Lett.* **1998**, *39*, 9289–9292.
53. Kreis, M.; Friedmann, C. J.; Bräse, S. Diastereoselective Hartwig-Buchwald Reaction of Chiral Amines with *Rac*-[2.2]paracyclophane Derivatives. *Chem. Eur. J.* **2005**, *11*, 7387–7394.
 54. Tagashira, J.; Imao, D.; Yamamoto, T.; Ohta, T.; Furukawa, I.; Ito, Y. Optically Active Palladium-Catalyzed Asymmetric Amination of Aryl Halide. *Tetrahedron Asymmetry* **2005**, *16*, 2307–2314.
 55. Kitagawa, O.; Takahashi, M.; Yoshikawa, M.; Taguchi, T. Efficient Synthesis of Optically Active Atropisomeric Anilides through Catalytic Asymmetric *N*-Arylation Reaction. *J. Am. Chem. Soc.* **2005**, *127*, 3676–3677.
 56. Kitagawa, O.; Yoshikawa, M.; Tanabe, H.; Morita, T.; Takahashi, M.; Dobashi, Y.; Taguchi, T. Highly Enantioselective Synthesis of Atropisomeric Anilide Derivatives through Catalytic Asymmetric *N*-Arylation: Conformational Analysis and Application to Asymmetric Enolate Chemistry. *J. Am. Chem. Soc.* **2006**, *128*, 12923–12931.
 57. Kitagawa, O.; Kurihara, D.; Tanabe, H.; Shibuya, T.; Taguchi, T. Catalytic Enantioselective Synthesis of Key Intermediates for NET Inhibitors Using Atropisomeric Lactam Chemistry. *Tetrahedron Lett.* **2008**, *49*, 471–474.
 58. Takahashi, M.; Tanabe, H.; Nakamura, T.; Kuribara, D.; Yamazaki, T.; Kitagawa, O. Atropisomeric Lactam Chemistry: Catalytic Enantioselective Synthesis, Application to Asymmetric Enolate Chemistry and Synthesis of Key Intermediates for NET Inhibitors. *Tetrahedron* **2010**, *66*, 288–296.
 59. Takahashi, I.; Morita, F.; Kusagaya, S.; Fukaya, H.; Kitagawa, O. Catalytic Enantioselective Synthesis of Atropisomeric 2-Aryl-4-Quinolinone Derivatives with an N-C Chiral Axis. *Tetrahedron Asymmetry* **2012**, *23*, 1657–1662.
 60. Takenaka, K.; Itoh, N.; Sasai, H. Enantioselective Synthesis of *C*₂-Symmetric Spirobilactams *via* Pd-Catalyzed Double Intramolecular *N*-Arylation. *Org. Lett.* **2009**, *11*, 1483–1486.
 61. Porosa, L.; Viirre, R. D. Desymmetrization of Malonamides *via* an Enantioselective Intramolecular Buchwald-Hartwig Reaction. *Tetrahedron Lett.* **2009**, *50*, 4170–4173.
 62. Li, H.; Belyk, K. M.; Yin, J.; Chen, Q.; Hyde, A.; Ji, Y.; Oliver, S.; Tudge, M. T.; Campeau, L.-C.; Campos, K. R. Enantioselective Synthesis of Hemiaminals *via* Pd-Catalyzed C–N Coupling with Chiral Bisphosphine Mono-Oxides. *J. Am. Chem. Soc.* **2015**, *137*, 13728–13731.
 63. Yang, W.; Long, Y.; Zhang, S.; Zeng, Y.; Cai, Q. Copper-Catalyzed Enantioselective Intramolecular *N*-Arylation, an Efficient Method for Kinetic Resolutions. *Org. Lett.* **2013**, *15*, 3598–3601.
 64. Shi, J.; Wang, T.; Huang, Y.; Zhang, X.; Wu, Y.-D.; Cai, Q. Pd-Catalyzed Asymmetric Intramolecular Aryl C–O Bond Formation with SDP(O) Ligand: Enantioselective Synthesis of (2,3-Dihydrobenzo[*b*][1,4]dioxin-2-yl)methanols. *Org. Lett.* **2015**, *17*, 840–

843.

65. Moncarz, J. R.; Laritcheva, N. F.; Glueck, D. S. Palladium-Catalyzed Asymmetric Phosphination: Enantioselective Synthesis of a *P*-Chirogenic Phosphine. *J. Am. Chem. Soc.* **2002**, *124*, 13356–13357.
66. Korff, C.; Helmchen, G. Preparation of Chiral Triarylphosphines by Pd-Catalysed Asymmetric P-C Cross-Coupling. *Chem. Commun.* **2004**, 530–531.
67. Bruner, T. J.; Anderson, B. J.; Blank, N. F.; Glueck, D. S.; Rheingold, A. L. Enantioselective Synthesis of *P*-Stereogenic Benzophospholanes *via* Palladium-Catalyzed Intramolecular Cyclization. *Org. Lett.* **2007**, *9*, 1109–1112.
68. Chan, V. S.; Bergman, R. G.; Toste, F. D. Pd-Catalyzed Dynamic Kinetic Enantioselective Arylation of Silylphosphines. *J. Am. Chem. Soc.* **2007**, *129*, 15122–15123.
69. Bhat, V.; Wang, S.; Stoltz, B. M.; Virgil, S. C. Asymmetric Synthesis of QUINAP *via* Dynamic Kinetic Resolution. *J. Am. Chem. Soc.* **2013**, *135*, 16829–16832.
70. Blank, N. F.; Moncarz, J. R.; Bruner, T. J.; Scriban, C.; Anderson, B. J.; Amir, O.; Glueck, D. S.; Zakharov, L. N.; Golen, J. A.; Incarvito, C. D.; Rheingold, A. L. Palladium-Catalyzed Asymmetric Phosphination. Scope, Mechanism, and Origin of Enantioselectivity. *J. Am. Chem. Soc.* **2007**, *129*, 6847–6858.
71. Cipiciani, A.; Fringuelli, F.; Mancini, V.; Piermatti, O. Synthesis of Chiral (*R*)-4-Hydroxy- and (*R*)-4-Halogeno [2.2]paracyclophanes and Group Polarizability. Optical Rotation Relationship. *J. Org. Chem.* **1997**, *62*, 3744–3747.
72. Takahashi, I.; Suzuki, Y.; Kitagawa, O. Asymmetric Synthesis of Atropisomeric Compounds with an N-C Chiral Axis. *Org. Prep. Proced. Int.* **2014**, *46*, 1–23.
73. Snell, R. H.; Durbin, M. J.; Woodward, R. L.; Willis, M. C. Catalytic Enantioselective Desymmetrisation as a Tool for the Synthesis of Hodgkinsine and Hodgkinsine B. *Chem. Eur. J.* **2012**, *18*, 16754–16764.
74. Nakazaki, A.; Miyagawa, K.; Miyata, N.; Nishikawa, T. Synthesis of a C-N Axially Chiral *N*-Arylisatin through Asymmetric Intramolecular *N*-Arylation. *Eur. J. Org. Chem.* **2015**, *2015*, 4603–4606.
75. Ishibashi, K.; Tsue, H.; Takahashi, H.; Tamura, R. Azacalix[4]arene Tetramethyl Ether with Inherent Chirality Generated by Substitution on the Nitrogen Bridges. *Tetrahedron Asymmetry* **2009**, *20*, 375–380.
76. Denning, R. A. Studies in Simultaneous Generation of Central and Axial Chirality *via* the Buchwald-Hartwig Reaction, M.Sc. Thesis, Ryerson University, 2014.
77. Surry, D. S.; Buchwald, S. L. Biaryl Phosphane Ligands in Palladium-Catalyzed Amination. *Angew. Chem. Int. Ed.* **2008**, *47*, 6338–6361.
78. Bringmann, G.; Wuzik, A.; Breuning, M.; Henschel, P.; Peters, K.; Peters, E.-M. Atropo-Enantioselective Synthesis of an Axially Chiral *C₁*-Symmetric Phosphine Ligand and Its Application in the Asymmetric Hydrosilylation of Styrenes. *Tetrahedron Asymmetry*

- 1999**, *10*, 3025–3031.
79. Hayashi, T. Axially Chiral Monophosphine Ligands (MOPs) and Their Use for Palladium-Catalyzed Asymmetric Hydrosilylation of Olefins. *Catal. Today* **2000**, *62*, 3–15.
 80. Fujita, K.-I.; Yamashita, M.; Puschmann, F.; Alvarez-Falcon, M. M.; Incarvito, C. D.; Hartwig, J. F. Organometallic Chemistry of Amidate Complexes. Accelerating Effect of Bidentate Ligands on the Reductive Elimination of *N*-Aryl Amidates from Palladium(II). *J. Am. Chem. Soc.* **2006**, *128*, 9044–9045.
 81. Teerlinck, C. E.; Bowyer, W. J. Reactivity of Magnesium Surfaces during the Formation of Grignard Reagents. *J. Org. Chem.* **1996**, *61*, 1059–1064.
 82. Garst, J. F.; Soriaga, M. P. Grignard Reagent Formation. *Coord. Chem. Rev.* **2004**, *248*, 623–652.
 83. Becht, J. M.; Ngouela, S.; Wagner, A.; Mioskowski, C. A Straightforward Anionic Coupling for the Synthesis of *ortho*-Bromobiaryls. *Tetrahedron* **2004**, *60*, 6853–6857.
 84. Leroux, F. R.; Bonnafoux, L.; Heiss, C.; Colobert, F.; Lanfranchi, D. A. A Practical Transition Metal-Free Aryl-Aryl Coupling Method: Arynes as Key Intermediates. *Adv. Synth. Catal.* **2007**, *349*, 2705–2713.
 85. Firouzabadi, H.; Iranpoor, N.; Amani, K. Heteropoly Acid Cesium salt/Cetyltrimethylammonium Bromide a Catalytic Heterogeneous System Which Highly Controls Regioselective Bromination of Aromatic Compounds with Bromine. *J. Mol. Catal. A: Chem.* **2003**, *195*, 289–294.
 86. SDBS Web http://sdb.sdb.aist.go.jp/sdb/cgi-bin/direct_frame_disp.cgi?sdbno=1753 (accessed Jan 1, 2014).
 87. Heller, B.; Gutnov, A.; Fischer, C.; Drexler, H. J.; Spannenberg, A.; Redkin, D.; Sundermann, C.; Sundermann, B. Phosphorus-Bearing Axially Chiral Biaryls by Catalytic Asymmetric Cross-Cyclotrimerization and a First Application in Asymmetric Hydrosilylation. *Chem. Eur. J.* **2007**, *13*, 1117–1128.
 88. Murata, M.; Buchwald, S. L. A General and Efficient Method for the Palladium-Catalyzed Cross-Coupling of Thiols and Secondary Phosphines. *Tetrahedron* **2004**, *60*, 7397–7403.
 89. Netherton, M. R.; Fu, G. C. Air-Stable Trialkylphosphonium Salts: Simple, Practical, and Versatile Replacements for Air-Sensitive Trialkylphosphines. Applications in Stoichiometric and Catalytic Processes. *Org. Lett.* **2001**, *3*, 4295–4298.
 90. Flegel, M.; Lukeman, M.; Wan, P. Photochemistry of 1,1'-Bi-2-Naphthol (BINOL) — ESIPT Is Responsible for Photoracemization and Photocyclization. *Can. J. Chem.* **2008**, *86*, 161–169.
 91. Uozumi, Y.; Hayashi, T. Catalytic Asymmetric Synthesis of Optically Active 2-Alkanols via Hydrosilylation of 1-Alkenes with a Chiral Monophosphine-Palladium Catalyst. *J. Am. Chem. Soc.* **1991**, *113*, 9887–9888.
 92. Hayashi, T. Chiral Monodentate Phosphine Ligand MOP for Transition-Metal-Catalyzed Asymmetric Reactions. *Acc. Chem. Res.* **2000**, *33*, 354–362.

93. Janesko, B. G.; Fisher, H. C.; Bridle, M. J.; Montchamp, J. L. P(=O)H to P-OH Tautomerism: A Theoretical and Experimental Study. *J. Org. Chem.* **2015**, *80*, 10025–10032.
94. Ikawa, T.; Barder, T. E.; Biscoe, M. R.; Buchwald, S. L. Pd-Catalyzed Amidations of Aryl Chlorides Using Monodentate Biaryl Phosphine Ligands: A Kinetic, Computational, and Synthetic Investigation Pd-Catalyzed Amidations of Aryl Chlorides Using Computational, and Synthetic Investigation. *J. Am. Chem. Soc.* **2007**, *129*, 13001–13007.
95. Hicks, J. D.; Hyde, A. M.; Cuezva, A. M.; Buchwald, S. L. Pd-Catalyzed *N*-Arylation of Secondary Acyclic Amides: Catalyst Development, Scope, and Computational Study. *J. Am. Chem. Soc.* **2009**, *131*, 16720–16734.
96. Xie, X.; Zhang, T. Y.; Zhang, Z. Synthesis of Bulky and Electron-Rich MOP-Type Ligands and Their Applications in Palladium-Catalyzed C-N Bond Formation. *J. Org. Chem.* **2006**, *71*, 6522–6529.
97. Baumgartner, M. T.; Tempesti, T. C.; Pierini, A. B. Steric Effects in the Synthesis of *Ortho*-Substituted 1,1'-binaphthalene Derivatives by the S_{RN}1 and the Stille Reaction. *Arkivoc* **2003**, *2003*, 420–433.
98. Lim, C. W.; Tissot, O.; Mattison, A.; Hooper, M. W.; Brown, J. M.; Cowley, A. R.; Hulmes, D. I.; Blacker, A. J. Practical Preparation and Resolution of 1-(2'-Diphenylphosphino-1'-Naphthyl)isoquinoline: A Useful Ligand for Catalytic Asymmetric Synthesis. *Org. Process Res. Dev.* **2003**, *7*, 379–384.
99. Mohar, B.; Čusak, A.; Modéc, B.; Stephan, M. *P*-Stereogenic Phospholanes or Phosphorinanes from *o*-Biaryllylphosphines: Two Bridges Not Too Far. *J. Org. Chem.* **2013**, *78*, 4665–4673.
100. Shifa, Z.; Wang, C.; Chen, L.; Liang, R.; Yu, Y.; Jiang, H. Modular Approach for Synthesis of Vicinal Diamines Containing Axial Chiral 1,1'-Binaphthyl from 1,2-Diaminoethane by Pd-Catalyzed *N*-Arylation Reactions. *Org. Lett.* **2011**, *13*, 1146–1149.
101. Hartwig, J. F. *Organotransition Metal Chemistry: From Bonding to Catalysis*; University Science Books, 2010.
102. Gawley, R. E.; Aubé, J. Kinetic Resolution. In *Principles of Asymmetric Synthesis*; Elsevier: Amsterdam, 2012; pp. 16–20.
103. Chojnacka, M. Towards the Synthesis of a New Pd-Phosphine Catalyst for the Buchwald-Hartwig Reaction, B.Sc. Thesis, Ryerson University, 2012.
104. Tatematsu, S.; Hibi, T.; Okuhara, T.; Misono, M. Preparation Process and Catalytic Activity of Cs_xH_{3-x}PW₁₂O₄₀. *Chem. Lett.* **1984**, 865–868.
105. Smith, C. J.; Hansch, C. The Relative Toxicity of Compounds in Mainstream Cigarette Smoke Condensate. *Food Chem. Toxicol.* **2000**, *38*, 637–646.